The Francis Crick Institute

Molecular Structure of Cell Signalling Laboratory

(Formerly the MRC National Institute for Medical Research)

Structural and functional basis for TRIM25 E3 ligase catalytic activity and NS1-mediated suppression

A thesis submitted by

Marios Grigorios Koliopoulos

In partial fulfilment of the requirements of

University College London

For the degree of Doctor of Philosophy

September 2017

Declaration

I, Marios Grigorios Koliopoulos, declare that the work presented in this thesis was performed in the laboratory of Dr Katrin Rittinger at the Francis Crick Institute in London, UK (Formerly the MRC National Institute for Medical Research). I confirm that the work presented in this thesis is my own. Where information has been derived from other sources, this has been indicated.

Marios G. Koliopoulos

Abstract

Ubiquitination is a post-translational modification of proteins with broad regulatory roles across cellular biology. This process involves the addition of ubiquitin molecules on target proteins, altering their cellular role and properties. Ubiquitination is performed by an enzymatic cascade consisting of three enzymes: ubiquitin activating enzymes (E1), ubiquitin conjugating enzymes (E2) and ubiquitin ligases (E3).

The tripartite motif (TRIM) family of proteins constitutes one of the largest subfamilies of RING E3 ligases and the majority of them are contributing to the regulation of innate immune responses. They are characterized by a conserved tripartite motif in their N-terminal region which comprises a RING domain, one or two B-box domains and a coiled-coil region. Self-association is believed to be crucial for catalytic activity of TRIM proteins, however, the precise molecular mechanism underlying this observation remains elusive.

The work presented in this thesis provides insights into the E3 ligase function of TRIM25 and shows how its oligomeric state is linked to its catalytic activity. The crystal structure of a complex between the TRIM25 RING domain and a ubiquitin-loaded E2 identifies the structural and mechanistic features that promote activation of E2~Ub allowing us to propose a model for the regulation of activity in the full-length protein. In the second part of this thesis, the molecular details of Influenza A NS1-mediated TRIM25 inhibition are presented. The crystal structures of NS1 bound to TRIM25 along with biochemical analysis allowed us to identify the interacting domains and propose a model for the inhibition of substrate ubiquitination during viral infection.

The results of this project extend our understanding of the mechanism, structure and regulation of TRIM E3 ligases and their substrates, leading to increased chances of targeting specific steps of the ubiquitination pathway during disease.

Impact Statement

Over the past few years, the ubiquitin system has emerged as a crucial regulator of almost every process required for sustaining life. This complex network is composed of a myriad of proteins all of which perform a dedicated task in a highly regulated and timely manner. Defects in this system are associated with cancer, neurodegenerative and autoimmune disorders. Many pathogenic microorganisms have also evolved mechanisms by which they directly inhibit proteins or hijack mechanisms of the ubiquitin system to avoid detection and escape immune responses. In the present thesis, the molecular details of an enzyme, TRIM25, which has a central role in averting viral infections including influenza, were explored. Structural and biochemical analysis promoted our understanding of the activation context and interacting partners on the atomic level. The general principles described for the mechanism of activity of TRIM25 seem also to apply to other enzymes of the same family with broad roles across immunity. Moreover, this project was aimed at characterizing, on a structural and mechanistic level, the observation that a protein from Influenza virus A directly inhibits the native function of TRIM25, in order to suppress an immunological response. The molecular details of TRIM25 inhibition upon influenza infection were presented in this study for the first time.

In 2016, Public Health England reported that moderate levels of influenza activity were observed in the UK, which nevertheless resulted in 209 documented deaths. The high pathogenicity caused by influenza A viruses has attracted much interest with the goal of developing drugs that specifically block the action of viral proteins and ultimately eliminate death risk and improve quality of life.

The results obtained during this project were presented in scientific conferences worldwide and published in scholarly open-access journals with the aim of a) raising awareness in the scientific community and b) forming a basis for further research in the field that will enhance our understanding of cell functions during healthy and diseased states.

Dedicated to Kalomoira, Nikos and Maria.

Acknowledgements

I would like to thank my academic supervisor Katrin Rittinger for trusting me with this PhD project, for providing me with all the resources ever required (and more) and for the freedom to pursue my ideas. Also, I thank you for supporting me in my applications and for believing in me all these years.

I wish to thank all the members of the Rittinger lab, past and present, for helping me throughout my time. My special thanks extends to Dr Diego Esposito for teaching me the secrets of powerful SAXS and for sharing my excitement about science. Dr Luigi Martino has been practically helping me in countless occasions, was always positive and encouraged me to pursue my "99% chance won't work" ideas -that is how one of the crystal structures was solved. I also thank Dr Abigail Davies, Ms Rebecca Stephens, Dr Henrik Johansson, Dr Isabella Tsai and Mr Marius Kausas for the fun in the lab (but mostly for all the baking).

Next, I wish to thank Dr Benjamin Stieglitz and Dr Aylin Morries-Davies for still sharing the same passion about ubiquitin thioesters since 2011 but mostly for being good friends. I would also like to show my gratitude to my friend Mr Evangelos Christodoulou for teaching me how do things in the right way. I wish to thank my second academic supervisor Dr Ian Taylor for teaching me how to do MALLS, how to express my frustration when things won't work and for being part of my thesis committee along with Dr Franca Fraternali and Prof Mike Blackman.

Importantly, this thesis would not have any structures without the precious help of Dr Philip Walker who screened more than 500 crystals for me; Dr Lesley Haire who inspired me to do crystallography; Dr Roksana Ogrodowicz who made magic potions for crystals; Dr Andrew Purkiss who is a crystallography guru; Dr Steve Smerdon who explained everything about symmetry operators. I also wish to thank Dr Laura Masino, Dr Stephen Martin and Dr Simone Kunzelmann of the Biophysics Lab for bearing with my "soluble aggregates". The same also extends to my friend and collaborator Dr Rodolfo Ciuffa (ETH Zurich) who has been trying to make sense out of my protein complexes using mass spectrometry.
Next, I would like to thank my efficient friend Dr Neil Ball for his encouragement during the last months of my PhD and for averting thesis-related IT disasters.

I also wish to thank all the people in the amazing Boehringer Ingelheim Fonds for the remarkable support and training they provided to me; getting the BIF PhD fellowship is definitely one of the highlights of my PhD. Additionally, I would like to thank the Medical Research Council and the Francis Crick Institute for funding my studies and my project.

I would also like to thank my parents, Nikolaos and Kalomoira for believing in me, for teaching me to be honest, patient and brave enough to go after my dreams. I would not have reached this stage in my studies without the emotional and practical support of my late grandmother Maria who I miss every day. I also want to thank my brother Giorgios for his support and for sharing the struggle of growing up. I am very grateful to my wife-to-be Christina for her constant encouragement and for believing in me even when I didn't. Lastly, I wish to thank Stephen and Rita for providing a home away from home.

Table of Contents

List of Figures

1. Introduction

3. Results

Structure and mechanism of TRIM25-RING activation

4. Results

Structure and mechanism of NS1-mediated TRIM25 inhibition

List of Tables

2. Materials and Methods

3. Results

Structure and mechanism of TRIM25-RING activation

4. Results

Structure and mechanism of NS1-mediated TRIM25 inhibition

Abbreviations

Å	Ångström
µL / µM	Micro-litre / micro-molar
AMP / ATP	Adenosine mono-phosphate / adenosine tri-phosphate
CARD	Caspase activation and recruitment domain
CC	Coiled-coil
CD	Circular dichroism
CTD	C-terminal domain
Da	Dalton
DNA	Deoxyribonucleic acid
DTT	Dithiothreitol
DUB	Deubiquitinating enzymes
E.coli	*Escherichia coli*
ED	Effector domain
EDTA	Ethylenediaminetetraacetic acid
EM	Electron microscopy
HECT	homologous to E6-AP carboxyl terminus
HEPES	4-(2-hydroxyethyl)-1-piperazineethanesulfonic acid
GST	Glutathione-S-transferase
HOIP	(Heme-oxidized IRP2 ligase 1)-interacting protein
IAV	Influenza virus A
IFN	Interferon
IEX	Ion-exchange chromatography
IκB	Inhibitor of κB
IKK	IκB kinase complex
IL	Interleukin
IPTG	Isopropyl β-D-1-thiogalactopyranoside
IRF	IFN regulatory factor
LB	Luria-Bertani broth
LR	Linker region
LIC	Ligation-independent cloning
LUBAC	Linear ubiquitin chain assembly complex
MALLS	Multi-angle laser light scattering
MAVS	Mitochondrial antiviral-signaling protein

MES	2-(N-morpholino)ethanesulfonic acid
mL / mM	Milli-litre / milli-molar
MR	Molecular replacement
MW	molecular weight
NEMO	NF-κB essential modulator
NF-κB	Nuclear Factor kappa-light-chain-enhancer of activated B cells
Ni-NTA	Nickel-nitrilotriacetic Acid
nM	Nano-molar
NMR	Nuclear magnetic resonance
NS1	Non-structural protein 1
OD	Optical density
o/n	overnight
PAMP	Pathogen-associated molecular patterns
PCR	Polymerase chain reaction
PDB	Protein data bank
PEG	Polyethylene glycol
pH	(the) power of hydrogen (-log10 of the hydrogen ion concentration)
pI	Isoelectric point
PML	Promyelocytic leukemia protein
RBCC	RING-Bbox-coiled coil domain
RBD	RNA-binding domain
RBR	RING-between-RING
RIG-I	Retinoic acid-inducible gene 1
RING	Really interesting new gene
RNA (ss/ds)	Ribonucleic acid (single-stranded/double-stranded)
SAXS	Small-angle X-ray scattering
SDS-PAGE	Sodium dodecyl sulfate polyacrylamide gel electrophoresis
SD	Standard deviation
SEC	Size-exclusion chromatography
Sf9 cells	Clonal isolate of *Spodoptera frugiperda* Sf21 cells
SUMO	Small ubiquitin-like modifier
TCEP	Tris(2-carboxyethyl)phosphine
TRIM	Tripartite motif
Tris	Tris (hydroxy methyl) aminomethane

Ub	Ubiquitin
UBA	Ubiquitin-associated
UBL	Ubiquitin-like
UBD	Ubiquitin-binding domain
UV	Ultraviolet

1. Introduction

Over the past two decades, the ubiquitin system has emerged as a crucial regulator of almost every cellular process. Ubiquitin is a highly conserved protein found in all eukaryotic cells. Upon appropriate upstream signaling events, it can be attached to target proteins or other ubiquitin molecules through a process called ubiquitination. This process is a highly regulated post-translational modification of proteins with broad regulatory roles across many aspects of cellular biology, including proteolysis, cell cycle progression, DNA damage repair, apoptosis and immune responses [1, 2]. Ubiquitination is mediated by an enzymatic cascade and is reversed by the action of de-ubiquitinating enzymes [1, 3]. Defects in this system are often associated with many diseases including cancer, neurodegenerative and autoimmune disorders [4].

1.1 Ubiquitin gene and protein structure

In humans, ubiquitin is encoded by four genes (UBB, UBC, UBA52 and RPS27A/UBA80) which produce different precursor forms. UBB (ubiquitin B) and UBC (ubiquitin C) genes encode three and nine fused head-to-tail ubiquitin repeats, respectively. UBA52 (ubiquitin A-52-residue ribosomal protein) and RPS27A (ribosomal protein S27A) each encode a single ubiquitin molecule fused to the ribosomal polypeptides L40 and S27, respectively [5-7]. All precursor forms are processed post-translationally by an ubiquitin C-terminal hydrolase to produce the monomeric functional form [8]. Not surprisingly, ubiquitin is one of the most abundant proteins in eukaryotic cells with measured levels in different cell types ranging between 17-85 μM (100-500 pmol/mg protein) [9-11]. Ubiquitin is a small (76 amino acid) highly stable globular protein that adopts a compact β-grasp fold with a flexible C-terminal tail composed of six residues (Figure 1.1A) [12, 13]. The β-grasp fold is composed of five strands forming a β-sheet which “grasps” a 3.5-turn α-helix. A large hydrophobic patch located on the solvent exposed region of the β-sheet and the inter-connecting flexible loops is formed by L8, I44 and V70 (Figure 1.1B) [14, 15]. This I44 patch has a key role in interactions of ubiquitin with proteins containing ubiquitin-binding domains (UBDs) and proteasomal receptors [16, 17]. A second hydrophobic patch is formed by I36 and L71/L73 which are located on the C-terminal tail (Figure 1.1B). The I36 patch is involved in interactions between different ubiquitin molecules but also with enzymes involved in ubiquitination [1, 18].

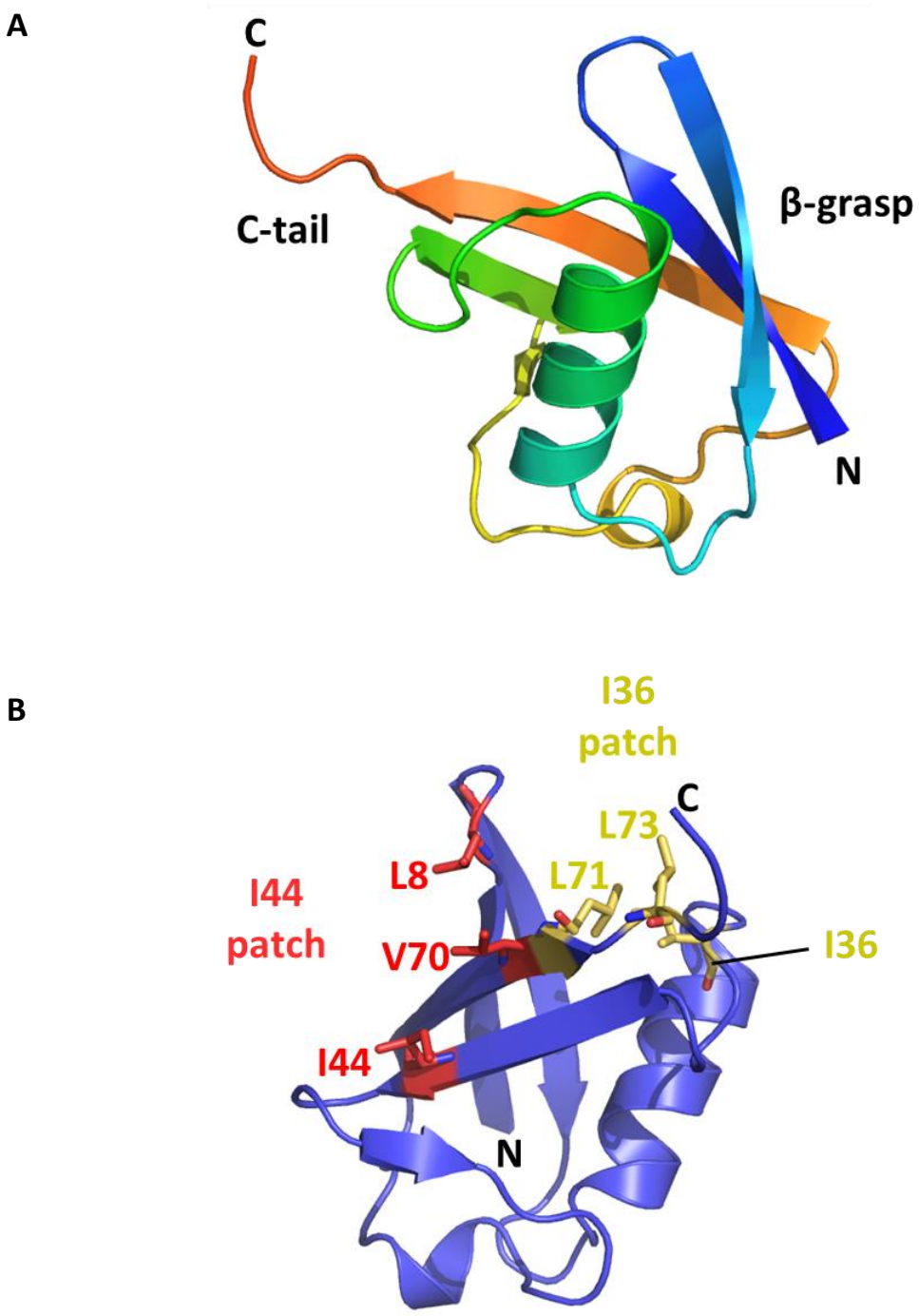

Figure 1.1: The structure of ubiquitin.

A) Ubiquitin adopts a compact β-grasp fold formed of a β-sheet composed of five β-strands and an α-helix with a flexible C-terminal tail. B) The hydrophobic patches formed around a.a. I36 (yellow) and I44 (red) of ubiquitin are indicated. These patches are important for interaction of ubiquitin with other proteins. Figures were generated in Pymol using 1UBQ.pdb [12].

1.2 Ubiquitin-like proteins

Eukaryotic cells have also evolved a cohort of structurally related proteins which are commonly referred to as ubiquitin-like proteins (UBL). These include SUMO (small ubiquitin-like modifier), NEDD8 (neural precursor cell-expressed, developmentally down-regulated 8), ISG15 (interferon-stimulated gene 15), ATG8 (autophagy 8) and FAT10 (HLA-F-adjacent transcript 10). Similar to ubiquitination, conjugation of UBLs is performed by dedicated machineries [19, 20]. The emerging roles of these proteins implicate them in numerous diverse cellular processes ranging from signal transduction and antiviral pathways to proteolysis and cell-cycle control. More recently, there have been numerous reports of a functional interplay between UBLs and ubiquitin to maintain cellular homeostasis and physiology [21, 22]. Despite the high significance of these proteins, the work presented in this study focuses on ubiquitin and therefore UBLs will not be discussed in any further detail.

1.3 Ubiquitin modifications are highly versatile

Ubiquitin modifications are highly dynamic and versatile and the physiological response generated depends mainly on the type of ubiquitin linkage formed between adjacent ubiquitin molecules. In the simplest form, a single ubiquitin molecule is attached to a lysine (Lys or K) residue of the substrate protein, a process known as mono-ubiquitination. This process controls numerous cellular responses, including receptor transport, DNA repair, viral budding but also proteasomal degradation [1, 23]. Moreover, multiple K residues on a substrate protein can be tagged with single ubiquitin molecules, a process referred to as multiple mono-ubiquitination. This type of modification is important for targeting activated receptor tyrosine kinases (RTKs) to the lysosome for degradation [24]. Apart from being attached directly to a lysine residue of the substrate protein, ubiquitin may also form poly-ubiquitin chains which are attached to substrates. Ubiquitin itself has seven lysine residues (K6, K11, K27, K29, K33, K48 and K63) all of which can be conjugated to another ubiquitin to form homotypic polymeric chains (Figure 1.2) [1]. In this reaction, the carboxyl group of G76 forms an isopeptide bond with the ε-amino group of a K residue. In addition, the C-terminus of one ubiquitin molecule can be linked to the α-amino group of methionine 1 of another ubiquitin to form linear (M1-linked) ubiquitin chains (Figure 1.2) [25]. Ubiquitin chains can be homotypic, i.e. when the same K is modified throughout

the chain (such as K6-, K48- and K63-linked) or mixed if different linkages are observed between ubiquitin molecules on the same chain. Complexity increases when a single ubiquitin is modified with multiple moieties which may then form homogeneous/heterogeneous chains (branched chains) [23].

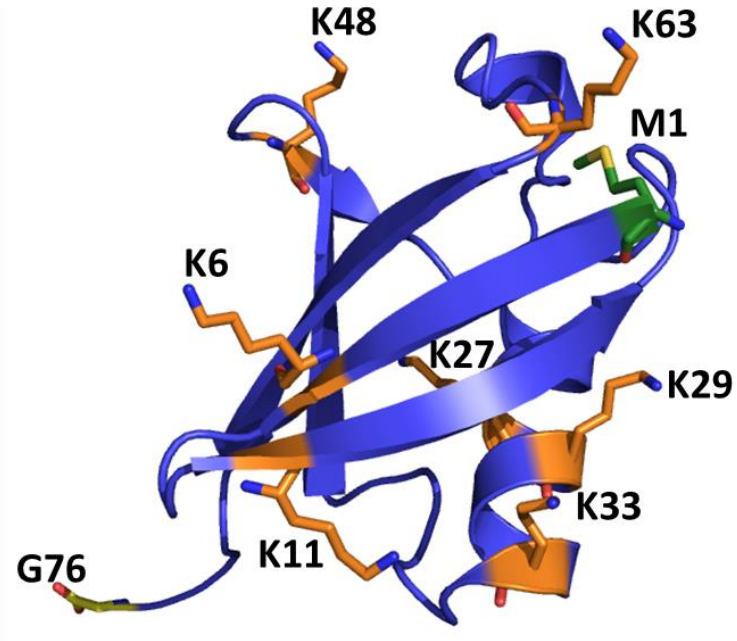

Figure 1.2: Ubiquitin residues mediating chain formation.

The side-chains of all residues involved in poly-ubiquitin chain formation are shown. Lysine residues are indicated in orange colour and the N-terminal methionine (M1) in green. An isopeptide bond is formed between K residues and the C-terminal G76 (yellow) of another ubiquitin, whereas a peptide bond is formed between ubiquitin molecules linked through M1/G76 linkage. Figure was generated in Pymol using 1UBQ.pdb [12].

1.4 Structure and function of ubiquitin chains

K48- and K63-linked chains, often referred to as canonical or conventional chains are best studied [23, 26]. However, recent studies have uncovered many interesting aspects of the other six types, the “atypical chains”. Structural analysis of different types of homotypic ubiquitin chains revealed how different linkages result in distinct chain conformations [1]. All of these linkages have been detected in cells and it has been shown that poly-ubiquitin chains bearing different linkages are recognised by different ubiquitin-binding receptors leading to propagation of distinct structural and functional information [27-29]. With the exception of K27-linked chains, crystal structures of all other types of linkages between two ubiquitin molecules have been reported (Figure 1.3) [30-36]. Chains linked by K48 adopt a compact conformation mediated through the I44 patch. A minimum of four K48-linked ubiquitin molecules have been known to target the substrate to the proteasome for degradation, a discovery that was awarded the Nobel Prize in Chemistry in 2004 [37]. Similar to K48-linked chains, ubiquitin linkages formed through K6 also adopt compact conformations but are mediating the removal of damaged mitochondria from cells and DNA damage repair [38, 39]. Chains linked via K11 are formed through the I36 patch, allowing the I44 patch to interact with other binding partners. K11-linked chains are indispensable in cell cycle progression and can also drive proteasome degradation of substrates [40].

In contrast to the K48-, K6- and K11-linkages, M1-, K63- and the less-studied K29- and K33-linked polymers display extended conformations: the two ubiquitin molecules resemble a dynamic configuration reminiscent of “beads on a string” (Figure 1.3). M1- and K63-linkages are now also well characterised, revealing pivotal roles in immune signalling and specifically in the activation of the NF-κB pathway [41]. K29 and K33 linkages have been linked to proteasomal degradation and protein trafficking through the trans-Golgi network, respectively, but still require further investigation [42]. K27 is not surface-exposed and therefore chains formed through this residue require local structural changes in the fold of ubiquitin [43, 44]. These chains have been implicated in regulating DNA repair and very recently in immunity [45, 46].

An additional level of complexity is added to the ubiquitination system by the recent observations that ubiquitin itself can be post-translationally modified [27, 29, 47, 48]. The physiological context for these modifications, which were mostly identified through proteomic analysis, remains relatively unknown with the

exception of the discovery that ubiquitin and poly-ubiquitin chains can be phosphorylated by PTEN induced putative kinase 1 (PINK1) at S65 [47, 49]. This phosphorylation event has been reported so far only in cells with mitochondrial damage as a potent signalling event for downstream activation of mitophagy [50, 51].

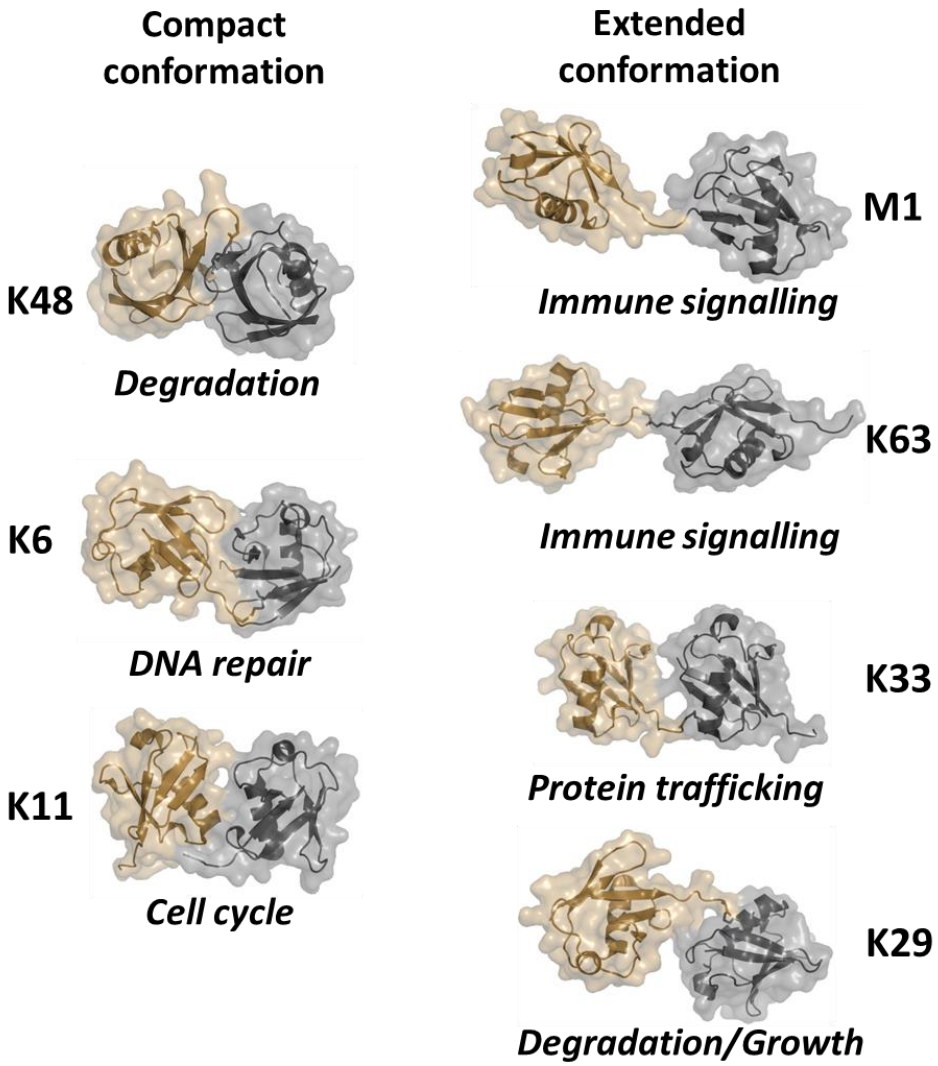

Figure 1.3: Ubiquitin chains.

Crystal structures are available for all different types of ubiquitin linkages with the exception of K27. The proximal Ub molecule is shown in gold and the distal in grey colour. Ubiquitin chains linked through K48 (1AAR.pdb) [36], K6 (2XK5.pdb) [35] and K11 (2XEW.pdb) [32] adopt a compact conformation where the two molecules pack against each other. Chains linked through M1 (2W9N.pdb) [30], K63 (3H7P.pdb) [30], K33 (4Y1H.pdb) [34] and K29 (4S22.pdb) [33] form an extended conformation with minimal interaction between linked ubiquitin molecules. Figure was generated in Pymol.

1.5 The ubiquitination cascade is a three-step process

The reversible process of ubiquitination is performed by an enzymatic cascade consisting of three enzymes: ubiquitin activating enzymes (E1), ubiquitin conjugating enzymes (E2) and ubiquitin ligases (E3). In humans there are genes encoding two E1 enzymes, 40 E2 enzymes and more than 600 E3 ligases which act in a sequential order to modify 1000s of substrates [52]. Although these gene numbers suggest a pyramidal organization, the ratio of expressed ubiquitin-specific E1:E2:E3 proteins in HeLa cells is estimated around 1:3:2 [53]. The organization of this multi-step system allows for a general pool of readily available ubiquitin-loaded enzymes to be directed specifically towards the desired physiological responses. Tight regulation at multiple levels ensures fine-tuning of the proteome in response to a changing environment.

The first step towards ubiquitination of a substrate is ubiquitin activation by an E1 enzyme (Figure 1.4). The C-terminal carboxyl group of ubiquitin is attached in an ATP-dependent reaction to the catalytic cysteine residue in the E1 enzyme through a covalent thioester bond [54]. Subsequently, structural re-arrangements on the E1 increase the affinity for E2 enzymes and facilitate ubiquitin transfer onto the active site cysteine of an E2 enzyme via a transthiolation reaction. E1 is subsequently released (Figure 1.4) [55]. Finally, E2 forms a complex with an E3 ligase and the substrate. Ubiquitin is then transferred through different mechanisms onto the lysine side-chain of the substrate protein or ubiquitin itself via the E3 (Figure 1.4) [56]. In the following sections, the main characteristics and properties of the E1, E2 and E3 ubiquitin enzymes will be discussed.

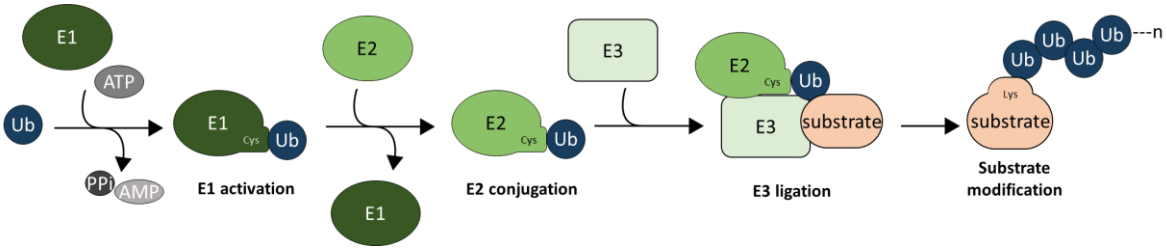

Figure 1.4: The ubiquitination cascade.

Ubiquitin is activated by E1 in an ATP-dependent manner. A thioester bond is formed between the C-terminus of Ub and the catalytic C of the E1. Ub is subsequently transferred onto the catalytic C of an E2 enzyme. An E3 enzyme can then mediate substrate ubiquitination.

1.5.1 Ubiquitin-activating enzyme E1

E1 enzymes are responsible for initiating ubiquitin conjugation. In humans, there are two E1 ubiquitin activating enzymes: Ube1 and Uba6. Recent data suggest non-redundant biological roles for the two E1 enzymes, highlighted by a preference towards distinctive substrates (E2 enzymes) leading to diverse signals across cellular regulatory networks [57].

Presently, structural information is only available for the *Schizosaccharomyces pombe* E1 (Uba1) which is highly homologous to human E1 (Ube1). The structure of the E1 was solved both in isolation and bound to cognate E2s, ubiquitin and ATP-Mg [58-62]. These structures reveal the precise mechanism of ubiquitin activation which involves structural rearrangements on the E1. E1 is a multi-domain protein composed of an adenylation domain involved in ubiquitin and ATP binding, a catalytic domain that encompasses the Ub thioester-forming cysteine and a C-terminal ubiquitin-fold domain (UFD) which participates in E2 enzyme recruitment (Figure 1.5) [54]. Initially, E1 binds ATP-Mg and Ub via the I44 patch leading to adenylation of the C-terminal glycine of Ub (Ub~AMP, where "~" indicates a thioester bond) [58]. Then, E1 undergoes conformational changes which allow nucleophilic attack of Ub~AMP by the sulphydryl group of the catalytic cysteine resulting in the formation of an E1~Ub thioester bond [62, 63]. The adenylation domain is then able to bind a second ATP-Mg and Ub to perform another round of adenylation [61]. Binding of the second Ub triggers displacement of the UFD which is then able to recruit an E2 enzyme (Figure 1.5) [58, 60]. Upon E2 binding, another structural rearrangement takes place which brings the E1~Ub

thioester close to the catalytic cysteine of the E2 [59, 60]. The precise mechanism by which the E1~Ub to E2 transthiolation reaction occurs is not fully characterised, although basic residues located on the N-terminal region of the E2 have been shown to be important for the transfer [58, 59]. It is also noteworthy that the large E1 structural changes occurring during Ub activation may be the underlying mechanism by which a single E1 can function with numerous E2 enzymes.

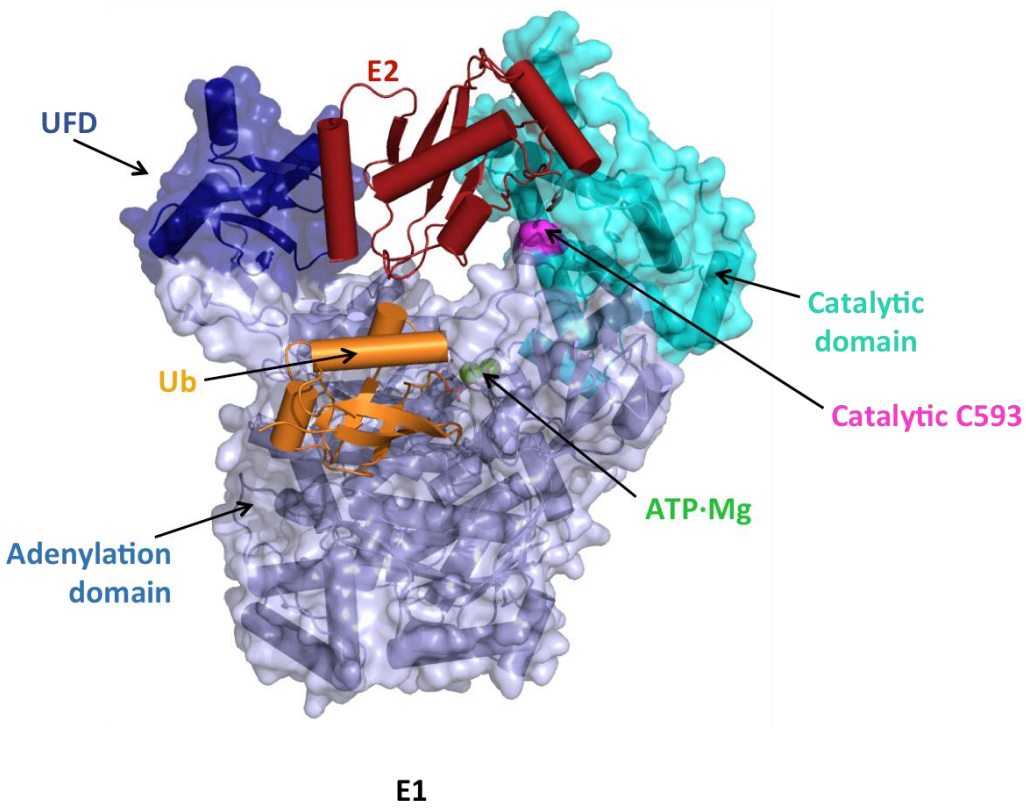

Figure 1.5: Structure of an E1/E2/Ub complex.

E1 (shown as surface representation and coloured by domain) binds to Ub (ribbon in orange), ATP-Mg (spheres in green) through the adenylation domain (light blue) and catalyses adenylation of the C-terminal G76 of Ub (Ub~AMP). Conformational changes lead to positioning of the Ub~AMP next to the active site cysteine of the E1 (magenta) in the catalytic domain (cyan) which results in thioester formation (E1~Ub). The E1 UFD domain recruits an E2 enzyme (ribbon in red) and thioester-bound Ub is then passed onto the active site cysteine. Figure was generated in Pymol using 4II2.pdb [60].

1.5.2 Ubiquitin-conjugating enzyme E2

E2 enzymes are the middle components in the ubiquitination cascade. They interact with an E1 enzyme and are able to recognize multiple E3 enzymes. Previous work by many groups has revealed that E2s may participate in substrate selection along with type and topology of modification [55, 64, 65]. All E2s contain a highly conserved ubiquitin-conjugating domain (UBC) formed by 150 amino acids and includes the catalytic cysteine that takes over the Ub thioester from the E1 to form E2~Ub ("~" indicates a thioester bond) [66]. E2 enzymes are divided in four classes, based on the presence of additional regions around the core UBC domain: class I consists of E2s that contain just the core UBC and no extensions; class II E2s contain N-terminal extensions whereas class III C-terminal extensions; class IV E2 enzymes contain additional regions at both ends [66]. In some cases these regions are intrinsically disordered but can adopt secondary structure upon interaction with other proteins [66]. The presence of these extensions affects the functionality of E2s and accommodates specific interactions with E1 and E3 enzymes [66]. To date, structural information is available for over 32 human E2 enzymes. The UBC domain is structurally conserved and adopts an α/β-fold formed by four α-helices and a four stranded β-sheet (Figure 1.6A) [67]. As discussed previously in section 1.5.1, the exposed UFD domain of E1 mediates interactions with the E2 [60]. On the E2, the interacting surface involves the N-terminal α-helix (α1) and the loop region (L1) connecting the first two β-strands of the UBC β-sheet (β1- β2) (Figure 1.6A) [68]. The same E2 region however is also involved in E3 binding indicating that E2 binding to E1 and E3 is mutually exclusive [68, 69]. This observation suggests a directionality of the ubiquitination cascade which probably allows for a more robust response as E2 enzymes occupy either an E1 in order to take over ubiquitin or an E3 to modify a substrate while E1 can recharge other E2s.

The E3 interaction site and the catalytic cysteine are located on flexible loop regions, thereby enabling the E2 to perform different reactions and function with multiple E3s (Figure 1.6A). Depending on the partnering E3 (will be discussed below in more detail), E2 enzymes are engaging in either aminolysis (transfer from the E2~Ub to an amino group (mostly Lys) on a substrate) or transthiolation (transfer to a catalytic cysteine on the E3 enzyme) [66]. In some cases, the activity of E2 enzymes is modulated through non-covalent interactions with either ubiquitin, E3s or other proteins. In most cases this E2 interface is referred to as

the “backside” surface of the UBC fold and is located at the opposite site of the catalytic pocket (Figure 1.6A) [66, 70]. In the absence of an E3, the reactivity of the E2~Ub remains low ensuring that non-productive hydrolysis of the Ub-thioester bond is prevented [66]. A more detailed account of the E2-E3 interactions and mechanism of ubiquitin transfer is given below.

In two special cases, ubiquitin E2 variant (UEV) proteins possess a UBC fold but lack the catalytic cysteine [71]. These E2s interact with catalytically active partners and enforce poly-ubiquitin chain linkage specificity [71, 72]. The only example described to date is the Ubc13/ Ube2V1 or Ube2V2 pair: Ubc13 forms a thioester with a donor ubiquitin (Ub_{donor}) via its catalytic cysteine; Ube2V2 binds to Ubc13~Ub_{donor} adduct and recruits an additional molecule of ubiquitin ($Ub_{acceptor}$) through non-covalent interactions (Figure 1.6B) [72]. Ube2V2 places $Ub_{acceptor}$ K63 in close proximity to Ubc13~Ub_{donor} enforcing chain formation of K63 linkage (Figure 1.6B) [72]. Both UEV isoforms (Ube2V1 and Ube2V2) mediate K63 chain formation in complex with Ubc13 in the same way but they differ in the cellular context that are activated: Ubc13-Ube2V1 is involved in NF-κB activation whereas Ubc13-Ube2V2 is required for DNA damage [73].

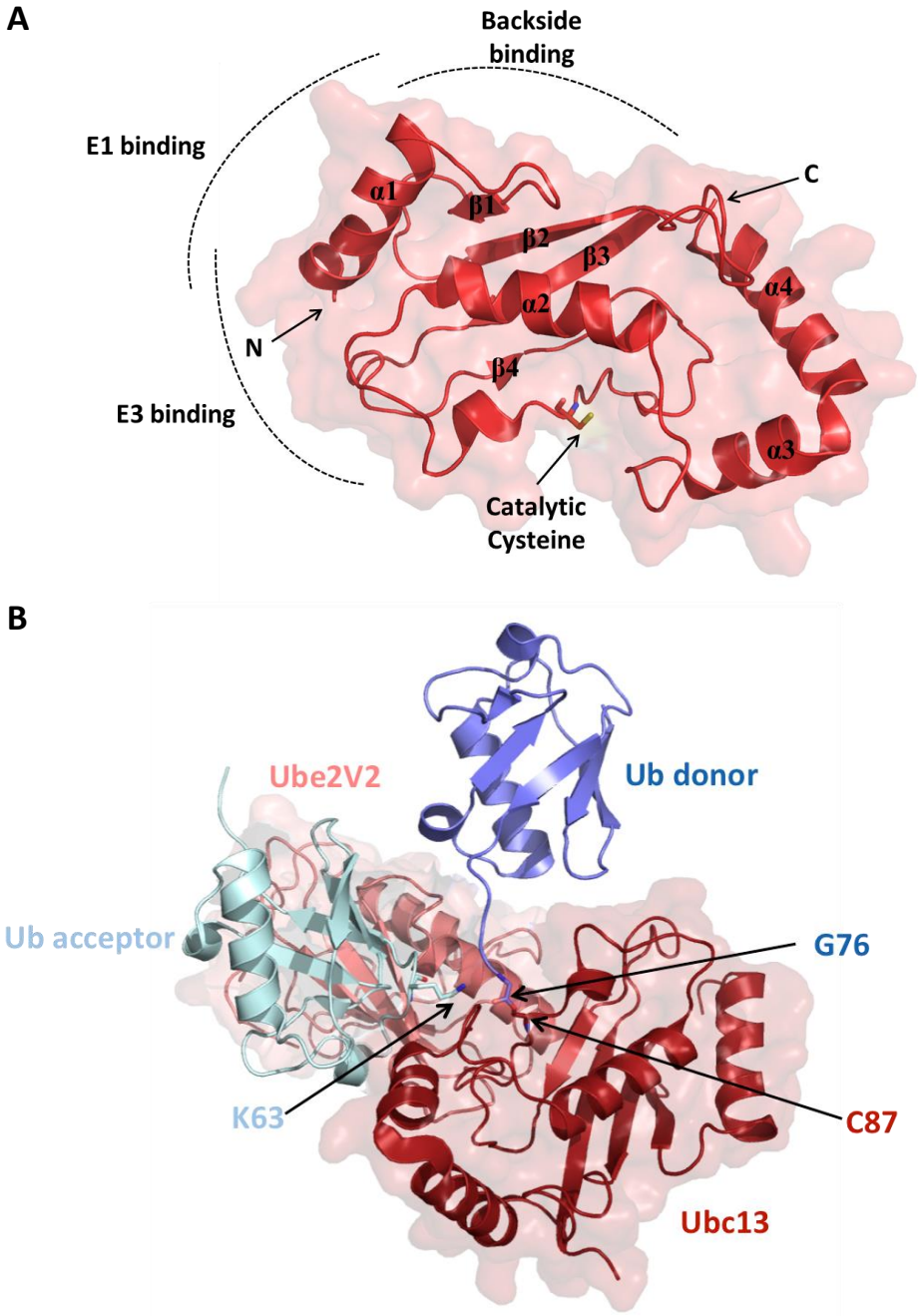

Figure 1.6: Structural characteristics of E2 enzymes.

A) E2 enzymes adopt a UBC fold formed of four α-helices and a four-stranded β-sheet as shown here for UbcH5c (2FUH.pdb) [70]. The E1- and E3-interacting surfaces of an E2 partially overlap. Some E2 enzymes bind Ub or other proteins through a "backside" interface located at the opposite site to the active site cysteine. B) The only heterodimeric E2 described to date is Ubc13(red)/Ube2V2(pink) (2GMI.pdb) [72]. Ubc13 forms a thioester with Ub (Ub donor, shown in blue) and Ube2V2 recruits another Ub (Ub acceptor, shown in light-blue). Ube2V2 positions Ub acceptor in a way that K63 points directly to the Ubc13~Ub donor thioester. Figures were prepared in Pymol.

1.5.3 E3 ubiquitin ligases

E3 ligases are the most diverse and critical components of this cascade and provide both efficiency and specificity to the ubiquitination machinery: they are mainly responsible for substrate selection and in some cases enforce the type of poly-ubiquitin chain linkage formed. The eukaryotic cell has evolved a small number of catalytic domains, which are incorporated usually in multi-domain proteins, or multi-protein complexes which contain a wide variety of substrate-recruiting modules and regulatory elements. These properties allow E3 ligases to operate in different cellular contexts and process diverse protein substrates in response to a multitude of cellular signals. There are three families of E3 ubiquitin ligases which operate with catalytically distinct ligation mechanisms (Figure 1.7). These include: the RING (really interesting new gene) or U-box E3s that function as scaffolds to bring the ubiquitin-loaded E2 and the substrate into close proximity [74]; the HECT (homologous to E6-AP carboxyl terminus) E3 ligases, which form a thioester intermediate with the ubiquitin, before transferring it to the substrate and the RING/HECT hybrids which combine the properties of RING and HECT ligases and are represented by the RBR (RING between RING) family of E3s (Figure 1.7) [56]. The vast majority of E3s belong to the RING/U-box subfamily (more than 600), with HECT and RBR ligases contributing 28 and 14 members to the E3 pool, respectively. The work presented in this study focuses on TRIM25, a RING E3 ubiquitin ligase. The following section will primarily focus on the general properties of RING E3 ligases including structure and mechanism, while the key characteristics of HECT and RBR E3s will be discussed in sections 1.5.3.2 and 1.5.3.3 below.

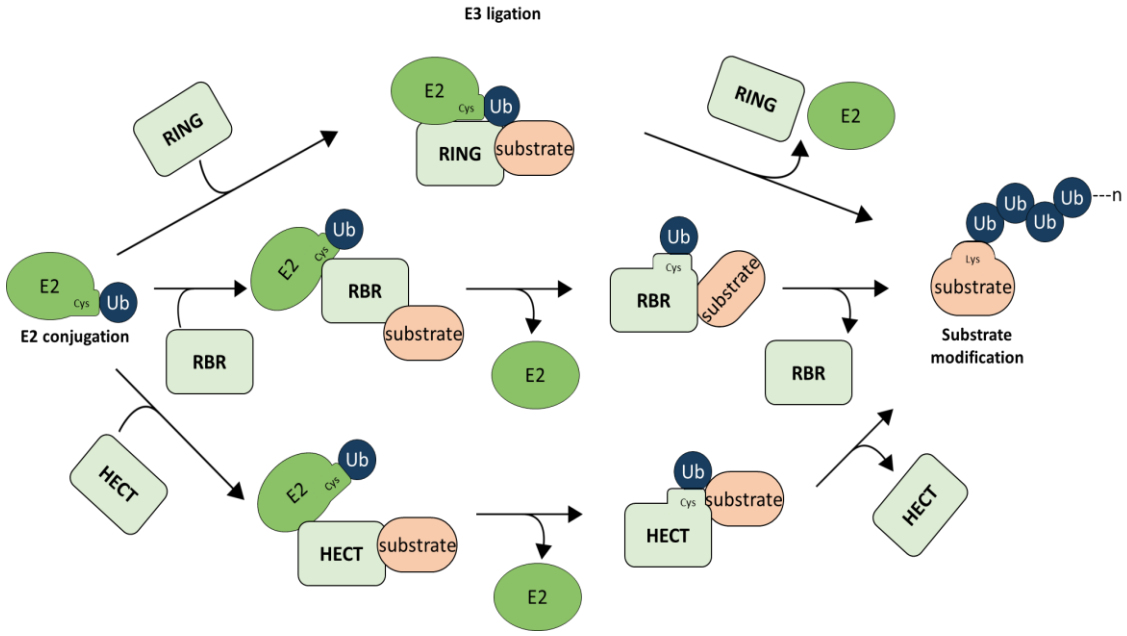

Figure 1.7: E3 ligases have distinct mechanisms of substrate ubiquitination.
RING E3 ligases bind the E2~Ub and the substrate and act as scaffolds, bringing the E2~Ub and the substrate in close proximity. Ubiquitin transfer takes place directly from the E2 onto a substrate. HECT and RBR E3 ligases form an E3~Ub bond through an active site cysteine and subsequently transfer it on a substrate.

1.5.3.1 RING E3s

1.5.3.1.1 RING sequence and structure

The RING (really interesting new gene) domain is a small domain formed by ~40-60 amino acids. RING domains are characterized by the presence of a signature sequence: C-X_2-C-X_{9-39}-C-X_{1-3}-H-X_{2-3}-C-X_2-C-X_{4-48}-C-X_2-C (where X can be any amino acid) (Figure 1.8A) [74]. Three-dimensional structures of RING domains revealed that the RING is a compact, globular domain composed of a central α-helix, two or more β-strands and two variable-length loop regions ($L1_R$ and $L2_R$) incorporating C/H residues which are buried within the hydrophobic core of the domain; this arrangement is stabilised through the coordination of two zinc ions in a cross-brace topology (Figure 1.8B) [75]. Sequence variations among RING domains include swapping of C/H residues or replacement of those with an aspartate which can also participate in zinc coordination [76]. Despite sequence variations, the fold is highly conserved among all RING domains but also U-box domains. The U-box domains however do not bind zinc atoms and the overall fold is maintained through a structural network of polar interactions [77, 78].

Many RING domains are reported to form homo- or hetero-dimers. Dimerization is mediated either by interactions through the β-sheets of the core RING element or requires further regions outside the core zinc-binding domain. For example, Rad18 (RNF73), a RING E3 ligase that mono-ubiquitinates PCNA (proliferating cell nuclear antigen) during DNA damage repair, forms a homodimer through α-helices adjacent to the core RING domains (Figure 1.8C) [79]. This four-helical bundle is formed through nonpolar interactions that involve hydrophobic residues which point their side-chains towards the core of the bundle. Such an arrangement is also observed in some heterodimeric RING E3s. For example, BRCA1 (breast cancer susceptibility gene 1) dimerizes with BARD1 (BRCA RING domain 1) through the formation of a four-helical bundle [80]. Even though BARD1 is inactive in isolation, upon heterodimerization with BRCA1 the E3 ligase activity of the complex is increased compared to BRCA1 on its own [81]. In other cases, heterodimerization occurs through a combination of interactions. Such a case is the Mdm2/MdmX (murine double minute 2/X homolog) complex, where Mdm2 -an active RING- dimerizes with an inactive counterpart (MdmX) to regulate the levels of tumor suppressor protein p53 by ubiquitination [82]. The Mdm2/MdmX complex is formed through interactions by the β-sheets of the core RINGs and the N-/C-terminal flanking residues (Figure 1.8D). The N-terminal

residues from each monomer form short α-helices which pack against each other at the base of the core RING (Figure 1.8D). The C-terminal residues form a short β-strand that is inserted in the β-sheets of the core RING, leading to the formation of a β-barrel-like fold shared between the two monomers (Figure 1.8D). In all cases described so far, dimerization is thought to enhance E3 ligase activity as disruption of this by mutagenesis abolishes E3 ligase activity [83].

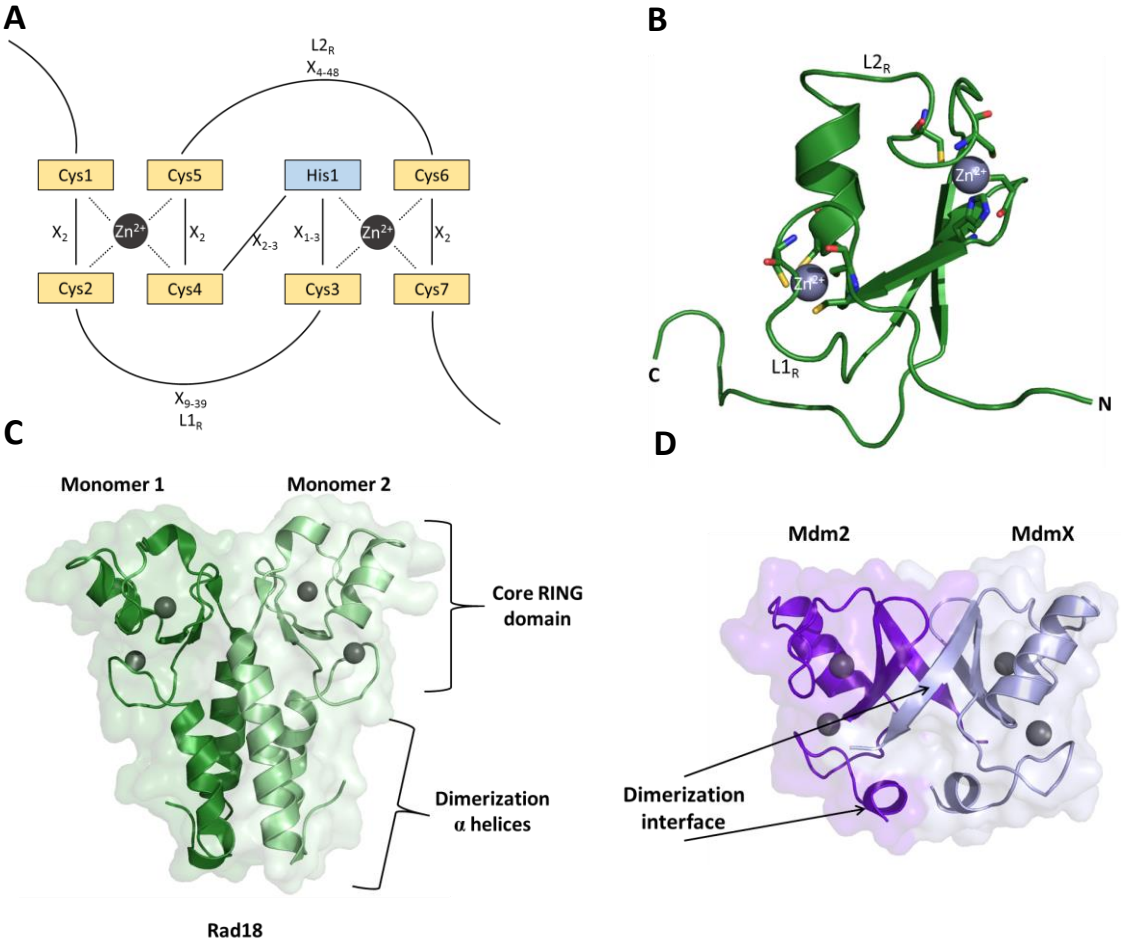

Figure 1.8: Structural features of RING E3 ligases.

A) Schematic representation of a typical consensus sequence of a RING domain. C/H residues bind Zn^{2+} atoms. X_n denotes the number of any amino acid residues located between two consecutive Zn^{2+}-binding residues. B) The first 3D structure of a RING domain (ICP0 protein from Human Herpesvirus 1) is shown in ribbon representation with the Zn^{2+} atoms as grey spheres and the side-chains of coordinating residues as "sticks" (1CHC.pdb) [75]. C) Dimerization of Rad18 RING domains is mediated through α-helices flanking the core Zn^{2+}-binding domain (2Y43.pdb) [79]. D) Dimerization of the Mdm2/MdmX RING complex (2VJE.pdb) is mediated through interactions by the β-sheets of the core RINGs and the N-/C-terminal flanking residues which form two short α-helices that pack against each other [82]. Figures were prepared in Pymol.

1.5.3.1.2 RING interactions with E2

Many structures of E2/E3 pairs have revealed that the α-helix and the two loop regions ($L1_R$ and $L2_R$) surrounding the zinc coordination sites of the RING domain and the α-helix $H1_{E2}$ and loop regions $L1_{E2}$, $L4_{E2}$ and $L7_{E2}$ of the E2 are required for E2/RING E3 interactions [66, 74, 78]. For example, in the structure of a complex of cIAP (cellular inhibitor of apoptosis) with Ube2D2 (UbcH5b), a $L1_R$ hydrophobic residue (V559), which is located in-between the first two zinc-coordinating C residues packs against two proline residues: P61 in $L4_{E2}$ and P95 in $L7_{E2}$ (Figure 1.9) [84]. This interface is further stabilized by polar interactions between the V559 backbone and the side-chain of R5 located on $H1_{E2}$. In addition, residues located on $L2_R$ (mainly P589 and R592) mediate interactions with S94 and Q92 which further stabilize the RING/E2 interface (Figure 1.9). Disruption of this key network abolishes the interaction between RING/E2 [84]. These interactions are observed in all RING/E2 structures described to date [74, 78]. Additional contacts between the E2 and regions outside the core RING/U-box element are observed in some cases and are thought to enhance specificity in RING/E2 binding [78, 85].

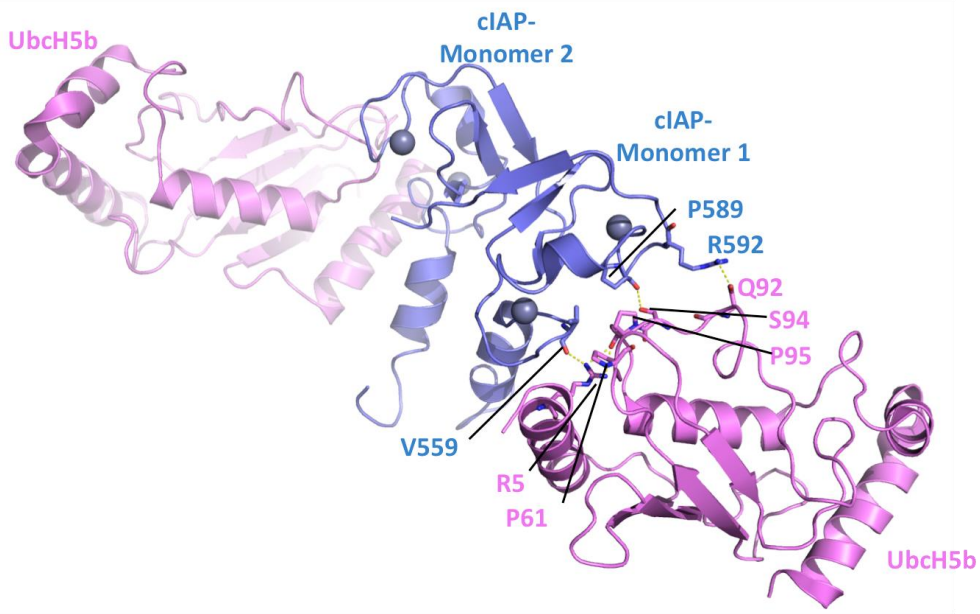

Figure 1.9: A RING E3/E2 structure.

The cIAP/UbcH5b complex structure (3EB6.pdb) shows that a dimeric cIAP RING domain (monomer 1 and 2 shown in blue) binds to two UbcH5b E2 enzymes (magenta) [84]. RING dimerization is mediated through interactions by the β-sheets of the core RINGs and the N-/C-terminal flanking residues. Each monomer contacts a single E2. RING/E2 interactions are mediated through residues which are located on the core Zn^{2+}-binding domain of the cIAP RING and the α1-helix and linker regions of UbcH5b. Figure was prepared in Pymol.

1.5.3.1.3 RING activation of the E2~Ub

RING E3 ligases activate the E2~Ub intermediate for subsequent nucleophilic attack by a substrate-derived lysine residue. In all three-dimensional structures of E2/RING E3 complexes described to date, the RING-E2 interface is distant to the catalytic cysteine of the E2, implying that multiple allosteric events and/or conformational changes are required for activation of the E2~Ub thioester [83, 86]. It was early evident however, that the E2 does not undergo conformational changes upon E3 binding to account for the increase in the E2~Ub reactivity [78, 86]. Additionally, many studies have shown that in some cases the weak interaction between a RING E3 and E2 is enhanced when the E2 is loaded with ubiquitin [74, 78, 87]. The underlying mechanism should therefore lie with ubiquitin recognition by the RING E3 ligase leading to activation of the E2~Ub conjugate. The UbcH5 (Ube2D) family of E2s is among the best characterized, both structurally and biochemically [70, 88]. The next section is primarily focused on the RING-mediated ubiquitin transfer from UbcH5~Ub; commonalities and differences shared by other E2/RING E3 pairs will be also briefly mentioned. In the absence of a RING E3 ligase, the UbcH5~Ub conjugate is shown to adopt a dynamic behavior and occupies multiple conformations [88]. These states are commonly referred to as open or extended conformations. Due to the labile nature of the thioester formed between the E2 and Ub, structural studies were only possible when a more stable thioester-mimic bond was generated. One approach was by mutation of the active-site cysteine to a serine (C85S). In this way, an oxyester-linked UbcH5-O~Ub was produced bearing similar properties with the thioester but exhibiting higher stability towards hydrolysis [88]-[89, 90]. For further stability, a second mutation was introduced on UbcH5 (N77A); this residue is essential for efficient ubiquitin transfer on the target substrate and mutation to an alanine reduces the reactivity of the UbcH5~Ub bond [89]. Another approach was to mutate the catalytic cysteine of the E2 to a lysine (C85K), which allows the formation of a non-hydrolysable isopeptide bond between the C-terminus of ubiquitin and the ε-amino group of the introduced lysine [91]. Both approaches generated a stable bond that mimics a thioester between UbcH5 and Ub (denoted as UbcH5-Ub with a “-“) and allowed crystallization of ternary complexes formed by RING E3s and UbcH5-Ub [89, 91]. A series of highly significant studies published in the last five years have shed light on the mechanism of E2~Ub activation by different RING E3s [89-96].

Activation of E2~Ub by dimeric RING E3

The first crystal structure of a RING E3/E2-Ub complex reported was that of RING finger (RNF)-containing protein 4 (RNF4) in complex with ubiquitin-loaded UbcH5a (Ube2D1)-Ub through an isopeptide bond (denoted as "-") [91]. RNF4 is a dimeric RING E3 ligase that interacts with and ubiquitinates protein substrates which are pre-modified with SUMO, marking them for degradation [87, 97]. To obtain this structure, it was necessary to fuse two RING domains in a linear manner, presumably to further stabilize RING dimerization and allow crystallization [91]. The structure shows an RNF4 dimer, with each RNF4 RING bound to a single UbcH5a-Ub conjugate (Figure 1.10A). The E2 binds to a single proximal RING via the canonical interface previously described in section 1.5.3.1.2 whereas there are no E2 contacts with the distal RING protomer (Figure 1.10A). The ubiquitin moiety from each E2-Ub conjugate is folded back away from the catalytic residue (mutated C85K) and towards the central helix of the E2 ($H2_{E2}$) in an orientation referred to as "closed" (Figure 1.10B). This interface is formed through an extensive network of interactions that includes the I44 hydrophobic patch of ubiquitin and L104, S105 and S108 of $H2_{E2}$ (Figure 1.10B). The UbcH5a-Ub closed state allows interactions of ubiquitin with both the proximal and distal RNF4 protomers explaining earlier studies reporting that RING dimerization is required for activity (Figure 1.10B) [78]. Residues located on $L2_{Ub}$, the I36 patch and the C-terminal tail of Ub contact the proximal RING whereas the top of the ubiquitin α-helix packs against an aromatic residue located on the distal RING monomer (Y193) (Figure 1.10A,B). An arginine located on the surface of the proximal RNF4 RING (R181), referred to as molecular "linchpin", contacts both the E2 and ubiquitin (Figure 1.10B) [90]. RNF4 residues which participate in the Ub interface appear to be primarily conserved in many dimeric RING E3s and mutation in any of those abolishes enzymatic activity [56, 87]. The same conclusions as described above were also reached independently in other structural studies, suggesting that a conserved mechanism applies for activation of E2~Ub by RING E3s [89, 90]. These data collectively establish that dimeric RING E3s activate the E2~Ub thioester by stabilizing a closed conformation of the E2~Ub, which is mediated through interactions of ubiquitin with both RING domains of a dimer. At this orientation, E2~Ub is primed for catalysis and transfer of ubiquitin to a lysine residue.

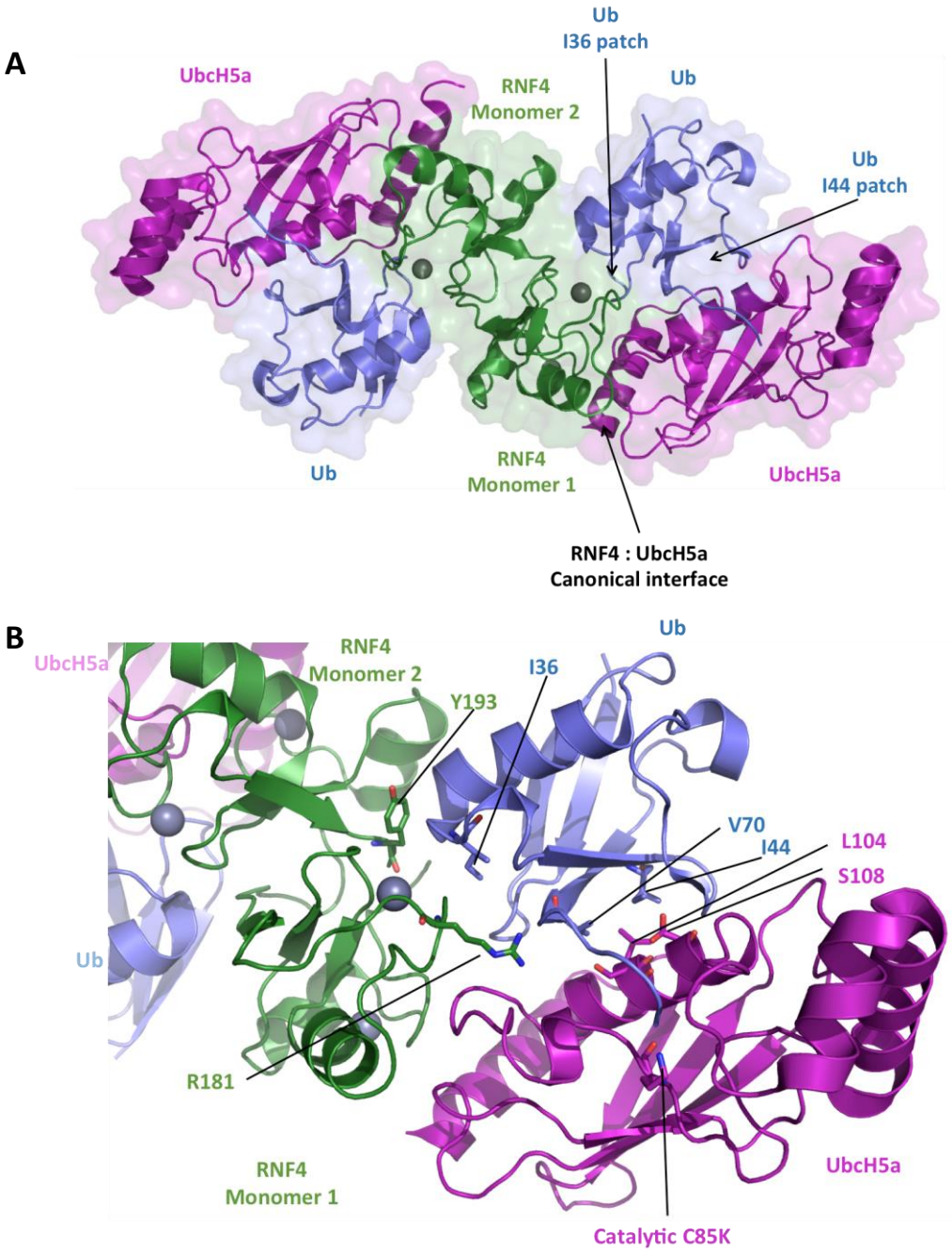

Figure 1.10: Structural details of dimeric RING-mediated E2~Ub activation.

A) The structure of a dimeric RING E3 ligase (RNF4, in green) bound to UbcH5a (magenta) charged with ubiquitin (blue) shows that each RING binds to a E2~Ub intermediate. Ubiquitin packs against the E2 through the I44 hydrophobic patch and the proximal RING domain through the I36 patch. B) A close-up of the RING/E2-Ub interface shown in A. The "linchpin" residue (R181) of the proximal RING domain contacts both E2 and Ub and an aromatic residue (Y193) from the distal RING domain are necessary for priming the E2~Ub intermediate. This structure shows that a dimeric RING domain binds to two E2~Ub conjugates and causes Ub to bind back towards the E2 and away from the E2 catalytic cysteine. This conformation is referred to as the "closed" conformation of an E2~Ub intermediate and is shown to be key for transfer of ubiquitin on a substrate. Figures were prepared in Pymol using 4AP4.pdb [91].

Activation of E2~Ub by monomeric RING E3

In dimeric RING E3 ligases, the RING domain of one subunit and tail of the second cooperate to prime Ub for transfer from E2~Ub to the substrate. The crystal structure of a monomeric RING E3 ligase CBL-B (Casitas B-lineage lymphoma proto-oncogene b) in complex with ubiquitin-loaded UbcH5b (UbcH5b-Ub) and a substrate fragment revealed that a different mechanism of Ub transfer is employed by monomeric RING E3 ligases [92]. Members of the CBL family of E3 ligases act by ubiquitinating and marking for degradation non-receptor and receptor tyrosine kinases, thereby attenuating downstream signaling [98]. Previous studies have established that phosphorylation of a highly conserved tyrosine (Y363) is a prerequisite for E3 ligase activity [99]. The crystal structure, obtained with the active/phosphorylated form of CBL-B (denoted as pCBL-B) shows that Ub is folded back towards the E2 via ubiquitin's I44 patch and adopts a closed conformation, an arrangement seen also in dimeric RING E3/E2-Ub structures (Figure 1.11). Similarly, the CBL-B RING/Ub interface is mediated through the I36 hydrophobic patch of ubiquitin (Figure 1.11). Intriguingly, pY363 is at the centre of these interactions. The phosphate moiety forms hydrogen bonding with $T9_{Ub}$ and a salt bridge with $K11_{Ub}$ (Figure 1.11). Phosphate absence or mutation of Y363 abolishes the catalytic ability of CBL-B [92, 100]. These observations indicate that a mechanism of E2~Ub activation by monomeric RING E3 ligases requires a non-RING structural element (the pY363 in the case of CBL-B), which functionally replaces the role of the aromatic residue observed in all the other dimeric RING E3/E2-Ub structures [87, 89, 91]. The structure of this complex reveals an additional level of regulation that is required for catalysis by a monomeric RING E3 and highlights the interplay between different post-translational modifications. Despite the structural differences observed between monomeric and dimeric RING E3s, both E3 ligase families achieve the same activation mechanism by inducing the closed conformation of the E2~Ub intermediate in which the ubiquitin is primed for transfer to a substrate lysine [56]. The structural elements that enhance the E3 ligase catalytic ability of other monomeric RING E3s remain to be uncovered. Importantly, these studies first established the mechanism of E2~Ub activation by RING E3s: in the absence of an E3, the Ub of the E2~Ub conjugate is in a conformational equilibrium which is shifted towards the open conformations; in the presence of a RING E3 the Ub

folds back onto the E2 and occupies mostly the closed conformation, an orientation favorable for thioester hydrolysis (Figure 1.12) [87, 89-92].

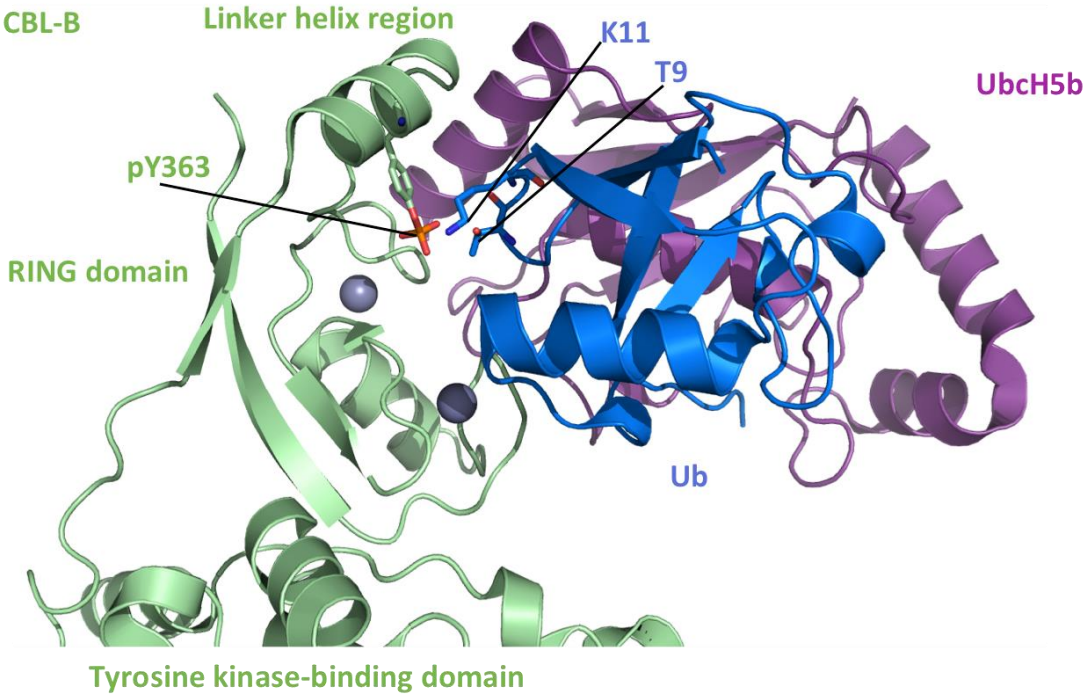

Figure 1.11: Structural details of monomeric RING-mediated E2~Ub activation.
The structure of a monomeric RING E3 ligase (CBL-B, in green) bound to UbcH5b (purple) charged with ubiquitin (blue) reveals a key role for an element outside the core RING domain. A phosphorylated tyrosine (pY363) is required for stabilizing the closed state of the E2~Ub thioester intermediate. Figure was prepared in Pymol using 3ZNI.pdb [92].

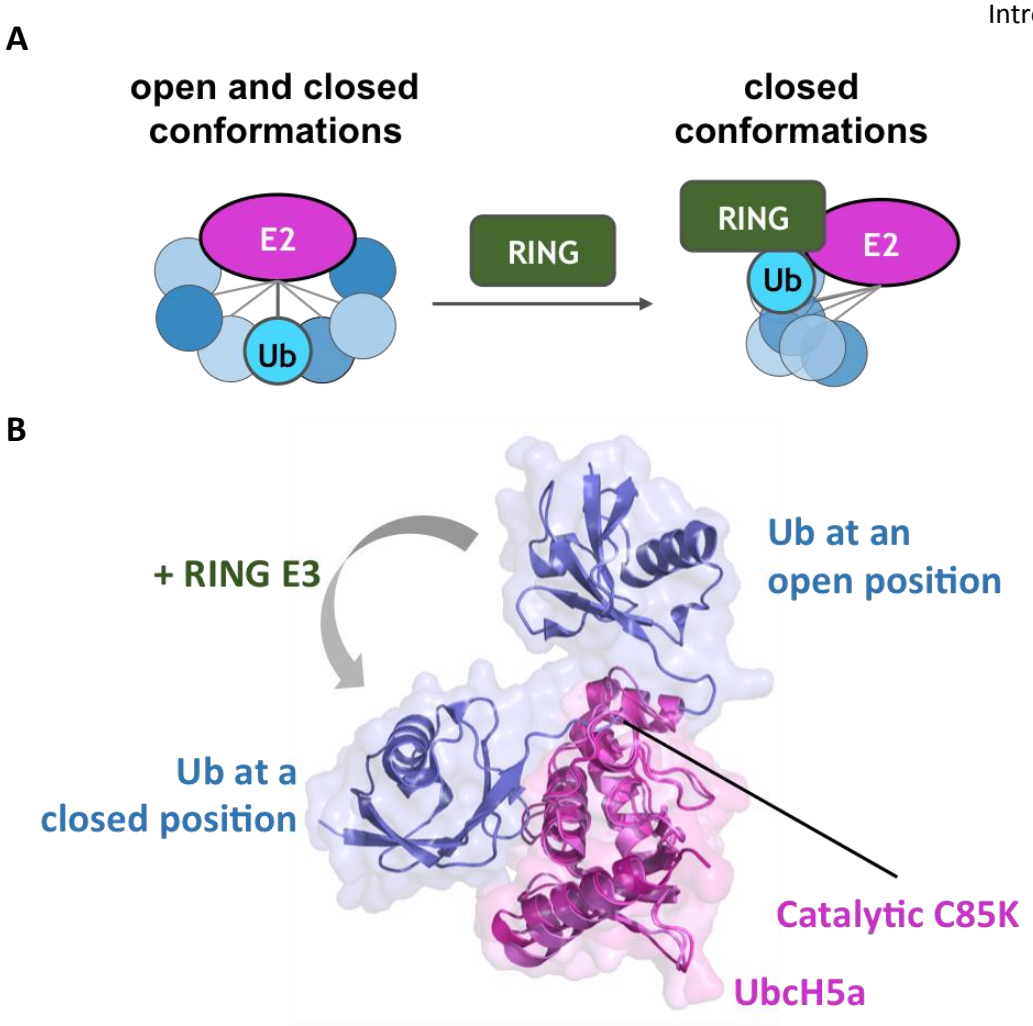

Figure 1.12: Structural changes on the E2~Ub by RING E3 ligases.

A) Schematic model of E2~Ub activation by RING E3s. In the absence of a RING E3, the Ub on a charged E2 occupies numerous positions around the E2 (open states). In the presence of a RING E3, the closed conformation of E2~Ub is stabilized through RING/Ub interactions. B) Alignment of UbcH5a~Ub structures solved in the absence (5ULF.pdb) and presence of a RING E3 (4AP4.pdb) reveal the large conformational change of Ub that takes place upon interaction with a RING E3 ligase [91]. Figure shown in B was prepared in Pymol.

Additional features enhancing the RING E3 efficiency

In all structures described so far in the literature, the key feature for activation of ubiquitin transfer employed by RING E3 ligases is the restraining of the E2~Ub in its closed conformation [56]. However, additional strategies which improve the catalytic efficiency of Ub transfer have also been recently described for some E2/RING E3 pairs. For example, the UbcH5 family of E2s can bind an additional ubiquitin molecule. This ubiquitin interacts non-covalently through the I44 patch with the beta strands β1-3 of UbcH5 (Figure 1.13A) [70, 101]. This interface is located away from the catalytic cysteine and across the thioesterified Ub, an event referred to as backside binding (see also section 1.5.2) (Figure 1.13A). The backside binding of Ub on UbcH5 increases the affinity towards RING E3 ligases and enhances the catalytic transfer of the donor ubiquitin to a substrate [70, 101]. Similarly, apart from the canonical E2/E3 interface, RING E3 ligases such as gp78, Cue1 and Rad18 harbor additional motifs which specifically bind to the backside of their cognate E2s (Ube2g2, Ubc7p and Rad6, respectively) [102-104]. The additional E2-binding of these E3s allosterically stimulates efficient Ub transfer and in the case of Rad6/Rad18 complex directs specificity towards mono-ubiquitination [104]. In a different mechanism, an additional Ub molecule binds directly to the monomeric RING E3 of Arkadia (RNF111) or the homologous Ark2C (RNF165) (Figure 1.13B) [105]. This interaction enhances ubiquitin transfer from the E2~Ub to a substrate and possibly reveals a mechanism by which Arkadia RING ligase facilitates poly-ubiquitin chain elongation on mono-ubiquitinated substrates [105].

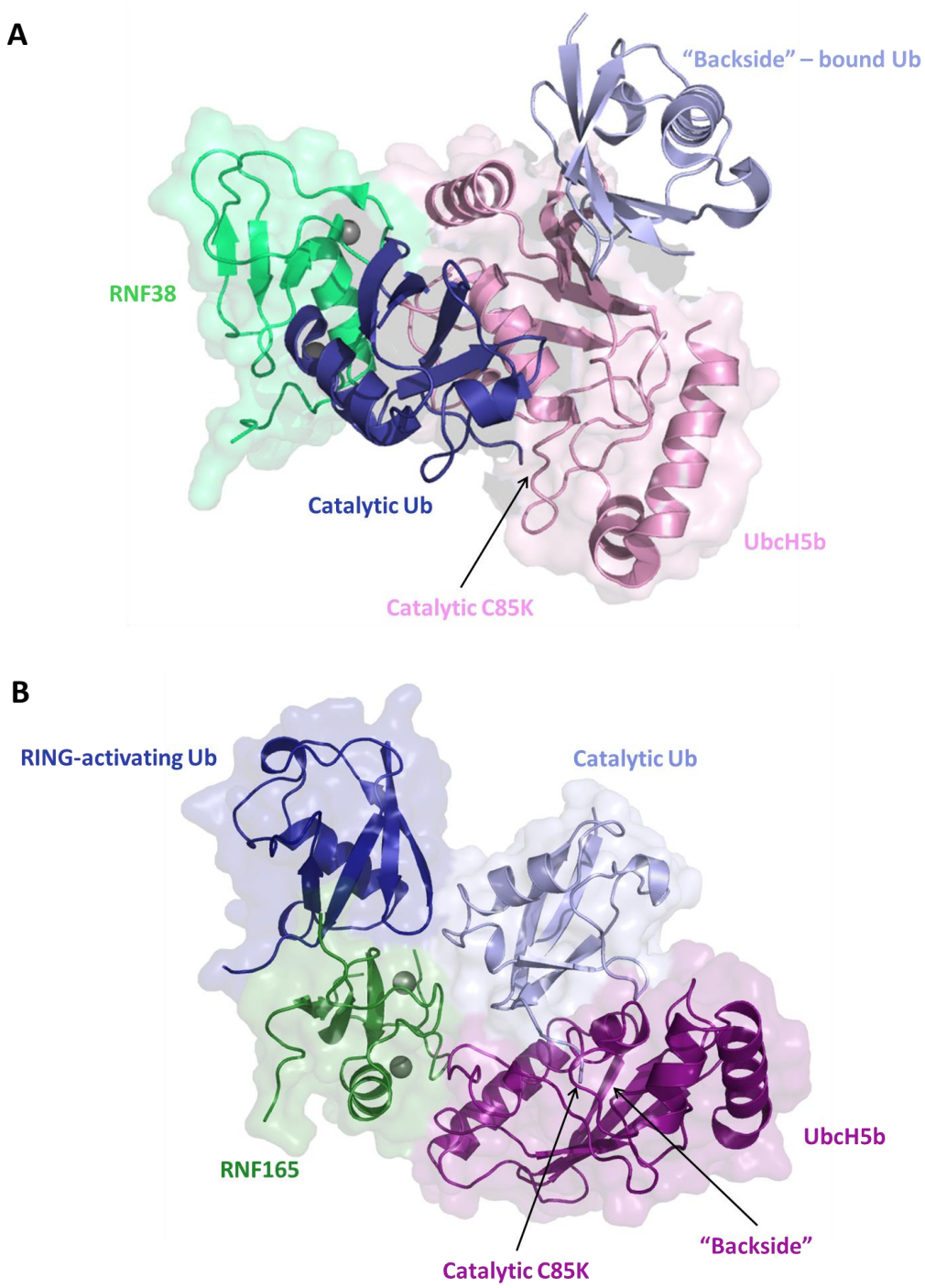

Figure 1.13: Non-covalent ubiquitin binding enhances RING processivity.

A) The structure of RNF38 RING domain (green) bound to UbcH5b (pink) charged with ubiquitin ("catalytic" Ub shown in dark blue) revealed that non-covalent binding of another Ub molecule (light blue) can occur on the E2. This binding takes place at the opposite site of the E2 catalytic site (referred to as the "backside" E2 surface). B) Non-covalent binding of Ub can occur directly on the RING domain, as seen in the case of RNF165/UbcH5b-Ub/Ub complex. A RING-activating Ub molecule (dark blue) binds to the RING domain and further stabilizes the canonical RING/E2~Ub interaction and priming of the E2~ub thioester. Figures A and B were prepared in Pymol using 4V3L.pdb [101] and 5D0K/5D0M.pdb [105], respectively.

1.5.3.1.4 Chain elongation by RING E3

Efficient Ub transfer from an E2~Ub intermediate to a substrate relies on the RING-mediated thioester activation. A substrate may be ubiquitinated at multiple lysine residues located in close proximity to the activated E2~Ub intermediate or at a single favourable lysine. In the case of a polyubiquitin chain formed on a single substrate lysine by RING E3s, this can be achieved by sequential addition of ubiquitin molecules to an extending chain built on the E2 and then transferred on a substrate (*en bloc*) or built directly on the substrate [106, 107]. Even though the type of the polyubiquitin chain linkage formed is a property of the E2 enzyme, E2/RING E3 enzymes cooperate to ensure that the substrate is sufficiently ubiquitinated before dissociating from the E3 [66]. In some cases a single E2 can mediate the formation of a Ub chain whereas in other cases different E2s are employed for chain initiation and elongation, respectively. For example, APC/C (anaphase promoter complex/cyclosome), a multi-subunit complex containing APC11 RING ligase cooperates with two E2 enzymes to specifically ubiquitinate substrates involved in cell cycle regulation with K11-linked polyubiquitin chains [108, 109]. Firstly APC11 interacts via the canonical RING E2/E3 interface with UBE2C (UbcH10) E2 and mono-ubiquitinates the substrate (a step referred to as initiation). Then, UBE2S E2 is recruited to generate a K11-linked poly-ubiquitin chain (elongation) [110] [111]. It is noteworthy that APC/C binds to mono-ubiquitinated substrates with higher affinity utilizing a “feed-forward” mechanism referred to as processive affinity amplification [111, 112]. During this process, a mono-ubiquitinated substrate preferentially binds to APC/C and can be further mono-ubiquitinated at a different lysine if UBE2C is bound or be subjected to K11-linked chain elongation through UBE2S E2 [111]. In this way, APC/C can engage in specific ubiquitination of multiple substrates which otherwise bind with weak affinity [111]. As described above, the processive affinity amplification mechanism might be a general property of RING E3 ligases as Arkadia RING facilitates a binding site for ubiquitin or ubiquitinated substrates for optimal activation of the E2~Ub intermediate [105].

1.5.3.1.5 Substrate recognition by RING E3

A substrate for ubiquitination is recruited to an E3 ligase by domains other than the catalytic RING. This is achieved in two ways: the RING domain is either part of a multi-domain polypeptide containing one or more substrate-binding domains

or participates in the formation of a multi-domain complex in which the substrate is recruited by a different protein of the same complex. In the first case, the RING domain generally modifies unique or structurally similar substrates [56]. Tripartite motif (TRIM) proteins belong to the first category where the RING and a substrate recruitment domain are located on the same polypeptide and will be discussed in detail in section 1.7. A representative example of multi-component RING-containing E3s is the family of Cullin-RING ligases (CRL) which target protein substrates for proteasomal degradation [113-115]. The CRL assemble into a functional complex composed of a Cullin scaffold protein, an adaptor protein, a receptor which recognizes a substrate and a small RING-containing protein [56, 115]. The eukaryotic cell has evolved seven Cullin proteins, many interchangeable adaptors and substrate receptors but only two RING-box proteins (Rbx1 and Rbx2) participating in the formation of more than 200 CRLs [113, 115]. In this way, many different combinations of CRL can be formed which allow the crucial specificity of this E3 towards its very diverse protein clientele using only a limited number of RING E3 proteins [115]. In certain cases, homo- or hetero-oligomerization of RING E3 ligases and post-translational modification of substrates have also been reported as crucial mechanisms for efficient substrate recruitment [56].

1.5.3.2 HECT E3s

HECT (homologous to E6-AP carboxyl terminus)-type E3 ligases are mechanistically distinct from RING E3 and form a thioester intermediate bond with Ub (E3~Ub) before transferring it to a substrate [1, 56, 116]. Located at the C-terminus of E3 ligases, the HECT domain is ~350 residues long and comprises two lobes separated by a flexible hinge linker: the N-terminal lobe which binds the E2~Ub and the C-terminal lobe which contains the active site cysteine [1, 56, 116]. Similarly to an E1/E2 pair, the ubiquitin is transferred from the catalytic cysteine of the E2 to that of the HECT-E3 via a transthiolation reaction in contrast to E2~Ub aminolysis performed by RING E3s [1, 116]. A series of structural and biochemical studies over the last few years revealed the mechanism of ubiquitin ligation by HECT E3 ligases [56]. For example, the crystal structure of the HECT domain of NEDD4L in complex with UbcH5b-Ub shows the position of the E2 binding site at the N-lobe and how the C-lobe is located close to the E2~Ub thioester to allow transfer of Ub to the catalytic cysteine of the HECT (Figure 1.14)

[18]. This structure established that the first step towards substrate ubiquitination is the binding of an E2~Ub intermediate to the N-lobe which triggers conformational changes on both the E2~Ub species and the E3 itself (Figure 1.14) [18]. In contrast to RING E3s which enforce a closed conformation of the E2~Ub conjugate, a key difference for HECT E3 ligases is that the N-lobe of HECT E3s promotes an open conformation in which the ubiquitin extends away from the E2 bringing it close to the E3 active site (Figure 1.14). These observations suggest that HECT E3s suppress the lysine reactivity of E2~Ub conjugates (including UbcH5b~Ub) by allowing an open conformation of Ub and hence favoring transthiolation rather than aminolysis [18, 56, 117, 118]. In the second step, ubiquitin transfer from the E2 to the active site cysteine of the E3 induces repositioning of the C-lobe closer to the substrate which is rightly placed with the help of the N-lobe (Figure 1.14) [118, 119]. These conformational changes in the HECT domain allow the activated E3~Ub thioester to be placed with the correct orientation next to a substrate lysine which mediates the nucleophilic attack [118]. Contrary to RING E3s which rely on their cognate E2s for ubiquitin chain linkage determination, HECT E3s are able to enforce a specific type of ubiquitin chain regardless of the E2 used. For example, E6AP (E6-associated protein) generates exclusively K48-linked polyubiquitin chains with UbcH7, a HECT-cognate E2 with no inherent chain linkage specificity [120]. The precise structural determinants of chain linkage specificity provided by HECT E3s remain unclear. An additional non-covalent binding site for ubiquitin located at the N-lobe of certain HECT E3s is shown to play a key role in chain elongation [56]. Mutational analysis has shown that disruption of this HECT/Ub interface abolished the ability of the HECT E3 to form multimeric Ub chains but did not affect the type of chain linkage. This observation likely suggests that the processivity of the HECT enzyme is enhanced by holding an internal ubiquitin in a growing ubiquitin chain [56].

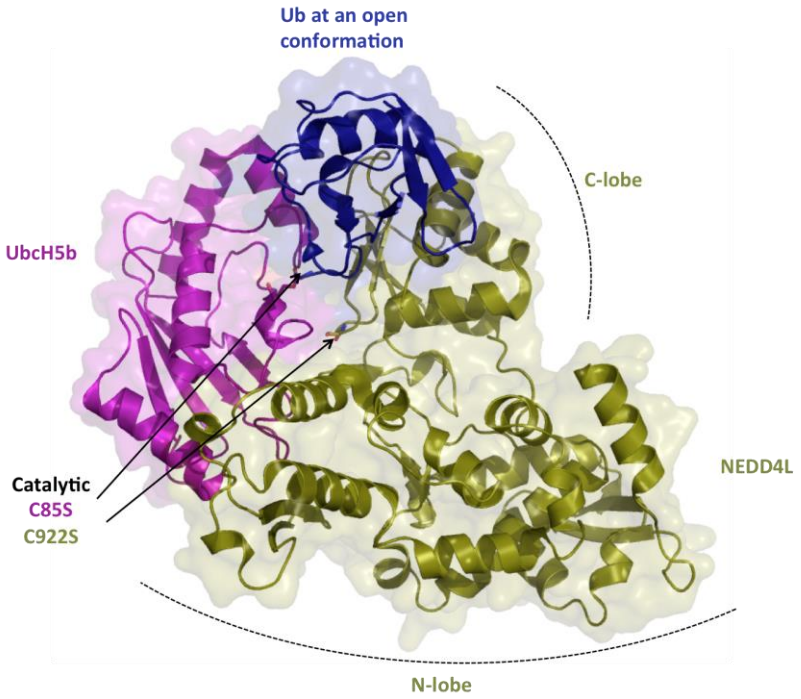

Figure 1.14: Structure of an active HECT E3/E2~Ub complex.

The structure of NEDD4L (olive green) HECT E3 bound to UbcH5b (magenta) charged with Ub (blue) shows the conformation of the complex during Ub transfer from the E2 to the E3. The HECT N-lobe binds the E2~Ub and, contrary to RING E3s, causes an open conformation of the E2~Ub which favours transfer of the thioester on the catalytic cysteine of the HECT E3 located at the C-lobe. Figure was prepared in Pymol using 3JW0.pdb [118].

1.5.3.3 RBR E3s

All 14 members of the RBR (RING between RING) family of E3s are characterized by the presence of a ~25 kDa RBR domain comprising two RING domains (RING1 and RING2) separated by a central in-between-RING (IBR) domain which also coordinates two Zn^{2+} atoms. Structural and biochemical analysis of several RBR E3s has now shown that RBR E3s mechanistically act as RING/HECT hybrids: RING1 resembles a canonical RING domain and recognizes the E2~Ub whereas the RING2 domain adopts an IBR fold and encompasses a catalytic C residue which similarly to HECT E3s forms a thioester bond with Ub [56]. A recent crystal structure of the HOIP (HOIL-1L interacting protein)-RBR domain bound to a stable UbcH5-Ub conjugate provided mechanistic insights into the E2~ubiquitin transfer employed by RBR E3s [121]. The HOIP-RBR is the catalytic centre of the large protein complex LUBAC (linear ubiquitin chain assembly complex) [25, 122, 123]. LUBAC is the only E3 ligase described to date to form M1-linked (also referred to as linear) ubiquitin chains [25, 124].

Despite the fact that the HOIP-RBR/UbcH5-Ub complex crystallized as a dimer, further biochemical analysis showed that in solution HOIP-RBR functions as a monomer and the dimer seen in the crystal structure is possibly due to crystal packing [121]. This structure shows that UbcH5~Ub binds to RING1 of HOIP-RBR and E2~Ub adopts an open conformation reminiscent of the one observed with HECT E3s (Figure 1.15A). The open conformation suppresses the lysine reactivity of UbcH5 and favors the transfer of Ub to the catalytic cysteine of the E3 [88, 117, 125]. The HOIP-RING2 domain is located across the RING1, a conformation that allows the RBR to wrap around the donor Ub (Figure 1.15A). At this orientation, the E2~Ub thioester bond is in close proximity to the active-site cysteine located on RING2 (Figure 1.15A). Similarly to HECT E3s, RBR ligases appear to rely on the open E2~Ub conformation and undergo structural rearrangements that allow transfer of the donor Ub to their active site [117, 125, 126]. In addition to the core RBR domain, different RBRs harbor additional domains with regulatory roles, located at the N- or C-terminus of the core RBR region. The role of such domains was highlighted in the two available crystal structures of full-length RBR-containing proteins: PARKIN and HHARI (human homologue of Ariadne). In both cases, the RING2 catalytic cysteine is shielded by a non-RBR element imposing an auto-inhibited state [127, 128]. Additional biochemical studies have shown that post-translational modifications are required to release the auto-inhibited state upon relevant upstream signaling and allow formation of E3~Ub. For example, activation of PARKIN requires phosphorylation of both PARKIN E3 and ubiquitin at S65 and activation of HHARI requires binding to a Cullin RING ligase which is pre-modified with NEDD8 [49, 128-133]. Similarly to HECT E3s, RBR ligases also enforce ubiquitin chain linkage specificity [125, 134]. The crystal structure of the RING2 domain plus an α-helical C-terminal extension of HOIP (LDD or Linear ubiquitin chain Determining Domain) revealed how this RBR specifically catalyzes the formation of linear chains (Figure 1.15B) [134]. An acceptor ubiquitin molecule is oriented with the help of the C-terminal extension in a way that the $M1_{acceptor}$ is pointing directly to the $G76_{donor}$ and the catalytic RBR cysteine (Figure 1.15B). The presence of this α-helical C-terminal extension is restricted only to HOIP explaining why this is the only E3 described to date to form M1-linked chains [134]. The mechanistic details by which other RBR E3 ligases dictate the linkage specificity remain to be seen.

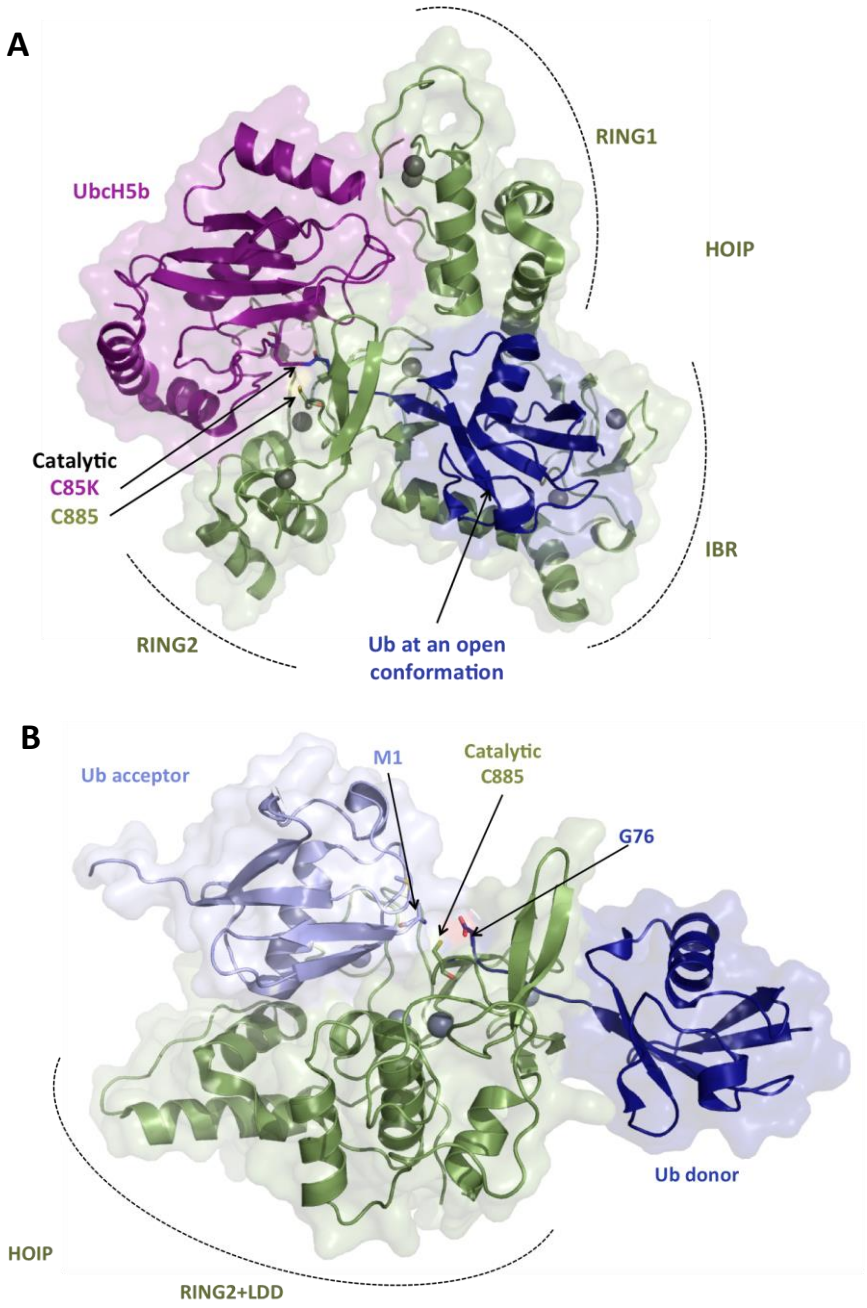

Figure 1.15: Active complexes of an RBR E3 ligase.

A) The structure of HOIP-RBR domain (green) bound to UbcH5 (magenta) charged with Ub (blue) shows that the RING1 of RBR binds the E2~Ub and, similarly to HECT E3s, induces an open conformation of the E2~Ub which favours transfer of the thioester on the catalytic cysteine of the RBR E3 located at the RING2. Additional contacts between the IBR region and Ub are required for efficient E2/E3 transthiolation. The RBR/E2~Ub crystallized with "swapped" domains which according to the authors was due to crystal packing [121]. Here, the functional monomeric RBR/E2~Ub complex is shown for clarity. B) HOIP-RING2 includes a helical region (LDD) (RING2-LDD shown in green) that recognizes an acceptor Ub (light blue). M1 of acceptor Ub is positioned next to the HOIP~Ub donor (in dark blue) thioester bond allowing formation of M1-linked polyubiquitin chains. Figures were prepared in Pymol using 5EDV.pdb and 4LJQ.pdb, respectively [121, 134].

1.6 Deubiquitinating enzymes (DUB)

E3 ligases are responsible for the remarkably diverse ubiquitin modifications of the proteome in every eukaryotic cell. Reversibility of these modifications is achieved by an equally diverse portfolio of deubiquitinating enzymes (DUBs) which are responsible for the cleavage of ubiquitin molecules from substrates and disassembly of ubiquitin chains. There are ~100 DUBs in the human genome divided into six distinct families, according to their structure [1, 3, 135]. These include five subfamilies of cysteine proteases: the ubiquitin-specific proteases (USPs with 54 members in humans), the ovarian tumour proteases (OTUs with 16 members), the motif interacting with ubiquitin (MIU)-containing proteases (MINDYs with 4 members), the ubiquitin C-terminal hydrolases (UCHs with 4 members) and the Josephin family proteases (with 4 members) [3]. The sixth family is composed of the Zn^{2+}-dependent JAB1/MPN/MOV34 (JAMM) proteases represented by 16 members in humans [3]. Detailed biochemical and structural studies have shed light into how different DUBs can recognise and process ubiquitin chains of distinct linkages and length [3, 135]. In certain cases, DUB enzymes bind to and cleave a single type of ubiquitin chains, as in the case of OTULIN (OTU DUB) which has only linear chain specificity, whereas other DUBs can process more than one type of ubiquitin linkage [3]. Additionally, DUB enzymes differ in their operating ability with some able only to remove a single ubiquitin moiety of a chain (exo-) and some other cleaving mid-chain (endo-cleavage) releasing an unanchored ubiquitin chain that can be further processed to regenerate mono-ubiquitin [3, 135].

Despite the key role of DUBs in regulating ubiquitin modifications and the medical relevance of these proteins in diseased states, this study is primarily focused on TRIM25, a RING E3 ligase and thus details of DUBs will not be further covered.

1.7 TRIM ligases are distinct members of the RING E3 family

The main part of this thesis is focused on TRIM25, a RING E3 ligase belonging to the TRIM family of proteins. The tripartite motif (TRIM) family constitutes the second largest subgroup of RING E3 ligases with 75 members in humans [136]. Members of the TRIM family are involved in the regulation of many cellular functions including cell growth, differentiation, innate immunity and apoptosis and are increasingly being implicated in oncogenesis [136-140]. The TRIM family of proteins is characterized by the presence of a unique supra-domain tripartite motif comprising a RING (R) finger closely followed by one or two B-box (B) motifs and a coiled-coil (CC) region (Figure 1.16). Even though these domains can be found in isolation in many other proteins, the presence of all three in the same polypeptide chain classifies the protein as a TRIM E3 [141-143]. In some cases, proteins are classified as TRIMs even if they contain two instead of three "signature" domains: for example, TRIM20 contains B-Box and CC motifs but the RING is replaced by a Pyrin domain [136, 143]. The tripartite motif (also referred to as RBCC) is present in the N-terminal portion of all TRIM proteins, whereas different C-terminal domains determine the main structural and functional differences within the family and often mediate interactions with other proteins (Figure 1.16) [136, 142-144]. When this project was initiated, it was not known if each domain of the RBCC operates as a separate functional unit or cooperates with the other domains to contribute to TRIM function. Additionally, the structural information available on these domains was very limited. Recent advances presented in this thesis (discussed in chapters 3 and 4) but also independently published during the course of this study promoted our understanding of structure and function of TRIM proteins and will be discussed in detail in the following sections.

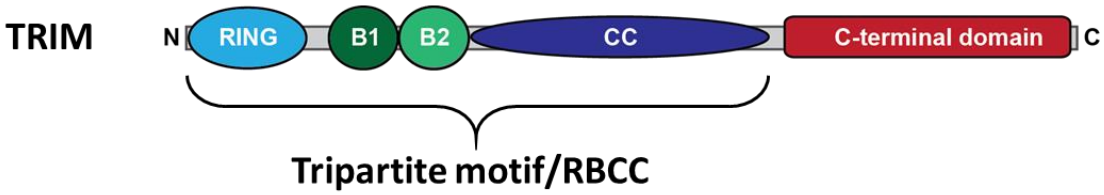

Figure 1.16: Schematic representation of TRIM proteins.

TRIM proteins contain a tripartite motif comprising a RING domain, one or two B-Box motifs and a CC region followed by a variable C-terminal domain involved in substrate recruitment.

RING domain

The RING domain is present in nearly all members of the TRIM family and encodes their E3 ligase activity [145]. Multiple structures of the core RING domain of several TRIM proteins available showed that the TRIM-RING spans 40-60 residues and adopts the two zinc-coordinating, cross-brace fold seen in other "canonical" RING E3s (and discussed in section 1.5.3.1.1 of this thesis) [142]. The structural similarity to other RING E3 domains and biochemical analysis led to the assumption that the TRIM-RING is responsible for binding of the cognate E2-ubiquitin thioester and facilitates transfer of ubiquitin onto a substrate. Prior to this study, the mechanistic details of the ubiquitin ligation employed by TRIM E3 ligases were very limited. Data presented in this study but also independently published during the course of this project reveal the molecular details of E2~Ub binding and thioester activation mediated by the TRIM-RING. These will be discussed in chapter 3.

B-box domain

B-box motifs are small, globular domains which coordinate two zinc ions by a combination of cysteine, histidine residues and in some cases aspartic acid residues, adopting a fold composed of a short α-helix and a β-sheet formed of two/three antiparallel β-strands which is reminiscent of the RING domain fold [146, 147]. These domains are located between the RING and CC domains in TRIM proteins and are thought to be evolutionarily-related to the RING fingers [146-148]. In most TRIMs, B-boxes are separated from the RING domain through a short linker region and are closely followed by the coiled-coil region. Two types of B-boxes are found in TRIM proteins which differ in the consensus sequence, size and spacing of the zinc-coordinating residues (B-box1 and B-box2) [142, 143]. The solution and crystal structures of several B-box domains of both types have been solved, revealing that the overall fold is shared between the two [146, 147, 149-153]. B-box2 however is ~8 residues shorter than that of type 1 and zinc coordination is achieved either by eight C/H residues or by seven C/H and one non-classical aspartic acid [142, 143]. All B-box1 domains described to date coordinate zinc ions using the classical C/H cross-brace motif [142, 143, 146]. The consensus sequence for B-Box1 is C-X_2-C-X_{6-17}-C-X_2-C-X_{4-8}-C-X_{2-3}-C/H-X_{3-4}-H-X_{5-10}-H (or C5(C/H)H2); for B-Box2 is C-X_{2-4}-H-X_{7-10}-C-X_{1-4}-D/C-X_{4-7}-

C-X_2-C-X_{3-6}-H-X_{2-5}-H (or CHC(D/C)C2H2) (Figure 1.17A) [142, 146]. TRIM proteins may contain one or two B-boxes in tandem. When both B-boxes are present, B-box1 always precedes B-box2 whereas when only one B-box is present it is always type 2 [143]. B-Box domains can also be found in non-TRIM proteins [154, 155]. Currently, the only available solution structure of the tandem B-boxes (B-box1 and B-box2) is that of TRIM18 (2JUN.pdb) (Figure 1.17B) [148]. In this structure, the two B-boxes pack closely against each other through their β-sheets and this interface covers more ~20% of their total surface. Further analysis of this B-box1,2 construct showed that this interaction increases the stability of the protein indicating that such orientation might be favorable in the cellular context [148]. Based on the structural similarity of the B-boxes to the RING domain, it has been suggested that B-box1 may contribute to the binding and activation of the E2~Ub intermediate whereas B-box2 might function by further regulating RING or B-box1 [142]. Further suggestions for functional roles include that B-Box domains may act as a protein-protein interaction motifs [155-157]. However, in the majority of cases, the precise role of these domains remains unclear. During the course of this study, several structures of different TRIM5α B-box2/CC constructs were solved [158, 159]. One of the key discoveries made by these structures is that the B-box2 closely packs against the coiled-coil region and these structures will therefore be discussed in conjunction with the coiled-coil in the next section [158, 159].

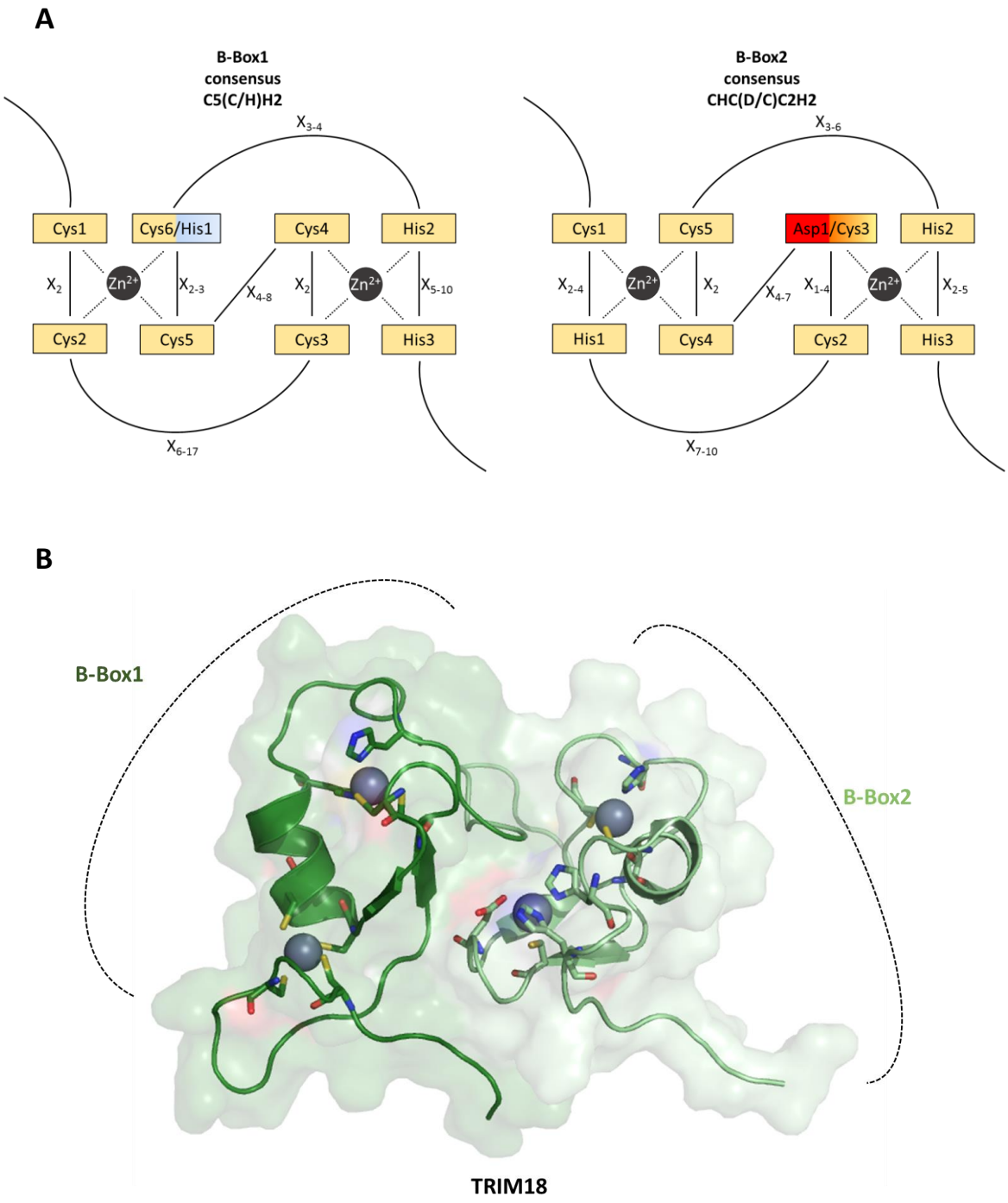

Figure 1.17: Sequence and structure of B-Box motifs.

A) Schematic representations of typical consensus sequences of a B-Box1 (left) and B-Box2 (right) domain. In B-box1, C/H residues bind Zn^{2+} atoms whereas in B-Box2 C/D residues are involved in Zn^{2+} coordination. B) Ribbon representation of the solution structure of TRIM18 tandem B-Box1(dark green)/B-Box2(light green) construct shows that the two are closely packing against each other. The side-chains of the residues which bind the Zn^{2+} atoms are shown. Figure was prepared in Pymol using 2JUN.pdb [148].

Coiled-Coil domain

The term coiled-coil was first introduced by Francis Crick and Linus Pauling in 1952 and refers to two α-helices which are coiled around each other [160, 161]. Coiled-coil domains are a common structural motif of many proteins known to mediate oligomerization [162]. Early primary sequence analysis of TRIM proteins including TRIM5α predicted the presence of three α-helices varying in length separated by non-structured linker regions [163]. Early studies have established that CC-mediated oligomerization of TRIM proteins is a prerequisite for biological function [142, 164]. In the absence of a TRIM-CC structure however, the precise CC-mediated oligomeric state and molecular details were not known. The first crystal structure of a TRIM coiled-coil region was that of TRIM25-CC closely followed by these of TRIM5α-B-box2/CC, TRIM69-CC and TRIM20-CC-PRYSPRY all of which became available during the course of this study [158, 165-167]. All TRIM-CC structures and subsequent biochemical analysis established that CC domains present in TRIMs form a symmetrical anti-parallel dimer composed of three α-helices per molecule, in a distinct manner (Figure 1.18A). In TRIM25-CC, helix1 (α1) is a ~170 Å long stem formed of 30 turns and packs closely to an antiparallel α1' of another monomer (Figure 1.18A). The second 3-turn α-helix (α2) is linked to α1 through a short 6-residue linker (L1) and packs back towards α1. The α2 is followed by a 14-residue linker (L2) which adopts an almost linear conformation and brings the third α-helix (α3) to the middle of the 170 Å stem. Importantly, α3 crosses over the top and packs closely to α1' forming a central four-helical bundle (Figure 1.18A). In general, coiled-coil regions are formed by heptad repeats, a term which refers to a repeating pattern of amino acids in every seven positions [162, 165]. The heptad repeat is normally occupied by HPPHCPC residues where H: hydrophobic, P: polar, C: charged. In TRIM25-CC, the α1-α1' coiled-coil interaction is formed by the canonical heptad (7-) repeats and additional hendecad (11-) residue repeats. These repeats are symmetrically arranged in a 7-7-7-7-11-11-11-11-7-7-7-7 pattern (Figure 1.18B). This combination of motifs produces two right-handed α-helices packing against each other into a left-handed supercoil at the ends but is slightly underwound in the middle to accommodate interactions leading to the formation of the four-helical bundle (Figure 1.18B) [165]. Comparison of amino acid sequences and structures of the coiled-coil regions described for TRIM5α and TRIM69 showed that the same anti-parallel orientation is adopted, indicating a common TRIM

feature [158, 165, 167]. Interestingly, the structures of all available TRIM-CC domains do not align very well and a closer inspection of their crystal structures shows unique features (Figure 1.19). To name a few, the curvature is different (TRIM20 arches more than TRIM69) and the α3 helix is kinked (TRIM20 and TRIM69) or is completely anti-parallel to the long α1 helix (Figure 1.19). The physiological relevance of these observations is not clear at this moment and both could be attributed to crystal lattice formation.

In the structure of TRIM5α B-box2/CC, the interface formed between B-box2 and CC domains was identified [158, 159]. This structure shows that the B-Box2 β-sheet packs against the α2' helix of the CC and is mainly mediated through hydrophobic interactions. Further studies are required to understand the orientation of the B-Box domain in relation to the CC-region in other TRIM proteins.

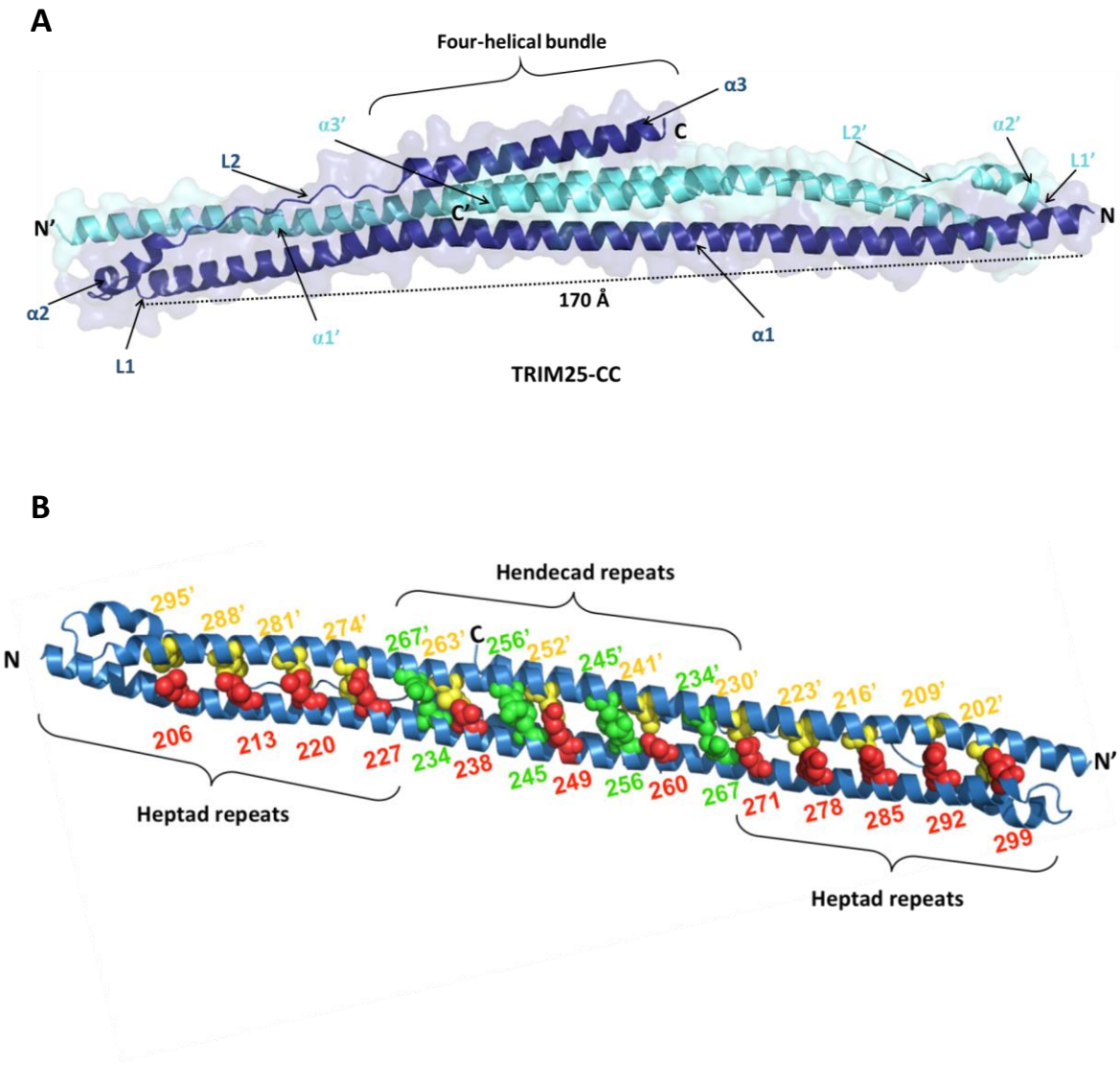

Figure 1.18: Structural analysis of TRIM-CC domains.

A) The structure of TRIM25-CC shows an antiparallel dimer comprising two long helices (α1- α1') followed by short linker (L1/L1') connecting α2/α2' helices at opposite sides that bind back towards the α1/α1'. Longer α3/α3' helices are separated by α2/α2' through a linker region (L2) and pack against α1'/α1, respectively. TRIM25-CC monomer 1 is shown in dark blue and monomer 2 in cyan. B) TRIM25 coiled-coil is formed by a symmetric pattern of repeating amino acids occurring every 7 (heptad repeat) or 11 (hendecad repeat) positions. Residues participating in interactions are numbered and shown as spheres. In red and yellow are hydrophobic residues of monomer 1 and monomer 2, respectively mediating dimerization of α1-α1' helices. In green are residues involved in hendecad repeats and mediate interactions that lead to the formation of the four-helical bundle in the middle of the antiparallel CC. Figure B was adapted from [165]. Figures were prepared in Pymol using 4LTB.pdb [165].

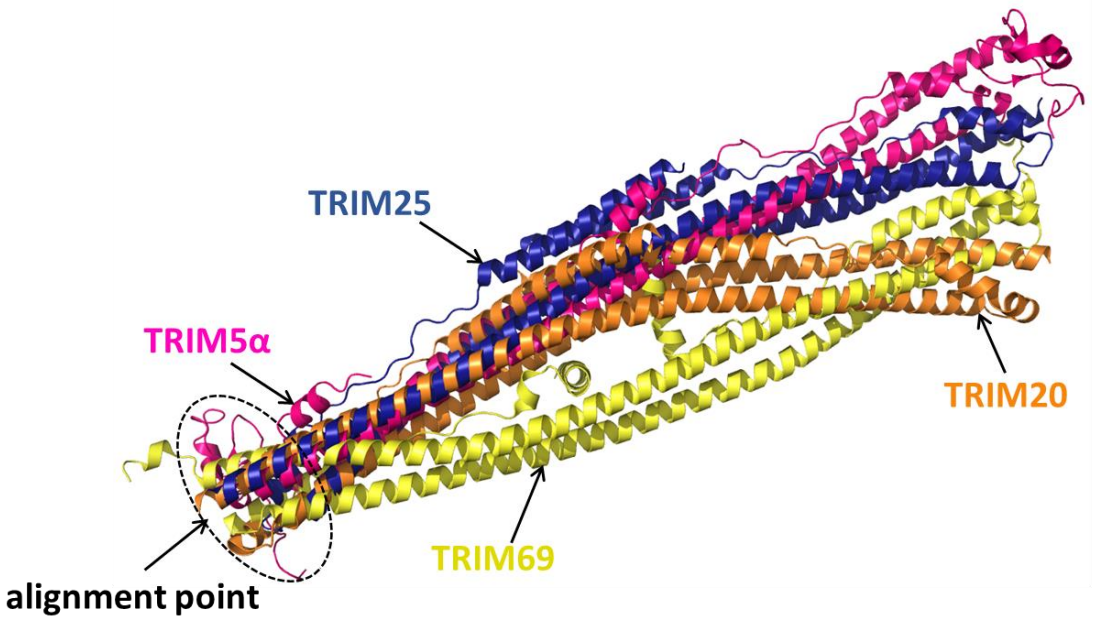

Figure 1.19: Structural alignment of TRIM-CC domains.

The structures of all TRIM-CC domains available to date were aligned as indicated. the formation of the four-helical bundle in the middle of the antiparallel CC. Differences are seen in curvature and position of the α3/α3' helices. Figure was prepared in Pymol using 4TN3.pdb (TRIM5α), 4CG4.pdb (TRIM20), 4LTB.pdb (TRIM25) and 4NQJ.pdb (TRIM69) [158, 165-167].

C-terminal domains

The RING, B-Box and CC domains is a common feature of the TRIM family and are present in (almost) all members, whereas there are marked differences in the C-terminal portion that accounts for the very diverse properties of TRIM proteins. To date, the main sub-categorization of TRIM proteins is based on their C-terminal domains [136, 168]. TRIM ligases are classified into 11 main families (I-XI) according to the type of C-terminal domain present (Figure 1.20) [136, 168]. Each family is further categorized into subgroups according to domain organization (Figure 1.20). The different C-terminal domains found in TRIMs along with their main functions described so far are: isolated PRY or SPRY domains with an unassigned function; fused PRYSPRY domains which are involved in protein-protein interactions; PHD (plant homeodomains) followed by BROMO (bromo-domain) which mediate transcriptional repression by binding to acetylated lysine residues of histones; COS (C-terminal subgroup one signature) which is involved in microtubule binding; FN3 (fibronectin type 3) which binds DNA and heparin; NHL (Ncl-1, HT2A, Lin-41) repeats which are protein-protein and protein-nucleic acid binding motifs; FIL (filament-type immunoglobulin) domains which are involved in actin binding; an ARF (ADP ribosylation factor-like) domain which are involved in intracellular vesicular trafficking; a MATH (meprin and TRAF-homology) domain for protein-protein interactions; an ACID (acid-rich) region of unassigned function; a TM (transmembrane) region [136, 138, 169]. The main role of the C-terminal domains is thought to be substrate binding [136, 142, 143].

Figure 1.20 shows the members of the TRIMs in each subgroup and also shows “non-canonical”/unclassified members of the TRIM family: i.e. TRIM proteins which do not contain a RING domain [136].

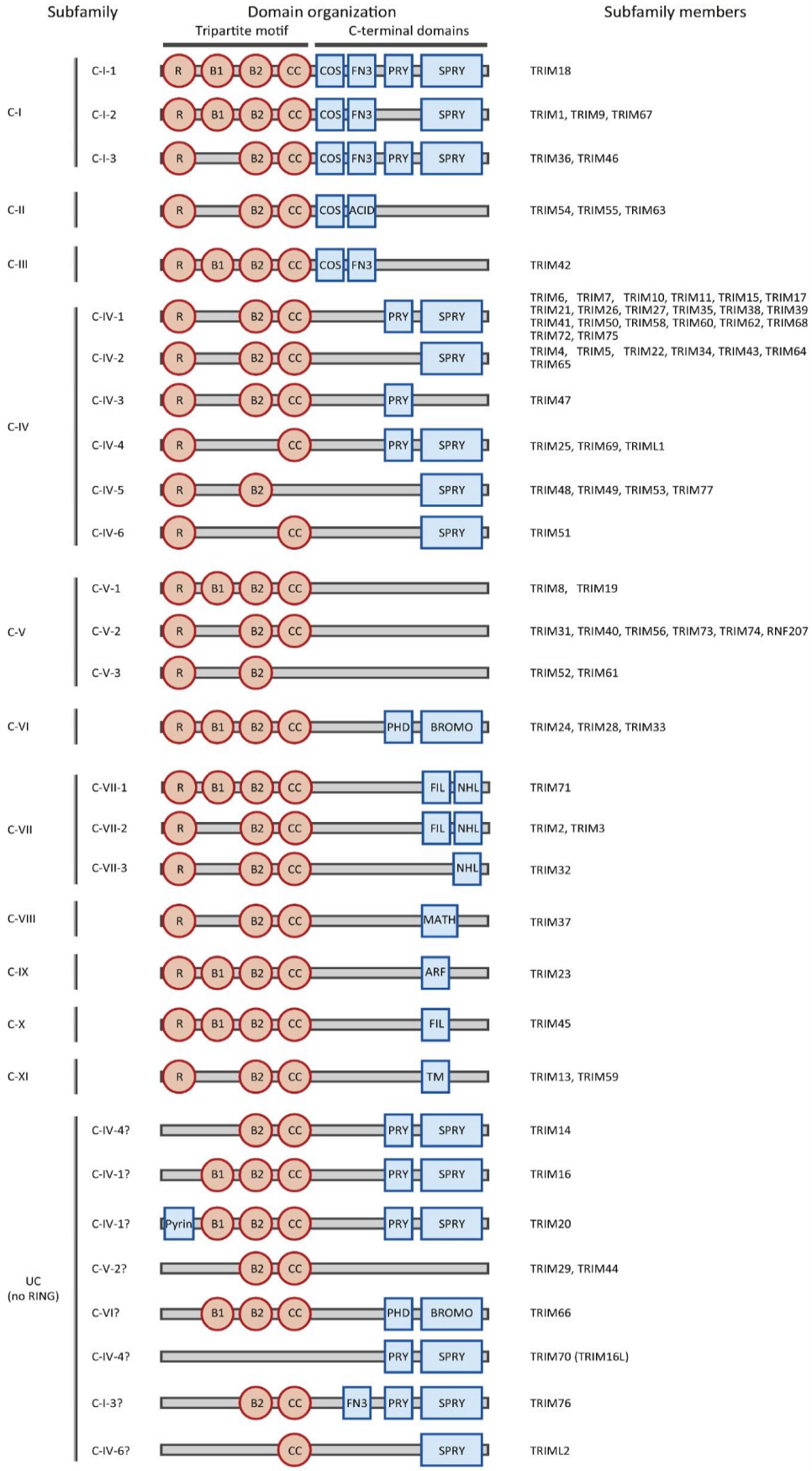

Figure 1.20: Categorization of TRIM proteins.

TRIMs are sub-divided in eleven families (I-XI) according to their C-terminal domain. Further subgroups are formed on the basis of domain organization. Figure was obtained from [136].

The most common C-terminal domain is the PRYSPRY domain which is present in nearly half of all TRIMs including TRIM25 (Figure 1.20) [136]. The PRYSPRY domain is formed by the fusion of two domains: PRY (~60 residues) and SPRY (~140 residues) [170]. Intriguingly, the SPRY domain can be found in animals, plants and fungi whereas the fused PRYSPRY is present only in vertebrates with an adaptive immune system indicating that these proteins have a major role in immunity [171]. The PRYSPRY domain is also known as the B30.2 domain, named after the B30.2 exon found in MHC (major histocompatibility complex) class I region [171]. As seen in the crystal structure of TRIM25, the PRYSPRY is a globular domain that adopts a characteristic β-sandwich fold formed of thirteen β-strands arranged in two antiparallel β-sheets held together by hydrophobic interactions and two N-terminal α-helices α1 and α2: α1 is parallel to the β-sheets and α2 which follows closely after α1 is perpendicular to the same β-sheet (Figure 1.21A) [172]. A structural overlap of the PRYSPRY domain from different proteins (including TRIM20, TRIM21, TRIM25, SPSB2 and TRIM72) shows that the overall fold is conserved [172]. This domain is proposed to mediate protein–protein interactions particularly in immune signalling proteins and is present in TRIM proteins either alone or preceded by COS and FN3 domains exerting less understood functions [136, 172]. Interestingly, to date, the only available structure of the TRIM coiled-coil region followed by the C-terminal domain is that of TRIM20 (Figure 1.21B) [166]. The crystal structure shows that the PRYSPRY domains of a CC-mediated TRIM20 dimer are located on top of the CC (Figure 1.21B). Further biochemical characterization revealed that despite the presence of a very short (3 a.a.) flexible linker linking CC and PRYSPRY, the PRYSPRY domain can occupy numerous positions in solution [166]. Based on structural analysis of symmetry-related molecules, the authors of this study further suggest that the PRYSPRY domain of TRIM20 may rotate around an “axis” passing through the short α1 of the PRYSPRY domain (Figure 1.21B). The flexibility seen for the PRYSPRY domain of TRIM20 might be necessary for substrate recruitment [166]. Further studies are required to understand if these observations apply also to other TRIM members.

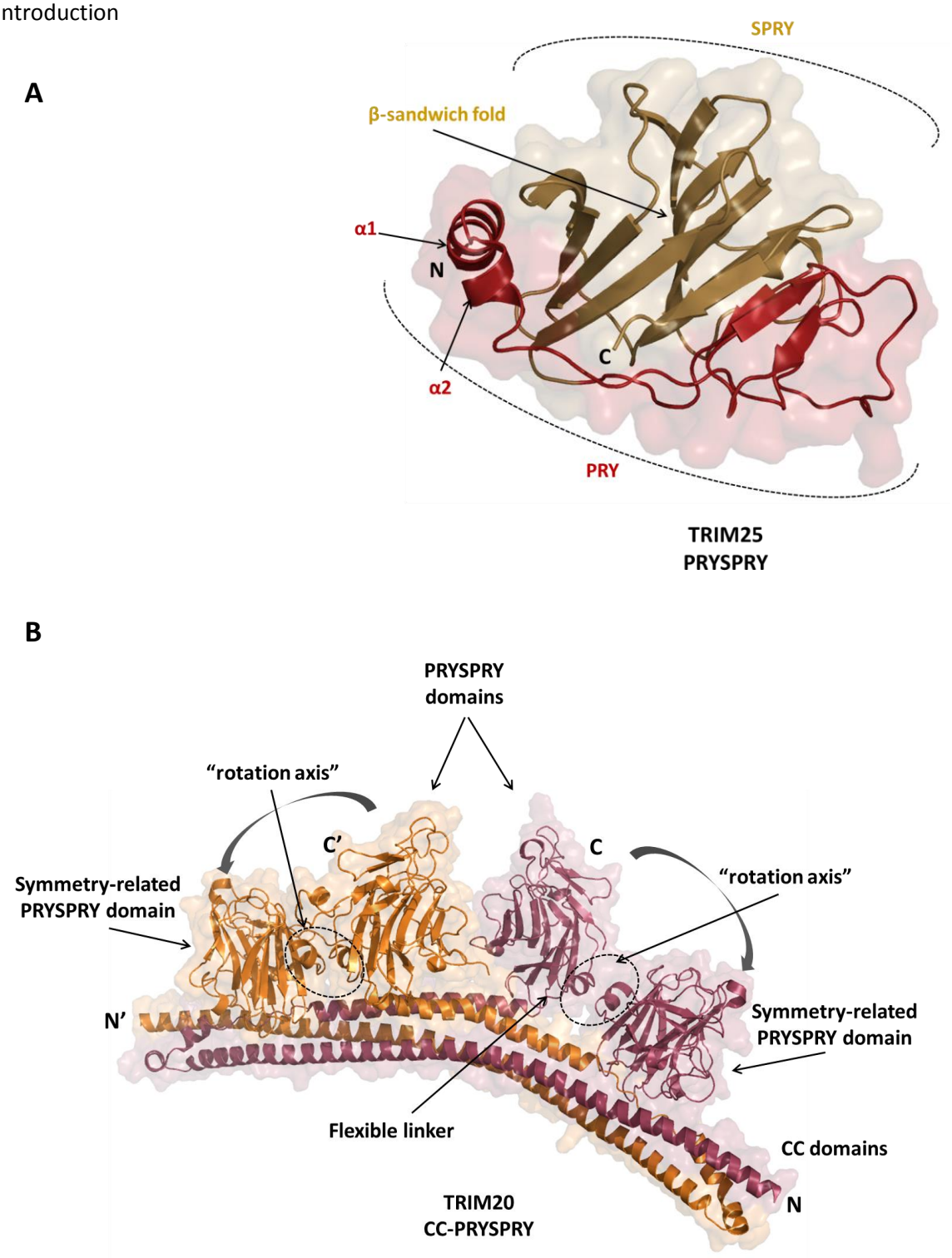

Figure 1.21: Structural characteristics of PRYSPRY domains.

A) The crystal structure of the TRIM25-PRYSPRY domain (4B8E.pdb) [172] shows the characteristic β-sandwich fold which is shared among all PRYSPRY-containing proteins**.** B) The structure of TRIM20-CC/PRYSPRY domain (4CG4.pdb) shows a CC-mediated antiparallel dimer with the two PRYSPRY domains located on top of the CC [166]. Based on crystal packing and biochemical analysis, the authors suggest a model in which the PRYSPRY domains can rotate about the short α-helix as indicated to form an extended conformation which allows substrate binding [166]. Figures were prepared in Pymol.

1.8 TRIM proteins in innate immunity

TRIM proteins are particularly important for the regulation of innate immunity and inflammation. It was shown that approximately half of all TRIM proteins identified to date enhance innate immune responses whereas several other reports have also implicated certain TRIMs to downregulation of immune signaling (Figure 1.22) [173-176]. Additionally, TRIM proteins have been shown to restrict viral infections and more recently were associated with marking intracellular bacteria for destruction [140, 176]. In the following sections, an overview of the key mechanisms by which certain TRIM proteins respond to infections will be discussed. The biological role of TRIM25 in antiviral immunity which is the main focus of this thesis will be discussed below in detail (section 1.9).

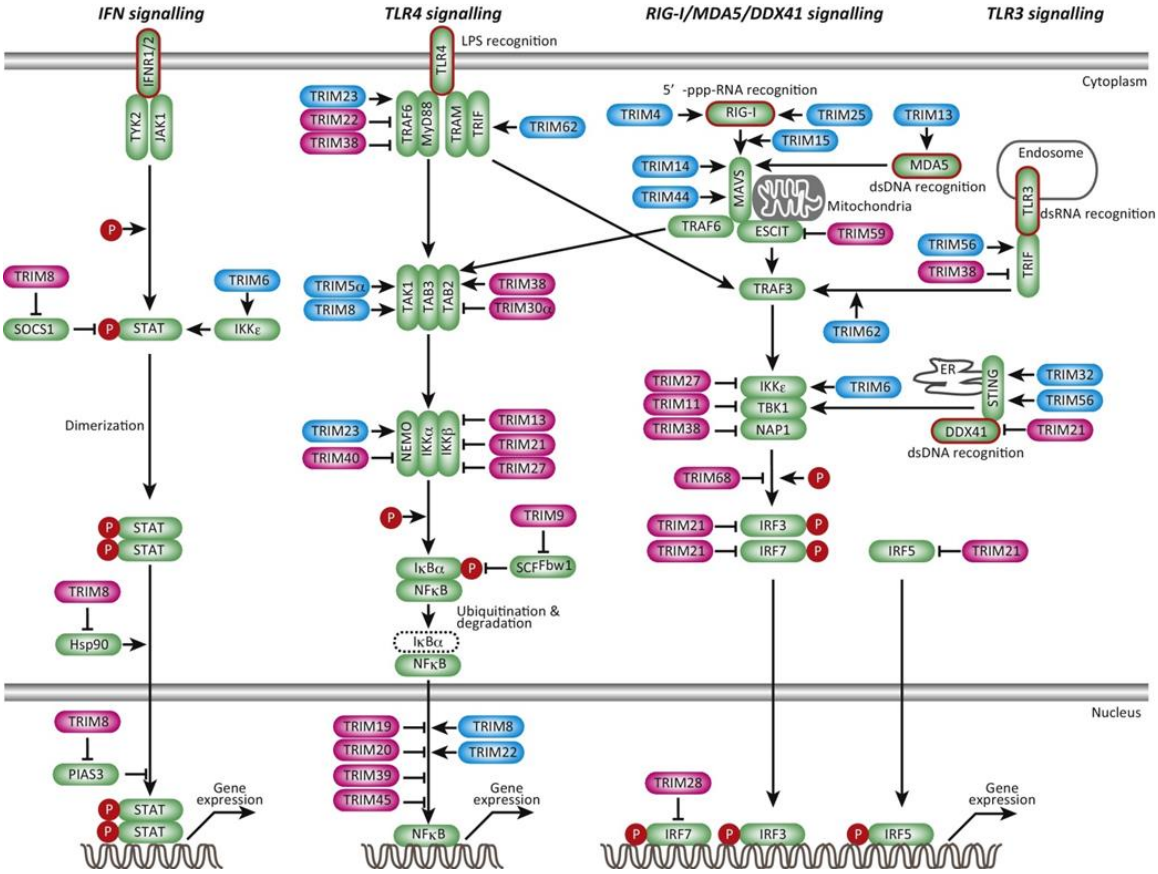

Figure 1.22: TRIM proteins as key regulators of innate immune responses.

A schematic overview of the numerous TRIM proteins which have been shown to regulate several innate immune responses. Pattern recognition receptors (shown in green with a red boundary-line) are molecules which recognize pathogenic invasion and activate complex signalling cascades involving many protein components. Some of those shown here in green are direct substrates of TRIM proteins. TRIM proteins shown in blue colour act as activators of downstream signalling whereas those in pink act as negative regulators. Phosphorylation (P) events are shown with a red circle. Several members of the TRIM family act synergistically to achieve fine-regulation of innate immunity. Figure is obtained from [136].

TRIM5α

TRIM5α is one of the best-studied members of the TRIM family to date, due to its high medical relevance. It is now well-established that in the cytosol of simian (rhesus monkey) cells, simian TRIM5α recognizes and directly binds to an incoming human immunodeficiency virus 1 (HIV-1) and protects the integrity of the host genome by viral destruction and downstream immune responses [177-180]. More recently, human TRIM5α has been shown to restrict HIV-1 infection but only in specific types of human cells [181].

The PRYSPRY domain of TRIM5α is required for the interaction with the large conical shell (~120 nm x 60 nm) made of protein repeats that surrounds the genetic material of the virus (retroviral capsid). The residues important for capsid binding are located on the flexible loop regions which have been suggested to undergo conformational changes upon interaction with the retrovirus [182]. Given that early studies showed that the isolated PRYSPRY domain binds with very weak affinity to the viral capsid, longer TRIM5α constructs were required to understand how TRIM5α recognises retroviral capsids [182, 183]. This was challenging, as TRIM5α B-Box2/CC constructs are prone to aggregation [184]. The crystal structure of rhesus TRIM5α B-box2/CC (previously described on section 1.7) was solved for a construct containing a double mutation on the surface-exposed region of the B-box2 [158]. These mutations (E120K/R121D) enhanced solubility of the B-box2/CC construct. In latter studies, the structures of an artificial chimeric TRIM5α B-box2/CC construct were obtained without these mutations and the role of B-box2 into the oligomerization of TRIM5α was uncovered [159, 178]. The structure of the chimeric Bbox2/CC showed a symmetric trimer (α, β, γ subunits) which is held together through reciprocal polar interactions between E120α:R121γ and R121α:E120β (Figure 1.23A) [159]. Biochemical analysis showed that TRIM5α B-box2, in isolation, is also forming a trimer in solution, further validating the crystal structures [185]. However, to date, this B-box2 behavior is thought to be TRIM5α-specific and contributes to the biological function of TRIM5α [149].

The TRIM5α higher-order oligomers are formed through coordination of the two oligomerization motifs (CC-mediated dimer and B-Box2-mediated trimer). This property is necessary for forming large hexagonal nets around the viral capsid (Figure 1.23B) [158, 159, 178, 185]. TRIM5α binding to the capsid induces RING activation and production of ubiquitin chains leading to capsid disassembly,

degradation of the viral proteins and also activation of inflammatory signaling pathways [186, 187]. The molecular details of capsid recognition by TRIM5α and the precise events that lead to HIV-1 neutralization are less understood.

TRIM21

Even when pathogenic microorganisms are coated with antibodies, in some cases they can still evade an adaptive immunity-mediated elimination such as phagocytic uptake by “hiding” in the cytoplasm of neighbouring cells [188]. It has been shown that upon invasion and cytosolic release, the immunoglobulin (Ig-)-coated microbes act as recruitment platforms for innate immunity-related proteins and subsequent immune signalling which leads to their destruction [189, 190]. TRIM21 acts as a cytosolic antibody receptor that uses its PRYSPRY domain to bind with high affinity to the Fc (heavy chain) portion of IgG, IgA or IgM found on the surface of internalised pathogens. This interaction combined with the E3 ligase activity of TRIM21 leads to proteasome-mediated degradation, autophagy initiation or activation of different immune signalling pathways (including NF-κB, AP-1 and IRF3/5/7) [191-193]. The crystal structure of TRIM21-PRYSPRY/IgG complex revealed the details of this interaction and helped identify aromatic residues on the Fc which can differ in primary sequence (Figure 1.24A). Nevertheless, the presence of structurally equivalent residues in other immunoglobulins allows wide cross-species reactivity [194]. This unique feature highlights the importance of TRIM21 in orchestrating cytosolic humoral immunity.

TRIM19/PML

TRIM19, also known as PML (promyelocytic leukemia protein), was first identified through its role in acute promyelocytic leukemia (APML), a subtype of leukemia. A reciprocal gene translocation between chromosomes 15 and 17 results in a *PML/RARα* (Retinoic Acid Receptor Alpha) fusion gene. The gene product that arises does not support the regulatory tumour suppressor functions of PML which include programmed cell death and cell division [195]. The loss of function of PML is therefore implicated in genome instability and cancer [196, 197].

Similarly to TRIM5α, TRIM19/PML is also shown to restrict viral infections. Upon infection by human cytomegaloviruses (HCMV), a subtype of Herpesviruses, TRIM19 forms large aggregates (sized ~0.3-1.0 μm) in the nucleus referred to as PML nuclear bodies (PML-NBs) [198, 199]. It was also recently shown that HIV-

1 infection triggers the formation of PML bodies in the cytoplasm and not in the nucleus of infected cells [200, 201]. However, these findings were challenged by a subsequent study which reports that TRIM19/PML is not involved in HIV-1 restriction in human cells [202]. Further studies are required to clarify the role of PML in HIV-1 infection. Nevertheless, the formation of PML bodies is dependent on the TRIM19 interaction with SUMO and SUMOylated proteins through its SIM (SUMO–interacting motif) but also on the E3 ligase activity of TRIM19 [198, 203]. These super-structures have been shown to activate downstream immune signaling processes by acting as recruitment platforms for other restriction factors such as the Daxx (death-domain-associated protein) and Sp100 (nuclear autoantigen 100) proteins [199].

The antiviral function of PML-NBs is antagonised by HCMV [199, 204]. A structural comparison of the central globular domain (IE1-CORE) of IE1 revealed that it resembles the structure of a TRIM CC region (Figure 1.24B) [205]. Subsequent biochemical analysis showed that the viral immediate early protein IE1 interacts directly with the CC domain of TRIM19 and this event inhibits TRIM19 SUMOylation [205, 206]. It was therefore suggested that complex formation between IE1 and TRIM19 abrogates the formation of PML-NBs by sequestering the available pool of TRIM19 and thus suppresses innate immune defence mechanisms [206]. The precise molecular details of this interaction remain to be uncovered.

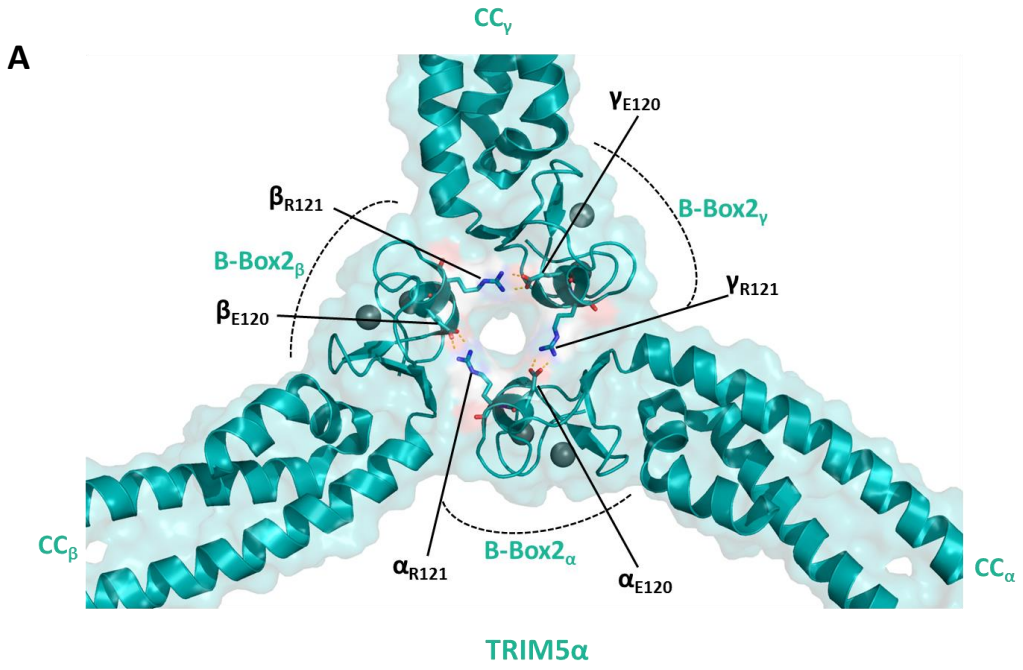

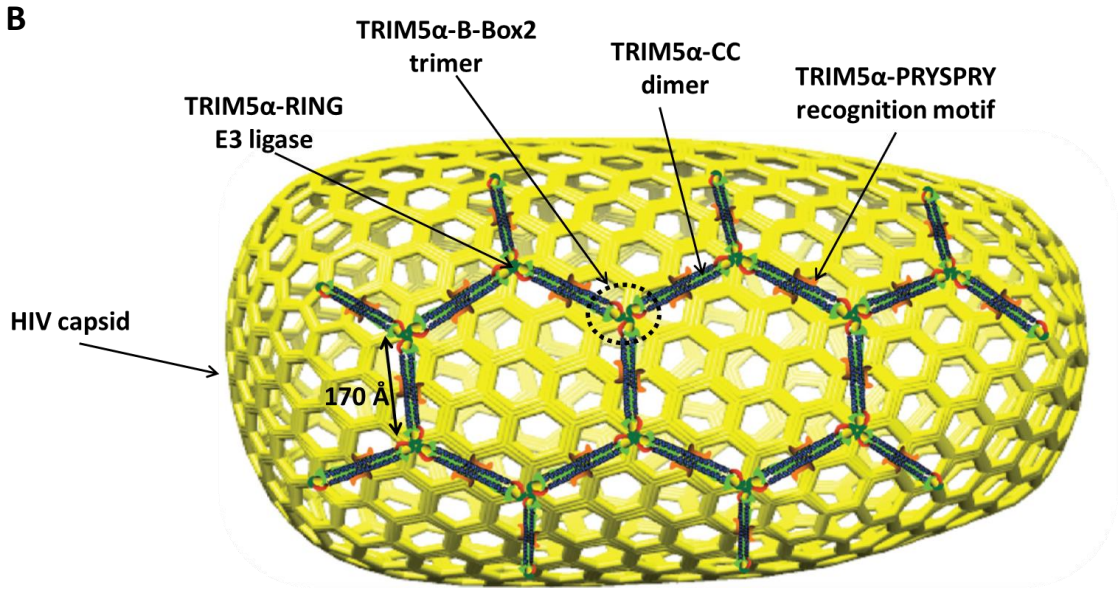

Figure 1.23: Oligomerization if a key feature of viral restriction factor TRIM5α.

A) The B-Box2 of TRIM5α forms a trimer which is required for higher-order oligomerization as shown in B. The side-chains of the residues mediating trimer-formation are highlighted. Figure was prepared in Pymol using 5IEA.pdb [159]. B) TRIM5α binds to proteins of a retroviral capsid through the PRYSPRY domain. Higher-order oligomerization of TRIM5α is achieved through the B-Box2 interfaces which allow formation of large hexagonal nets that lead to coating of the whole capsid. Figure B was adapted from [159].

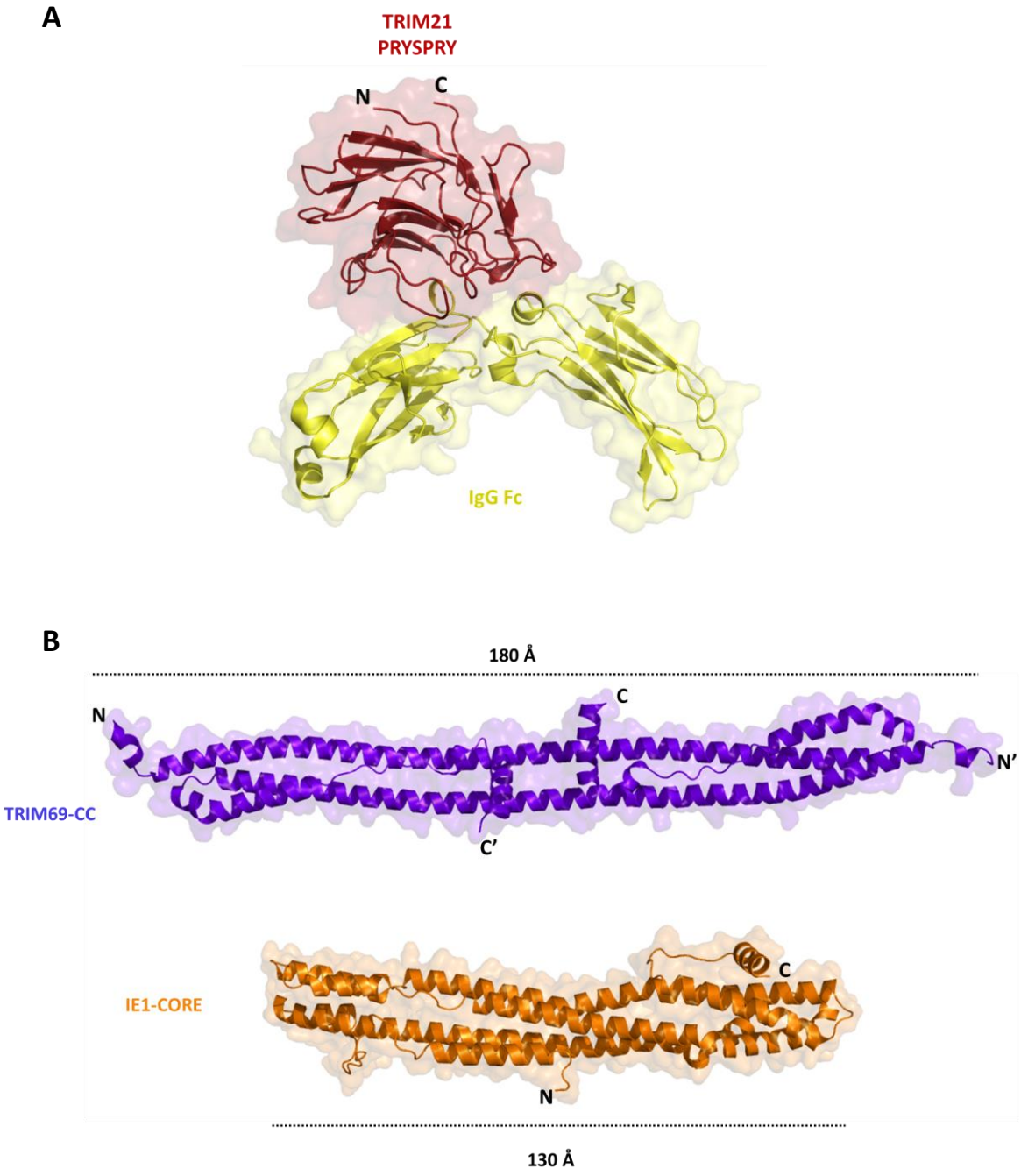

Figure 1.24: TRIM proteins involved in innate immunity.

A) The structure of the TRIM21-PRYSPRY domain (red) bound to IgG-Fc shows how TRIM21 can recognize antibody-coated pathogens in the cytoplasm. B) IE1 protein of HCMV directly binds to TRIM19/PML and suppresses its function. The IE1-CORE domain (shown in orange) reportedly mimics the structure of the TRIM19/PML-CC domain. Here, in the absence of a TRIM19/PML structure, the TRIM69-CC structure (purple) is shown for comparison. Figures were prepared in Pymol using 2IWG.pdb (TRIM21/IgG) [194], 4WID.pdb (IE1) [205] and 4NQJ.pdb (TRIM69) [167].

1.9 The antiviral role of TRIM25

TRIM25 is one of the better-studied TRIM proteins which mediates immune responses and protects cells against viral infections. The main substrate of TRIM25 is retinoic acid-inducible gene I protein (RIG-I), also known as DEAD (Asp-Glu-Ala-Asp or DEAD in one-letter code) box protein 58 (DDX58) [207]. RIG-I belongs to the RIG-I-like receptor (RLR) family of intracellular pattern recognition receptor (PRR) proteins. Soluble PRRs are molecules which survey the cytoplasm of cells and recognize conserved features of microorganisms and viruses commonly referred to as pathogen-associated molecular patterns (PAMPs) [208, 209]. Common PAMPs are nucleic acids, proteins and carbohydrates. RIG-I, as most other intracellular PRRs, is an ubiquitously expressed protein found in almost all mammalian cell types contributing to maintaining a sterile environment [208, 209]. RIG-I is a 925 amino-acid long protein composed of an N-terminal tandem caspase activation and recruitment domains (CARDs), a central DExD/H-box RNA helicase and a C-terminal domain (CTD) [210]. In healthy cells, RIG-I resides in an auto-inhibited state which entails a globular shape where multi-phosphorylated CARDs bind back to the DExD/H-box and C-terminal domain, in an orientation that does not allow RNA binding [211-213]. Upon viral infection, RIG-I has multiple levels of regulation that ultimately lead to production of type I interferon (IFN) through a multistep signalling cascade. Initially, RIG-I senses the presence of viral RNA and binds to a magnesium ion, ATP and the viral RNA through the central DExD/H-box helicase and C-terminal domain (CTD) [211, 214, 215]. The binding of RNA and ATP triggers major conformational changes leading to release of the autoinhibited state which exposes the N-terminal tandem CARDs (2CARDs) that are subsequently de-phosphorylated [216, 217]. This extended conformation is further stabilized by K63-linked polyubiquitination of the RIG-I-CTD by RING E3 ligase Riplet (RNF135) [218]. Subsequently, the now activated dsRNA-bound polyubiquitinated RIG-I is recognised by TRIM25 which further modifies the 2CARDs with K63-linked polyubiquitin [207]. TRIM25-mediated RIG-I ubiquitination is crucial as it induces and stabilizes a higher-order oligomeric state of RIG-I [207, 219]. The mitochondrial trafficking protein 14-3-3ε is responsible for translocation of the oligomerized RIG-I to mitochondria where it binds to the mitochondrial antiviral-signalling protein (MAVS) [220]. MAVS is embedded in the outer mitochondrial membrane and, upon interaction with RIG-I oligomers, is itself

forming filamentous structures [221]. These large aggregates act as a signalling platform containing multiple proteins including TRAFs and the IκB kinase complex (IKK) which activate multi-component transcription factors such as NF-κB, IFN regulatory factor 3 (IRF3) and IRF7 that control the expression of antiviral genes (e.g. type I IFN, tumour necrosis factor (TNF) and interleukins (IL-6,8)) [209, 210]. Intriguingly, it has been reported that in cells, overexpression of a RIG-I construct which contains the CARDs but lacks the central RNA helicase and C-terminal domains leads to IFN activation. This suggests that the CARDs are effectively the minimal requirement for initiating an innate immune response [210, 216]. Figure 1.25 summarizes key TRIM25-mediated activation and inhibition events that lead to type-I IFN response.

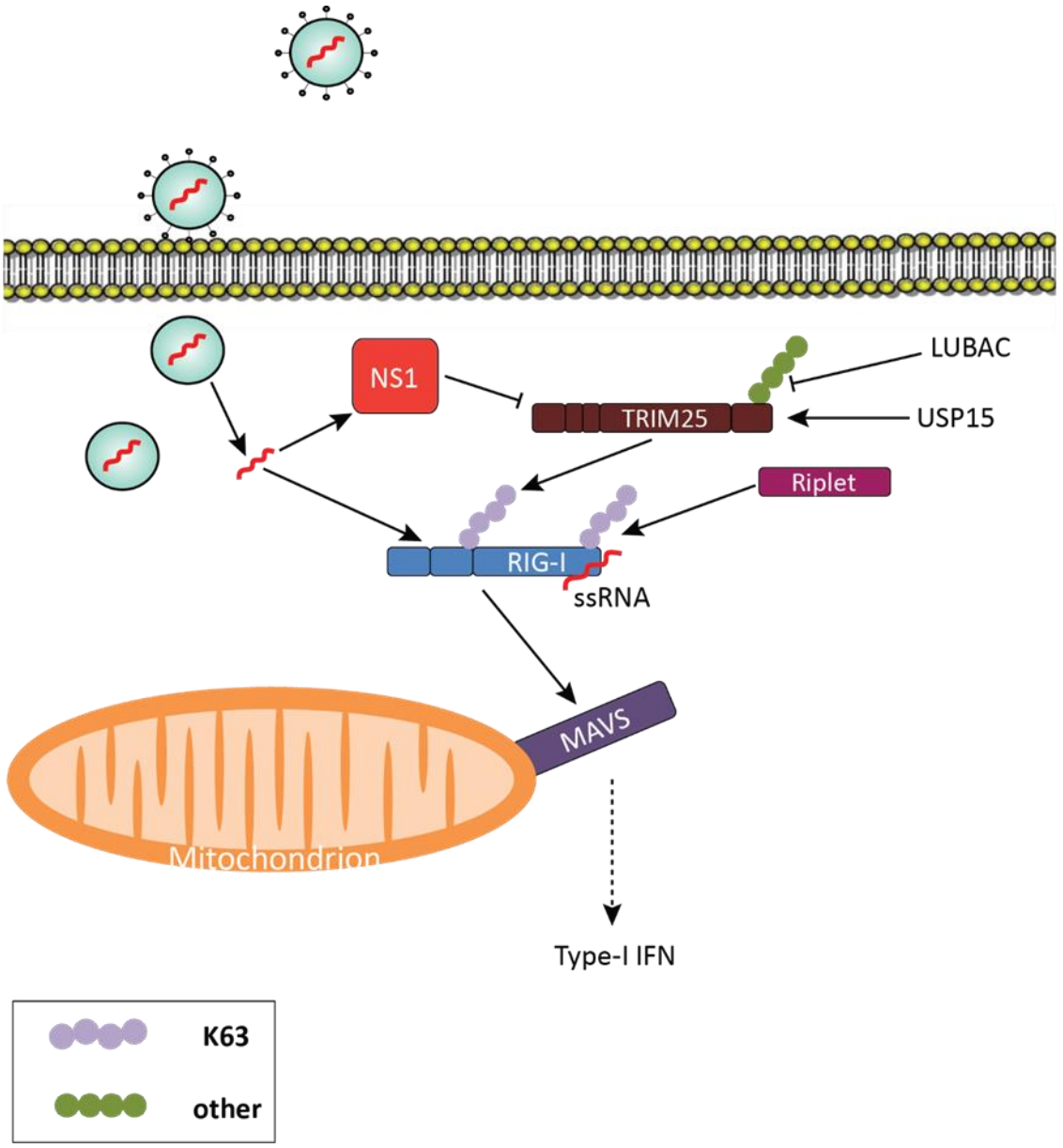

Figure 1.25: The TRIM25 antiviral signalling cascade.

Viral infection leads to RNA release in the cytoplasm which is recognised by RIG-I. TRIM25 and Riplet E3 ligases modify an RNA-bound RIG-I molecule with K63-linked poly-ubiquitin chains to stabilize it to an active state. RIG-I downstream binds to mitochondrial membrane-bound MAVS which becomes activated and leads to IFN production. LUBAC and USP15 perform regulatory roles on TRIM25, the former inhibiting and the latter promoting the E3 ligase function of TRIM25. The antiviral role of TRIM25 is antagonised by viral proteins such as NS1 which directly bind and inhibit its function.

1.9.1 RIG-I ubiquitination by TRIM25

TRIM25 recognises the tandem CARD motifs of RIG-I through the C-terminal PRYSPRY domain and mediates its ubiquitination [207]. The crystal structure of the mouse TRIM25-PRYSPRY domain (see also section 1.7) along with mutational studies identified the key TRIM25 residues responsible for RIG-I-2CARD binding as D488 and W621 which are also conserved in the human protein (E483 and W616, respectively) [172]. D488 is located on a flexible loop region (L3) whereas W621 is found on strand β12 of the β-sheet of PRYSPRY, in close proximity to other aromatic residues (such as F528, F559 and F623). Mutation of D488 and W621 abolishes the interaction with RIG-I-2CARD, whereas mutation of any other aromatic residue only modestly affects it [172]. Based on deletion studies, the TRIM25-interacting surface of RIG-I has been mapped to the N-terminal CARD (CARDa) of RIG-I (mutation of T55I abolishes interaction) whereas the lysine residues targeted for ubiquitination are located on the C-terminal CARD (CARDb) [207]. Initial studies identified several lysine residues as the target of TRIM25-mediated RIG-I ubiquitination (namely K99, K169, K172, K181, K190 or K193) but further mass-spectrometry-based analysis showed K172 as the primary site for K63-linked polyubiquitination [207]. Unsurprisingly, the RING domain of TRIM25 is shown to be indispensable for TRIM25-mediated RIG-I ubiquitination [207]. Cell-based studies further established that members of the UbcH5 (Ube2D) and Ubc13 (Ube2N) families of E2s are necessary for RIG-I activation [216]. In the absence of a TRIM25-RIG-I complex structure, the molecular details of this interaction remain obscure.

1.9.2 K63-linked polyubiquitin is required for RIG-I activation

Apart from covalent linkage of Ub on RIG-I, cell-free biochemical reconstitution assays have shown that unanchored K63-linked poly-ubiquitin chains can also activate the RIG-I/MAVS signalling pathway [216]. A subsequent structural study established that K63-linked polyubiquitin chains non-covalently wrap around the tandem CARDs of RIG-I and form a helical assembly [219]. In this structure, four RIG-I-2CARDs form a helical tetramer through CARD/CARD interactions which is further held together by three K63-Ub_2 chains which bind on the outer surface of this arrangement (Figure 1.26) [219]. The authors performed further biochemical and binding studies and suggested that longer K63-Ub_n (where n>3) chains are required for RIG-I-2CARD tetramer formation in solution [219]. This

helical tetrameric structure of RIG-I-2CARD was proposed and later also proven to act as a seed for MAVS nucleation and filament formation [221]. MAVS, which also contains a CARD, recognises the tetrameric RIG-I and forms itself a tetrameric structure which follows the helical trajectory of the RIG-I tetramer, leading to the formation of long filaments [219, 221, 222]. Activation of the RIG-I/MAVS signalling pathway is primarily based on the presence of K63-linked ubiquitin conjugates. Even though biochemical and structural studies have established the role of unanchored K63-linked chains in RIG-I oligomerization, further reports suggest that mutation of K172 on CARDb abolishes completely RIG-I-mediated signalling [207]. This, along with the crystal structure-based observation that unanchored K63-linked Ub dimers are not contacting K172 possibly suggest a cooperative mechanism in which RIG-I is subject to both covalent attachment of Ub at K172 and binding of K63-linked chains to ensure a robust signalling response (Figure 1.26). Regardless of the covalent or non-covalent nature of the K63-linked poly-ubiquitin chains involved in RIG-I activation, which is still debatable, it is well established that the catalytic activity of TRIM25 is absolutely required for their synthesis and activation of downstream antiviral signalling.

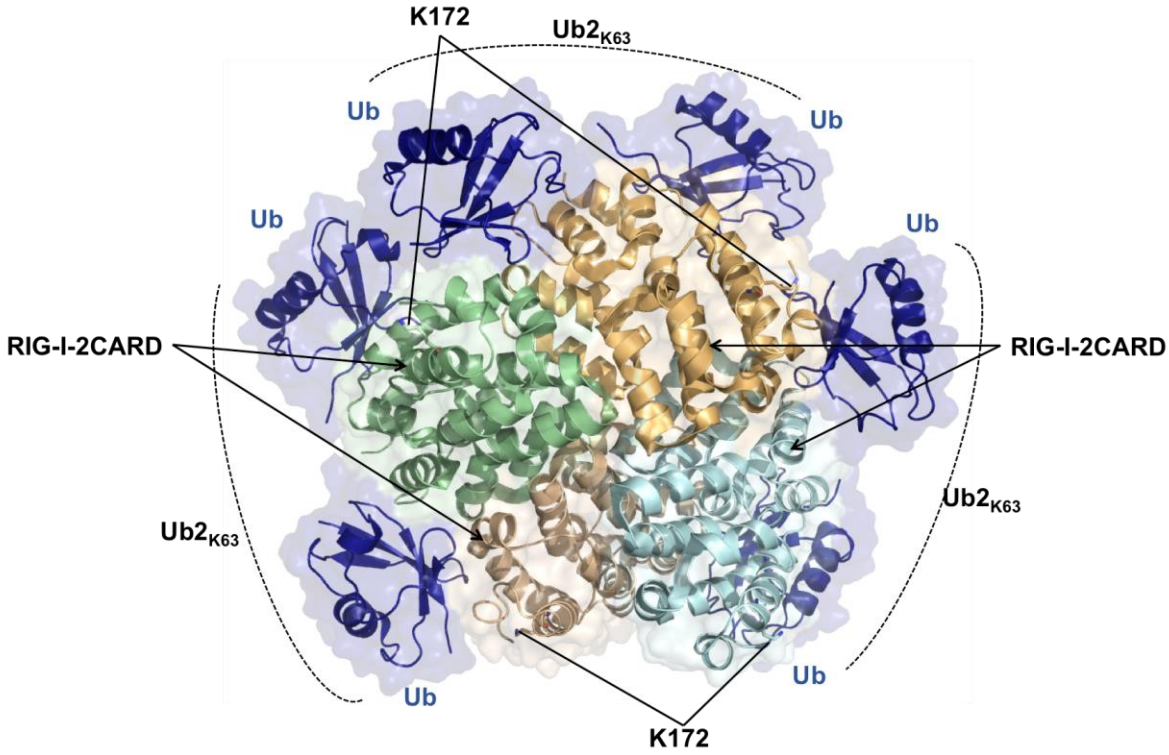

Figure 1.26: Structure of the active RIG-I-2CARD/UbK63 complex.

The structure of a RIG-I-2CARD/Ub_{K63} complex shows that four RIG-I-2CARDs (shown in green, yellow, light blue and light brown) are held together by three non-covalently-bound K63-linked diubiquitin molecules (dark blue). K172, which is the primary lysine for ubiquitin modification by TRIM25 is in close proximity with the C-terminal G76 of ubiquitin, indicating that a similar complex is formed through covalent attachment of K63-linked ubiquitin chains. Figure was prepared in Pymol using 4NQK.pdb [219].

1.9.3 RIG-I inactivation requires TRIM25 suppression

To prevent excessive production of interferons, cytokines and to fine-tune immune signaling responses, cells have developed sophisticated feedback inhibitory mechanisms. For example, the RIG-I-mediated signaling pathway is negatively regulated by LUBAC. LUBAC, the only E3 described to date to form M1-linked chains (see also section 1.5.3.3), recognizes the PRYSPRY domain of TRIM25 and mediates polyubiquitination that disrupts its function, thereby disrupting RIG-I activation [223]. It is reported that in cells TRIM25 undergoes mono-ubiquitination either by itself or by another unidentified to date E3 ligase [223]. The mono-ubiquitinated TRIM25 species are highly susceptible to further polyubiquitination by LUBAC (see also Figure 1.25 in section 1.9). The authors of this study have further identified HOIP-RBR-LDD (which is the main catalytic domain of LUBAC as described in section 1.5.3.3) as the minimal catalytic requirement for TRIM25 recognition and modification [223]. Hence, it can be further speculated that the conjugated-to-TRIM25 ubiquitin molecule is recognized by the ubiquitin-interacting-LDD region of the HOIP-RBR which leads to polyubiquitin chain elongation with M1-linked chains. However, the authors of this study suggest that the main ubiquitin-chain linkage identified in their experiments is through K48, an observation which likely suggests the involvement of a different E3 ligase [223]. The precise mechanism and structural details of the LUBAC/TRIM25 interaction remain largely unknown.

TRIM25 polyubiquitination with K48-linked ubiquitin chains acts as a signal for degradation and dampening of immune signaling [223]. On the contrary, the RIG-I-mediated response is maintained by the actions of USP15. USP15 is a DUB enzyme which interacts with the B-Box domains of TRIM25 and removes K48-linked ubiquitin chains from TRIM25 thereby sustaining IFN production [224]. Recently, a study showed that disrupting the interface of USP15/TRIM25 by a point mutation on USP15 (L749R) abolishes tissue inflammation [225]. Therefore, targeting of the USP15/TRIM25 complex might be used to treat acute or chronic states of inflammatory diseases [225].

The above fine-regulation mechanisms highlight the importance of TRIM25 in regulating an innate immune response against viruses.

1.10 Additional roles of TRIM25 in cells

TRIM25 is the second most abundant RING E3 in HeLa cells (with ~5 x 10^5 copies per cell) [9]. It is thus not surprising that additional RIG-I-independent roles have been attributed to TRIM25. Many of these roles are novel and ubiquitin-independent. Intriguingly, UV cross-linking experiments in living cells coupled to mass spectrometry have shown that TRIM25 can directly bind to RNA. In embryonic stem cells, TRIM25 is highly expressed and binds to yet unidentified sequences of RNA via the CC domain [226]. The precise role of this interaction is not currently known.

In a separate study, TRIM25 is shown to be involved in the suppression of a specific microRNA (miRNA) [227]. MiRNAs are short non-coding RNA molecules involved in mRNA silencing and thereby regulate gene expression. TRIM25 is reported to specifically recognize a conserved sequence and the secondary structure of a miRNA (pre-let-7). TRIM25 mediates ternary complex formation with pre-let-7 and two classical RNA-binding proteins (Lin28a/TuT4). This complex then allows uridylation (addition of uridine nucleosides at the 3' tail of miRNA) mediated by (Lin28a/TuT4). This modification targets pre-let-7 for degradation and can only proceed in the presence of TRIM25 [227]. Further studies are required to determine how the specificity towards certain miRNAs is achieved by TRIM25.

Early studies have also suggested that TRIM25 acts as an E3 ligase for ISG15 (see also section 1.2). The RING domain of TRIM25 was shown to be able to activate the E2~ISG15 intermediate and catalyse the transfer of ISG15 to substrates including 14-3-3σ and TRIM25 itself [228, 229]. However, later studies on the mechanism of ISG15 ligation on a substrate argue that a) a RING ligase cannot transfer ISG15 and rather a HECT-like mechanism is required and b) ISG15 ligation of proteins is exclusively performed by the E3 HERC6 (HECT domain and RCC1-like domain-containing protein 6) [230, 231]. Further studies are required to clarify these observations.

These novel functions have opened exciting new routes for further studies on TRIM25.

1.11 TRIM25 is directly targeted by pathogens

A very recent report has indicated that dengue virus (DENV) infection which is responsible for dengue fever in humans causes direct TRIM25 inhibition in an intriguing manner [232]. DENV, which belongs to the family of pathogenic Flaviviruses, produces accessory 300-500-nucleotide-long RNA molecules (referred to as subgenomic flaviviral RNAs or sfRNAs) which accumulate upon infection and have direct roles to disease. sfRNAs form complex RNA secondary structures which are highly dependent on conserved nucleotide sequences. One such sfRNA, PR-2B is derived from DENV serotype 2 (DENV-2) and specifically binds to TRIM25 and prevents deubiquitination which, as described in section 1.9.3, is necessary for sustained RIG-I-mediated IFN response [224, 232]. The molecular determinants of the TRIM25/sfRNA interaction remain to be uncovered.

The Influenza type A (IAV) family of viruses cause seasonal flu epidemics every year affecting the majority of the world's population. Human IAV infection triggers both adaptive and innate immune responses and viruses have developed specific mechanisms to suppress these [233]. Given the key role of TRIM25 as mediator of innate immune responses during viral infections it is not surprising that viral pathogens including influenza A viruses (IAV) have evolved systems to directly target TRIM25 and challenge the RIG-I-mediated IFN and cytokine production. One key protein produced by the short genome of IAV is non-structural protein 1 (NS1) [233]. NS1 has been shown to directly bind to the CC region of TRIM25 and inhibit its E3 ligase function thereby suppressing ubiquitination of RIG-I [234]. Given the medical relevance of this interaction, part of this study was focused on characterizing the structural details of this mechanism that could provide novel drug targets in the future. The results are presented and discussed in chapter 4 of this thesis. Therefore, the next section will form an introductory basis on IAV and specifically focus on describing some of the key characteristics and interactions of NS1.

1.12 Influenza A viruses

Influenza viruses belong to the *Orthomyxoviridae* family with a genomic negative-sense single-stranded RNA encoding eleven proteins [235]. There are four antigenic types of influenza viruses, A, B, C and D of which type A is the most virulent human pathogen. Influenza A viruses (IAV) cause influenza, commonly referred to as “flu” which is an acute, highly contagious respiratory illness that mainly affects the upper respiratory tract (nose, throat and bronchi). Symptoms include fever, rhinorrhea, sore throat and coughing, myalgia and fatigue and in some cases IAV infection can lead to death [235]. Many pandemics caused over the years have established IAV as a threat to public health and its circulation is highly monitored across the world [236]. Influenza A viruses are further categorized into different subtypes and named accordingly. The nomenclature criteria involve: the host of origin (e.g. equine, swine, avian with the exception of humans); the geographic location of the first isolation; the strain number; the year of isolation; the antigenic type of the two viral glycoproteins hemagglutinin (HA) and neuraminidase (NA) found on its surface with subtypes H1-H18 and N1-N11. For example, A/Puerto Rico/8/1934 (H1N1) is a type A influenza virus, first isolated in humans in Puerto Rico in 1934 with hemagglutinin and neuraminidase of types H1 and N1, respectively [235].

1.13 Non-structural protein 1

Influenza infections are restricted by host proteins which activate innate immune responses that lead to destruction of the virus. As described previously in section 1.9, IAV RNA is recognised by RIG-I which requires ubiquitination by TRIM25 to induce the production of IFN [207]. This pathway is challenged by viral proteins which act as virulence factors inhibiting innate immune responses, thereby allowing efficient viral replication in host cells. IAV non-structural protein 1 (NS1) is a multifunctional protein responsible for mediating numerous interactions with host proteins and therefore actively contributes to the prevalence of IAV infection [233, 237]. NS1 is a ~26 kDa protein expressed during the early stages of infection. NS1 proteins from different influenza A strains differ in their length ranging from 202 to 237 amino acids [237, 238]. They consist of an N-terminal RNA binding domain (RBD, a.a. 1-73) and a C-terminal effector domain (ED, a.a. 85-202), followed by an unstructured C-terminal tail. A short linker (NS1-LR, a.a. 80-84) is present in all viral strains apart from the highly pathogenic H5N1 and

connects the two domains [237-240]. Multiple structures of individual domains from different strains are available and these have provided insight into the fold of these domains, their role in self-association of NS1 and details of their interaction between RBD and dsRNA and ED with different host proteins [239, 241, 242]. A limited number of full-length NS1 structures have revealed the conformational flexibility of the RBD and ED architecture owing to the presence of the LR [243, 244]. The key structural characteristics of NS1 are detailed below.

1.13.1 Structural analysis of NS1

RNA-binding domain (RBD)

It was twenty years ago when the first crystal structures of an IAV RBD were reported [242, 245]. The role of this domain as an RNA-binding motif was described even earlier and the crystal structures of the unbound and dsRNA-bound NS1-RBD helped mapping of the interaction surfaces and identification of the residues involved [242, 245-247]. The NS1-RBD is a three-α-helix-containing motif (α1, α2 and α3) (Figure 1.27A) [245]. α1 is composed of 22 amino acids and is followed by a 4-residue turn. α2 (20 residues) is then closely followed by a 3-residue turn that connects it to the shorter (15 amino acids) α3. α2 is antiparallel to α1 and α3 packs across the former two. The functional NS1-RBD is composed of two antiparallel monomers forming a six-helical arrangement related by two-fold symmetry (Figure 1.27A). The dimerization of this domain is mediated by hydrophobic interfaces which bury more one third (~1,500 $Å^2$) of its total surface (~4,300 $Å^2$) [245]. Binding of dsRNA is mediated by the two α2 helices of the RBD dimer which recognise the major groove of the RNA and R38 acting as a key “anchor” residue for this interaction (Figure 1.27B) [246, 247]. A recent study has also provided evidence that NS1-RBD from certain viral strains directly recognises RIG-I-CARDb and this interaction potentially has inhibitory roles for IFN production [248].

Effector domain (ED)

Multiple structures of NS1-ED from different strains have revealed a highly conserved fold comprising seven β-strands and three α-helices (Figure 1.27C) [237, 239, 241, 249]. Six (1-6) β-strands form an antiparallel, slightly twisted β-sheet surrounding the central α-helix (α2) that is held in place through hydrophobic interactions. α1 is a short (1- turn) helix packing against the backside

of the β-sheet and α3 (2.5-turn) helix is almost parallel to α2 and connects to it through the short (parallel to the main β-sheet) seventh β–strand (Figure 1.27C). This NS1-ED fold is referred to as an α-helix/β-crescent fold due to the crescent-like shape of the β-sheet around the α-helix [241]. The effector domain of NS1 mediates numerous interactions with host proteins and has been reported to dimerize independently from the constitutively dimeric NS1-RBD [249, 250]. Dimerization of NS1-ED is achieved mainly through W187 residues which are reciprocally inserted into the α-helix/β-crescent fold of each participating monomer (Figure 1.27D) [239, 249-252]. Dimerization through NS1-ED allows further higher order oligomerization of NS1, a property which is necessary for many functions described so far, including dsRNA binding [239, 243, 252].

The full-length NS1 structures available to date have confirmed that the fold of the individual domains (RBD and ED) is the same as described by the isolated RBD and ED structures, respectively: the RBD is forming the six-helical bundle and the ED has the characteristic α-helix/β-crescent fold and mediates further oligomerization through W187 residue [243, 244]. Interestingly, when the FL-NS1 structures are aligned on the RBD, it becomes evident that the ED can occupy numerous positions around it and this is due to the presence of the flexible linker region (LR) that connects the two domains which was not resolved in the previous structures of the isolated RBDs and EDs (Figure 1.28) [243, 244]. One of the crystal structures available is that of the highly pathogenic H5N1 strain (A/Vietnam/1203/2004(H5N1)) that has an evolutionary conserved 4-residue deletion (LR Δ80-84) (Figure 1.28) [243]. This structure shows that the EDs cross-over the RBD dimer and closely pack against it. The structure of a NS1-FL (strain A/blue-winged teal/MN/993/1980(H6N6)) that has a longer LR and represents the majority of NS1 proteins in all strains with the exception of H5N1 shows that the two EDs are shifted upwards in regards to the RBD and are not crossing over as seen in H5N1-NS1 (Figure 1.28) [240, 244]. Both of these structures were solved for constructs containing a double mutation (R38A/K41A) in the RBD which according to the authors was necessary for crystallographic studies [243, 244].

Structural studies have shown that NS1 binds to different host proteins through the ED [237, 239]. The structure of NS1-ED in complex with p85β, a regulatory subunit of the phosphoinositide 3-kinase (PI3K) complex, revealed that this interaction is mediated through the highly conserved NS1-ED α1 helix comprising residues 95-99 which binds to the rigid elongated coiled coil domain (β-iSH2) of

p85β forming a four-helical bundle (Figure 1.29A) [253]. This interaction is shown to stimulate PI3K activity which then exerts its catalytic activity to non-physiological substrates and allows viral replication [253]. In a different example, NS1-ED binds to the host mRNA processing factor CPSF30 (cellular 30-kDa subunit of the cleavage and polyadenylation specificity factor) (Figure 1.29B) [254]. NS1-ED utilizes the α2 interface and specifically W187 to bind the second and third zinc finger (F2F3) domains of CPSF30 in a tetrameric complex composed of two head-to-head NS1-EDs and two CPSF30 proteins. This interaction is key to viral suppression of innate immune responses as it directly inhibits global host-mRNA processing [254]. Based on the current evidence, it is clear that NS1 is a multifunctional protein that binds multiple host factors to interfere with host antiviral responses on multiple levels [237, 239].

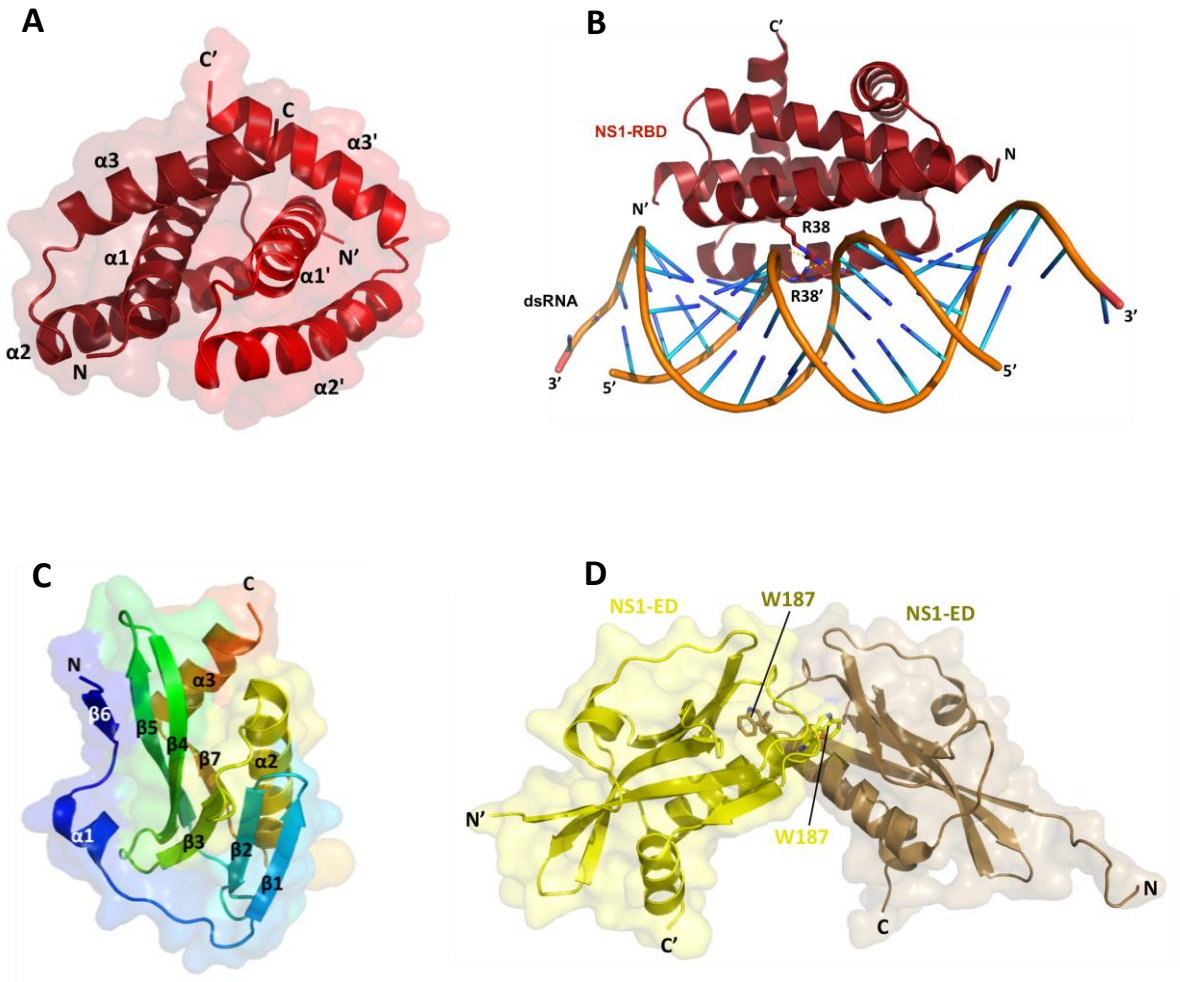

Figure 1.27: Structural features of NS1-RBD and ED.

A) The structure of RNA-binding domain (RBD) of NS1 (1AIL.pdb) [242] shows a symmetric six-helical arrangement which leads to the formation of a stable homo-dimer. Monomers are coloured in red and dark red for clarification. B) The structure of the NS1-RBD in complex with double-stranded RNA (dsRNA) (2ZKO.pdb) [246] shows the importance of R38 and R38' in mediating interactions with the RNA backbone of the major groove. C) The structure of NS1 effector domain (ED) (2GX9.pdb) [241] shows a conserved fold α-helix/β-crescent formed of seven β-strands and three α-helices. D) NS1-ED dimerization seen in the crystal structure (2GX9.pdb) [241] is mediated through reciprocal interactions of residues centred around W187 in both monomers. Monomers are shown in yellow and brown. Figures were prepared in Pymol.

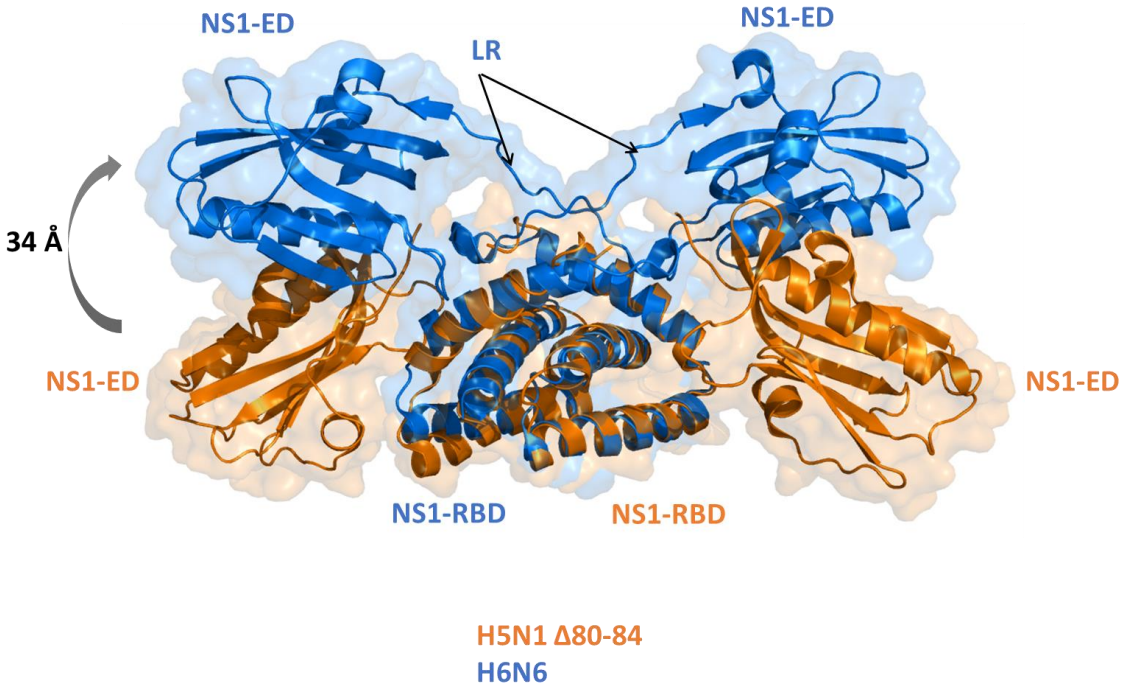

Figure 1.28: Full-length NS1 structures show inter-domain flexibility.

The structures of the NS1-FL from H5N1 strain (shown in orange) and H6N6 strain (in blue) are aligned on the RBD. H6N6-NS1 has a longer linker region (LR) connecting RBD and ED, whereas H5N1 has an evolutionary conserved 4-residue deletion (LR Δ80-84). The H6N6-NS1-EDs extend further compared to H5N1-NS1-EDs which pack against the RBDs, indicating that a longer LR allows more flexibility. Figures were prepared in Pymol using 3F5T.pdb [243] and 4OPH [244].

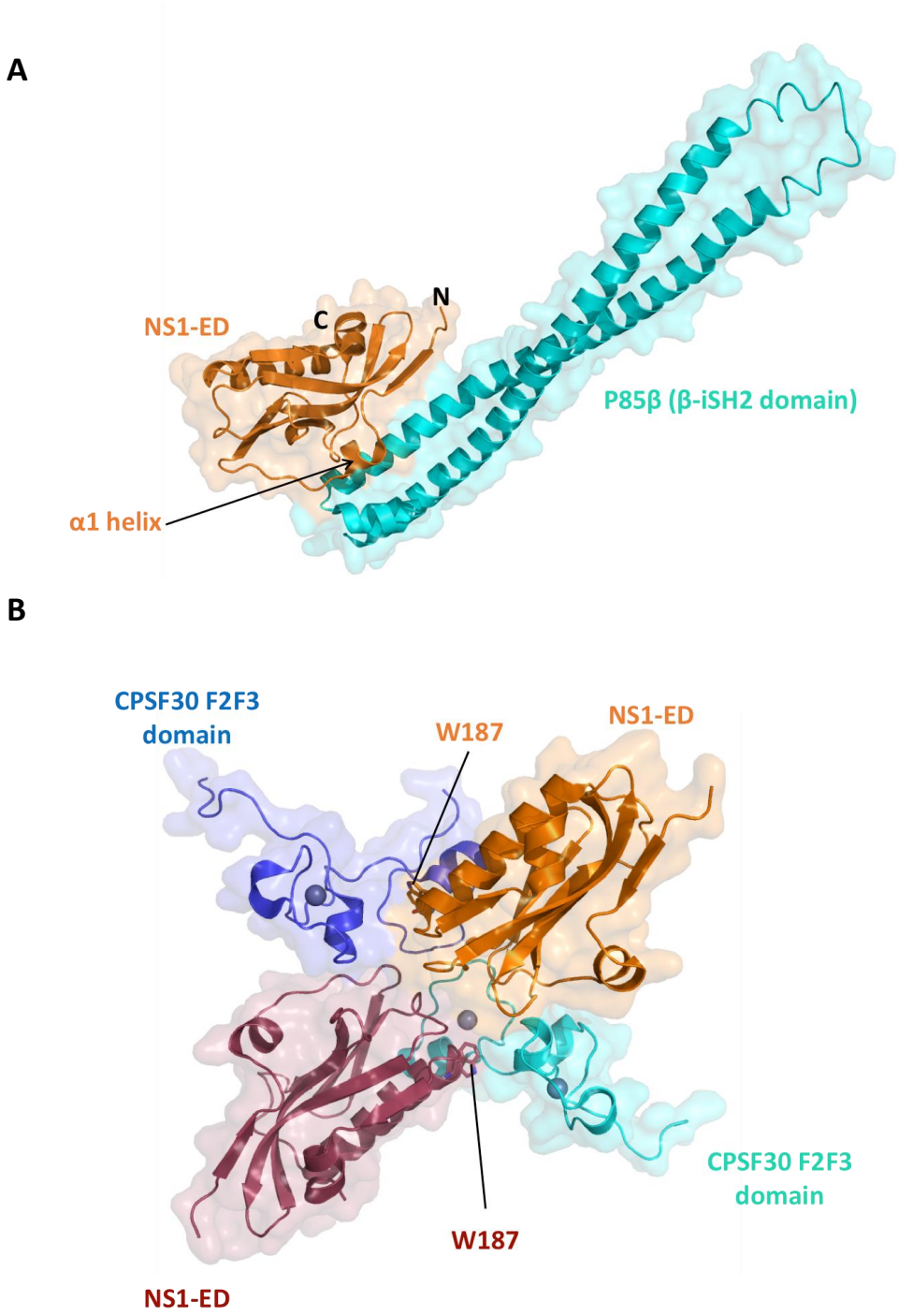

Figure 1.29: Interactions between NS1-ED and host proteins.

A) Structure of NS1-ED (shown in orange) bound to host p85β protein (cyan) shows that NS1-ED recognizes the elongated coiled coil domain of p85β through the short α1 helix, forming a four-helical bundle. B) Structure of NS1-ED (orange and deep red) bound to the Zn^{2+}-fingers of CPSF30 (blue and cyan) shows that two NS1-EDs adopt a "head-to-head" orientation and interact with CPSF30 through the two W187 residues. Figures were prepared in Pymol using 3L4Q.pdb (NS1/p85β) [253] and 2RHK.pdb (NS1/CPSF30) [254].

1.14 Objectives of study

TRIM proteins compose one of the largest subfamilies of RING E3 ligases and their involvement in the regulation of processes such as innate immune signalling and carcinogenesis suggest that they could constitute interesting targets to combat disease. TRIM ligases share a conserved domain architecture that consists of an N-terminal TRIM motif and a variable C-terminal region involved in substrate-recruitment. Previous studies have primarily focused on elucidating the mechanism of action of the viral restriction factor TRIM5α. However, prior to the present study, the mode of action and the molecular mechanisms underlying function of other TRIM proteins were less understood. Specifically, it was not known how TRIMs operate as E3 ubiquitin ligases and how their oligomeric state contributes to their observed function. The main aim of this project was thus to understand the precise molecular determinants required for catalytic TRIM E3 ubiquitin ligase function and substrate ubiquitination using *in vitro* biochemical and structural approaches.

This study was exclusively focused on TRIM25 which is a TRIM protein with a crucial role in antiviral innate immunity. Previous reports have established that activity of TRIM25 is required for recognition and ubiquitination of the cytosolic pattern recognition receptor RIG-I which initiates a pathway that culminates in the production of type 1 interferon. Intriguingly, this response is suppressed by direct inhibition of TRIM25 by Influenza A viral protein NS1.

The present study was aimed at obtaining information on a) the functional interplay between domains of the TRIM motif; b) their contribution to oligomerization and the E3 ligase function of TRIM25; c) the structural details of the TRIM25/NS1 interaction and the precise mechanism of virus-mediated E3 ligase suppression.

2. Materials and Methods

2.1 Materials

Chemicals and reagents used in the present study were purchased from Abcam, Expedeon, Fluka, GE Healthcare, Hampton Research, Invitrogen, Novagen, Promega, Pierce, Qiagen, Roche, Santa Cruz Biotechnology and Sigma-Aldrich and Stratagene. Specific chemicals and reagents are detailed throughout this chapter. Oligonucleotide primers were obtained from Sigma-Aldrich or Eurofins and DNA sequencing reactions were performed by GATC Biotech.

2.2 Molecular biology

2.2.1 Bioinformatics

The NCBI website (https://www.ncbi.nlm.nih.gov) was used to obtain nucleotide sequences of target genes; the NCBI Basic Local Alignment Search (BLAST) Tool (https://blast.ncbi.nlm.nih.gov/Blast.cgi) was used to identify homologues to the provided nucleotide and protein sequences. Pairwise nucleotide or protein sequence alignment was performed using EMBL-EBI EMBOSS Matcher tool (http://www.ebi.ac.uk/Tools/psa/emboss_matcher). Prediction of protein domain boundaries and secondary structure was performed using the PSIPRED server (http://bioinf.cs.ucl.ac.uk/psipred) and Crystallization Construct Designer (CCD) tool (https://xtal.nki.nl/ccd). Uniprot (http://www.uniprot.org) and the Expasy ProtParam tool (http://web.expasy.org/protparam) were used to determine biophysical parameters of proteins including molecular weight (MW), isoelectric point (pI) and extinction coefficient (ε). The ligation independent cloning (LIC) primers were designed with the aid of the CCD tool (https://xtal.nki.nl/ccd). Mutagenesis nucleotide primers were designed using Primer X (http://www.bioinformatics.org/primerx).

2.2.2 Plasmids

Details for all expression plasmids as well as sources of template DNA for all proteins used in this study can be found in Table 2.1. The plasmids of the E1, all E2s, RIG-I-2CARD construct and ubiquitin variants used were available in the lab (Table 2.1). Briefly, E1, all E2 proteins, RIG-I-2CARD and Ub variants were cloned into vector pGEX-6P1 or pET49b (Merck Millipore) to generate GST

(Glutathione S-transferase) or pDEST-17 (gift from H. Walden) and pET47b or pET21b for His_6-tagged proteins. A Human Rhinovirus 3C Protease (HRV-3C) protease cleavage site is included in the pGEX-6P1 and pET vectors to allow GST-tag or His_6-tag removal. Ubiquitin mutants K48C, K63A and K0-(all K residues in a.a. positions 6, 11, 27, 29, 33, 48, 63 are substituted to R) were cloned into pET21b vector in which the tags are removed. All E3 ubiquitin ligase (with the exemption of the full-length TRIM25) and NS1 constructs described here were cloned by ligation-independent cloning (LIC) into pET47, pET52b or pET-5247-SUMO to produce an HRV-3C cleavable His_6-, Strep-Tag-II- or His_6-SUMO-amino-terminal fusion protein, respectively.

The pET-5247-SUMO was vector constructed by Mr Evangelos Christodoulou (The Francis Crick Insititute) and produces MA**HHHHHH**SDSEVNQEAKPEVKPEVKPETHINLKVSDGSSEIFFKIKKTTPLRRLMEAFAKRQGKEMDSLRFLYDGIRIQADQTPEDLDMEDNDIIEAHREQIGG*LEVLFQGP*G-target fusion protein, where the underlined sequence is SUMO, the sequence in italics is the HRV-3C cleavage site and in bold is the His_6-tag. Details of all genes and protein constructs used in this study can be found in Tables 2.1 and 2.4.

Protein	Origin	UniProt identifier	Source	Vector	Mutations	Boundaries
TRIM25	Human	Q14258	Clone available in the lab	pET5247 or pET52 or pIEX-Bac3	P358L(natural variant)	see Table 2.4
NS1	Influenza A virus	P03496	Commercial (GeneArt)	pET47b or pET52	see Table 2.4	see Table 2.4
Ubiquitin	Bovine/human	P62992	Clone available in the lab	commercial or pET47b or pET21b	wt, M1C, K48C, K63A	FL
UBE1	Mouse	Q02053	Clone available in the lab	pET21b	wt	FL
UbcH5A (UBE2D1)	Human	P51668	Clone available in the lab	pGEX6P1	wt, C85K/S22R	FL
UbcH5C (UBE2D3)	Human	P61077	Clone available in the lab	pGEX6P1	wt	FL
UbcH7 (UBE2L3)	Human	P68036	Clone available in the lab	pGEX6P1	wt	FL
UbcH8 (UBE2E2)	Human	Q96LR5	Clone available in the lab	pGEX6P1	wt	FL
UbcH10 (UBE2C)	Human	O00762	Clone available in the lab	pDEST17	wt	FL
Ubc13 (UBE2N)	Human	P61088	Clone available in the lab	pGEX6P1	wt, K92A	FL
Uev1a (UBE2V1)	Human	Q13404	Clone available in the lab	pGEX6P1	wt	FL
Ube2G2 (UBE2G2)	Human	P60604	Clone available in the lab	pET49b	wt	FL
E2-25K (UBE2K)	Human	P61086	Clone available in the lab	pDEST17	wt	FL
RIG-I-2CARD (DDX58)	Human	O95786	Clone available in the lab	pET49b	wt	2-200

Table 2.1: Details of all proteins used in the presence study.

Details of TRIM25 and NS1 protein constructs can be found on Table 2.4.

2.2.3 Ligation-independent cloning (LIC)

Protein domain boundaries are shown in Table 2.4. Primers for PCR were designed with universal 21 base pair overhangs suitable for LIC (Forward primer: 5' CAGGGACCCGGT 3' and Reverse primer: 5' GGCACCAGAGCGTTA 3' which includes stop codon). In total, 50 TRIM25 and 3 NS1 constructs of varying length were designed. PCRs were set up with 10 ng of TRIM25 or NS1 templates with different extension times depending on construct length, using KOD Hot Start Master Mix DNA Polymerase (Merck Millipore) according to manufacturer's instructions (Table 2.2 and 2.3). PCR products were purified using a PCR Purification Kit (Qiagen). Purified PCR products and pre-cut and column-purified pET vector containing complementary overhangs (kindly provided by Mr Evangelos Christodoulou, The Francis Crick Institute) were treated separately with T4 DNA polymerase: ~0.2 pmole of PCR inserts were treated with dATP while ~0.06 pmole of vector was treated with dTTP for 20 mins at room temperature followed by 20 mins incubation at 75°C to heat-inactivate the enzyme. Following heat-inactivation, LIC reactions were carried out by adding 2 µl insert to 1 µl vector (~50 ng/µl) with 5 mins incubation at room temperature; 1 µl EDTA was then added to each reaction followed by 5 mins incubation. Finally, 1 µl of LIC reaction was transformed into 50 µl of chemically competent BL21 (DE3) GOLD *E. coli* cells (Stratagene) by heat-shock treatment at 42°C followed by plating onto LB-agar supplemented with ampicillin or kanamycin at 100 or 30 µg/ml, respectively to select for transformed colonies. Plates were incubated o/n at 37°C. Two or more colonies from each construct were used to inoculate o/n cultures which were then used to screen for insert by colony PCR. Plasmid DNA extraction of positive colonies was performed using a Spin Miniprep Kit (Qiagen). All plasmids were verified by DNA sequencing (GATC) and stored at -20°C. In most cases, a glycerol stock containing 70% culture and 30% glycerol as a cryo-protectant was flash-frozen in liquid nitrogen and stored at -80°C.

Component	*Volume (µl)*
1. Template DNA (~10-20 ng)	*X*
2. Forward primer (100 pmole)	*1.5*
3. Reverse primer (100 pmole)	*1.5*
4. KOD Hot Start Master Mix (0.04 U/µl)	*25*
5. dH_2O	*X*
Total volume	*50*

Table 2.2: Standard PCR components for LIC reactions.

	Target size	
Step	***< 500 base pairs (bp)***	***500-1000 bp***
1. Polymerase activation	*95°C for 2 min*	*95°C for 2 min*
2. Denaturation	*95°C for 20 sec*	*95°C for 20 sec*
3. Annealing	*60°C for 10 sec*	*60°C for 10 sec*
4. Extension	*70°C for 10 sec/1000bp*	*70°C for 15 sec/1000bp*
Repeat steps 2-4	*30 cycles*	*30 cycles*

Table 2.3: PCR protocol for LIC reactions.

2.2.4 Mutagenesis

Site-directed mutagenesis was performed using forward and reverse oligonucleotide primers containing the desired base substitution designed with the aid of PrimerX website. Two separate protocols were followed: Protocol A, in which the QuikChange site mutagenesis kit (Stratagene) was used according to manufacturer's instructions and Protocol B which included a two-step overlapping reaction. Briefly, in protocol A, a single PCR reaction was performed with overlapping primers annealing to the mutation site and the entire plasmid was amplified; this resulted in a re-circularized plasmid containing the gene of interest with the desired mutation and *Dpn* I endonuclease treatment removed the parental (unmutated) template. Protocol B achieves site-directed mutagenesis by primer extension and relies on two consecutive PCR reactions. For this protocol, two flanking primers (namely A and D) which anneal to the ends of the target sequence were combined with two internal primers with complementary ends (B

and C) containing the substitution of interest in two reactions: reaction 1 with primers A and C and reaction 2 with primers B and D, generating constructs AC and BD, respectively. In a second PCR reaction, the two AC and BD products were combined and due to complementary ends, they hybridized and further amplified using primers A and D, resulting in fragment AD containing the desired mutation. The products derived from protocol B were followed by LIC. Positive inserts were verified in all cases by sequencing.

2.3 Protein expression

2.3.1 Small-scale protein expression/purification

Small-scale over-expression was performed using 0.5 ml cultures (in 48-well 2 ml blocks) grown in rich media supplemented with 0.1 mM $ZnCl_2$ at 37 °C until an optical density at 600 nm (OD_{600}) of 6.0 was reached. The temperature was then decreased to 18°C and protein expression was induced by the addition of 1 mM IPTG (isopropyl β-D-thiogalactoside) with o/n incubation. Cells were harvested by centrifugation at 6000 x g for 20 mins at 4°C, supernatant was discarded and pellets were resuspended in buffer containing 50 mM Tris/HCl pH 7.7. Subsequently, buffer containing 50 mM Tris/HCl pH 7.7, 3 mM EDTA, lysozyme (1.5 mg/ml) and 60% w/v sucrose was added as it allows shrinking of the cells. H_2O was added to re-swell the cells and aid the lysis performed in lysis buffer (50 mM Tris/HCl pH 7.7, 900 mM NaCl, 90 mM imidazole, 15% v/v glycerol, 30 mM $MgSO_4$, 25u/ml Universal Nuclease (Thermo Fisher Scientific), 0.7% OTG (Octylthioglucoside), 3 mM TCEP (tris-(2-carboxyethyl)phosphine), 0.3 mM PMSF (Phenylmethanesulfonyl fluoride). Clarified lysates were applied to Ni Sepharose 6 Fast Flow beads (GE Healthcare) pre-equilibrated with binding buffer containing 50 mM Tris/HCl pH 7.7, 300 mM NaCl, 40 mM imidazole, 0.02% OTG and 1 mM TCEP. After binding, Ni beads were washed with 4 column-volumes binding buffer to remove any unbound proteins. His_6-tagged proteins were eluted with elution buffer containing 50 mM Tris/HCl pH 7.7, 300 mM NaCl and 500 mM imidazole and 1 mM TCEP. Samples were analysed by SDS-PAGE.

2.3.2 Large-scale protein expression

A starter culture was produced by o/n incubation at 37°C in a shaking incubator at 200 rpm; a 1/100 dilution was then used as inoculum for larger cultures, typically 1-6 litres. Cells were grown in 0.8 L Luria Bertani (LB) or Terrific Broth (TB) media in 2 L flasks in a shaking incubator at 37°C to a mid-log phase OD_{600} of 0.8 (LB) or 3.0 (TB) at which point the temperature was decreased to 22°C. All Zn^{2+}-containing proteins were expressed in LB and supplemented with 0.1 mM $ZnCl_2$. Protein expression was induced by the addition of 0.4 mM IPTG with 16 h incubation. Cells were harvested by centrifugation at 4,500 x g for 30 mins at 4°C in a Beckman J6-M1, the supernatant was discarded and cell pellets were stored at -20°C.

2.3.3 ^{15}N labelling of TRIM25-RING for NMR studies

In order to allow incorporation of ^{15}N isotope in the protein of interest, in this case TRIM25-RING, cells were grown in M9 minimal medium supplemented with $^{15}NH_4Cl$. A 10x stock solution of M9 salts was prepared for a total volume of 0.5 L containing: 30 g Na_2HPO_4, 15 g KH_2PO_4, 2.5 g NaCl, 5 g $^{15}NH_4Cl$ and dH_2O with pH adjusted to 7.4 using 10 M NaOH. The 10x ^{15}N-enriched M9 stock was autoclaved to sterilize. Each litre of M9 media for bacterial growth was prepared by diluting 100 mL 10x media solution with 900 mL autoclaved dH_2O; $MgSO_4$, $CaCl_2$ and $ZnCl_2$ were also added to final concentrations of 2 mM, 0.1 and 0.1 mM, respectively. Finally, a source of carbon was added to the media as filter-sterilized glucose solution to a final concentration of 0.3% w/v. A total volume of 4 litres was inoculated with the starter culture at a 1/100 dilution. Cells were incubated in a shaking incubator at 37°C to a mid-log phase OD_{600} of 0.7 at which point the temperature was decreased to 22°C. Protein induction commenced with the addition of 0.25 mM IPTG and 16 h incubation. As with cultures grown in LB/TB, cells were harvested by centrifugation at 4,500 x g for 30 mins at 4°C in a Beckman J6-M1, the supernatant was discarded and cell pellets were processed.

2.4 Protein purification

All buffers using for protein purification were made using deionised water (MilliQ or dH_2O), filtered through a 0.22 µm membrane filter and degassed. The pH of buffers was fixed to ± 1 pH unit from the target protein's pI (isoelectric point).

TCEP or DTT (dithiothreitol) (Sigma-Aldrich) were added to the buffers to prevent oxidation of cysteine residues. Details of the different TRIM25 and NS1 constructs purified during this study can be found on Table 2.4.

construct	*a.a.*	*MW (Da)*	*pI*	*ε*	*Purification steps*	*Mutations*
TRIM25-R	*1-82*	*9059*	*4.86*	*8480*	*Ni; SEC*	*wt, E9R, E10R, R54A, K65A, T67A, V72R*
TRIM25-RB1	*1-152*	*16716*	*5.21*	*13980*	*Ni; IEX; SEC*	*wt*
TRIM25-RB1B2	*1-202*	*22397*	*5.76*	*13980*	*Ni; IEX; SEC*	*wt*
TRIM25-RBCC	*1-438*	*48984*	*7.98*	*19940*	*Ni; IEX; SEC*	*wt*
TRIM25-B1B2CC	*103-379*	*31700*	*7.69*	*5960*	*Ni; IEX; SEC*	*wt*
TRIM25-CC	*189-379*	*21959*	*8.55*	*5960*	*Strep or Ni; SEC*	*wt*
TRIM25-FL	*1-630*	*70973*	*8.44*	*63830*	*Ni; IEX; SEC*	*wt*
NS1-FL	*1-230*	*25868*	*6.21*	*23490*	*Ni or Strep; SEC*	*wt, R38A/K41A, R38A/K41A/W187A, W187A*
NS1-RBD	*1-73*	*8569*	*8.16*	*5500*	*Ni; SEC*	*wt*
NS1-ED	*79-230*	*16840*	*5.87*	*17990*	*Ni; SEC*	*wt, L95A/S99A, R140A*

Table 2.4: TRIM25 and NS1 constructs used in the present study.
Boundaries, molecular weight, theoretical pI, extinction coefficient (in units of M^{-1} cm^{-1}), purification steps and mutations are mentioned for each construct. Sequence of purification steps was: affinity chromatography (Ni/Strep); ion exchange (IEX) and size-exclusion chromatography (SEC).

2.4.1 Cell lysis

In general, *E.coli* cell pellets were re-suspended and incubated for 60 min. in 10 ml of lysis buffer (per gram of pellet) containing: 100 mM HEPES, 500 mM NaCl, 1 mM TCEP, 5 mM Mg_2Cl, DNase I (2 µg/ml), lysozyme (1 mg/ml) (both from Sigma-Aldrich) and one Complete EDTA-free Protease Inhibitor cocktail tablet (Roche) per 50 ml of lysis buffer. If fusion protein was His_6-tagged, lysis buffer was supplemented with 20-40 mM imidazole. Cells were kept on ice and lysed by sonication at 40% duty cycle, with intervals of 5 sec ON and 10 sec OFF for 5 min per 100 ml in a Branson Sonifier SFX250. Lysate was clarified by centrifugation at 55,000 x g for 45 mins at 4 in a Beckman JA-25.50 rotor and the supernatant collected. Samples of lysate, supernatant and pellet were analysed by SDS-PAGE.

2.4.2 Affinity chromatography

For proteins containing a GST-, Strep-II- or His_6-tag, affinity chromatography was carried out as an initial purification step.

GST-tagged protein

Clarified supernatant was applied to pre-equilibrated in buffer A^{GST} (100 mM HEPES, 500 mM NaCl, 1 mM DTT) Glutathione Sepharose High Performance (HP) beads packed in a XK16 column (GE Healthcare). Beads were washed with 20 CVs with buffer A^{GST} to remove unbound proteins. The GST-tagged protein was eluted with buffer B^{GST} (100 mM HEPES, 500 mM NaCl, 1 mM DTT, 20 mM reduced glutathione (Sigma-Aldrich)) and incubated o/n with 150-200 µg of 3C protease at 4°C while dialysing against a large excess of buffer A^{GST} to remove the glutathione. Cleaved protein was then re-applied to the GST-binding column to remove the GST-tag and non-cleaved fusion proteins including GST-HRV-3C. Eluent was stored for subsequent purification steps.

Strep-II-tagged protein

Clarified lysate was applied to StrepTactin Sepharose High Performance (HP) beads packed in a XK16 column (GE Healthcare) which was pre-equilibrated in buffer A^{Strep} containing 100 mM HEPES, 300 mM NaCl, 1 mM DTT. Beads were washed with 20 CVs with buffer A^{Strep} to remove unbound proteins. The fusion protein was eluted in buffer B^{Strep} containing 100 mM HEPES, 300 mM NaCl, 1 mM DTT and 2.5 mM desthiobiotin (IBA) followed by o/n incubation with His-HRV-3C protease at 4°C. Eluted fractions were further purified by size-exclusion chromatography (SEC).

His_6-tagged protein

Clarified supernatant was applied to a His-Trap HP 5ml or HiTrap TALON crude 5ml column (both GE Healthcare). His-Trap utilises immobilized Ni^{2+} to capture histidine tagged proteins whereas TALON resin is coated with Co^{2+} metal. The main difference between the two resins is that TALON binds with lower affinity to His-tag enabling higher specificity and increased purity in some cases. In both cases, columns were pre-equilibrated in buffer A^{His} (100 mM HEPES, 500 mM NaCl, 0.5 mM TCEP, 20-40 mM imidazole). Beads were washed with 40 CVs using buffer A^{His} to remove unbound proteins. The His_6-tagged proteins were eluted with buffer B^{His} containing 100 mM HEPES, 500 mM NaCl, 0.5 mM TCEP, 300-400 mM imidazole. Eluted fractions were incubated o/n with His-HRV-3C protease at 4°C while dialysing against a large excess of buffer C^{His} containing 50 mM HEPES, 200 mM NaCl, 1 mM DTT. Samples of eluted protein fractions were analysed by SDS-PAGE and relevant fractions were pooled, concentrated

and further purified by ion-exchange and/or SEC. The same procedure was followed with His_6-SUMO-tagged proteins.

2.4.3 Ion-exchange chromatography

Buffers for ion-exchange chromatography (IEX) were prepared by taking into consideration the pI of the proteins. In most cases, after affinity chromatography protein samples were dialysed/diluted into buffer A^{IEX} (50 mM HEPES, 50 mM NaCl, 1 mM DTT) and applied to a pre-equilibrated 5 ml HiTrap HP Q or S column or a 1 ml / 6 ml Resource Q/S column or a Mono Q/S 5/50 GL connected to an ÄKTA Prime or Purifier system (all from GE Healthcare). Proteins were generally eluted with a 1M NaCl gradient over 20 CVs. Samples of eluted protein fractions were analysed by SDS-PAGE and relevant fractions were pooled, concentrated and further purified by size-exclusion chromatography.

2.4.4 Size-exclusion chromatography

Size-exclusion chromatography (SEC) was carried out on all protein samples as a final purification step to remove high-molecular weight contaminants, aggregated species but also smaller peptides (His_6- or Strep-II-Tag) or small molecules such as salts. In general, proteins were concentrated to 5 or 2 ml and applied to either a Superdex-75 or a Superdex-200 (16/60 or 26/60) column (GE Healthcare), depending on size and amount of protein. SEC columns were connected to an ÄKTA Prime and pre-equilibrated in buffer (50 mM MES or HEPES or Tris pH 6-8 (depending on protein pI), 150 mM NaCl, and 1 mM DTT). Relevant fractions were analysed by SDS-PAGE, pooled, concentrated and stored.

2.5 Insect cell expression and purification of full-length TRIM25

Full-length TRIM25 (TRIM25-FL) was expressed and purified from insect cells using the following protocol. TRIM25-FL was cloned into pIEX-Bac3 vector (Merck Millipore) with an N-terminal His_{10}-tag and an HRV 3C protease cleavage site using LIC cloning strategy. Protein was expressed in Sf9 insect cells using a protocol established and performed by Mr Evangelos Christodoulou (The Francis Crick Institute). Cells from 2.1 L of culture were resuspended in lysis buffer (100 mM HEPES, pH 7.0, 500 mM NaCl, 5% (v/v) glycerol, 1 mM TCEP, 20 mM Imidazole, 10 mM $MgCl_2$), supplemented with 1 mM PMSF, 2 tablets of EDTA-

free protease inhibitor cocktail tablets, and 25 units/mL Benzonase nuclease (Sigma-Aldrich). Cells were lysed by sonication and debris was removed by centrifugation (55,000 g for 45 min at 4°C). The supernatant was incubated with 5 mL of TALON superflow resin (GE Healthcare) for 3 h on a rocker at 4°C. The resin was washed extensively with wash buffer (100 mM HEPES, pH 7.0, 500 mM NaCl, 10% (v/v) glycerol, 1 mM TCEP, 40 mM Imidazole). Bound protein was eluted in wash buffer containing 300 mM Imidazole in a total volume of 5 mL and incubated with HRV-3C to remove the His_{10}-tag. The protein was purified to homogeneity on a HiLoad 16/600 Superdex 200 gel filtration column in size-exclusion buffer (50 mM HEPES, pH 7.0, 100 mM NaCl, 1 mM DTT). Centrifugal concentration of this protein resulted in aggregation and yield reduction and alternative methods were pursued: protein-containing fractions were diluted in buffer containing 50 mM HEPES pH 7.0, 50 mM NaCl, 1 mM DTT and applied to a 1 ml SP FF IEX column (GE Healthcare) as a means of protein concentration. Protein was eluted in buffer containing 50 mM HEPES pH 7.0, 300 mM NaCl, 1 mM DTT and flash-frozen in liquid nitrogen and stored at -80°C. The highest achieved concentration was ~2.5 mg/ml and typical overall yield was 1.35 mg/L of culture.

2.6 SDS-PAGE electrophoresis

SDS-PAGE (sodium dodecyl sulphate polyacrylamide gel electrophoresis) was used to analyse protein samples. Typically, 10-15 µl of each sample was mixed with 2X NuPAGE LDS Sample buffer and loaded on NuPAGE 4-12% Bis-Tris Novex pre-cast gels (both from Invitrogen). Novex Sharp Stained/Unstained Protein Standards (Invitrogen) were used as a molecular weight marker. Gels were run at 200 V in MES buffer (Invitrogen) for 30-35 min and stained with Coomassie-based InstantBlue protein stain (Expedeon).

2.7 Protein concentration determination

Purified proteins were concentrated using centrifugal concentrators (Sartorius) with appropriate molecular weight cut-off according to the manufacturer's instructions. Protein concentrations were determined by UV absorption spectroscopy on a NanoDrop spectrophotometer (Thermo Fisher Scientific) using the theoretical 280 nm molar extinction coefficients calculated for each construct based on the primary amino acid sequence. The absorbance was measured

between 220-350 nm. Residues containing aromatic side-chains (such as W, Y and F) absorb in the near-UV spectrum (250-350 nm) and the reading at 280 nm was used.

Protein concentration was determined using the Beer-Lambert law:

Equation 2.1: $A = \varepsilon \; C \; L$

where A = absorbance at 280 nm, ε = molar extinction coefficient (M^{-1} cm^{-1}), C = molar protein concentration (M) and L = cell path length (1 cm). Protein extinction coefficients were determined from the primary amino acid sequence using the ExPASy ProtParam tool available online.
All proteins were aliquoted (typically in 10-50 µl aliquots), flash-frozen in liquid nitrogen and stored at -80°C.

2.8 Ubiquitin fluorescence labeling and charging of E2 enzymes

2.8.1 Ub (M1C) Atto647N labelling

To label ubiquitin, Atto647N maleimide dye (Sigma-Aldrich) was used. Atto647N label is modified with a maleimide moiety that reacts with the thiol group of cysteine residues. Wild-type ubiquitin does not have any C residues and therefore M1 was mutated to a C to allow stable labelling. Ub (M1C) was extensively dialysed against degassed buffer containing 50 mM HEPES pH 7.4, 150 mM NaCl, 0.5 mM TCEP in order to remove any label-reactive species (such as “free” thiols from the buffer) and to ensure that the target C of Ub(M1C) is reduced (not forming a disulphide bond). Atto647N maleimide was dissolved in dimethylformamide (DMF) (Sigma-Aldrich), according to the manufacturer’s instructions. The concentration of Atto was determined at 644 nm using NanoDrop spectrophotometer and dilutions (1:100 and 1:1000). Protein was mixed with the fluorescent dye in a 1:2 ratio and incubated in the dark at 25°C for 2 hours. Reaction mixture was passed through a 5 ml Desalting column (GE Healthcare) to remove excess dye and protein-containing fraction was eluted in 2 ml according to the manufacturer’s instructions. The absence of a reducing agent in the reaction buffer allows formation of disulphide bonds in the unlabelled fraction of ubiquitin. Thus, to further purify the labelled protein, the protein mixture was passed onto a pre-equilibrated (in buffer containing 50 mM HEPES, 150 mM

NaCl) S75 16/60 SEC column to separate the labelled protein from cross-linked non-labelled species. Fractions containing the labelled protein were pooled, concentrated to 0.5 mM and stored at -80°C. The final concentration of Atto647N-Ub(M1C) (referred to as Ub_{Atto} or AttoUb throughout this thesis) was determined using the extinction coefficient of Atto647N (250,000 M^{-1} cm^{-1}). Approximately ¾ of the starting protein material was labelled.

2.8.2 E2 charging reactions

The E2~Ub thioester intermediates were produced using a protocol which was previously established in the lab [122, 134]. Briefly, His-Ube1 (1 μM), E2 (UbcH5a or UbcH5c) (250 μM), Ub or Ub^{Atto} (500 μM) and ATP (3 mM) (Sigma-Aldrich) were incubated in reaction buffer containing 50 mM HEPES pH 7.5, 150 mM NaCl, 20 mM $MgCl_2$ for 60 min at 25°C. The E2~Ub thioester-linked intermediate was purified by SEC using a HiLoad 16/60 Sephadex 75 gel filtration column (GE Healthcare) pre-equilibrated in 50 mM HEPES pH 7.5, 150 mM NaCl. Similarly, the isopeptide-linked UbcH5a-Ub used in structural studies was prepared as described previously [91]. In this case, His-Ube1 (1 μM), UbcH5a (S22R/C85K) (200 μM), Ub (300 μM) and ATP (adenosine triphosphate) (3 mM) were incubated in reaction buffer containing 50 mM Tris pH 10, 150 mM NaCl, 20 mM $MgCl_2$ for 16 h at 30°C and subsequently purified by SEC as above. The reaction is performed at pH 10 to allow de-protonation of the lysine and subsequent nucleophilic attack to ubiquitin's Gly76. The S22R mutation prevents E2 "back-side" binding of ubiquitin and enhances crystallization [91].

2.9 In vitro ubiquitination assays

2.9.1 E3 auto-ubiquitination assays

In the absence of the physiological substrate, the rate of E2 discharge on the E3 itself is commonly employed to qualitatively monitor E3 ligase activity. In general, TRIM25 auto-ubiquitination assays were carried out in the presence of 1 μM UBE1 (E1), 2.5-30 μM of the indicated E2, 2.5-30 μM of the various TRIM25 constructs (E3), 100 μM mono-ubiquitin (bovine, Sigma-Aldrich) and 10 mM ATP (Sigma-Aldrich). The reaction buffer contained 50 mM HEPES pH 7.5, 150 mM NaCl and 20 mM $MgCl_2$. All components were mixed together and incubated at the indicated temperature (25-30°C), for the indicated time-points. Samples of 10 μl were taken at set time intervals (e.g. 0, 5, 10, 20, 40, 60 min), mixed 1:1 with

2x NuPAGE LDS Sample buffer (Invitrogen) containing 500 mM DTT and analysed by SDS-PAGE. Timepoint at 0 min indicates the sample taken prior to the addition of ATP.

2.9.2 E2~Ub discharge assays

E3 auto-ubiquitination assays are a useful tool to directly compare how the E3 ligase activity of one construct changes in response to different experimental conditions. On the contrary, comparison of the activity of different E3 constructs, which vary in length and thus contain different number of lysine residues available for modification, is more difficult when auto-ubiquitination assays are used. For this reason, ubiquitin discharge assays with pre-charged E2~Ub (UbcH5a or UbcH5c) were performed with 10 µM UbcH5a~Ub adduct and 4 µM TRIM25 construct in buffer containing 50 mM HEPES pH 7.5, 150 mM NaCl and 50 mM L-lysine. Under these conditions, L-lysine acts as a "pseudo-substrate" and allows monitoring of the E2 discharge rate without being affected by the number of the available lysine residues on the E3. Samples were taken over time with timepoint 0 indicating the sample taken immediately after the addition of the E2~Ub conjugate, on ice to prevent thioester hydrolysis. Samples were analysed by SDS-PAGE and protein were visualised by staining with InstantBlue (Expedeon).

To quantify the effect of longer TRIM25 constructs on the rate of E2~Ub discharge, reactions containing 1 µM UbcH5c~Ub^{Atto} adduct, 4 µM TRIM25 construct and 20 mM L-lysine were incubated at 25°C for up to 30 min, and samples were quenched with 2× SDS sample buffer at the described time intervals and resolved by SDS–PAGE. For quantification by fluorescence detection, gels were scanned with a Storm 869 Scanner and the bands for E2~Ub^{Atto} and Ub^{Atto} were integrated using ImageQuant (both from GE Healthcare). It was not possible to use the ratio of E2~Ub^{Atto}/Ub^{Atto} as a readout as a small portion of ubiquitin was transferred to the E3, especially for longer constructs. The reduction of E2~Ub^{Atto} was plotted over time. Experiments were performed in duplicate (TRIM25-RING mutants) or triplicate (all other TRIM25 constructs).

2.9.3 K63-linked ubiquitin chain formation

Ubiquitination assays with Ubc13/Ube2V1, which mediate the formation of unanchored K63-linked poly-ubiquitin chains were performed with 1 µM E1, 10 µM each Ubc13/Ube2V1, 4 µM TRIM25 construct and 100 µM ubiquitin in buffer containing 50 mM HEPES pH 7.5, 150 mM NaCl, 20 mM $MgCl_2$ and 10 mM ATP. Reactions were incubated at 25°C for up to 30 minutes and samples were quenched with 2x SDS sample buffer at the described time intervals and resolved by SDS-PAGE and stained with InstantBlue (Expedeon).

For quantification, assays were carried out with 0.5 µM E1, 2.5 µM of each Ubc13/Ube2V1, 4 µM TRIM25 construct and 50 µM ubiquitin, supplemented with 1 µM Ub^{Atto}. Gels were scanned and the bands for free Ub^{Atto} integrated. Experiments were performed in triplicate.

2.9.4 RIG-I ubiquitination assays

In vitro substrate ubiquitination assays were performed in two ways, either in the presence of UbcH5 or Ubc13 using two procedures detailed below.

In the case of UbcH5, RIG-I ubiquitination experiments were performed using a pre-charged UbcH5c~Ub^{Atto} conjugate (Ub^{Atto} labelling and UbcH5c charging as described above in section 2.8). Single turnover reactions were performed to avoid unanchored chain formation as seen in previous assays with UbcH5 and TRIM25. Each reaction was set up with 4 µM of UbcH5c~Ub^{Atto}, 0.5 µM TRIM25-FL, 20 µM RIG-I-2CARD and 0, 40 or 100 µM of different NS1 mutants/constructs (NS1-RBD, NS1-ED, NS1-FL (R38A/K41A/W187A or W187A)) in buffer containing 50 mM HEPES pH 7.5, 150 mM NaCl and 20 mM $MgCl_2$. As control, a reaction without RIG-I-2CARD and NS1 was set up. Further control reactions include TRIM25-FL and RIG-I-2CARD in the absence of NS1. These were used to set a baseline for TRIM25-FL-mediated RIG-I-2CARD ubiquitination. Given that some NS1 constructs (FL and ED) were ubiquitinated in the presence of TRIM25-FL, control reactions with TRIM25-FL and NS1 were performed (in the absence of RIG-I-2CARD). The reactions were monitored over 30 min. Samples were taken at the indicated time points (0 and 30 min). Time point 0 indicates the sample taken immediately after the addition of UbcH5c~Ub^{Atto}, while the reaction was on ice. Subsequently the reactions were incubated at 30˚C. Each sample was treated with loading dye (with DTT) followed by SDS-PAGE analysis. SDS-PAGE was scanned at 635 nm wavelength (which is the Atto647N emission

wavelength). The band corresponding to RIG-I-2CARD-AttoUb$_1$ was integrated and was plotted as the average of experimental duplicates (± s.d.).

RIG-I-2CARD ubiquitination reactions with Ubc13 and TRIM25 were performed with 0.5 µM His-Ube, 5 µM Ubc13 (K92A to supress E2 auto-ubiquitination [93]), 0.5 µM TRIM25-FL, 20 µM RIG-I-2CARD, 1 µM Ub^{atto} and 0 or 100 µM NS1 constructs/mutants (NS1-RBD, NS1-ED, NS1-FL (R38A/K41A/W187A or W187A)) in buffer containing 50 mM HEPES pH 7.5, 150 mM NaCl, 20 mM $MgCl_2$ and 10 mM ATP. As a negative control, a reaction without TRIM25 was set up. In the presence of TRIM25 and Ubc13, TRIM25 was auto-ubiquitinated (positive control). In the presence of TRIM25-FL and NS1-FL or ED, NS1 is ubiquitinated. A reaction with TRIM25 and RIG-I-2CARD was used to set a baseline for TRIM25-FL-mediated RIG-I-2CARD ubiquitination. The reactions were monitored over 60 min. Samples were taken at the indicated time points (0, 30, 60 min). Time point 0 indicates the sample taken before addition of ATP. The reactions were incubated at 30 ˚C and each sample was treated with loading dye (with DTT) followed by SDS-PAGE analysis. SDS-PAGE was scanned at 635 nm wavelength (which is the Atto647N emission wavelength). The band corresponding to RIG-I-2CARD-AttoUb$_1$ was integrated and was plotted as the average of experimental triplicates (± s.d.). Same SDS-PAGE was also stained with InstantBlue to visualize total protein content.

2.10 Protein-protein interaction analysis and visualization

2.10.1 Analytical size-exclusion chromatography

To test if E2~Ub binding to the TRIM25-RING domain stabilizes RING dimerization as described in chapter 3, the samples of UbcH5c-Ub, TRIM25-RING and a covalently linked RING dimer (referred to as TRIM25R-Li-R and used as control) were subjected to analytical size-exclusion chromatography (SEC). Samples of TRIM25R, TRIM25-R-Li-R and UbcH5c-Ub were run individually as controls followed by TRIM25R/UbcH5-Ub and TRIM25R-Li-R/UbcH5c-Ub complexes. 100 µl of each sample at a concentration of 500 µM was applied to an S75 10/300 GL column (GE Healthcare) pre-equilibrated in buffer containing 50 mM HEPES, 150 mM NaCl, 0.5 mM and 0.5 mM TCEP and run at a flow rate of 0.5 ml/min in an AKTA purifier (GE Healthcare). The applied concentration of the sample is diluted ~10-fold while on the SEC column.

2.10.2 Pull-down experiments

To analyse the interaction between TRIM25 and NS1 (described in chapter 4), Strep-tag II-tagged pull-down experiments were performed in 200 µl pull-down buffer (50 mM HEPES pH 7.5, 150 mM NaCl, 1 mM dithiothreitol (DTT)). StrepTactin (GE Healthcare) beads (40 µl) were incubated for 30 min. with either Strep-tag II-tagged TRIM25-CC (50 µM) or buffer (control) and then further incubated with different NS1 constructs and mutants (200 µM) for 3 h at 4 °C with gentle agitation. Beads were transferred to mini spin columns (Generon) and washed 8 times with 100 µl pull-down buffer. Beads were incubated for 10 min and eluted in pull-down buffer containing 2.5 mM desthiobiotin (IBA). Samples were analysed by SDS-PAGE. The bands for Strep-tag II-TRIM25-CC (24.5 kDa) and NS1-FL (26.1 kDa) are not well-resolved by SDS-PAGE and were thus immunoblotted using anti-NS1. The only commercially available anti-NS1 antibody specific for strain A/Puerto Rico/8/1934 I had access to, is a monoclonal antibody raised against an epitope mapping to the N-terminal domain of NS1 (sc-130568 HRP, Santa Cruz Biotechnology) and is thus not suitable for detecting NS1-ED. The size of NS1-ED (16.8 kDa) differs sufficiently from that of TRIM25-CC and it was thus stained with InstantBlue (Expedeon) for analysis. Input represents sample taken prior to bead-washing with pull-down buffer.

2.10.3 Western Blotting

A (10x) filtered stock TBS buffer containing 24.23 g Trizma HCl pH 7.6, 80.06 g NaCl, in 1L dH_2O was prepared; a working TBST buffer containing 100 mL TBS in 900 mL dH_2O and 1 mL Tween 20 (final concentration 0.1%) was used.

Protein bands were transferred to a polyvinylidene difluoride (PVDF) membrane under dry transfer conditions, using iBlot equipment (Invitrogen) according to manufacturer's instructions. After the transfer, membrane was briefly washed with TBST buffer. Blocking of the membrane was done for 1h at room temperature (RT) with TBST + 5% w/v milk. Different antibody dilutions and incubation times were tested to obtain the best results. A 1:500 v/v dilution of the anti-NS1 (sc-130568 HRP, Santa Cruz Biotechnology) in TBST + 5% milk (i.e. 80 µL in 40 mL) and incubation for 3h at RT was the optimised condition used for this antibody. Subsequently, the blotted membrane was washed four times in TBST for 20 min at RT to remove antibody excess. In this case, anti-NS1 was already conjugated to horseradish peroxidase enzyme (HRP) so there was no

need for incubation with a secondary antibody. Enhanced chemiluminescence (ECL) was used to visualize the protein bands on an Imagequant 600 RGB (GE Healthcare).

2.11 Biophysical analysis of proteins

2.11.1 Circular dichroism (CD) spectroscopy

Circular dichroism (CD) spectroscopy is a technique based on the absorption of circularly polarized light by chiral/achiral molecules in an asymmetric environment which can be used to determine the presence of secondary structure in proteins in solution. Proteins were prepared at a concentration of 0.15 mg/ml in 50 mM PBS (phosphate buffered saline) buffer. CD measurements were performed using a Jasco J-715 spectropolarimeter. All spectra were corrected for buffer signals. Far-UV CD was used to study secondary structure content and samples were scanned from 260 nm to 195 nm at 25°C, using a 2 mm path length quartz cuvette and the acquired spectra were used to estimate the secondary structure content of the target protein. The final spectra were averages of 20 separate scans. Data collection and analysis were performed with the help of Dr Simone Kunzelmann and Dr Laura Masino and the results were analysed using software written by Dr Steve Martin (The Francis Crick Institute).

The recorded intensities (S, in millidegrees) for far-UV can be converted to Δεmrw according to the:

Equation 2.2: $\Delta\varepsilon mrw = S \; mrw / (3290 \; C_{mg/ml} \times L)$

Where:
Δεmrw - mean residue CD extinction coefficient
S: CD signal (in millidegrees)
mrw: mean residue weight (Da) = (molecular weight M_w) / (number of peptide bonds N)
$C_{mg/ml}$: concentration (in mg/ml)
L: path length (in cm)

2.11.2 Thermofluor

ThermoFluor assay is a temperature-based assay which can be used to determine the thermal stability of a protein in different conditions such as pH and NaCl concentration [255-257]. Here, 5µg/well of $TRIM25_{RBCC-S}$ were mixed with 100 mM of the condition of interest from Slice pH screen (Hampton Research), 150-1000 mM NaCl, 2.5 µl of 10x SYPRO Orange dye (Invitrogen) and balanced with H_2O to a total volume of 25 µl/well. As the temperature increases from 25°C to 95°C in 0.5°C increments, $TRIM25_{RBCC-S}$ unfolds and SYPRO Orange binds to hydrophobic patches/denatured protein/molten globules and fluoresces. For data analysis, the fluorescence intensity is plotted as a function of temperature. The ideal resulting curve is sigmoidal and can be used to estimate the melting temperature (T_m) of the protein of interest, which corresponds to the midpoint of the transition curve. The temperature increments and fluorescence monitoring are done using a qPCR machine (Stratagene Mx3005P). Data analysis and T_m calculations were performed in Excel (Microsoft).

2.11.3 SEC-MALLS

Size-exclusion chromatography coupled to multi-angle laser light scattering (SEC-MALLS) is a technique which allows determination of the absolute molecular mass of a molecule during analytical gel filtration and is independent of shape and therefore well-suited to the determination of the oligomeric state of proteins. MALLS is a type of static light scattering in which an incident laser beam (light) is scattered as it passes through a solution due to particles (protein). The time-averaged intensity of this scattered light is proportional to the molar mass of the scattering particle. The light scattering varies significantly with angle and hence MALLS data are collected at several angles to the incident laser beam [258-260]. Three detectors are employed, one for light scattering (LS), one for absorbance (UV) and one for refractive index (RI). RI detector measures the refraction of light as it passes through the protein solution and allows determination of the concentration of the sample independently of UV absorbance. The applied concentration of the sample is diluted ~10-fold while on the SEC column. For SEC-MALLS analysis, 120 µl of filtered sample at a range of concentrations (e.g. 0.3 mg/ml to 16 mg/ml) were applied to either an S75 or S200 10/300 GL column (GE Healthcare) attached to a Jasco HPLC pre-equilibrated in buffer containing 50 mM HEPES, 150 mM NaCl, 0.5 mM TCEP

and 3 mM NaN_3 and run at a flow rate of 0.5-1 ml/min. Scattered light intensity of the eluent was recorded at 16 angles using a DAWN-HELEOS laser photometer (Wyatt Technology). The protein concentration of the eluent was determined from the refractive index RI(n) change (dn/dc=0.186), where c is the solute concentration, using an OPTILAB-rEX differential refractometer (Wyatt Technology). Average molecular mass and poly-dispersity of samples contained in the chromatographic peaks were determined using the ASTRA software version 6 (Wyatt Technology). Data collection and analysis were performed with the help of Dr Ian Taylor (The Francis Crick Institute).

2.11.4 NMR spectroscopy

Data collection and analysis were performed by Dr Diego Esposito (The Francis Crick Institute). All spectra for TRIM25-RING were recorded at 25 °C on Bruker AVANCE spectrometers operating at 14.1 T, 16.5 T and 18.8 T in NMR buffer (20 mM HEPES, pH 7.5, 100 mM NaCl, 0.5 mM TCEP, 5% D_2O). Data were processed with NMRPipe/NMRDRAW and analysed with CCPN software [261, 262]. ^{15}N Relaxation Measurements and ^{1}H-^{15}N heteronuclear NOE were collected with standard methods previously described [263]. R1 and R2 values were determined for each residue by fitting an exponential decay to the peak intensity of data collected in an interleaved manner to minimize time dependent temperature or stability effects with delay times in random sequence. T1 longitudinal recovery delays were set to 10, 100, 200, 400, 600, 800, 1200 and 1600 msec. T2 transverse recovery delays were set to 8, 16, 24, 40, 56, 80, 104 and 128 msec. In each case the error was determined from the fit according to a procedure implemented in CCPN Analysis. Residues were excluded in which overlap in the data precluded accurate measurement of the peak intensity and where the value of heteronuclear NOE (calculated from the ratio [Peak $Intensity_{saturated}$]/[Peak $Instensity_{unsaturated}$]), indicative of local motion or chemical exchange, was below 0.7. Isotropic correlation times were determined using the programme TENSOR2 [264]. Isotropic correlation time projections were obtained by the program HYDRONMR [265].

2.11.5 SAXS Data Collection and Analysis

Macromolecular small-angle X-ray scattering (SAXS) is a technique widely used to obtain low-resolution information of proteins in solution [266-268]. In most

cases, SAXS is complementary to high resolution methods (such as NMR and X-ray crystallography or recently even cryo-EM) and further biochemical analysis. Its main advantage is that information can be obtained about the size, shape, oligomeric state and flexibility of multi-domain proteins using a non-labelled sample in close-to-native conditions. A low resolution three-dimensional molecular "envelope" can be reconstructed *ab initio*, i.e. without any prior information which might introduce model bias. Compared to X-ray crystallography (see also section 2.12), SAXS can be performed on non-crystalline objects including proteins. A typical protein SAXS experiment includes exposing a protein in solution (can be in a cell or in-flow) to a synchrotron-produced high-intensity, monochromatic (same frequency) and collimated (same direction of travel) X-ray beam. X-ray photons interact with the atoms of the protein which causes them to scatter and this scattering pattern is recorded using an X-ray detector. The measured scattered intensity of each photon (I) depends on the scattering angle (2θ). Scattering intensities are recorded for both the protein-containing buffer and the protein sample, with the former subtracted from the latter to remove background scattering "noise" and allow data processing. The resulting scattering profile is expressed as a function of the amplitude of the scattering vector (referred to as momentum transfer (q) and measured in nm^{-1} or $Å^{-1}$) as described by the:

Equation 2.3: $q=4\pi \sin\theta/\lambda$

where λ is the wavelength (nm or Å) of the incident radiation and 2θ is the scattering angle. The wavelength (λ) is fixed and scattering angle θ is small (typically <3˚) and thus I(q)/q depends only on the scattering angle [267]. The momentum transfer q is proportional to the scattering from a single particle averaged over all orientations as well as to the protein concentration. Geometrical parameters of the particle such as the molecular mass (MM) and its radius of gyration (R_g) can be derived from analysis of the slope produced in Guinier plot which is described by the:

Equation 2.4: $\ln(I(q))/q^2$

Additionally, the volume (V) and surface (S) of a particle, obtained using the

Porod plot, provide information about the oligomeric state of a protein. The D_{max} value, calculated by the Fourier transformed SAXS pattern, expresses the maximum distance within the analyzed particle and the Kratky plot expressed by the:

Equation 2.5: $(I(q) \times q)/q^2$

provides further information about the folding state of the protein but also about the flexibility of multi-domain macromolecules. All of the above parameters provide useful information about the overall state of the protein analysed (i.e. folding, aggregation, oligomeric state) and should be critically judged and cross-examined by other biophysical techniques if possible. For well-behaved and monodisperse samples, the scattering profile can be used to reconstruct molecular envelopes *ab initio*.

Synchrotron SAXS batch data for TRIM25-R, RB1 and RB1B2 constructs were collected at the Diamond Light Source on beamline B21. SEC-SAXS data for the TRIM25-RBCC construct were collected at the SWING beamline, SOLEIL. The Diamond data were recorded on a Pilatus 2M detector with a fixed camera length of 3.9 m and 12.4 keV energy allowing the collection of a momentum transfer range, q between 0.015-0.3 $Å^{-1}$. All samples were extensively dialysed against the background buffer and measured for three construct dilutions in the concentration range that gave a monodisperse molecular weight according to SEC-MALLS. The data at SOLEIL were recorded over a momentum transfer range of 0.01-0.60 $Å^{-1}$. TRIM25-RBCC constructs, which tends to oligomerize was injected at 2.5 mg/mL onto an SEC-3 300 Å Agilent column and eluted at a flow rate of 0.2 mg/mL at 15 °C. Frames were collected during the fractionation of the protein. Frames collected before the void volume were averaged and subtracted from the signal of the elution profile to account for background scattering. Data reduction, subtraction and averaging were performed with the help of Dr Diego Esposito (The Francis Crick Institute) using the software FOXTROT (SOLEIL).

The scattering curves were analysed using the programs Scatter and the package ATSAS to obtain the radius of gyration (Rg), the maximum particle dimension (Dmax), the excluded particle volume (Vp), the cross-sectional radius and the pair distribution function (P(r)) [269]. The molecular mass of the scattering

particles were estimated using a method described by Rambo [270]. Low resolution three-dimensional *ab initio* models for the different constructs of TRIM25 (with applied P2 symmetry for the dimeric constructs) were generated by program DAMMIF, averaging the results of 25 independent runs using the programs SUPCOMB and DAMAVER [271]. The SAXS-derived dummy atoms models were rendered with Pymol (Schrödinger, LLC).

2.12 Protein crystallization and structure determination

To date, X-ray crystallography is the most widely used technique to obtain high resolution structural information of proteins [272, 273]. Contrary to other structural techniques (NMR or cryo-electron microscopy) which can be restricted by the size of the macromolecule of interest, X-ray crystallography has no such limitations. The requirements for this technique however may restrict the chances of success: a highly pure and monodisperse sample is required in large quantities (~10 mg/ml) which may not always be possible. A major bottleneck for the acquisition of a protein structure using X-ray crystallography is that the protein needs to form a crystal. A protein crystal is composed of protein molecules which are arranged in a lattice of identical unit cells (described by three dimensions a, b and c and three inter-axial angles α, β and γ). Crystal symmetry operations can be applied to the minimal asymmetric unit to generate the unit cell and thus the whole crystal.

2.12.1 Crystallization experiments

Crystallization of a protein may only occur when its concentration is greater than the limit of its solubility (a state referred to as super-saturation). In this state, the sample may precipitate and thus not crystallize. In cases where precipitation does not occur, crystal nuclei can be formed (nucleation) and then the crystal lattice expands (crystal growth). The early stages of this process are critical and for this reason different precipitants (varying pH, salt concentration, additives, polymers and organic solvents) and protein concentrations are normally tested. Protein crystallization trials were performed using the vapour diffusion method. In this technique, the protein is mixed with a precipitant solution in a crystallization drop located adjacent to a reservoir containing a larger and more concentrated amount of precipitant. The well is sealed and the two components are allowed to equilibrate over time. This leads to a slow diffusion of water vapour from the

protein solution, which is absorbed by the precipitant reservoir, driving the protein/precipitant solution into a supersaturated state that favours protein nucleation and crystallogenesis. The nucleation depletes the protein in the crystallization droplet and leads to the formation of protein crystals which can be used for X-ray diffraction analysis.

Initial crystallization experiments for TRIM25 and NS1 were carried out on an Oryx 6 or NanoOryx (Douglas Instruments) or Mosquito LCP (TTP Labtech) crystallization robot using the sitting-drop vapour diffusion method (with 100 nl of protein solution and 100 nl of precipitant solution) in standard 96-well polystyrene MRC plates (Molecular Dimensions) containing 60-75 µl of precipitant solution. Crystallization conditions were screened using a variety of commercially available and 'in-house'-produced screens. In addition, optimization experiments were also set up manually using the hanging drop vapour diffusion method in 24- or 48-well pre-greased plates (Qiagen or Hampton Research) with 1 µl of protein solution mixed with 1 µl of precipitant solution on a siliconized coverslip. Each coverslip was turned around and used to seal the reservoir containing 100-200 µl of precipitant solution. In order to obtain crystals large enough for X-ray diffraction analysis, different parameters were altered such as incubation temperature (4°C or 18°C), pH, precipitant concentration and protein concentration (ranging from 3 to 10 mg/ml depending on the size and solubility of the construct). Variable screens and pipetting schemes were manually prepared in Excel (Microsoft Office). Crystallization procedures for protein crystals used in structure determination are described in detail in Chapters 3 and 4.

2.12.2 Crystal harvesting and data collection

Collection of diffraction data is routinely performed from cryo-protected protein crystals. Crystals were harvested from the crystallization drop under a microscope. A single crystal was scooped out of the crystallization drop using an appropriately sized nylon cryo-loop (Hampton Research or MiTeGen) attached to a steel pin with a magnetic base. The size of the cryo-loop must be as small as possible to avoid excess of crystallization buffer but big enough to fit the crystal. The captured crystal is then cryo-protected by soaking for 30-60 sec into a 2 µl solution composed of an appropriate cryo-protectant and the crystallization reservoir's solution. This is necessary for two reasons: 1) to avoid formation of crystalline ice around the cryo-loop upon freezing and 2) to reduce radiation

damage of the crystallized protein during data collection, both of which massively affect the diffraction quality of the crystal. Glycerol, low molecular weight PEG (polyethylene glycol) and sugars are some of the most commonly used cryo-protectants and the effect of different percentages on the diffraction behaviour was tested (may vary from 10-30%). Cryo-protected crystals were then flash-cooled by dipping into liquid nitrogen and stored into a pre-cooled cryo puck for transportation to the synchrotron for diffraction data collection.

Synchrotrons produce high intensity X-ray beamlines necessary for macromolecular crystallography and structure determination. Diffraction data for all crystals described in this study were collected in Diamond Light Source following unique data collection strategies for each crystal. All data were collected on beamline IO4: TRIM25-RING/UbcH5a-Ub (λ = 1.2829 Å) and TRIM25-CC/NS1-ED and TRIM25-CC/NS1-FL (both at λ = 0.9795 Å). Beamline IO4 is equipped with a direct Pilatus 6M-F detector (Dectris) used for image collection.

2.12.3 Data processing and reduction

Diffraction images contain information about the position and intensity of the observed spots (also known as reflections). A sub-set of these reflections is indexed using programs such as iMOSFLM [274] and XDS [275]. Indexing is a procedure in which the reflections are assigned to their Miller indices (h,k,l) and allows the calculation of the unit cell dimensions and subsequent assignment of a potential space group on the crystal. Then, the intensities of all measured reflections are integrated in a process in which the intensities of each reflection are averaged. Subsequently, scaling of integrated data allows normalization of all reflections in relation to each other and signal-to-noise ratio calculation. Next, symmetry related and partial reflections dispersed over different images (frames) are combined in a process referred to as merging. Data integration, scaling and merging were performed using AIMLESS program [276] which is available through the CCP4 software suite [277]. In all cases, 5% of randomly assigned data was flagged as an R_{free} value and will be further explained in section 2.12.6.

2.12.4 Experimental phasing

An X-ray beam is an electromagnetic wave characterized by properties including the wavelength, the wave amplitude and the phase. Diffraction images contain information about the measured intensity of a given reflection which allows the

calculation of the wave amplitude. The wavelength of the X-ray is on the order of 0.1 nm (1Å) which is comparable with the spacing between protein atoms. However, in order to solve the macromolecular crystal structure, determining the phase of the corresponding electromagnetic wave is also crucial. The phase of the X-ray cannot be measured directly and other methods are employed to overcome the so-called “phase problem” in X-ray crystallography [278].

In cases when homologous structural information is not available, experimental phasing is required to solve the crystal structure. The presence of Zn^{2+} or other heavy atoms in the structure allows for anomalous diffraction. The structure of TRIM25-RING/UbcH5a-Ub was solved by single anomalous dispersion (SAD) using the Zn^{2+} atom at 2.34 Å resolution. A single dataset collected at the Zn^{2+} absorption edge (λ = 1.2829 Å) was used for heavy-atom search, density modification and initial model building which were performed using the automated pipeline in Phenix AutoSol [279]. The resulted electron density maps were examined in COOT [280, 281] and further improved by an iterative process of manual model building and refinement further discussed in section 2.12.6. Details of this structure are presented and discussed on chapter 3.

2.12.5 Molecular replacement

The phase problem for a structure with available structural homologous models can be solved by molecular replacement (MR) [282]. Structural similarity between the target protein and the replacement model is key for successful MR. In most cases, structural homology can be assumed when the primary amino acid sequence identity is over 40%. Programs like Chainsaw in CCP4 software suite [283] may be used to remove side chains of amino acids or flexible loop regions that are not conserved between the target and MR model. A Fourier transformation of the measured intensities is used to obtain a Patterson map, which is then compared to the Patterson map from the replacement model and is closely correlated if MR is successful [284]. The correct position and orientation of the molecule is determined by rotational and translational operations performed automatically in Phaser and the phase problem is resolved [285]. Among other parameters which need to be considered, Z-scores, log likelihood gain (LLG) scores and number of solutions give an indication whether a MR operation is successful. Generally, a translation function Z-score (TFZ) above 8 and a minimal number of solutions (i.e. the less solutions indicate higher

confidence) might indicate a probable phase solution using MR. Nevertheless, the derived electron density maps need to be critically examined in COOT [280, 281] after each operation. MR was used to solve the structures of TRIM25-CC/NS1-ED and TRIM25-CC/NS1-FL described in chapter 4.

2.12.6 Model building and refinement

The initial electron density map obtained after phase determination is usually of low quality and in most cases the model is incomplete. It was thus necessary to perform an iterative process of polypeptide chain building to further improve the model and electron density by many rounds of refinement.

Model building was performed automatically in Phenix Autobuild software [286] or manually in COOT [280, 281]. Restraints on the peptide bond length, bond angles, torsion angles and individual Ramachandran restraints were employed to ensure that the model does not deviate from the ideal geometry typically found in proteins. Measure of such inconsistencies can be given by the root mean square deviation (RMSD) between the structural model and the ideal geometrical parameters and the Ramachandran plot which shows local deviation of amino acids from the preferred geometry [287]. In each amino acid, the torsion angle of the N-Cα (Φ) and the Cα-C (Ψ) bond is limited to allowed regions in accordance to steric repulsions which can be observed in the Ramachandran plot. The absence of Ramachandran outliers is a good indication of the quality of the model but in some cases, due to weak electron density these restraints might slightly differ.

Structural refinement was performed using Phenix [288] and Refmac [289] software and applying different parameters including atom coordinates in real space, occupancy and B-factors (temperature factors). Non-crystallographic symmetry restraints can be activated when the asymmetric unit contains more than one copies of the same molecule which leads to improved symmetry of the protein molecules [290]. The experimental phases can be further improved by TLS refinement and rigid body refinement where individual regions of the model are treated as rigid bodies and translational or rotational operations improve the positions of these groups [291]. The use of different refinement strategies varies according to parameters such as the resolution of the experimental data and the number of copies contained in the asymmetric unit and ultimately leads to greater agreement between the structural model and the experimental data. The

convergence of the observed data with the calculated structure can be expressed by the R-factor which is calculated through the

Equation 2.5: $$R = \frac{\sum||Fobs|-|Fcalc||}{\sum|Fobs|}$$

where $|Fobs|$ and $|Fcalc|$ represent the amplitude of the observed and calculated structure factor, respectively.

The R_{work} / R_{free} factors are indicative of the refinement quality of the calculated structure. The R_{work} includes all the reflections that were used during refinement whereas R_{free} excludes reflections which were "flagged" during data processing and were used to calculate the $|Fobs|$. Correct refinement strategies cause decrease of the R values. Consideration of the values of these two R factors throughout refinement prevents over-fitting of the model into the electron density and overall leads to improved agreement of the calculated model with the observed data.

3. Results

Structure and mechanism of TRIM25-RING activation

3.1 Overview

TRIM proteins share a tripartite domain organization: an N-terminal RING (R) domain closely followed by one or two B-box (B) motifs and a coiled coil (CC) region. The presence of the tripartite motif (also referred to as RBCC) is confined to the TRIM family of proteins yet until initiation of this project, its precise functional role remained elusive. In particular it was not known whether each domain of the RBCC operates as a separate functional unit or cooperates with the other domains. Previous work on TRIM proteins was mostly focused on the retroviral restriction factor TRIM5α and indicated that self-association is essential for catalytic activity. To determine the role of the individual domain in self-association and catalytic activity, a systematic analysis on TRIM25 was performed and the results are presented in this chapter. TRIM25 was chosen as it has a crucial role in the anti-viral response.

3.2 TRIM25 constructs

Initial efforts were focused on identifying well-expressed and soluble constructs of TRIM25 containing a) the individual domains of the RBCC motif and b) a combination of all domains of interest (RING, B-Box1,2 and CC) allowing us to examine the role of each domain in TRIM25 self-association and E3 ligase activity. Constructs containing RING (R), RING/B-box1 (RB1), RING/B-box1/2 (RB1B2), B-box1,2/CC (B1B2CC) and CC (CC) were expressed and purified using a two or three-step purification protocol. The yields of these constructs were approximately 2-5 mg per 1L bacterial culture and they could be concentrated up to 4-8 mg/ml (Figure 3.1, lanes 1-5). Additionally, longer constructs which contained a combination of all domains of interest (RING, B-Box1,2 and CC) were pursued. The full-length TRIM25 construct (FL) and a construct containing the tripartite motif (RING, B-box1,2 and CC) plus a C-terminal extension but lacking the PRYSPRY domain (referred to as $RBCC_L$) were cloned and expressed in *E. coli*. The full-length protein was poorly expressed and resulted in very low yield (12 µg per 1L bacterial culture) and degradation of the sample (Figure 3.1, lane 7). Therefore, a baculovirus-based expression system was set up and optimized in order to increase the yield and purity of the full-length protein (described in detail in section 4.11). The TRIM25-$RBCC_L$ construct containing the whole tripartite motif, was well-expressed and could be purified to homogeneity using an optimised three-step purification procedure that resulted in approximately 1 mg of pure protein per 1L bacterial culture (Figure 3.1, lane 6).

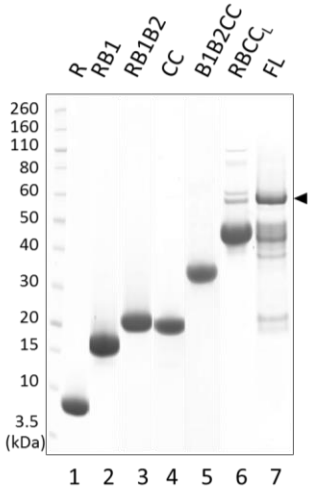

Figure 3.1: Final protein yield and purity of TRIM25 constructs.

The different TRIM25 constructs expressed, purified and used throughout this thesis as assessed by SDS-PAGE. Arrow indicates intact full-length TRIM25 expressed in *E. coli* cells whereas bands below are degraded species.

3.2.1 Additional TRIM25-RBCC constructs

In an effort to further improve the yield and quality of the longer TRIM25-RBCC construct, a number of constructs containing different domain boundaries was generated using a highly efficient ligation independent cloning (LIC) technique and small-scale expression and purification tests were performed. In total, 19 new constructs which contained the tripartite motif of TRIM25 were designed with the C-terminal boundary being either shortened or elongated, in order to examine if this would affect the stability/solubility of the protein (Figure 3.2A). Interestingly, the protein becomes insoluble when the C-terminal boundary is extended towards the PRYSPRY domain and it appears to behave better when the linker spanning between the CC region and the PRYSPRY is removed (Figure 3.2B). Of note, this linker region is predicted to be unstructured and contains a large number of positively charged residues which might interfere with solubility of the protein. During the time that the expression experiments were performed, the structure of the CC region of TRIM25 (a.a. 189-379) was published, suggesting that this linker region was not necessary for the correct folding of this domain (see also section 1.7) [165]. Therefore, it was decided to further examine the construct containing the tripartite motif without the C-terminal linker extension (termed as TRIM25-RBCC$_S$).

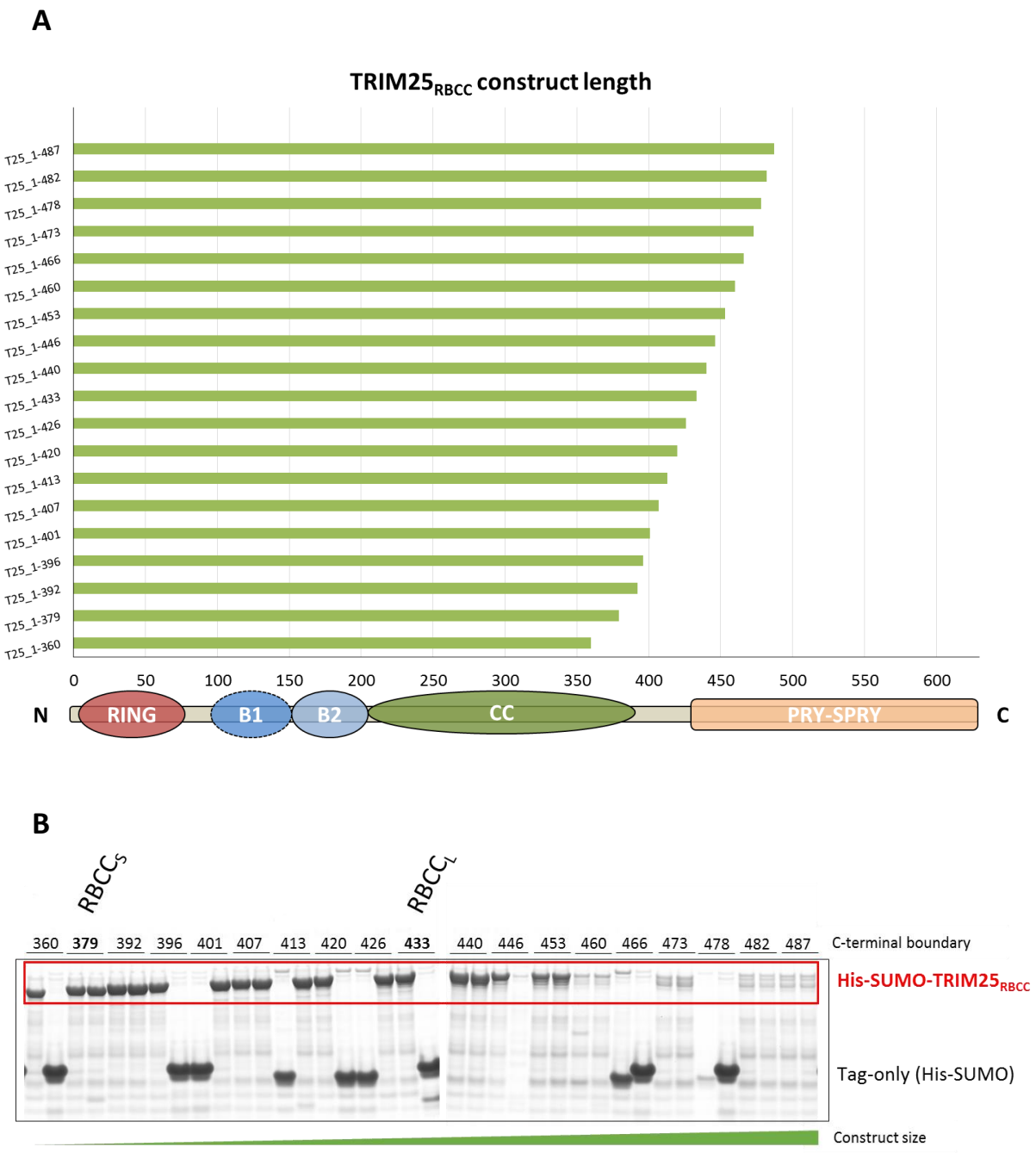

Figure 3.2: TRIM25-RBCC construct optimization.

A) Schematic representation of the TRIM25-RBCC constructs generated by LIC. Different C-terminal boundaries were tested. Genes were cloned in pET-5247 vector expressing a His_6-SUMO-TRIM25 fusion protein. B) LIC-obtained plasmids were transformed in BL21(DE3)GOLD *E. coli* cells and two colonies per construct were picked for analysis. Each colony was grown in 0.5 mL cultures in 48-well blocks with O/N induction at 18°C. Cells were lysed enzymatically; lysate was applied to Ni^{2+} beads in 96-well column plates, followed by wash and elution as His-SUMO-TRIM fusion protein. Negative colonies (i.e. no gene inserted) express His-SUMO as indicated. TRIM25-$RBCC_S$ (a.a. 1-379) and TRIM25-$RBCC_L$ (a.a. 1-433) were chosen for further analysis.

3.2.2 Optimisation of the purification protocol for TRIM25-RBCCs

Initial small-scale purification procedures for TRIM25-RBCCS resulted in a pure and well-behaved protein which however could not be concentrated above 1 mg/ml in the standard purification buffer (50 mM HEPES pH 7.5, 150 mM NaCl, 1 mM DTT) using centrifugal concentrators. Therefore, in order to try and identify a different buffer, pH and NaCl concentrations which might stabilise the protein further, a high-throughput buffer screening experiment was performed (Thermofluor). Thermofluor is a fluorescence-based thermal denaturation assay which utilizes a fluorophore (SYPRO orange) that binds to exposed hydrophobic surfaces of the protein [255-257]. When the protein is correctly folded at low temperatures, small hydrophobic areas are exposed and thus there is low fluorescence signal. Upon an increase in temperature, the protein starts to unfold and hydrophobic patches become exposed, resulting in fluorophore binding and an increase in fluorescence signal. In this way, the effect of different buffers conditions on the protein stability can be assessed.

In this experiment, eight buffers (ranging from pH 5 to pH 9) and four NaCl concentrations (150-1000 mM) resulting in 32 different conditions were tested (Figure 3.3). At pH 5, the protein is unfolded as indicated by the shape of the curve and the high fluorescence signal observed even at 25°C. At pH 6, a typical thermal-shift curve is observed suggesting that the protein is folded up to ~55°C and then unfolds, as indicated by the sharp increase in the fluorescence signal (Figure 3.3). The NaCl concentration does not have an effect on the thermal stability of TRIM25-RBCCS. In buffers with pH range 6.5-8, the protein displayed similar melting-temperature values (average T_m ranging 61-62°C) (Figure 3.3). These values are higher than the ones observed in buffers pH 6, 8.5 and 9, indicating that the protein is more stable at a pH range of 6.5-8. Further analysis and comparison of the thermal-shift spectra obtained for MES pH 6.5, Bis-Tris pH 7, HEPES pH 7.5 and Tricine pH 8 shows that while MES and Bis-Tris buffers show similar transition states and a large increase in the fluorescence units upon thermal unfolding (~ 13000 units max. increase on the Y axis), HEPES and Tricine show smaller increase in fluorescence signal (~ 6000 units max. increase on the Y axis) and broader peaks (Figure 3.3). This observation may be due to thermal unfolding proceeding in multiple steps or the protein being less stable in the HEPES and Tricine buffers tested here. For example, in HEPES pH 7.5, 250 mM NaCl condition (Figure 3.3, red trace), two peaks are observed and this

behaviour can be attributed to different domains unfolding separately or dimerization disruption.

Therefore, I decided to test the effect of MES pH 6.5 on the stability of TRIM25-RBCC$_S$, as in this condition a typical thermal-shift transition state was observed. Protein expression was scaled up to 4L and the buffer-exchange was performed during SEC. Despite this, TRIM25-RBCC$_S$ precipitated during centrifugation-mediated protein concentration and the highest yield achieved was less than 1 mg/ml. In addition, co-concentration was tested with TRIM25-RBCC binding partners including Ubc13, UbcH5-Ub or Ub (these observations are discussed below in detail in section 3.3) (Figure 3.4A). However, this approach did not result in higher concentration of the TRIM25-RBCC$_S$ construct.

It is noteworthy that other constructs containing variable C-termini boundaries were scaled-up and purified but showed no improvement in the final yield. It was therefore decided that all subsequent experiments would be done with TRIM25-RBCC$_L$ which could be concentrated up to 2.5 mg/ml without aggregation issues (Figure 3.4B). The quality of this protein was assessed using CD spectroscopy to determine the presence of secondary structure. The CD spectrum observed is typical of a folded protein which contains α-helices and β-sheets (Figure 3.4C).

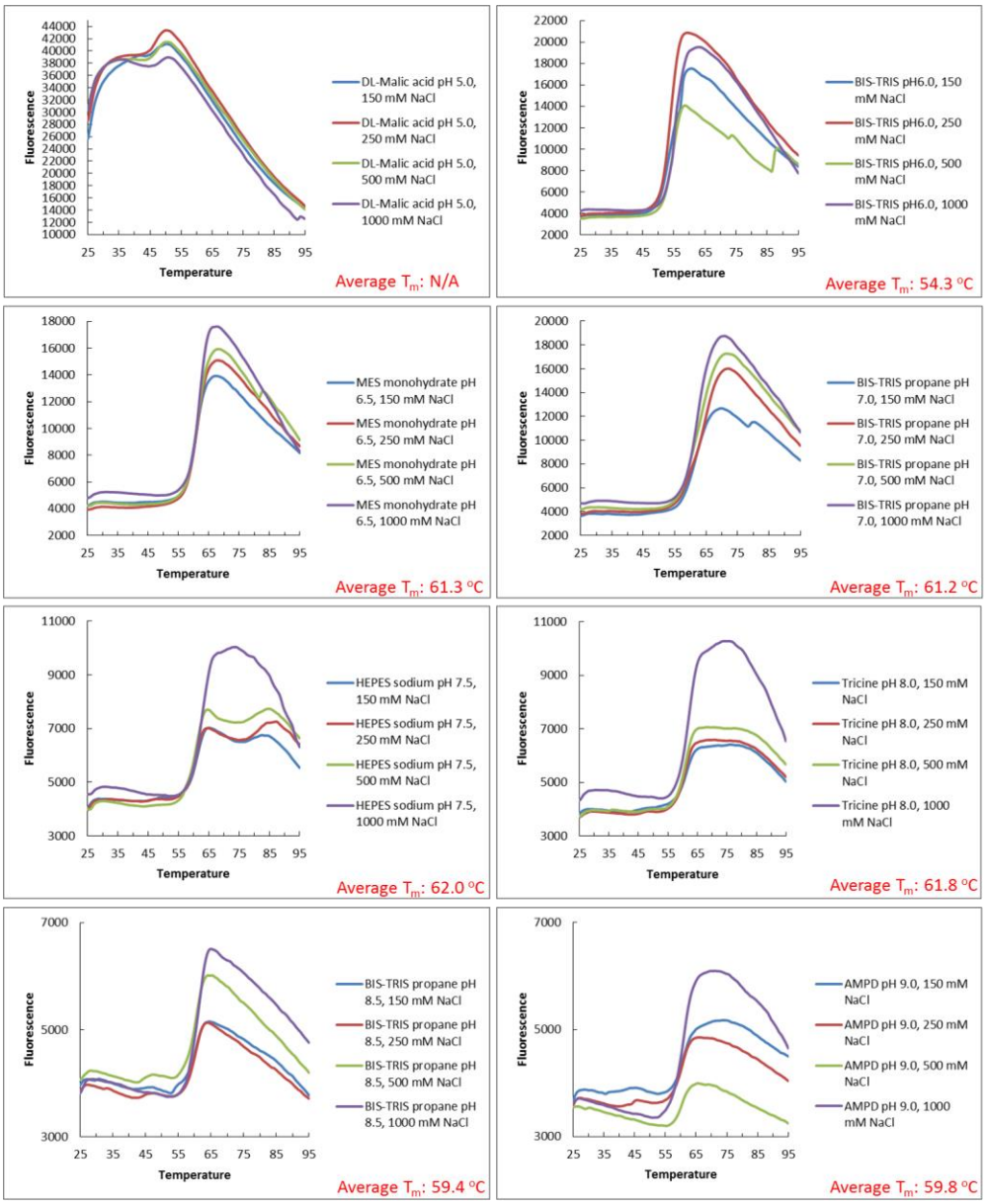

Figure 3.3: Buffer effect on thermal stability of TRIM25-RBCCs.

To identify a buffer that improves protein behaviour, a high-throughput buffer screening experiment was set up to test the effect of eight different buffers (DL-Malic acid pH 5; Bis-Tris propane pH 6, pH 7 and pH 8.5; MES pH 6.5; HEPES pH 7.5; Tricine pH 8; AMPD pH 9). Each buffer was tested with four different NaCl concentrations (150, 250, 500 and 1000 mM) as indicated in each graph. In total, the effect of 32 different buffer conditions on the thermal stability of TRIM25-RBCCS was evaluated. A low fluorescence signal indicates a folded protein. At pH 5, the protein shows a spectrum typical of an unfolded protein. In buffers with pH 6, 8.5 and 9 the TRIM25-RBCCS construct has a melting temperature (T_m) of 54-59°C whereas in buffers with pH 6.5-8 the protein is more stable, with a T_m = ~ 61°C. NaCl concentration does not affect thermal stability of the TRIM25-RBCCS construct. Panel C, D are examples of typical denaturation curves whereas E and F show non-ideal denaturation profiles (non-sigmoidal curves and low fluorescence signal in the transition state).

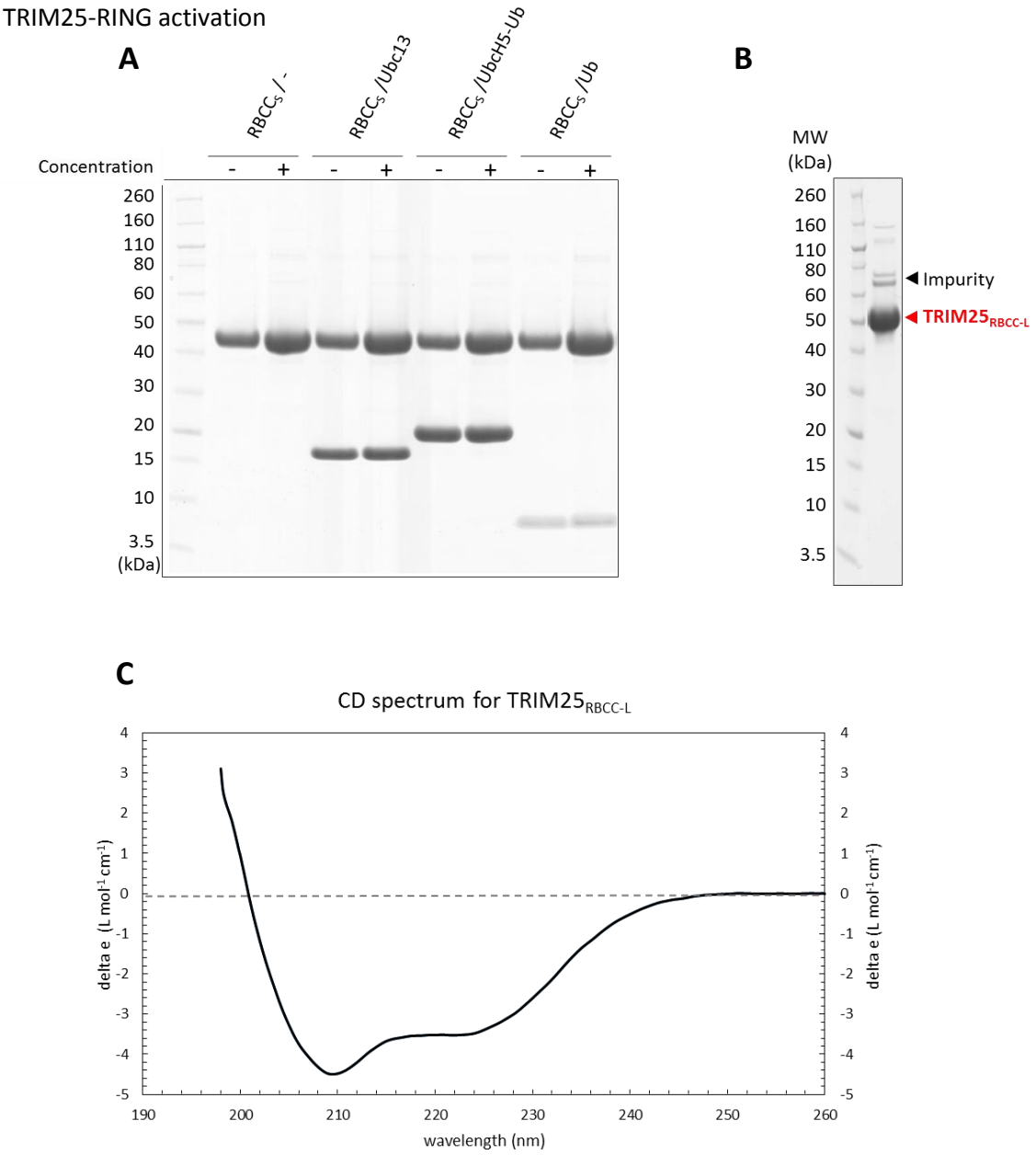

Figure 3.4: Characterization of the TRIM25-RBCC construct.

A) In an effort to examine if interaction partners allows TRIM25-RBCC$_S$ concentration above 1 mg/ml (which is the highest concentration achieved for this protein on its own), co-concentration of TRIM25-RBCC$_S$ with Ubc13, UbcH5-Ub and Ub was tested. TRIM25-RBCC$_S$ was concentrated on its own as control. Samples before and after concentrating were run on an SDS-PAGE to estimate protein concentration. No yield improvement was observed with any of the potential interaction partners. B) Analysis of final yield and purity of the longer RBCC construct (TRIM25-RBCC$_L$) on SDS-PAGE. C) Circular dichroism (CD) qualitative analysis of TRIM25-RBCC$_L$. The far-UV spectrum of TRIM25-RBCC$_L$ at 0.15 mg/ml at 25°C is typical of a folded protein which contains α-helices and β-sheets as indicated by the positive peak at ~200 nm and negative peaks at ~220 nm.

3.3 Assessing the E3 ligase function of TRIM25

Ubiquitination assays were performed to test if the catalytic activity of TRIM25 could be assessed *in vitro*. The ATP-dependent enzymatic cascade was reconstituted using purified E1, E2, TRIM25 as the E3 and ubiquitin. Reactions were incubated over time and samples taken were resolved by SDS-PAGE (Figure 3.5). The TRIM25-RBCC$_L$ construct is active as indicated by multiple bands that appeared over time, corresponding to the molecular weight of TRIM25-RBCC$_L$ conjugated with Ub$_1$, Ub$_2$, Ub$_3$…Ub$_n$. This was coupled to the reduction of the TRIM25-RBCC$_L$ band which indicates that TRIM25 transfers ubiquitin onto itself - a process referred to as auto-ubiquitination (Figure 3.5). Auto-ubiquitination is commonly used as readout of E3 ligase activity, especially when the native substrate of the E3 is not available. In this case, the assays were all performed with the TRIM25-RBCC$_L$ construct which has the C-terminal PRYSPRY domain removed. The PRYSPRY is reported to be the substrate-recruitment domain and it was thus evident that the activity assays at this stage could not involve the physiological substrate of TRIM25, RIG-I and instead had to rely on auto-ubiquitination.

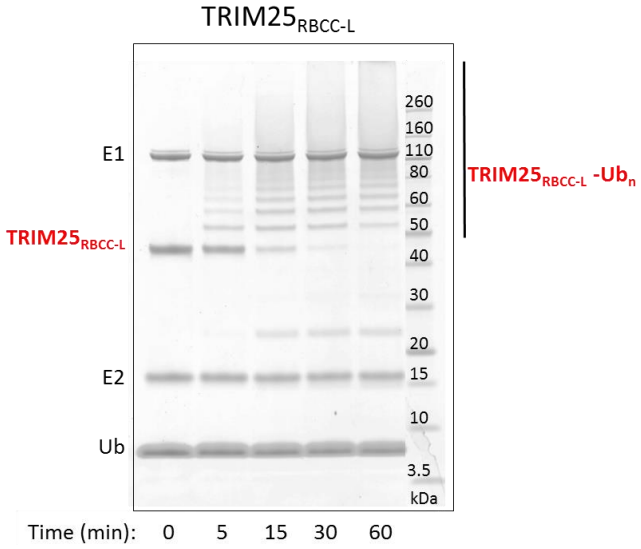

Figure 3.5: TRIM25 ubiquitination assay.

The E3 ubiquitin ligase activity of TRIM25-RBCC$_L$ was tested *in vitro* using purified proteins. 1 µM E1, 5 µM E2, 2.5 µM E3 (TRIM25), 100 µM Ub and 10 mM ATP were incubated at 25 °C over time. Samples removed from the reaction at the indicated time points: 0 (before the addition of ATP), 5, 15, 30 and 60 minutes were analysed by SDS-PAGE. Reduction of the TRIM25-RBCC$_L$ band over time is due to auto-ubiquitination.

3.3.1 TRIM25 has E2 specificity

Ubiquitination assays using UbcH5a and UbcH5c E2 enzymes, which are suggested in the literature to be active with TRIM25 resulted in robust auto-ubiquitination of the E3 ligase (Figure 3.6A,B). TRIM25-RBCC$_L$ was also tested with a number of other E2 ubiquitin-conjugating enzymes available in the lab but appeared to be active only with members of the UbcH5 family (Figure 3.6A-E). No E2-independent Ub conjugation was observed in the presence of E1 and TRIM25-RBCC$_L$ alone (Figure 3.6F).

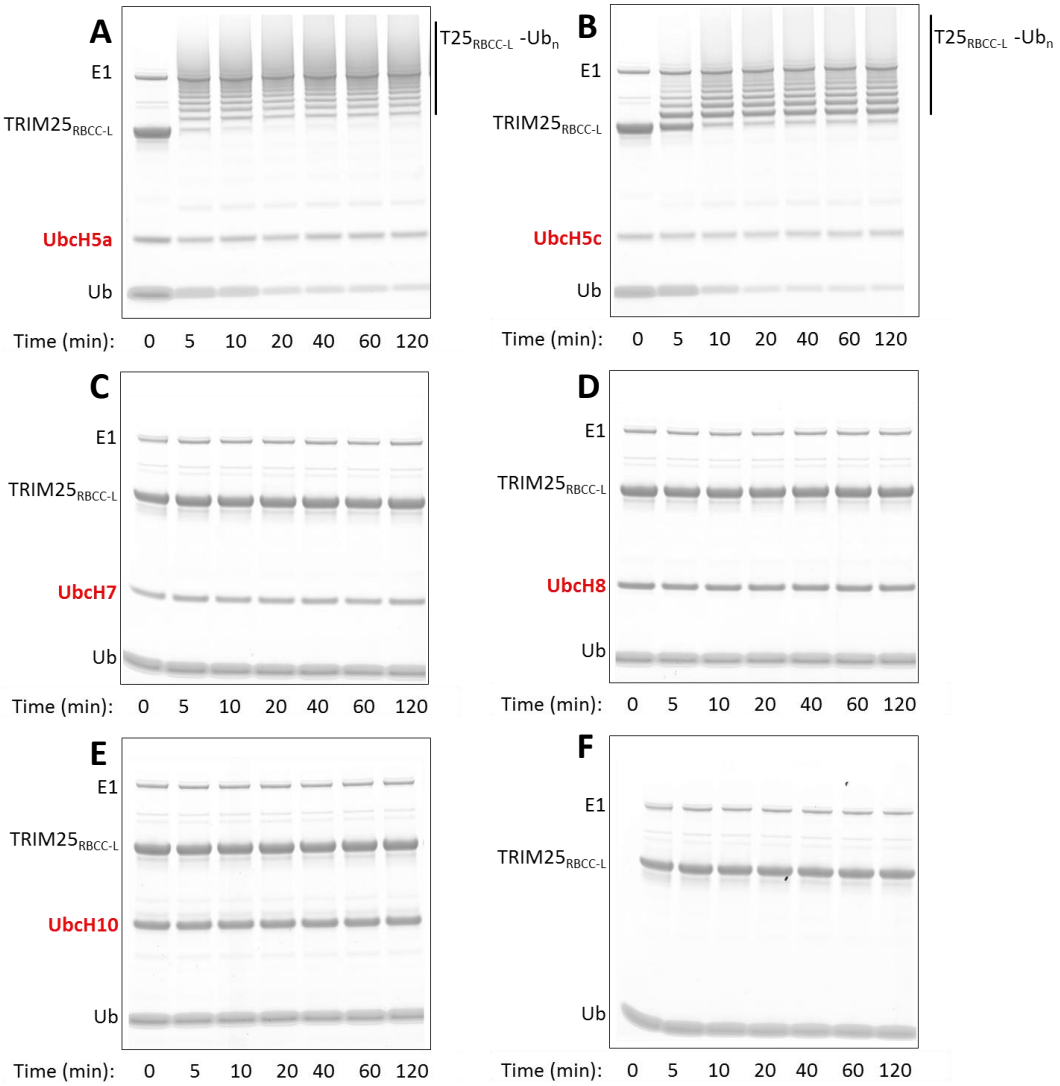

Figure 3.6: TRIM25-RBCC$_L$ has E2 specificity.

In vitro ubiquitination assays with TRIM25-RBCC$_L$ and different E2 enzymes to examine enzymatic activity. The corresponding E2 is A) UbcH5a, B) UbcH5c, C) UbcH7, D) UbcH8, E) UbcH10. As control, no E2 was included in F. Time points: samples at 0 (before the addition of ATP), 5, 10, 20, 40, 60 and 120 min were analysed by SDS-PAGE. Protein concentrations: 1 µM E1, 5 µM E2 (except F), 10 µM E3 and 100 µM Ub.

TRIM25 has been also shown to be active with Ubc13/Ube2V1, a heterodimeric E2. Ubc13/Ube2V1 is a well-characterised E2 complex which is able to synthesize unanchored K63-linked Ub chains even in the absence of an E3 ligase (see also section 1.5.2) (Figure 3.7A). Ubc13 has the active site cysteine and forms a thioester bond with activated ubiquitin (donor) whereas Ube2V1 is inactive on its own. Instead, Ube2V1 binds and positions K63 of another ubiquitin (acceptor) for nucleophilic attack on the thioester formed between Ubc13 and the donor ubiquitin [71, 93]. Notably, in the presence of TRIM25-RBCC$_L$, the formation of unanchored Ub chains proceeds much more quickly, whereas no auto-ubiquitination of TRIM25-RBCC$_L$ takes place (Figure 3.7B).

Interestingly, TRIM25-RBCC$_L$ was also active with isolated Ubc13, which is believed to be active only when forming a hetero-complex with Ube2V1. However, in the absence of Ube2V1, TRIM25-RBCC$_L$ appears to be predominantly mono-ubiquitinated (Figure 3.7C). As a control, Ube2V1 which lacks catalytic activity is not active with TRIM25-RBCC$_L$ (Figure 3.7D).

In order to gain further insight into the reaction and distinguish between auto-mono-ubiquitination of TRIM25-RBCC$_L$ by Ubc13 and unanchored chain formation occurring with Ube2V1, the reaction was initiated in the absence of Ube2V1, in order to “prime” TRIM25-RBCC$_L$ with Ub and then Ube2V1 was added to this reaction. Strikingly, TRIM25-RBCC$_L$-Ub$_1$ became predominantly the substrate of the heterodimer Ubc13/Ube2V1 instead of Ub (Figure 3.7E) and was further ubiquitinated indicating that Ube2V1 may be involved in Ub chain elongation if TRIM25 is already ubiquitinated by an E2 or even another E3 (Figure 3.7F). However, this observation may also be interpreted in a different way: once TRIM25-RBCC$_L$ is ubiquitinated, it can no longer promote the formation of unanchored Ub chains by Ubc13/Ube2V1, which might have an implication in the biological function of TRIM25 (see also section 1.9.3).

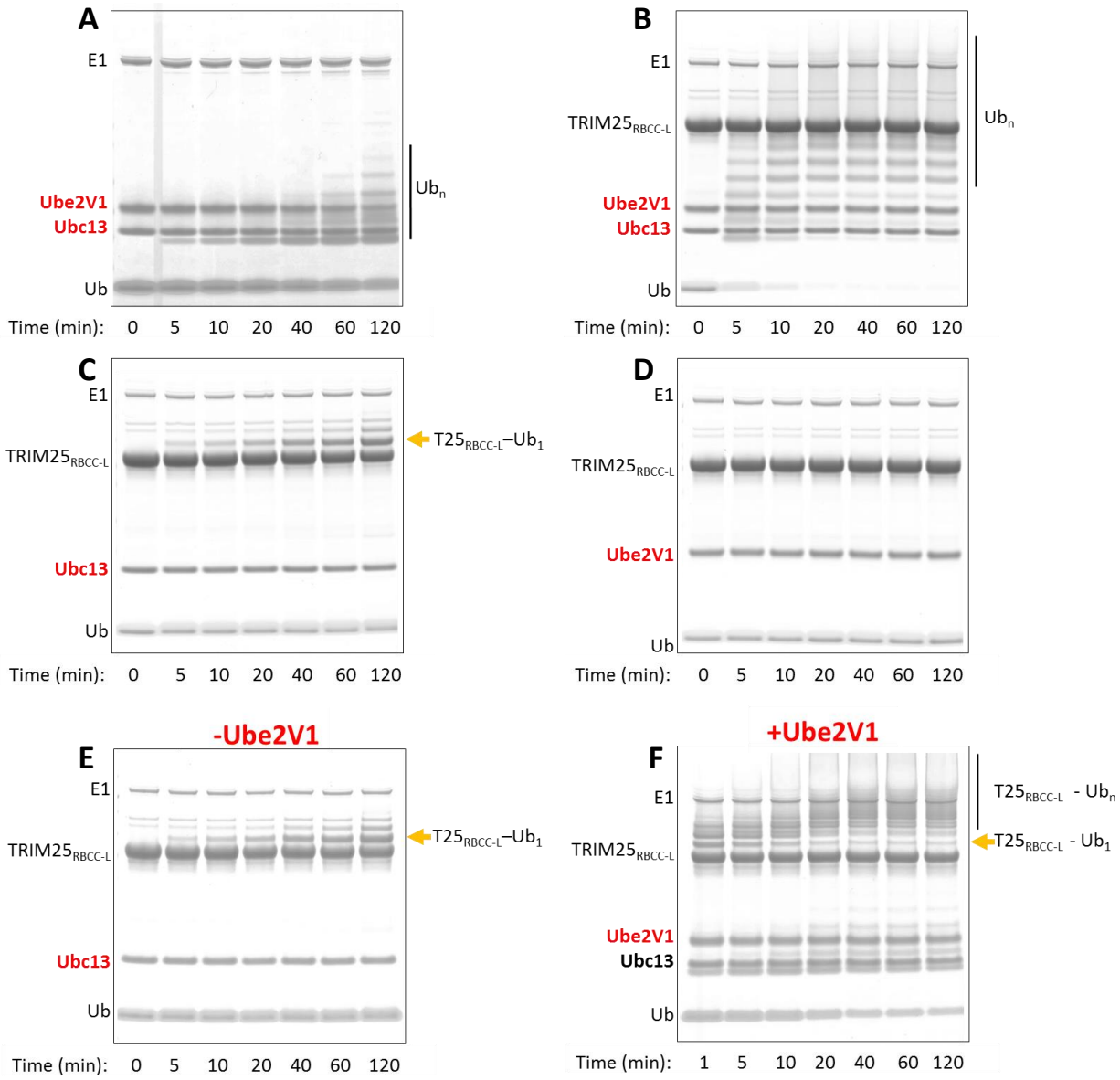

Figure 3.7: TRIM25-RBCC$_L$ enhances the activity of Ubc13/Ube2V1.

A) Ubc13/Ube2V1 synthesizes unanchored Ub chains in the absence of an E3. B) TRIM25-RBCC$_L$ greatly enhanced the formation of unanchored Ub chains by Ubc13/Ube2V1. C) TRIM25-RBCC$_L$ appeared to be auto-mono-ubiquitinated in the presence of Ubc13 only (yellow arrow). D) Ube2V1 lacks catalytic activity. Time points: samples at 0 (before the addition of ATP), 5, 10, 20, 40, 60 and 120 min were analysed by SDS-PAGE. E and F) TRIM25-RBCC$_L$ was auto-mono-ubiquitinated in the presence of Ubc13 (yellow arrow); as soon as Ube2V1 was added to the reaction (first sample taken 1 min after the Uev1a addition) TRIM25-RBCC$_L$-Ub acted as the preferred substrate over Ub and unanchored chain synthesis did not proceed. Time points in E: samples at 0 (before the addition of ATP), 5, 10, 20, 40, 60, 120 min; in F: samples taken 1, 5, 10, 20, 40, 60, 120 min after the addition of Ube2V1. Protein concentrations: 1 µM E1, 10 µM E2, 20 µM E3 (except A) and 100 µM Ub.

3.3.2 Chain synthesis by TRIM25

To identify the preferred type of ubiquitin chains built by TRIM25, enzymatic assays were performed with TRIM25-RBCC$_L$ and the E2s that showed activity, UbcH5 and Ubc13/Ube2V1 (shown in 3.3.1).

E2: UbcH5c

When an ubiquitin mutant which has all seven K residues mutated to R (UbK0) was used, there were multiple TRIM25-RBCC$_L$-Ub$_n$ species observed at a rate similar to the one observed when wild-type ubiquitin (wt Ub) was used (Figure 3.8A,B). The main difference was that in the presence of UbK0 the high-molecular weight species (above the band of E1) were absent when compared to wt Ub. UbK0 can only be attached to a target lysine residue once and cannot form polyubiquitin chains. Since there were multiple polyubiquitinated TRIM25-RBCC$_L$ species observed, this leads to the conclusion that there are multiple lysine residues on TRIM25-RBCC$_L$ targeted for multi-mono-ubiquitination *in vitro*. The differences observed in these assays suggest that apart from multiple K residues on TRIM25-RBCC$_L$ being targeted, polyubiquitin chains were formed with wt Ub. To determine the type of these chains, the K63A ubiquitin mutant was used next. The rate and the species formed in this reaction are closely similar to the assay with wt Ub (Figure 3.8C). Subsequently, a K48C ubiquitin mutant was used and this massively decreased the rate and the polyubiquitination levels formed on TRIM25-RBCC$_L$ (Figure 3.8D). In order to ensure that any of these mutations on ubiquitin did not affect thioester-formation on the E1 and E2, the loading of UbcH5c was examined and did not reveal any differences (Figure 3.8E). These results likely suggest that under assay conditions TRIM25-RBCC$_L$ is multi-mono-ubiquitinated on many different K residues and that the type of poly-Ub-linkage formed is mainly through K48 but may include other chain linkages too.

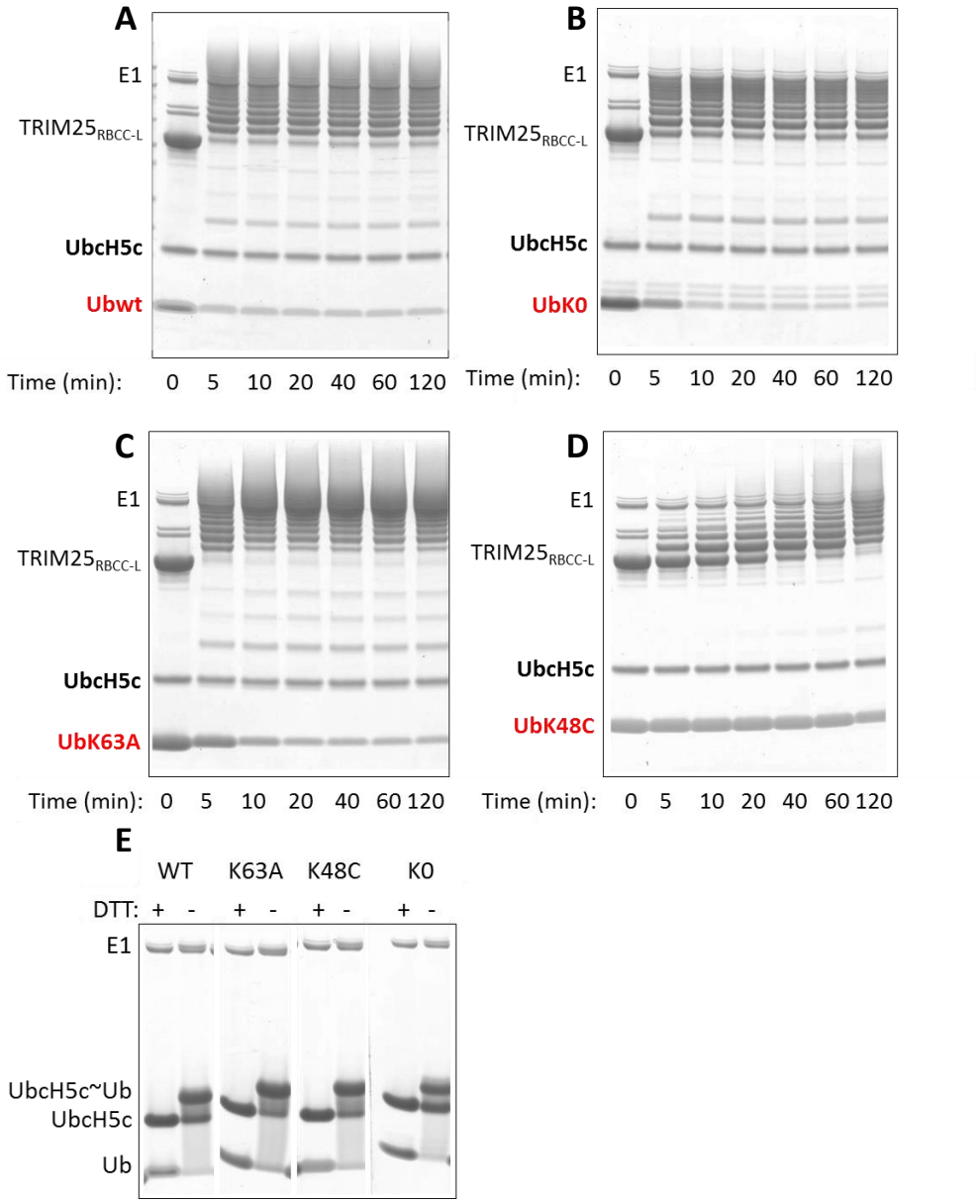

Figure 3.8: Polyubiquitin with TRIM25-RBCC$_L$ and UbcH5c.

A) As a reference of enzymatic activity, wt Ub was used. B) In the presence of UbK7R (all seven K of Ub have been substituted by R), TRIM25-RBCC$_L$ was predominantly mono-auto-ubiquitinated at multiple lysine residues. However, large molecular weight species were absent compared to panel A. C) In the presence of UbK63A, TRIM25-RBCC$_L$ was auto-ubiquitinated at a similar rate to wt Ub. D) In the presence of UbK48C, TRIM25-RBCC$_L$ was auto-ubiquitinated at a slower rate compared to wt Ub. Time points: samples at 0 (before the addition of ATP), 5, 10, 20, 40, 60 and 120 min were analysed on SDS-PAGE. This assay was performed at 20 ˚C as UbK7R was unstable at higher temperature. Protein concentrations in A-D: 1 µM E1, 10 µM E2, 20 µM E3 and 100 µM Ub. E) Control reaction showing that E1 and UbcH5c can be charged with the mutant Ub equally well as with wt Ub. Reactions were incubated at incubated at 20 ˚C over time and samples removed after 15 min and treated with loading dye (+/- DTT) followed by analysis on SDS-PAGE.

E2: Ubc13 and Ubc13/Ube2V1

In the presence of Ubc13, TRIM25-RBCC$_L$ was predominantly mono-ubiquitinated regardless of the type of Ub used (wt Ub or UbK63A) (Figure 3.9A,B). However, in combination with the heterodimeric Ubc13/Ube2V1, when UbK63A was used TRIM25-RBCC$_L$ was predominantly mono-ubiquitinated compared to the unanchored Ub-chains with wt Ub and strikingly over time Ube2V1 was also auto-ubiquitinated (Figure 3.9C,D). This observation indicates that, in the presence of TRIM25-RBCC$_L$, the heterodimeric E2 retains its intrinsic specificity for generating poly-ubiquitin chains linked via K63.

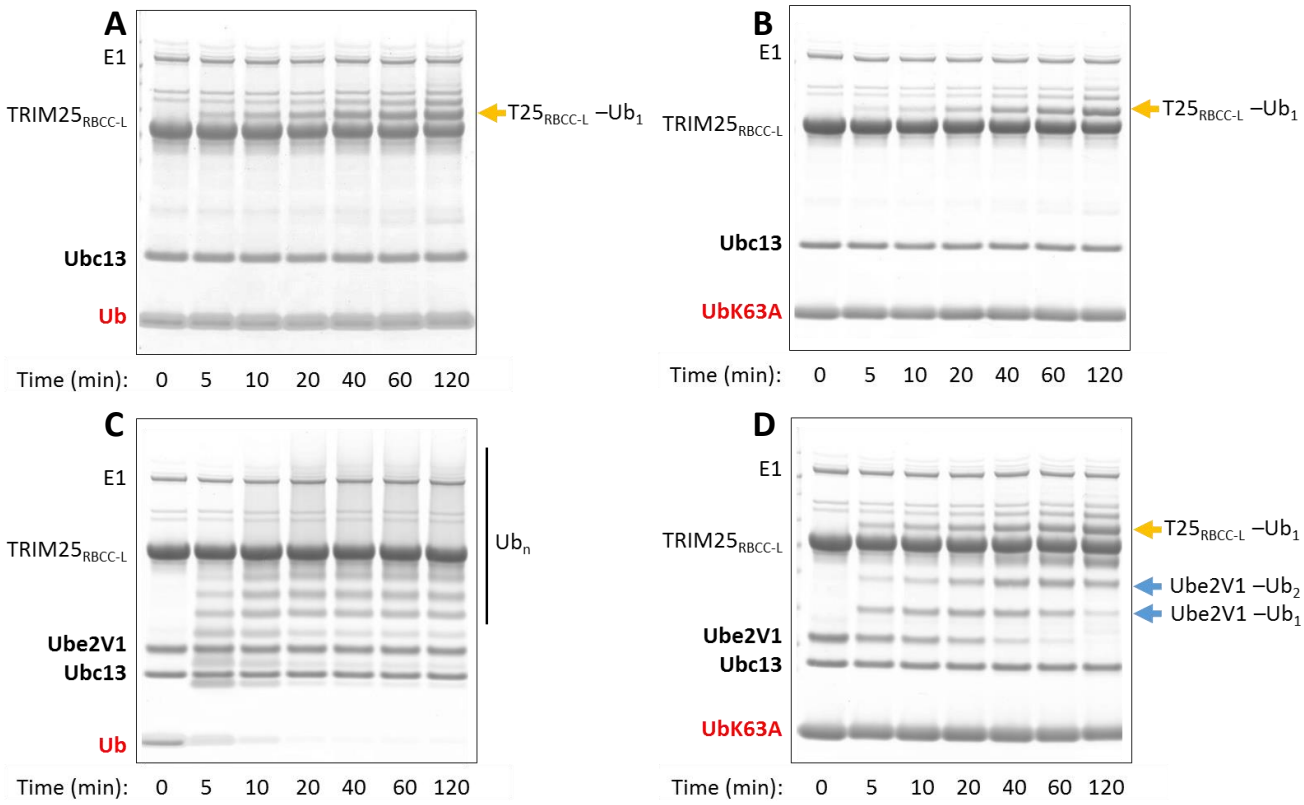

Figure 3.9: Polyubiquitin with TRIM25-RBCC$_L$ and Ubc13/Ube2V1.

A) As a reference of enzymatic activity, wt Ub and Ubc13 was used. B) Even in the presence of UbK63A and Ubc13, TRIM25-RBCC$_L$ displayed similar auto-mono-ubiquitination as with wt Ub (yellow arrow). C) As a reference of activity, wt Ub and Ubc13/Ube2V1 were used. D) In the presence of UbK63A and Ubc13/Ube2V1, TRIM25-RBCC$_L$ was auto-mono-ubiquitinated (yellow arrow). Unanchored chains were not formed. Over time, Ube2V1 itself gets auto-ubiquitinated (blue arrows). Time points: samples at 0 (before the addition of ATP), 5, 10, 20, 40, 60 and 120 min were analysed by SDS-PAGE. Enzyme concentrations: 1 µM E1, 10 µM E2 and 20 µM E3.

3.4 The oligomeric state of TRIM25

Prior to this study there was no systematic study about the contribution of the individual RBCC domains to self-association of TRIM25. The crystal structures of the coiled coil regions of TRIM5α, TRIM20, TRIM25 and TRIM69 all show an anti-parallel dimer for this region and based on sequence conservation it has been suggested that this behaviour might be a general property of the TRIM family [158, 165-167]. Further work on TRIM25 suggested that the CC region is required for the dimerization of the full-length protein [167]. Moreover, structural and biochemical data on TRIM5α indicated that B-Box2 (TRIM5α-RB2) is involved in mediating self-association which is required for the physiological role of TRIM5α as a restriction factor against retroviral infection [153, 158, 159, 178, 185, 292].

To analyse the oligomeric behaviour of the individual domains of the RBCC of TRIM25, analytical size-exclusion chromatography coupled to multi-angle light scattering (SEC-MALLS) was employed on the R, RB1, RB1B2, B1B2CC, CC and $RBCC_L$ constructs. All constructs lacking the CC region appear monomeric at concentrations up to 4 mg/ml (Figure 3.10). Extension of the RING-containing TRIM25 fragment to include the CC region renders the protein primarily dimeric with a propensity to form higher molecular weight species in the explored concentration range (≥ 0.5 mg/ml). A construct of TRIM25 which includes the two B-box domains and the CC (TRIM25-B1B2CC) is dimeric, in agreement with the behaviour of the isolated TRIM25-CC. Finally, the PRYSPRY domain is monomeric, an observation in agreement with the previously reported crystal structure (Figure 3.10) [172].

These results allowed me to draw several conclusions regarding the contribution of each domain to the oligomeric state of TRIM25: a) the TRIM25-RING domain is monomeric at the explored concentration; b) the B-Box domains do not contribute to higher-order self-association of TRIM25 as observed in TRIM5α; c) the combination of RING and CC domains on the $RBCC_L$ construct appears to induce a higher-order oligomeric state. The TRIM25-B1B2CC and –CC constructs have a different C-terminal boundary (last amino acid is at 379) compared to the TRIM25-$RBCC_L$ construct which spans to residue 433 for reasons explained in sections 3.2.1 and 3.2.2. Although it cannot be formally dismissed, it seems unlikely that this short (54 a.a.) extension towards the C-terminus, which is not conserved in TRIM25 across different species, would have an effect on the oligomeric state of TRIM25. It is therefore suggested that

incorporation of the (monomeric on its own) RING domain to the CC domain allows the protein to form species which are larger than a dimer. The oligomeric state of each TRIM25 domain tested in the present report and also previously described is summarized on Table 3.1.

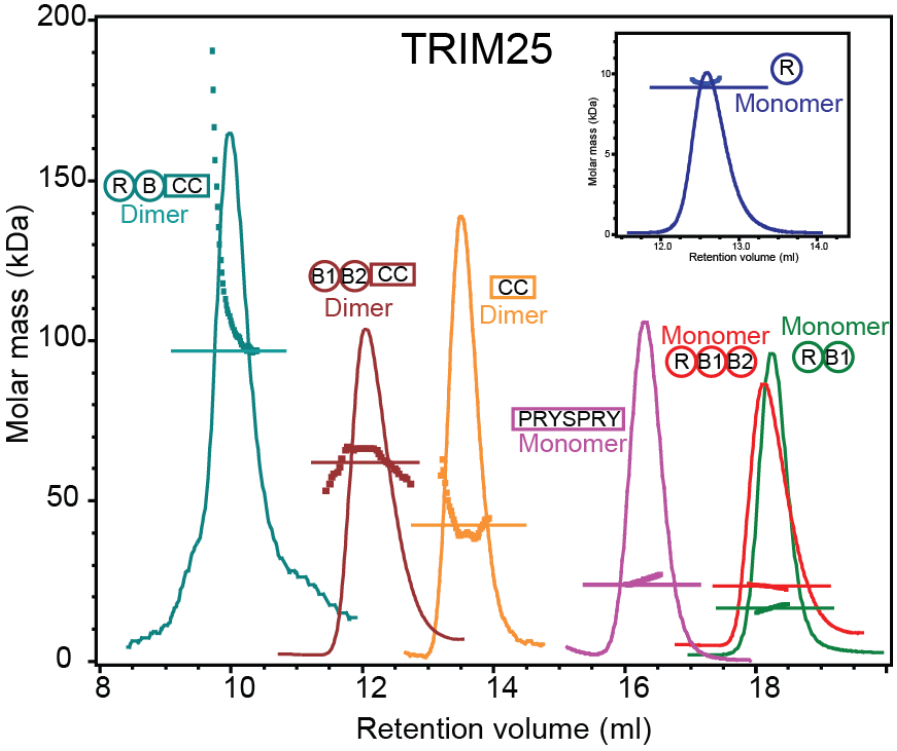

Figure 3.10: SEC-MALLS analysis of TRIM25.

The chromatogram shows the UV absorbance at 280 nm (curve) and the weight-averaged molecular masses of the samples (dotted-line). The theoretical/expected molecular mass for each construct is shown as a straight line and is parallel-to-the-X-axis. Constructs containing the CC domain were expected to be dimeric. Only the elution peaks of each sample are shown for clarity. The proteins are colour coded and the domain architecture is reported next to the respective MALLS curve. All TRIM25 samples were run on an S200 10/300 column with the exception of RING (shown in top-right inner panel) which has a small size (~9 kDa) and was run on an S75 10/300 column. Concentrations of each sample are indicated below on Table 3.1.

Domains	*Boundaries*	*Oligomeric state*	*Concentration*	*Reference*
R	*1-82*	*Monomeric*	*4 mg/ml*	*Present report*
RB1	*1-152*	*Monomeric*	*4 mg/ml*	*Present report*
RB1B2	*1-202*	*Monomeric*	*4 mg/ml*	*Present report*
B1B2CC	*103-379*	*Dimeric*	*1.5 mg/ml*	*Present report*
CC	*189-379*	*Dimeric*	*2 mg/ml*	*Present report and Sanchez et al., 2014. 4LTB.pdb*
RBCC	*1-433*	*>Dimeric*	*1 mg/ml*	*Present report*
PRYSPRY	*435-630*	*Monomeric*	*4 mg/ml*	*Present report and D'Cruz et al., 2013; 4B8E.pdb*

Table 3.1: SEC-MALLS data and oligomeric analysis of TRIM25.

Summary of SEC-MALLS data shown in Figure 3.10.

3.5 Oligomerization of TRIM25 enhances the E3 ligase activity

To assess the role of CC-mediated oligomerization in the ligase function of TRIM25, enzymatic assays were performed with shorter constructs that do not contain the CC region and compared with $RBCC_L$. When UbcH5 was used, TRIM25 is auto-ubiquitinated in the absence of its physiological substrate (see also section 3.3). However, as shown in Figure 3.8 and further described in section 3.3.2, auto-ubiquitination takes place on multiple lysine residues of TRIM25. Therefore, this assay was not suitable to compare the relative catalytic activity of TRIM25 constructs with a vastly varying number of lysine residues. To overcome this, a single-turnover lysine-discharge assay was utilized instead, which monitors the ability of a given construct to activate a pre-charged UbcH5c~Ub conjugate for transfer of ubiquitin onto free lysine included in the reaction buffer. In this assay the R, RB1, RB1B2 and RBCC fragments of TRIM25 were able to discharge the UbcH5~Ub conjugate (Figure 3.11). Unsurprisingly, B1B2CC which lacks the RING domain was completely inactive, an observation which further dismisses earlier reports which, based on structural similarities of the B-Box with the RING fold, have suggested a probable catalytic role for the B-Box domains [142]. Instead, these data indicate that the RING of TRIM25 is the minimal catalytic core of TRIM25 and is active as a monomer (Figure 3.11).

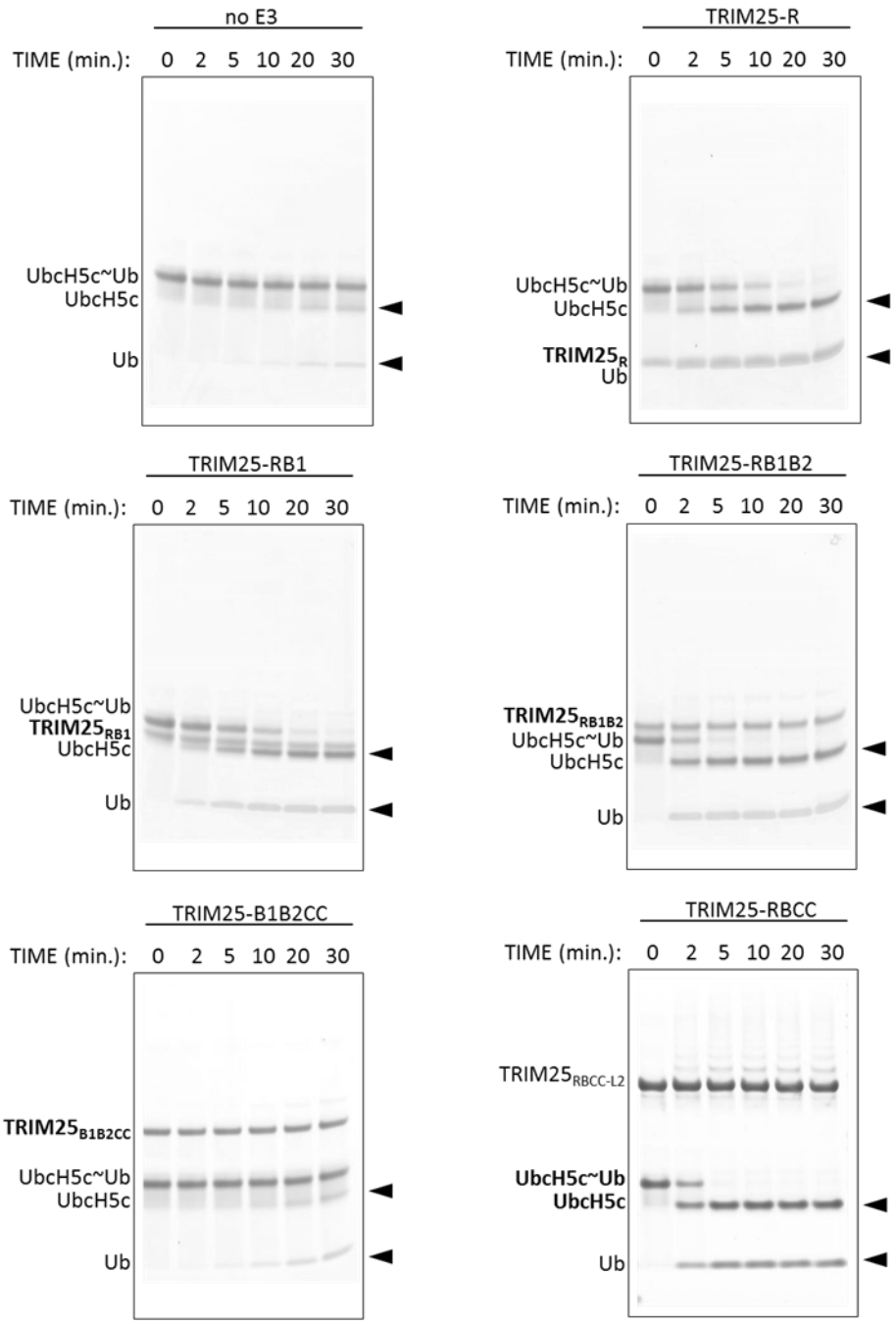

Figure 3.11. UbcH5c~Ub discharge assays with TRIM25 constructs.

Assays were carried out with 10 μM UbcH5c~Ub and 0 μM (control) or 4 μM of different TRIM constructs as indicated in buffer containing 50 mM L-Lysine. The reaction was monitored over 30 min. Samples taken at the indicated time points (0, 2, 5, 10, 20, 30 min) were treated with loading dye (without DTT) followed by SDS-PAGE analysis. The absence of reducing agents (such as DTT) allows monitoring of the E2~Ub thioester loss due to TRIM25 E3 ligase activity. Time point 0 indicates the sample taken immediately after the addition of UbcH5c~Ub, while the reaction was on ice. Subsequently the reactions were incubated at 25 ˚C. Black triangles indicate UbcH5c (top) and Ub (bottom) bands produced due to UbcH5c~Ub thioester hydrolysis.

The above assay gave a qualitative indication about the enzymatic activity of TRIM25 constructs that contain the minimal catalytic RING domain. In order to further quantify and plot the differences observed in the catalytic activity of each TRIM25 construct, ubiquitin was labelled with Atto647N fluorophore and charged onto UbcH5 as described in section 2.8. The E2 discharge rate was measured over time (Figure 3.12). The plotted differences show that activity of the RING domain is slightly increased in the presence of B-box1 and even further with the tandem B-box1,2. Intriguingly, the reaction is significantly enhanced in the presence of the entire RBCC motif (Figure 3.12). These results further confirm that the RING of TRIM25 is the minimal catalytic core for E3 ligase activity but that the CC-induced dimerization further enhances its activity.

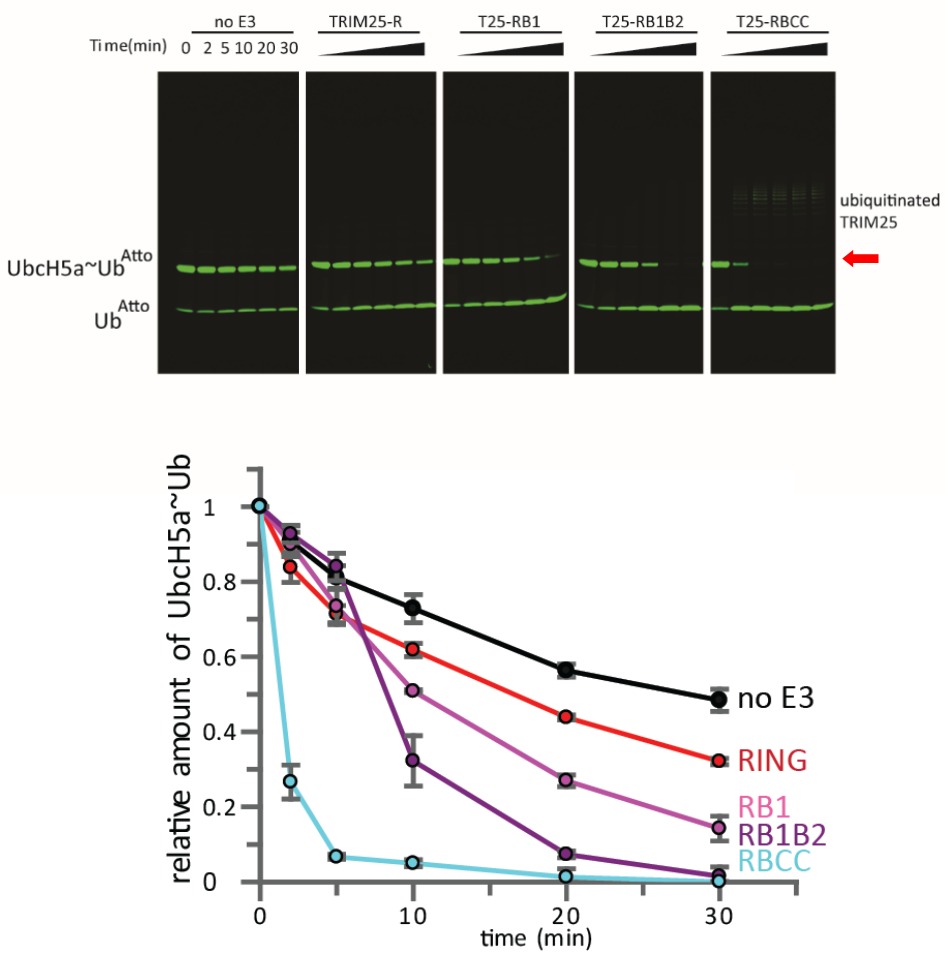

Figure 3.12. Quantitative analysis of TRIM25 UbcH5a~UbAtto discharge.

The use of fluorescently-labeled Ub^{Atto} allows quantitative monitoring of the UbcH5a~Ub^{Atto} discharge rates in the presence of different TRIM25 constructs. Assays were carried out with 1 μM UbcH5a~Ub^{Atto} and 0 μM (control) or 4 μM of different TRIM constructs as indicated in buffer containing 20 mM L-Lysine. The reaction was monitored over 30 min. Samples were taken at the indicated time points (0, 2, 5, 10, 20, 30 min). Time point 0 indicates the sample taken immediately after the addition of UbcH5a~Ub^{Atto}, while the reaction was on ice. Subsequently the reactions were incubated at 25 ˚C. Each sample was treated with loading dye (without DTT) followed by SDS-PAGE analysis. Top panel shows SDS-PAGE scanned at 635 nm wavelength (which is the Atto647N emission wavelength). The UbcH5a~Ub^{Atto} band (indicated by red arrow) was integrated and was plotted as the average of experimental triplicates (± s.d.). Figure was adapted from [94].

In the preliminary assays shown above (see 3.3.1), TRIM25 was shown to be active with the heterodimeric Ubc13/Ube2V1 that catalyses formation of unanchored K63-linked poly-ubiquitin chains. As with UbcH5, the catalytic activity of constructs containing the RING domain and extensions to include the B-Box domains and the CC region was qualitatively assessed (Figure 3.13). Similarly to the assays with UbcH5, TRIM25-RING is sufficient to initiate the formation of K63-linked chains (Figure 3.13). Additional domains of the TRIM motif do not appear to enhance the formation of unanchored K63 ubiquitin chains under these experimental conditions.

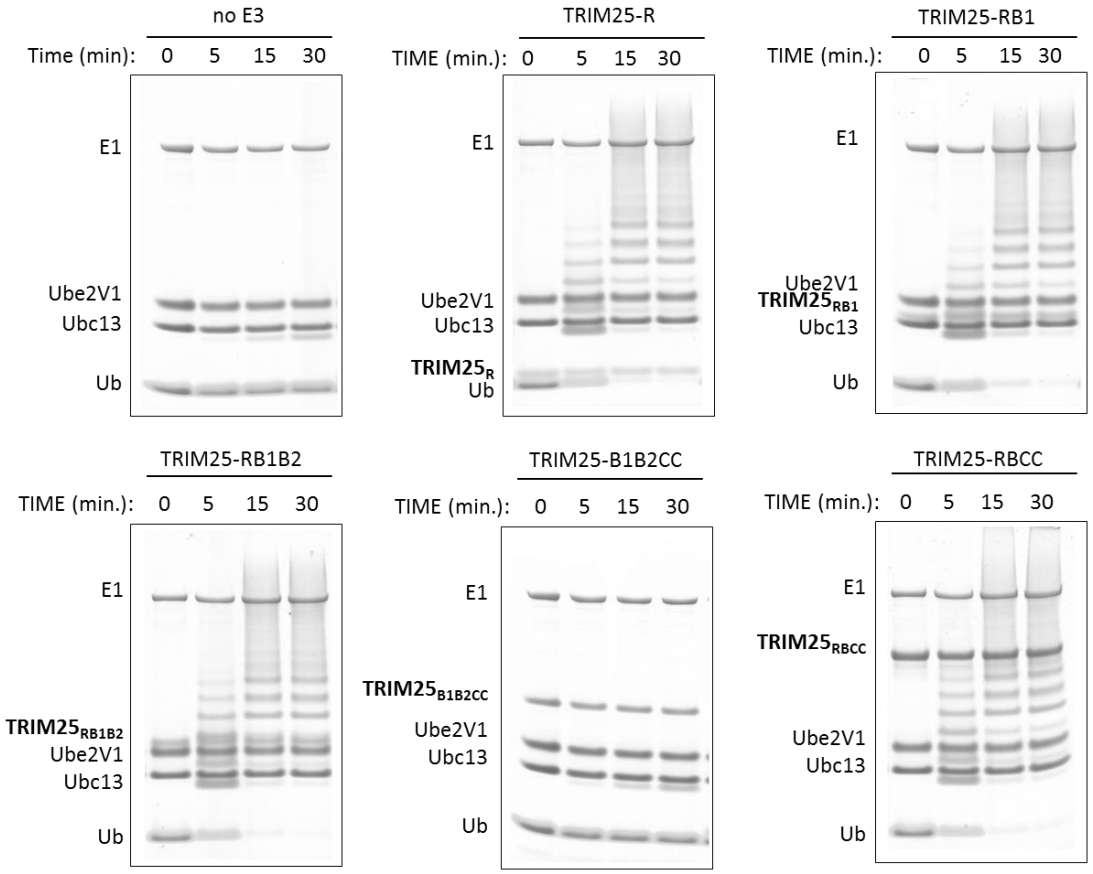

Figure 3.13. K63-linked chain formation by different TRIM25 constructs.

Ubiquitination assays with Ubc13/Ube2V1 were performed with 1 μM E1, and 10 μM of each E2, 0 μM (control) or 4 μM of different TRIM constructs as indicated and 100 μM Ub. The reaction was monitored over 30 min. Reaction was incubated at 25 ˚C and samples taken at the indicated time points (0, 5, 15 and 30 min) were analysed by SDS-PAGE. Sample at 0 min. was taken before the addition of ATP.

To quantify and plot any differences between TRIM25 constructs, the assays were performed in the presence of fluorescently labelled ubiquitin and the rate of Ub^{Atto} (fluorescent Ub) incorporation into unanchored K63-linked chains (Ub^{Atto} band disappearance over time) was quantified (Figure 3.14). The results obtained indicate that the RING domain is the minimal requirement for activation of Ubc13 which closely resembles the observations in assays with UbcH5. The main difference between the assays using the two E2s appears to be that there is no significant enhancement of activity in RB1, RB1B2 or RBCC constructs, in contrast to the results from the discharge assays with UbcH5 (Figure 3.14). These data confirm that the RING is the main catalytic unit of TRIMs. The presence of the B-boxes moderately enhances the catalytic activity during discharge of the UbcH5~Ub conjugate onto free lysine but does not enhance the synthesis of unanchored poly-ubiquitin chains. This is an interesting observation and further experiments are required to further examine a potential role of the B-Box domains in catalytic activation.

Taken together, these results suggest that the RING of TRIM25 does not appear to require dimerization for catalytic activity, in contrast to previous suggestions that TRIMs require self-association for activity. To gain molecular insight into the mechanism of ubiquitin transfer, the crystal structure of the RING domain of TRIM25 in complex with ubiquitin-loaded UbcH5a was solved.

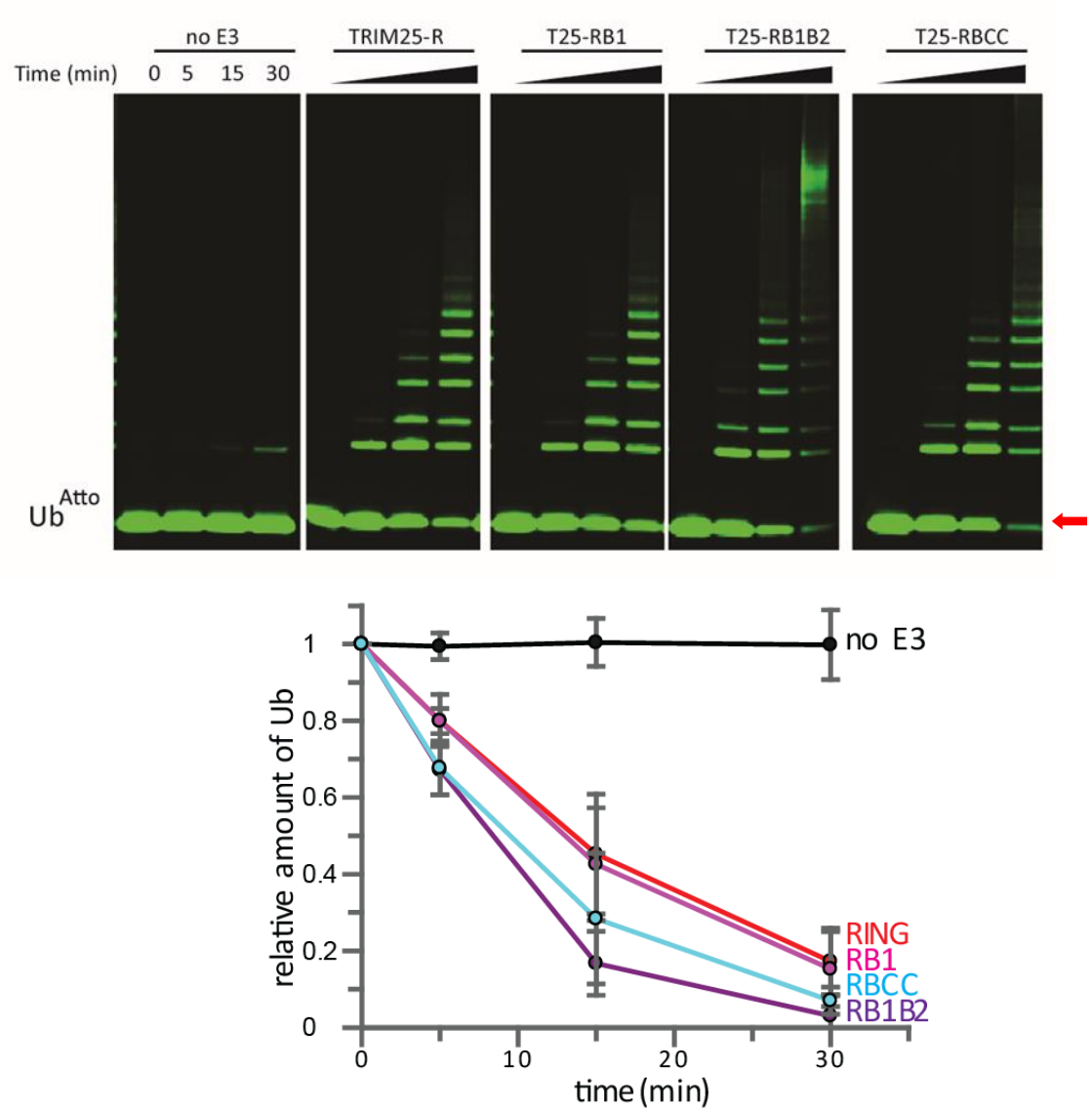

Figure 3.14. Quantitative analysis of K63-linked polyubiquitin formation.

The use of fluorescently-labeled Ub^{Atto} allows quantification of K63-linked chains in the presence of different TRIM25 constructs. Assays were carried out with 0.5 μM E1, 2.5 μM of each E2 (Ubc13 and Ube2V1), 0 μM (as control) or 4 μM TRIM construct, 50 μM unlabeled Ub supplemented with 1 μM Ub^{Atto}. It was not possible to use labeled-only Ub (Ub^{Atto}) as the fluorophore interfered with K63-chain formation. Combination of a large excess of unlabeled Ub with Ub^{Atto} ensured that Ub^{Atto} acted mostly as a donor (i.e. the last molecule on a growing K63 chain). The reaction was monitored over 30 min. Samples were taken at the indicated time points (0, 5, 15, 30 min). Time point 0 indicates the sample taken before addition of ATP. The reactions were incubated at 25 ˚C and each sample was treated with loading dye (+ DTT) followed by SDS-PAGE analysis. Top panel shows SDS-PAGE scanned at 635 nm wavelength (which is the Atto647N emission wavelength). The Ub^{Atto} band (indicated by red arrow) was integrated and is plotted as the average of experimental triplicates (± s.d.). Figure was adapted from [94].

3.6 Structure and mechanism of TRIM25-RING activity

3.6.1 Crystallization of the TRIM25-RING/UbcH5a-Ub complex

To obtain the crystal structure of the TRIM25-RING bound to charged UbcH5a~Ub, it was necessary to mutate the catalytic cysteine of the E2 into a lysine (C85K). This strategy was previously described for other RING/E2~Ub structures and allows the formation of a non-hydrolysable isopeptide bond which mimics the thioester bond (here denoted as "-" in UbcH5a-Ub) [89, 91]. Additionally, the UbcH5a backside binding interface with Ub was disrupted (S22R) to allow crystal lattice formation as previously described [91].

The TRIM25-RING domain (8 mg/ml) was mixed with UbcH5a-Ub (10 mg/ml) at a 1:1 molar ratio. Initial hits were optimized by hanging-drop vapour diffusion at 18 °C with a reservoir solution containing 100 mM Tris pH 8.5 and 10% PEG 20000 reaching full size (~0.5 mm) after 3 days (Figure 3.15). Crystals were flash-frozen in the reservoir solution containing 20% glycerol.

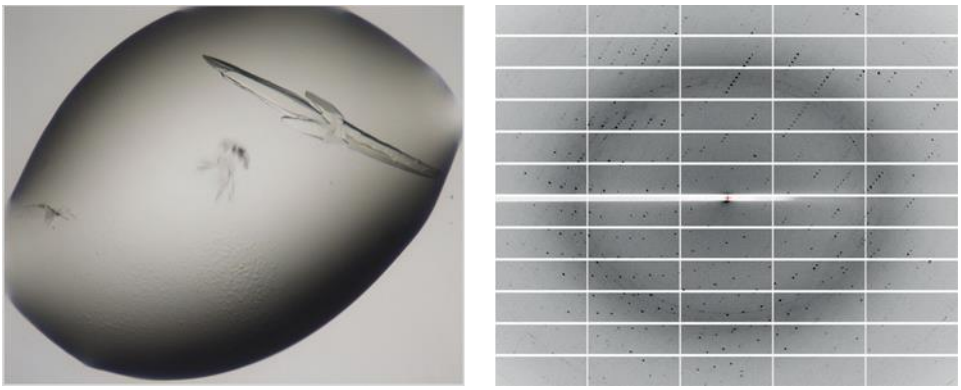

Figure 3.15. Crystal of the TRIM25-R/UbcH5a-Ub complex.

Left panel: Initial hits obtained for this complex included a crystal that resembled the Excalibur sword. Further optimization resulted in single crystals which were used for X-ray diffraction. Right panel: typical image showing good quality diffraction pattern and well-resolved spots reaching ~2.3 Å without any major common pathologies observed such as ice-rings or multiple lattices.

3.6.2 Structure determination of the TRIM25-RING/E2-Ub complex

The structure of TRIM25-RING/UbcH5a-Ub was solved by single anomalous dispersion (SAD) at 2.34 Å resolution (Figure 3.15). A single dataset collected at the Zn^{2+} absorption edge (λ = 1.2829 Å) was used for heavy-atom search, density modification and initial model building, which were performed using the automated pipeline in Phenix AutoSol. The resulting electron density maps were examined in COOT and the model was further improved by an iterative process of manual building and refinement using REFMAC5 and Phenix. The model of TRIM25-RING:UbcH5a-Ub has 94.4% of its residues in favoured regions, 4.5% in allowed regions and 0.5% (1 residue) outliers. Structural figures were prepared in Pymol. The data collection and refinement statistics are summarized in Table 3.2. Coordinates and structure factors were deposited in the Protein Data Bank under the accession code 5FER.

Crystal	**TRIM25-R/UbcH5a-Ub**
Resolution	30.28–2.34 (2.42–2.34)
Space group	$P2_12_12_1$
Cell dimensions	
a,b,c (Å)	60.48, 71.70, 160.43
α, β, γ (°)	90.0, 90.0, 90.0
R_{merge}	0.139 (1.918)
Total reflections	384,013
Unique reflections	30,000
Redundancy	12.8
Completeness (%)	99.32
$\langle I/\sigma(I)\rangle$	13.75 (1.53)
$CC_{1/2}$	0.998 (0.523)
Refinement	
R_{work}	0.227
R_{free}	0.273
Number of atoms	4,832
Protein	4,760
Zn^{2+}	4
Water	68
Average B-factor (Å^2)	56.0
RMS bonds (Å)	0.002
RMS angles (°)	0.539
Ramachandran statistics	
Favoured region (%)	96.11
Allowed region (%)	3.38
Disallowed region (%)	0.51

Table 3.2: X-ray crystallography data collection and refinement statistics.

Data for the highest resolution shells are given in parenthesis.

3.6.3 The crystal structure of the TRIM25-RING/UbcH5a-Ub complex

The TRIM25-RING/UbcH5a-Ub complex crystallised with two molecules of each protein in the asymmetric unit related by a two-fold symmetry axis (Figure 3.16). Surprisingly and in contradiction to the SEC-MALLS experiments described in section 3.4, the RING domain crystallized as a dimer with the dimer interface burying ~1000 Å of solvent accessible surface. As described previously for a number of other RING ligases such as Rad18 (see also 1.5.3.1.1), TRIM32 and BRCA1/BARD1 dimerization is mediated by two α-helices located N-and C-terminal to the core Zn^{2+}-binding RING domain that form a 4 helix-bundle [79, 80, 94]. The TRIM25-RING dimerization interface is also conserved in other TRIM proteins as shown by an alignment of the TRIM25-RING with TRIM5α-RING (4TKP.pdb and [187]) and TRIM32-RING (5FEY.pdb and [94]) (Figure 3.17A). The RING/RING interface is formed predominantly by hydrophobic residues (L4, L7, L11, V68, L69, V72 and F76) that project their side-chains into the interior of the four-helix bundle (Figure 3.17B).

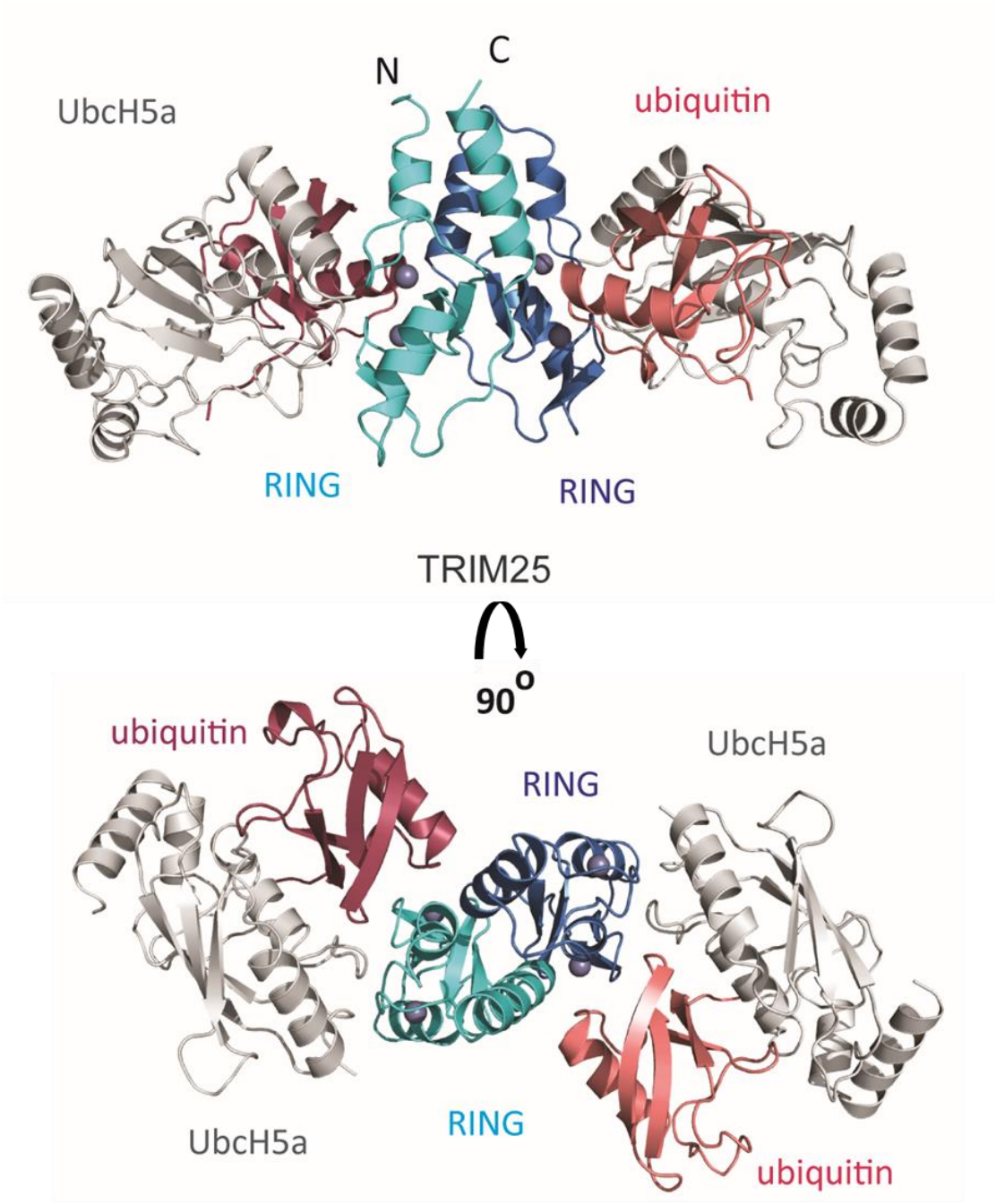

Figure 3.16. Structure of the TRIM25-R/UbcH5a-Ub complex.

Ribbon representation of the TRIM25-RING/UbcH5a-Ub complex structure is shown in two orientations. The asymmetric unit in the crystal shows two TRIM25-RING molecules (blue and cyan) and two UbcH5a-Ub conjugates (UbcH5a in light grey and Ub in red and salmon) related by two-fold symmetry. Each TRIM25-R interacts with one UbcH5a-Ub intermediate. UbcH5a-Ub adopts the closed conformation which is stabilized by RING/Ub interactions. Each E2 interacts with one TRIM25-R domain. The two RING domains interact with each other through the N/C-terminal regions that encompass the core Zn^{2+}-binding domain. These regions form a four α-helical bundle. Each RING coordinates two Zn^{2+} atoms (shown as grey spheres) in a canonical manner (cross/brace topology). Figure was adapted from [94].

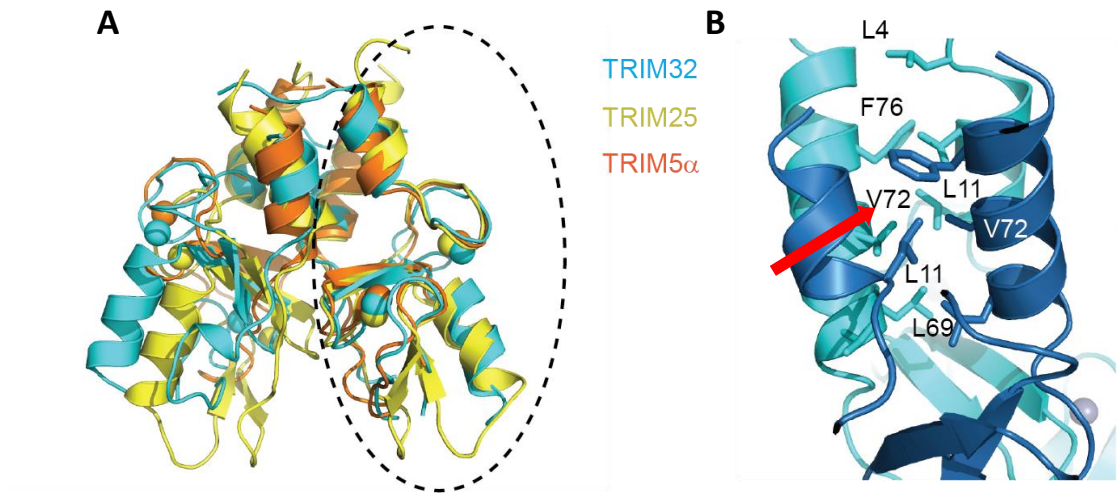

Figure 3.17. Structural analysis of the TRIM25-R dimer.

A) Structural alignment of TRIM-RING domains. TRIM32 (cyan), TRIM5α (orange) and TRIM25 (yellow) are aligned on one TRIM-R monomer (circled region). All RING domains dimerize through the N/C-terminal α-helices packing against each other. The RING domains of these TRIMs align well but slightly differ on the relative orientations of the RINGs; i.e. in TRIM32-R the α-helices of one monomer are almost perpendicular to the α-helices of the other monomer, whereas in TRIM25 and TRIM5α the four α-helices are almost parallel to each other. B) Close-up of the TRIM25-R dimerization interface which is formed primarily by hydrophobic interactions within the N/C-terminal α-helices. The side-chains of the participating residues are indicated. Each RING monomer is coloured (blue or cyan). Red arrow shows V72, the effect of which is further examined below. Figure was adapted from [94].

To examine the role of dimerization in the enzymatic activity of TRIM25, V72 which resides at the centre of the helical bundle was mutated to a polar arginine (V72R) (Figure 3.17B). Mutation of the equivalent hydrophobic residue to arginine has previously been shown to interfere with catalytic activity of TRIM5α, another TRIM ligase whose RING is monomeric in solution but crystallizes as a dimer [187]. Given that it was not possible to detect dimerization in solution (see also section 3.4) and hence it was not able to test if the V72R indeed disrupted the ability of TRIM25-RING to dimerize, a tandem RING-linker-RING construct was produced as a positive control. Such a covalent RING dimer would be expected to enhance any weak dimerization affinity present. The effect of these mutations on the enzymatic activity of TRIM25-R was examined in UbcH5a~Ub^{Atto} and UbcH5c~Ub discharge assays (Figure 3.18A-C). The results obtained from both

experiments are comparable and in the case of UbcH5a~Ub^{Atto}, the use of the fluorescently-labelled Ub^{Atto} allows quantification as described previously in section 3.5 (Figure 3.18A,B). The V72R mutant TRIM25-R construct was devoid of activity. In contrast, the RING-linker-RING construct was able to discharge the E2~Ub much faster compared to the single wt RING domain (which was used as a control) and all E2~Ub thioester was discharged already after 2 min (Figure 3.18A-C). Additionally, V72R was introduced into the covalently linked RING dimer and this construct was further tested for its catalytic ability. It appears that its activity was significantly reduced but not to the same extent as in the monomeric RING (Figure 3.18A-C). These observations were further confirmed in K63-chain formation assays with Ubc13/Ube2V1 (Figure 3.19). The V27R RING was inactive whereas the RING-linker-RING construct was equally active as the monomeric RING domain which was used as control (Figure 3.19).

Overall, these data suggest that the activity observed in assays using the monomeric RING constructs probably derives from a proportion of dimeric species that is present under the experimental conditions. Furthermore, it is possible that RING dimerization is enhanced by binding of the E2~Ub intermediate (further discussed in section 3.7 below). In contrast, synthesis of K63-linked chains by Ubc13/Ube2V1 was not enhanced by the fused RING dimer in agreement with the previously shown data (Figure 3.14) that suggested that CC-mediated dimerization does not have a significant effect on the formation of free K63 chains. The differences observed in the assays with the two different E2 enzymes (UbcH5 and Ubc13) could be attributed to the fact that the Ubc13~Ub intermediate adduct has been shown to occupy mostly the “closed” state that is primed for Ub transfer [88]. This observation could also help explain the catalytic ability of Ubc13 when in complex with Ube2V1 even in the absence of an E3 [71]. On the contrary, UbcH5~Ub occupies primarily the “open” state and is thus dependent on the E3 in order to stabilize the “closed” conformation [88-92].

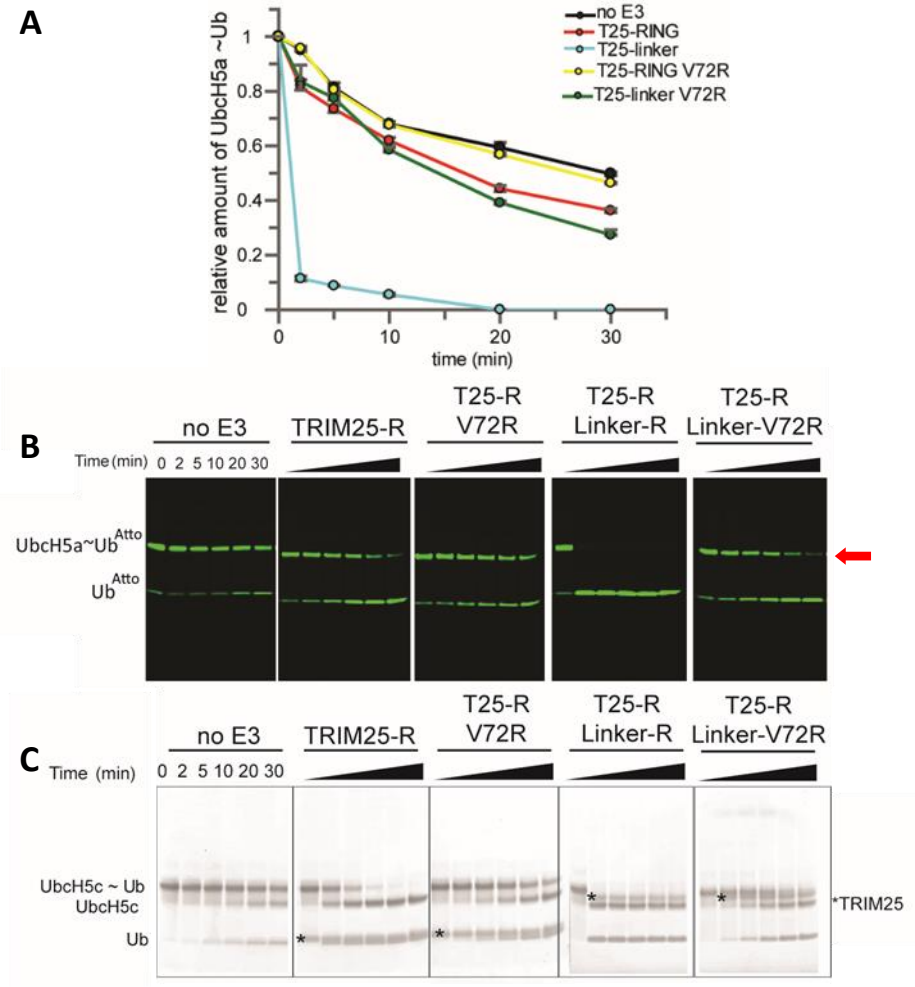

Figure 3.18. Catalytic role of RING dimerization in UbcH5~Ub priming.

A) Quantitative analysis of UbcH5a~Ub^{Atto} discharge (using SDS-PAGE shown in B) on its own (control) and in the presence of wt/mutant version of TRIM25-RING including: wt, V72R, covalently-linked RING dimer (denoted as T25R-Linker-R) and covalently-linked RING dimer bearing the V72R mutation on both RINGs (denoted as T25R-Linker-R V72R). B) Assays were carried out with 1 μM UbcH5a~Ub^{Atto} and 0 μM (control) or 4 μM of different TRIM-R constructs as indicated in buffer containing 20 mM L-Lysine. The reaction was monitored over 30 min. Samples taken at the indicated time points (0, 2, 5, 10, 20, 30 min). Time point 0 indicates the sample taken immediately after the addition of UbcH5a~Ub, while the reaction was on ice. Time point zero for the T25-R-Linker-R and T25-R-Linker-R-(V72R) samples was taken before the addition of E3 as discharge is very fast. Subsequently the reactions were incubated at 25℃. Each sample was treated with loading dye (without DTT) followed by SDS-PAGE analysis and scanning at 635 nm wavelength (which is the Atto647N emission wavelength). The UbcH5a~Ub^{Atto} band (indicated by red arrow) was integrated and is plotted as the average of experimental duplicates (± s.d.). C) Assays were carried out as described in B but with 10 μM UbcH5c~Ub and 0 μM (control) or 4 μM of different TRIM constructs as indicated in buffer containing 50 mM L-Lysine. Asterisk shows the different TRIM constructs. Figure was adapted from [94].

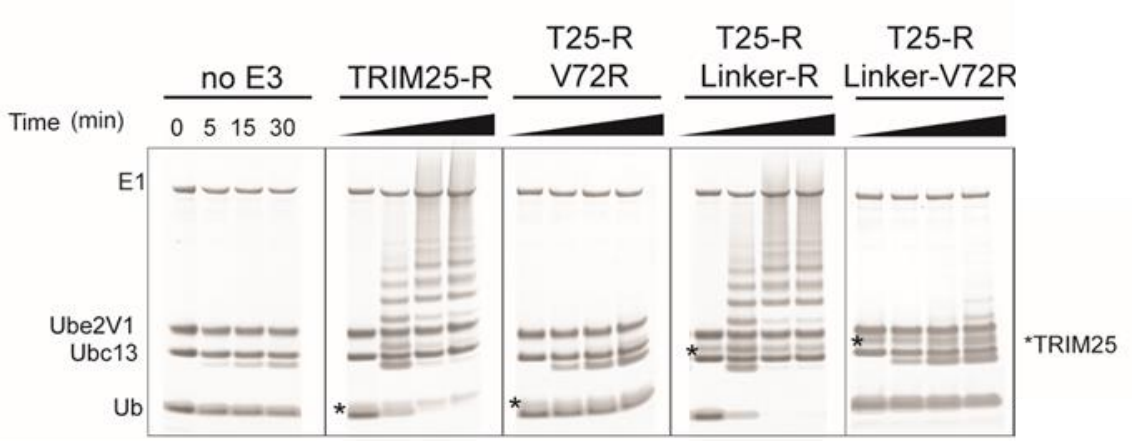

Figure 3.19. Catalytic role of RING dimerization in K63-chain formation.

Ubiquitination assays with Ubc13/Ube2V1 were performed with 1 μM E1, and 10 μM of each E2, 0 μM (control) or 4 μM of different TRIM-RING constructs as indicated and 100 μM Ub. The reaction was monitored over 30 min. Reaction was incubated at 25℃ and samples taken at the indicated time points (0, 5, 15 and 30 min) were analysed by SDS-PAGE. Sample at 0 min. was taken before the addition of ATP. Asterisk shows the different TRIM constructs. Figure was adapted from [94].

3.6.4 Mechanism of ubiquitin transfer mediated by TRIM25-RING

Close inspection of the TRIM25-RING/UbcH5a-Ub complex structure shows that the mechanism of catalysis by the RING of TRIM25 involves key residues conserved in most TRIM proteins but also shared by other members of RING E3 ligases, both dimeric and monomeric.

Each RING monomer contacts a single UbcH5 molecule via the canonical E2-E3 surface (described in section 1.5.3.1.2). Each ubiquitin molecule is folded back onto the E2 resulting in the “closed” conformation, which includes contacts between the I44 hydrophobic surface of Ub and the E2, an orientation in which the thioester bond is activated and the ubiquitin is primed for transfer. Structural analysis shows that R54 residue of TRIM25 plays the role of the “linchpin” residue and is involved in the formation of electrostatic interactions with Q92 of UbcH5 and Q40/R72 residues of Ub. This basic residue has been previously reported for other RING E3s and is involved in activation of the E2~Ub conjugate (see also section 1.5.3.1.3). Mutation of R54A reduced the catalytic potential of TRIM25-R in discharging UbcH5~Ub and in the formation of K63-linked chains by Ubc13/Ube2V1 (Figure 3.20B-E). These data indicate that the E2-E3 interface involves residues of the core Zn^{2+}-binding domain of the RING and is not affected by dimerization through the 4-helix bundle.

Additionally, instead of an aromatic residue seen for other dimeric RING E3s, the distal TRIM25-R contributes to catalysis via C-terminal residues K65 and T67 which contact D32 and E34 of Ub respectively (Figure 3.20A). Mutation of K65A and T67A reduces the catalytic ability of TRIM25-R both with UbcH5 and Ubc13/Ube2V1 (Figure 3.20B-E). R33 and L80 occupy similar area in the TRIM32 RING structure and also in TRIM37 (R67, E71) and TRIM5 (N76, E79).

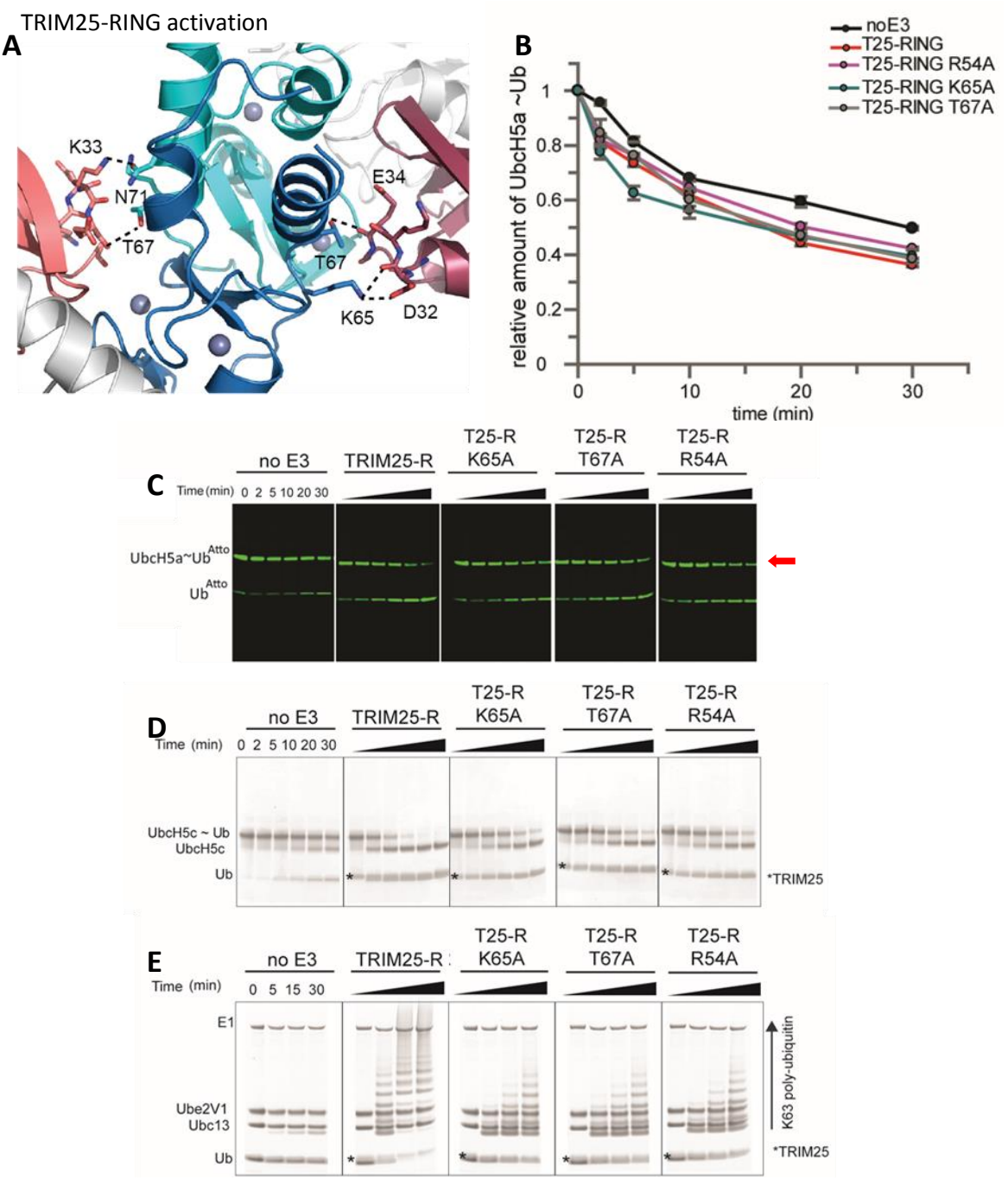

Figure 3.20. Catalytic role of RING interaction with Ub.

A) Close-up of interactions between TRIM25-RING (blue or cyan) and proximal Ub (dark red or salmon) molecule. UbcH5a is shown in grey. The side-chains of RING residues involved in polar interactions with Ub are shown: $K65_{RING}/D32_{Ub}$ and $T67_{RING}/E34_{Ub}$ in blue/red pair and $T67_{RING}/E34_{Ub}$ $N71_{RING}/K33_{Ub}$ in cyan/salmon pair respectively. B, C) Quantitative analysis of UbcH5a~Ub^{Atto} discharge (using SDS-PAGE shown in (C) in the presence of TRIM25-R bearing R54A ("linchpin" residue) and K65A or T67A involved in RING/Ub interaction. Conditions as described in Figure 3.18. Red arrow indicates band used for quantification. D) Discharge assays with UbcH5c~Ub and RING mutants. Conditions as shown in Figure 3.18. E) Ubiquitination assays with Ubc13/Ube2V1 and TRIM25-RING mutants as described in Figure 3.19. Asterisk indicates TRIM25-R constructs. Figure was adapted from [94].

The structures of several dimeric RING E3s in complex with E2-Ub have been reported revealing that the proximal RING binds the E2~Ub via the I36 surface patch of Ub, while an aromatic residue from the distal RING makes additional contacts with the same Ub surface. In contrast, in monomeric RINGs other structural elements have been shown to play the role of the second RING [92]. For example CBL-B requires phosphorylation of a Y residue outside the core RING domain that in turn contacts Ub.

Interestingly, in the case of the TRIM25-R/UbcH5-Ub complex, apart from R54 which is required to activate the E2~Ub, the proximal RING domain employs an acidic residue (E10), which forms a salt bridge with K11 of Ub but also with N71 from the C-terminal α-helix of the proximal TRIM25-R (Figure 3.21A). Mutation of E10R completely abolished the ability of TRIM25-R to discharge UbcH5~Ub but also to form K63-linked Ub chains with Ubc13/Ube2V1 (Figure 3.21B-E). Due to the close proximity of E9 to K11 of Ub, the E9R mutation was also introduced and enzymatic assays were performed. E9R is equally able to discharge UbcH5~Ub as the wt-TRIM25-R indicating that the dual function of E10 (to contact the distal TRIM25-R and Ub) is crucial for activity (Figure 3.21B-E). This observation gains significance by inspecting sequence alignments that indicate that the acidic motif with either one or two Glu residues is conserved in nearly all TRIMs containing a PRYSPRY C-terminal domain (subgroup I & IV) and in many other members of the TRIM family [167]. Moreover, structural and sequence comparison of TRIM25-R, TRIM32-R (solved in our group, 5FER.pdb and [94]), TRIM5α-R which was recently described (4TKP.pdb and [187]) and TRIM37 (3LRQ.pdb) shows that E16 (TRIM32), E11/E12 (TRIM5) and E11 (TRIM37) occupy similar positions. This key acidic residue is also conserved in other E3 RING/U box ligases such as CHIP (D230) [293]. A structural alignment of TRIM25-R and monomeric CBL-B shows that CBL-B has Y363, which needs to be phosphorylated for full activation of the E3 ligase activity, in the corresponding position of TRIM25 E10 [92]. Therefore, it appears that an acidic residue that is capable of contacting ubiquitin molecule and stabilizing the “closed” conformation is a feature shared by both monomeric as well as dimeric RING E3s.

In conclusion, these data suggest that the dimerization of the TRIM RINGs allows for contacts of the proximal Ub with the opposing RING monomer and in most cases involve salt bridges and hydrophobic interactions with the D32, K33, E34 residues of Ub. Intriguingly, the data suggest that the 4-helix bundle is involved

in optimal activation of the thioesterified Ub, as mutations (V72R or E10R) which affect the formation of the α-helices and thus dimerization of the RING domains completely abolish activity.

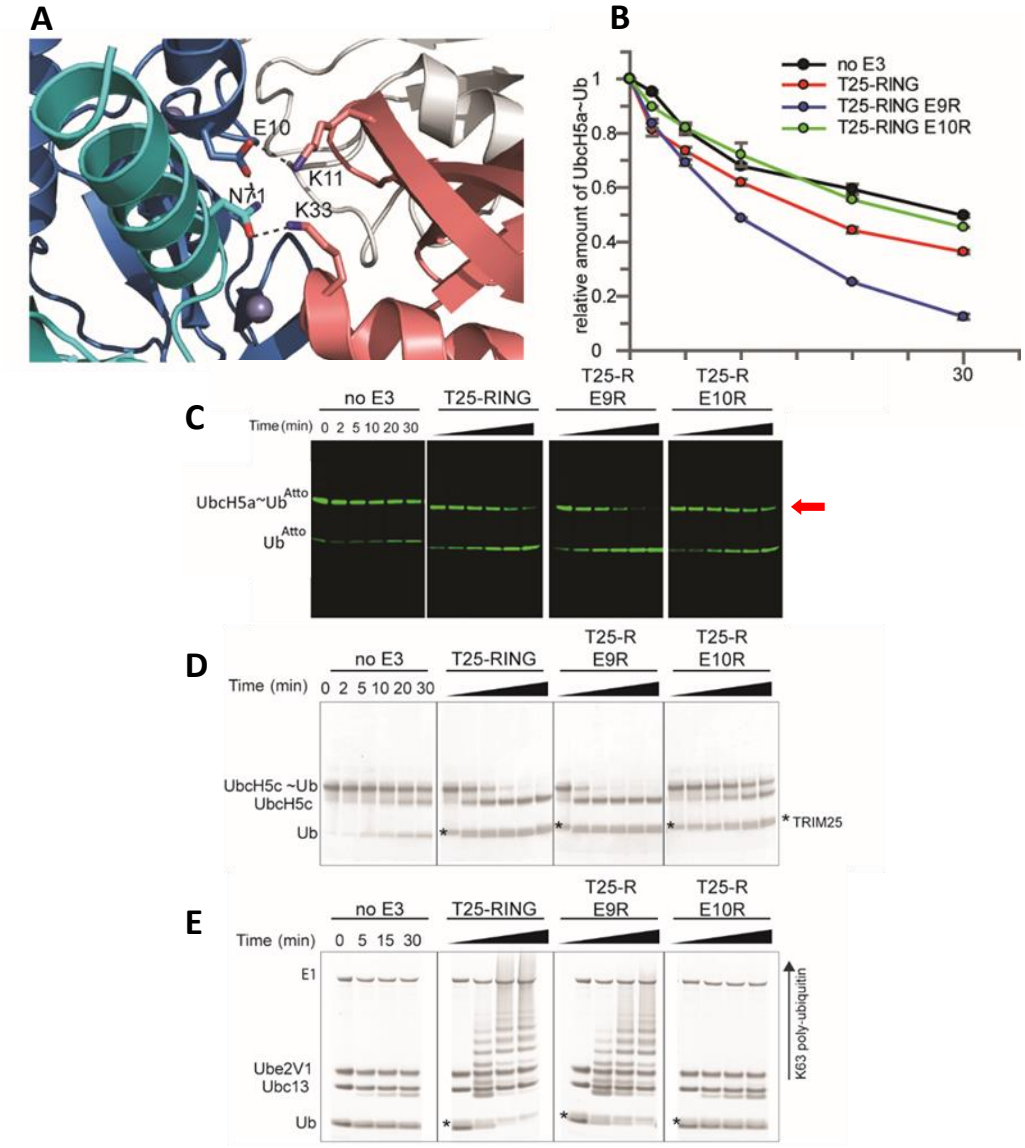

Figure 3.21. Atomic details of UbcH5a-Ub priming by TRIM25-RING.

A) Close-up of interaction network formed between TRIM25-RING (monomers coloured in blue and cyan) and proximal Ub (salmon) molecule. E2 is shown in grey. The side-chains of RING residues involved in a network of polar interactions with proximal Ub are shown: $E10_{RING1}$/$N71_{RING2}$/$K11_{Ub}$/$K33_{Ub}$. B, C) Quantitative analysis of UbcH5a~Ub^{Atto} discharge (using SDS-PAGE shown in C) in the presence of TRIM25-R bearing E9R and E10R mutations. E9 is in close proximity and was also tested. Conditions as described in Figure 3.18. Red arrow indicates band used for quantification. D) Discharge assays with UbcH5c~Ub and RING mutants. Conditions as shown in Figure 3.18. E) Ubiquitination assays with Ubc13/Ube2V1 and TRIM25-RING mutants as described in Figure 3.19. Asterisk indicates TRIM25-R constructs. Figure was adapted from [94].

3.7 Dimerization of TRIM25-RING in solution

The SEC-MALLS data shown in 3.4 revealed that the TRIM25-R domain is monomeric at concentrations up to 4 mg/ml (or 440 μM). However, the sample will be diluted on the SEC column around ~10-fold, meaning that the concentration evaluated will be lower. On the other hand, during crystallization the protein concentration increases dramatically for nucleation and crystal formation to take place. Given that TRIM25-RING dimerization was observed in the crystal structure and I have shown that it is necessary for the enzymatic activity of TRIM25, it was decided to examine if there is a weak tendency for TRIM25-R to dimerize at higher concentrations. For this reason, NMR was employed and the results were analysed with the help of Dr Diego Esposito (The Francis Crick Institute). The 2D ^{1}H-^{15}N-HSQC spectra of the ^{15}N-labelled TRIM25 RING construct were recorded at a concentration range between 125 μM and 1000 μM. Spectra show variable intensities and linewidths of the cross-peaks (Figure 3.22A). Close inspection of the spectra obtained for 125 μM and 570 μM revealed that despite the fact that the resonances are overall well-dispersed, the linewidth of most peaks is quite broad compared to the spectrum of a similar-sized monomeric RING construct of TRIM32 which shows sharp peaks (Figure 3.22A). Both a monomeric TRIM32-RING and a dimeric TRIM32-RING construct spectra were previously recorded at the same concentration and is presented here as control (kindly provided by Dr Diego Esposito). Intriguingly, the spectra of TRIM25-RING appear more similar to the one obtained for the dimeric TRIM32-RING (Figure 3.22A).

Further comparison of the two TRIM25-RING spectra recorded at different concentration (125 μM and 570 μM) reveals only slight chemical shift variations for some well-dispersed peaks, indicating that the overall structure of the domain is retained regardless of the protein concentration. These results likely imply that there is a dynamic exchange between a monomeric and a dimeric form of the protein.

In order to further validate the above observations, the hydrodynamic properties of the TRIM25-RING were examined by ^{15}N-nuclear relaxation measurements. Relaxation experiments monitor the loss of magnetization when radiofrequency (RF) pulses are applied to a macromolecule in solution in a strong magnetic field. The atoms enter an excited state due to the energy absorbed from the RF pulse which deteriorates over time, as atoms return to their equilibrium state. The

measurement of the longitudinal (R1) and transverse (R2) relaxation rates allows the estimation of a protein isotropic rotational correlation time which is the time required for a molecule to rotate through an angle of one radian and is dependent on its size and dynamics properties. The calculated value for the isotropic rotational correlation time of the TRIM25 RING is 6.42 ± 0.07 nsec (at 125 µM), 7.67 ± 0.09 nsec (at 570 µM) and further increases to 9.3 ± 0.1 nsec (at 1000 µM) (Figure 3.22B). This indicates a concentration-dependent increase in the size of TRIM25-RING. Interestingly, the theoretical values for TRIM25-RING derived from the crystal structure presented in 3.6.3 are 6.65 nsec for the monomer and 11.0 nsec for the dimeric RINGs whereas the calculated value for the TRIM32-RING-monomer is 6.80 nsec and 11.3 nsec for the TRIM32-RING-dimer (Figure 3.22B). Taken together, these NMR data suggest that TRIM25-RING has a weak tendency for dimerization, which is more prominent at higher protein concentrations. This ability is likely enhanced in the context of the full-length protein or by additional binding partners such as the E2~Ub conjugate.

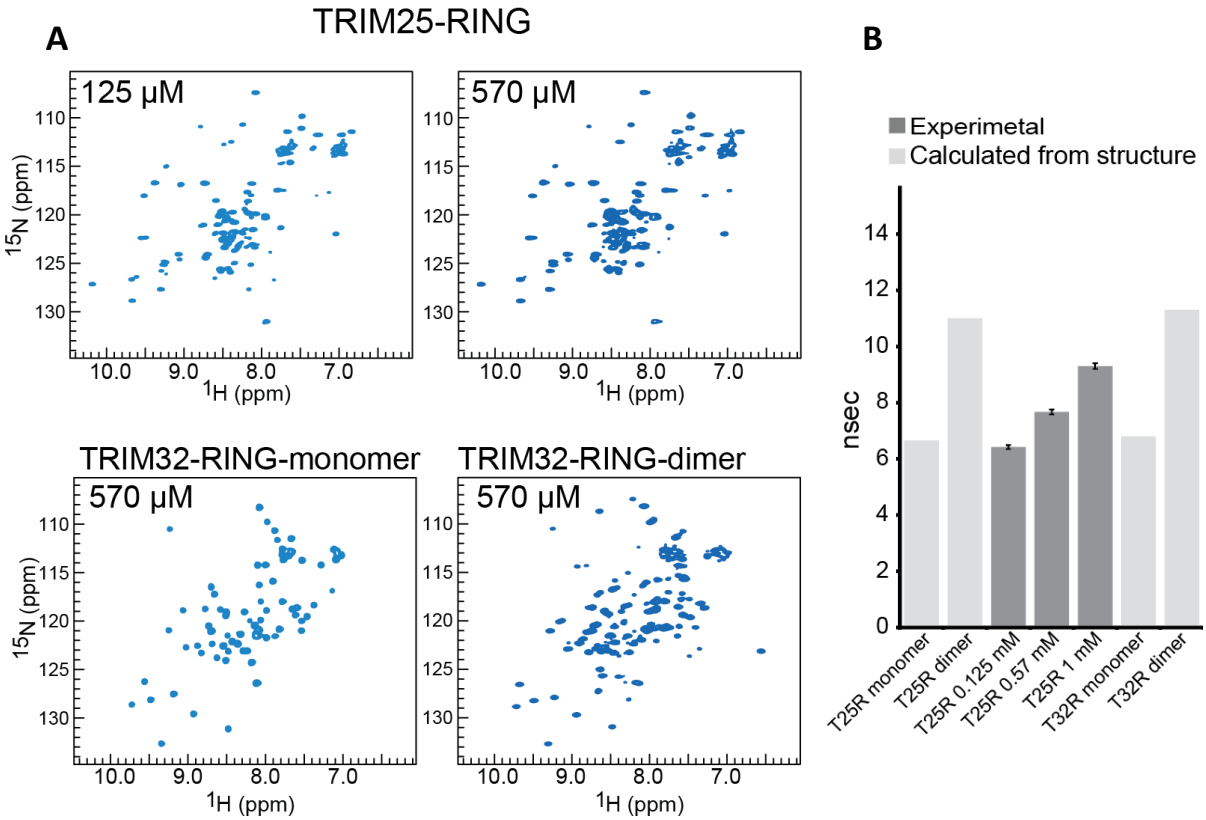

Figure 3.22. TRIM25-RING analysis in solution by NMR.

A) 2D ^{1}H-^{15}N-HSQC spectra were recorded for TRIM25-RING construct at two concentrations (125 and 570 µM) show well-dispersed intensity peaks with broad linewidth. For comparison, the spectra of a monomeric (results from partial deletion of the N-terminal α-helix and spans a.a. residues 10-84) and a dimeric (a.a. 1-93) TRIM32-RING construct with similar size (monomer is ~9 kDa) to TRIM25-RING (kindly provided by Dr Diego Esposito) are shown. The resonances observed for TRIM25-R spectra resemble more those seen in the spectrum of the TRIM32-R-dimer. B) Graph showing the calculated isotropic rotational correlation times of TRIM25-R and TRIM32-R constructs. These values were obtained from the relaxation analysis of resonances in the corresponding 2D ^{1}H-^{15}N HSQC spectra (dark grey bars, measured at 125, 570 and 1000 µM) or calculated from available structures (light grey bars) as comparison standards. Figure was adapted from [94].

Structural and biochemical analysis of the TRIM25-R/UbcH5a-Ub complex showed that contacts between both RING domains and each of the ubiquitin molecules are required for stabilization of the “closed” conformation. To further examine if binding of the E2~Ub conjugate promotes RING dimerization of the TRIM25-RING in solution, the elution profiles of TRIM25-R and UbcH5a-Ub were analysed using an analytical 10/300 S75 SEC column. Further experimental details are described in section 2.10.1.

As a control, UbcH5a-Ub and TRIM25-R were tested separately and eluted at a retention volume of V_e= 10.8 ml and V_e= 11.5 ml respectively (Figure 3.23A). The TRIM25-R/UbcH5a-Ub complex, which was reconstituted by mixing an equimolar concentration of UbcH5a and TRIM25-R (~400 µM each), was subjected to SEC and eluted at V_e= 10.5 ml. The SEC elution profile and analysis of the eluted species on an SDS-PAGE shows that the formation of a small proportion of the RING/E2~Ub complex could be observed (Figure 3.23A,B). This possibly indicates that TRIM25-R interacts weakly with UbcH5a-Ub which leads to complex dissociation during SEC. To further validate these observations, the experiment was repeated with the covalently-linked RING dimer. In this case, the retention volume of the TRIM25-R-linker-R construct was shifted from V_e= 10.4 ml (when tested on its own) to V_e= 9.4 ml (when in presence of UbcH5a-Ub). Analysis of the eluted fractions on an SDS-PAGE shows formation of a stoichiometric complex as judged by the similar intensity of the bands which correspond to the TRIM25-R-linker-R construct and UbcH5a-Ub (Figure 3.23C,D).

Comparison of the elution profiles observed for TRIM25-R/UbcH5a-Ub (V_e= 10.5 ml) and TRIM25-R-linker-R/UbcH5a-Ub (V_e= 9.4 ml) further indicate that dimerization and complex formation are linked but that complex formation is too weak for the isolated RING domain to be followed by SEC (Figure 3.23).

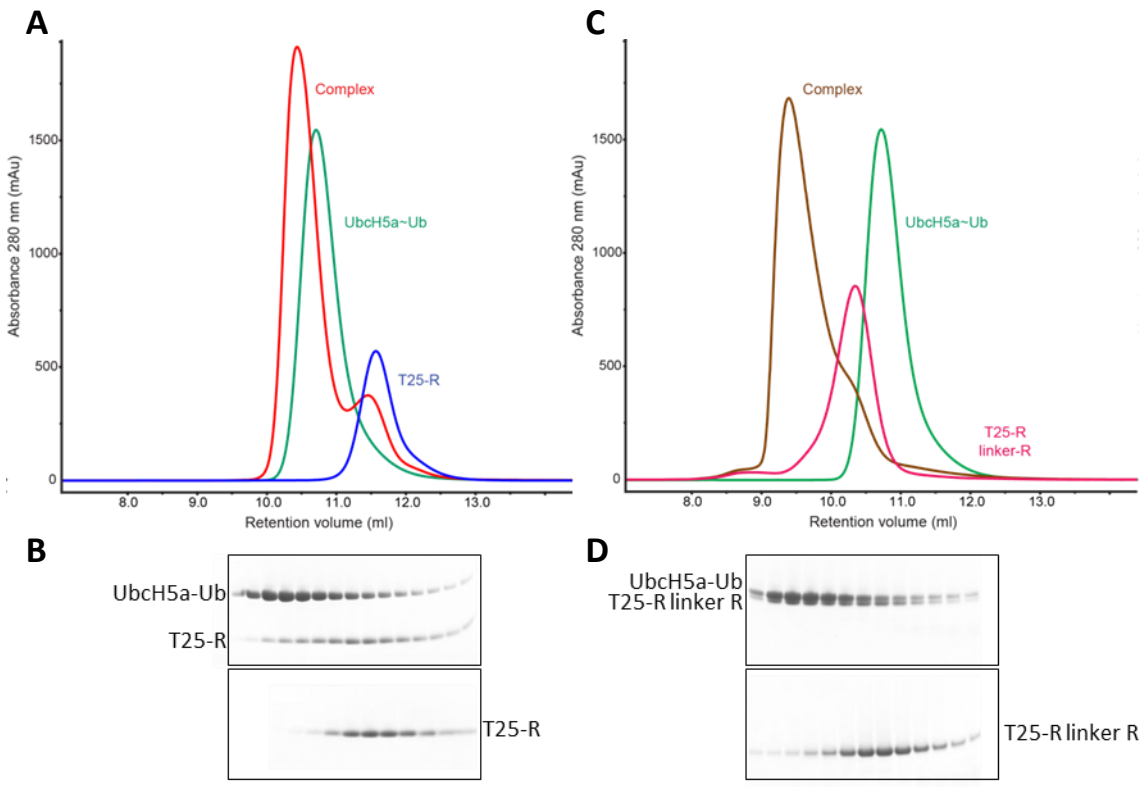

Figure 3.23. Analysis of TRIM25-RING/UbcH5a-Ub complex by SEC.

A) Chromatograms for TRIM25-R (blue trace), UbcH5a-Ub (green) and TRIM25-R/UbcH5a-Ub complex (red) obtained by SEC. Each protein was analysed at a concentration of 400 μM, both individually and in complex. B) The same eluted protein fractions of the complex (top panel) and the RING in isolation (lower panel) were collected and analysed by SDS-PAGE as shown. The elution volume of the sample with both components (RING and E2-Ub) indicates complex formation but SDS-PAGE analysis suggests complex dissociation. C,D) The same experiment as shown in A,B was repeated but with the covalently-linked TRIM25-R dimer as control. In this case, there is a clear difference in the elution volume of the TRIM25-R-linker-R/UbcH5a-Ub (brown trace) compared to SEC runs with individual components. SDS-PAGE confirmed that a stoichiometric complex was formed.

3.8 Crystallisation trials with TRIM25-RBCC$_L$

Next, in an effort to obtain further structural insights about the TRIM25 RING dimerization in the context of the RBCC construct, a number of crystallization trials were performed with TRIM25-RBCC$_L$ in isolation but also with interaction partners previously identified through the enzymatic assays described in this thesis. These included UbcH5a-Ub, Ubc13 and Ubc13-Ub. Ubc13 C87K/K92A (C87K allows the formation of a non-hydrolysable isopeptide bond and K92A mutation suppresses non-specific auto-ubiquitination) was charged with Ub in a similar way as described for UbcH5a-Ub and previously established [91, 93]. Crystallization trials were performed with a concentration of 2.5 mg/ml (~60 μM) TRIM25-RBCC$_L$ (which was the highest concentration achieved for this construct –see also section 3.2.2) and different concentrations of E2/E2-Ub (60 and 120 μM). Crystallization trials for the above components were carried out using ten different crystallization screens, containing approximately 1000 different conditions and two different incubation temperatures (4° and 18° C). Initial hits included spherullites and microcrystals and appeared only in trays containing the combination of TRIM25-RBCC$_L$/Ubc13-Ub (60 μM each) at 18° C. The spherullites are transparent clusters formed of protein without the characteristic edges of a crystal (Figure 3.24). Microcrystals included small elongated crystals with a size of ~5 μm which are not appropriate for collection of X-ray diffraction data. Extensive optimisation trials were performed and included streaking ("breaking" the spherullites using micro-tools) and seeding using microcrystals in several different buffer/precipitant screens. These approaches are well-established and have proved successful in the past. In this case, larger crystals (up to 15 μm) appeared on the seeded plates after 5 days and subsequent optimization rounds did not increase the size (Figure 3.24). These crystals were harvested and tested for X-ray diffraction both in-house and in Diamond Synchrotron without success (less than ~ 7 Å). Therefore, in order to gain structural insight into the overall conformation of TRIM25-RBCC$_L$, it was decided to adapt a different strategy detailed below.

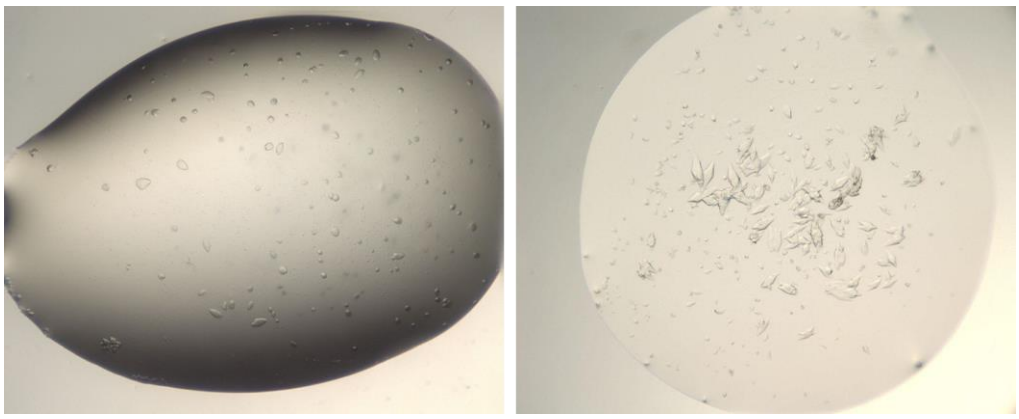

Figure 3.24. Crystals of TRIM25-RBCC$_L$/Ubc13-Ub.
Initial hits (left image) included crystalline material and sphellulites which are not suitable for X-ray diffraction. Further optimization resulted in small crystals (right image) which did not diffract well.

3.9 Solution structure of TRIM25

To gain further insight into the low-resolution structure of longer constructs of TRIM25, small-angle X-ray scattering (SAXS) experiments were performed on R, RB1, RB1B2 and RBCC$_L$ constructs with the help of Dr Diego Esposito (The Francis Crick Institute). Data were collected at Diamond and Soleil Synchrotrons and details of data collection and analysis are described in section 2.11.5.

One of the key observations derived from analysis of the SAXS data and serves as a quality control for the SAXS measurements is that the calculated molecular masses for all TRIM25 constructs are in good agreement with the oligomerization pattern observed by SEC-MALLS (shown in 3.4). The *ab-initio* models of the molecular envelopes for all TRIM25 constructs were calculated and fitted with available structural coordinates using the program CRYSOL. Monomeric TRIM32-RING and dimeric TRIM32-RING constructs were used as controls.

The molecular envelope calculated for the TRIM25-RING domain is that of an elongated sphere with a maximum dimension (D_{max}) of 48 Å and a cross section corresponding to the maximum of the P(r) distribution of ~16 Å (Figure 3.25A,B). Interestingly, the monomeric TRIM32-RING construct and TRIM25-RING have very similar scattering profiles and pair-distribution functions indicating a similar overall structure (Figure 3.25A,B). The TRIM32-RING-2mer is slightly larger (~60 Å) and the maximum of the P(r) function is shifted to the right, indicating a larger

cross section (Figure 3.25A,B). The monomeric form of the TRIM25-RING seen in the crystal structure has a good fit to the calculated SAXS envelope (χ^2 = 1.2) (Figure 3.25B). Similarly, both the NMR structure of TRIM32-RING-1mer and the crystal structure of the TRIM32-RING-2mer fit the corresponding SAXS envelopes with χ^2 = 0.4 and χ^2 = 0.5 respectively, indicating a very good fit and providing a good comparison control for TRIM25-RING to both a monomeric and dimeric protein in solution (Figure 3.25B). These data collectively indicate that the TRIM25-RING is monomeric under the experimental conditions, which is good agreement with the NMR data discussed in section 3.7.

The calculated envelopes for TRIM25-RB1 and TRIM25-RB1B2 have elongated cylindrical shapes with D_{max} values of 94 Å and 110 Å respectively (Figure 3.26A,B). The value of the peak in the pair-distribution plot is comparable to that of the monomeric RING indicating an arrangement of domains similar to beads on a string. Comparison of the D_{max} value for RB1 and RB1B2 shows that they differ by approximately 16 Å in length, which coincides with the diameter of the B-box (calculated from available structures). Given that there is only a short linker present between the two B-boxes, it is reasonable to speculate that the two B-boxes are closely packed to each other, an orientation reminiscent of the only available NMR structure of the tandem B-Boxes from TRIM18.

Next, the TRIM25-RBCC$_L$ construct was analysed using size-exclusion chromatography coupled to SAXS (SEC-SAXS) (Figure 3.27A,B). This technique was employed to ensure that the sample was monodisperse and occupies a single oligomeric state (i.e. dimeric species only) (Figure 3.27A). The profile in the pair-distribution function (Figure 3.27C) points to an elongated shape and is similar to previously reported profiles for the CC-containing regions of TRIM5α and TRIM20 [158, 166]. Surprisingly, the D_{max} value for TRIM25-RBCC$_L$ (183 Å) is very similar to that of TRIM5α-BCC construct (180 Å) and to TRIM25-CC (170 Å) (calculated from the crystal structures) (Figure 3.27C,D). However, the cross-section of the TRIM25-RBCC$_L$ is calculated at 61 Å, which is larger than that calculated from the TRIM25-CC structure (48 Å). These observations suggest that the RB1B2 domains are not protruding from the CC but possibly fold back towards the middle of the CC. This model is further supported by the structure of the TRIM5α-BCC construct, in which the two B-Box2 domains pack against either side of the CC region. Moreover, further analysis suggests that the RB1B2 domains are flexibly linked to the CC region of TRIM25, which implies that RB1B2

may occupy different conformations and could potentially end up dimerizing on top of the CC domain (Figure 3.27E). In this case however, SAXS data represent the average of all different conformations that the protein adopts in solution and no conclusions about sub-populations can be drawn from the present data.

Furthermore, the crystal structure of the TRIM25-CC was solved for the construct spanning amino acid residues 189 to 379 but the model shows only residues 189-360, indicating that the last 19 residues are part of a flexible linker. Given that the TRIM25-RBCC$_L$ construct used for SAXS analysis has C-terminal boundary residue 433, it is reasonable to speculate that this ~70 residue linker, which was necessary for achieving a higher protein concentration (see also section 3.2.2), might have an effect on the size of the calculated molecular envelope for TRIM25-RBCC$_L$ and further studies are hence required, using a TRIM25-CC construct that spans residues 189-433.

Overall, the SAXS data suggest that the TRIM25-RING domain is a monomer and is flexibly linked to the B-Box domains, which appear though to pack closely to each other. A first view of the low resolution TRIM25-RBCC$_L$ structure was obtained and allows us to propose a model for RING dimerization where the two RB1B2 domains bind back towards the middle of the CC bringing the two RING domains together (Figure 3.27E,F).

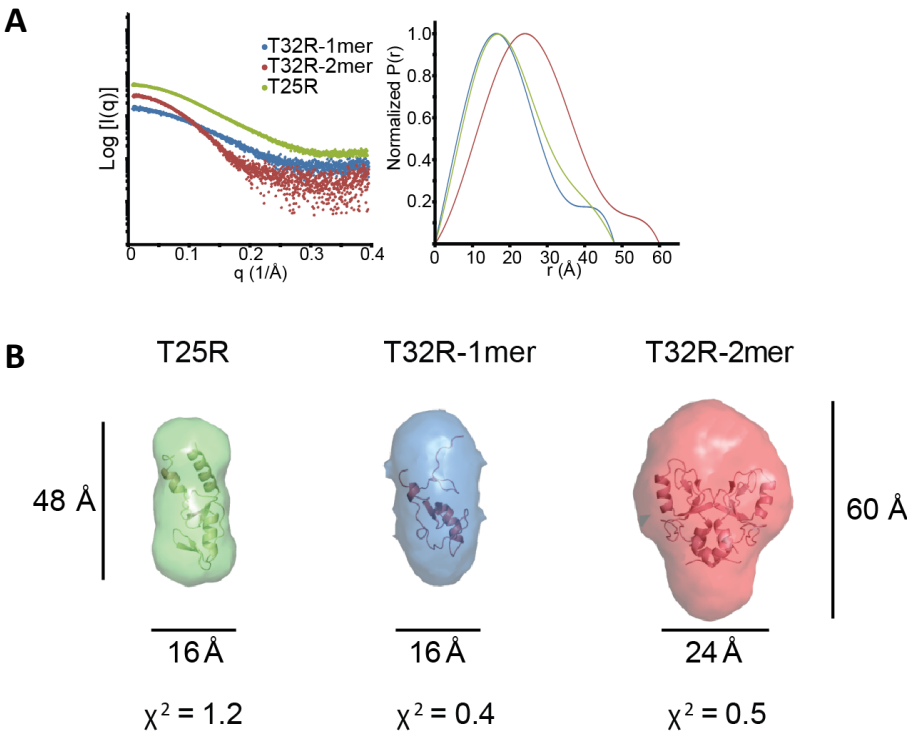

Figure 3.25. SAXS analysis of TRIM-RING.

A) X-ray scattering profiles of TRIM25-R (green), TRIM32-R-1mer (blue) and TRIM32-R-2mer (left panel) and their normalised pair-distribution functions P(r) used for calculations of the molecular dimensions (right). B) The low-resolution *ab initio* models derived from the SAXS data analysis fitted with the available structures. The χ^2 values shown indicate a good agreement between the envelopes and the structures. Bars indicate dimensions. Figure was adapted from [94].

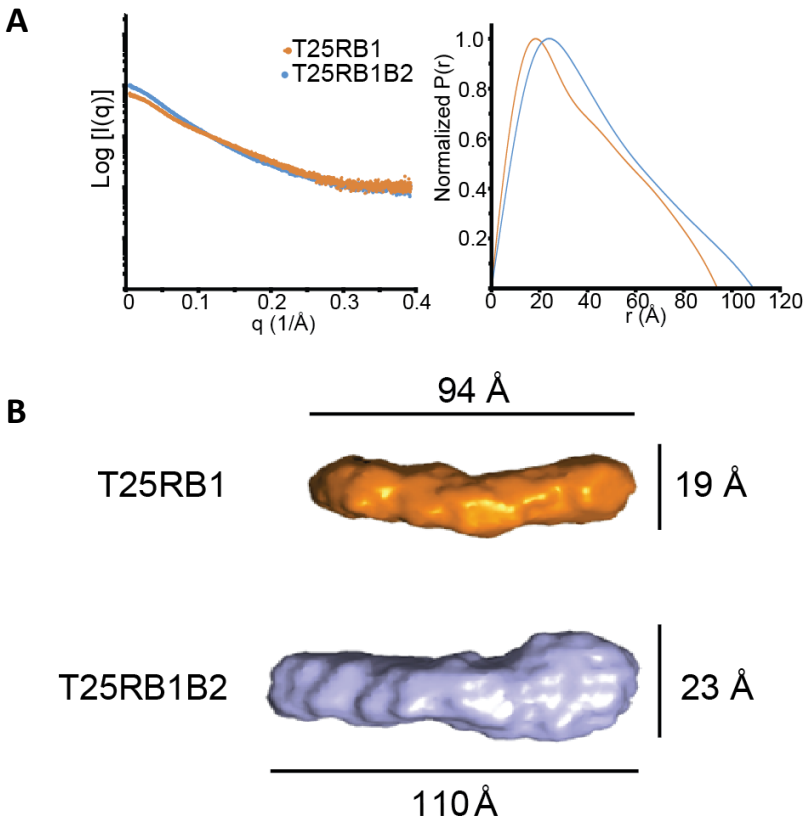

Figure 3.26. SAXS analysis of TRIM25-RB1 and RB1B2.

A) X-ray scattering profiles of TRIM25-RB1 (orange) and TRIM25-RB1B2 (light blue) and their normalised pair-distribution functions P(r) used for calculations of the molecular dimensions (right). B) The low-resolution *ab initio* models derived from the SAXS data analysis. Bars show dimensions. Figure was adapted from [94].

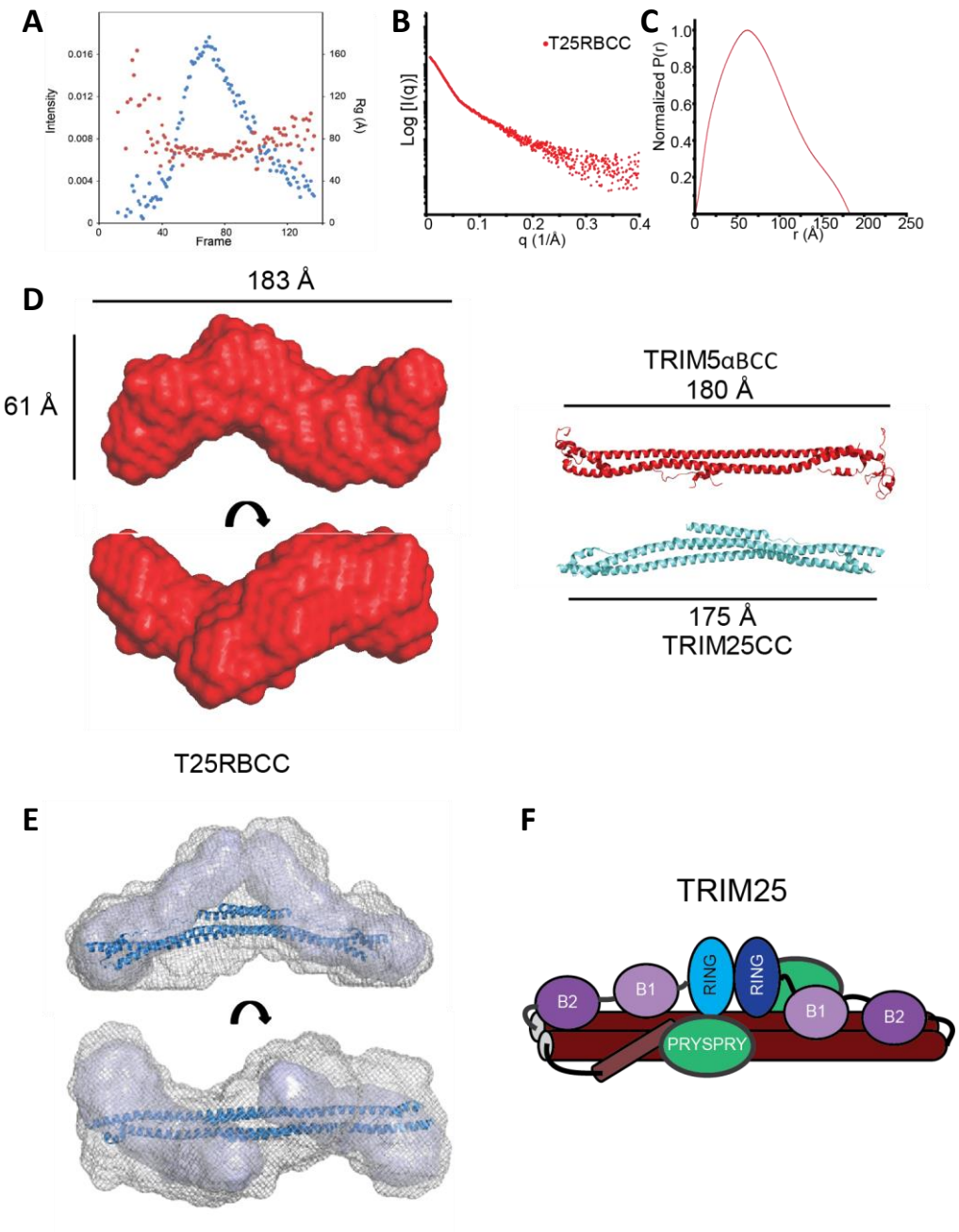

Figure 3.27. SEC-SAXS analysis of TRIM25-RBCC$_L$.

A) Size-exclusion chromatography in-line with SAXS data recording for TRIM25-RBCC$_L$. The intensity (left X-axis) and radius of gyration (Rg) (right X-axis) profiles are reported as a function of the frames recorded at equal time intervals. B) X-ray scattering profile of TRIM25-RBCC$_L$. C) Normalised pair-distribution function P(r) used for calculations of the molecular dimensions. D) The low-resolution *ab initio* model derived from the SEC-SAXS data analysis shown in two orientations and presented in scale with the structures of TRIM5α-BCC (4TN3.pdb) and TRIM25-CC (4LTB.pdb). Bars indicate dimensions. E) The TRIM25-RBCC$_L$ envelope (shown as grey mesh) can accommodate two RB1B2 envelopes (shown as surface representations in light blue. The TRIM25-CC is shown as ribbon (blue). F) Cartoon representation of a RING dimerization model for TRIM25. Figure was adapted from [94].

3.10 Summary and Discussion

The work presented in this chapter was aimed at obtaining insights into the catalytic function of the tripartite motif in TRIM25. Initially, the activity of TRIM25-RBCC construct was tested using a number of *in vitro* ubiquitination assays. Results obtained showed that the RBCC domain is active with UbcH5 isoforms A and C (isoform B and D are also active as described recently [95]. TRIM25-RBCC was further shown to activate the heterodimeric E2 formed of Ubc13/Ube2V1. Ubiquitination assays with TRIM25-RBCC and UbcH5 or Ubc13/Ube2V1 further showed that chain linkage specificity relied on the E2s and not on TRIM25. In the context of RING E3s, UbcH5 does not enforce a single type of polyubiquitin chains. This was validated using ubiquitination assays with TRIM25, UbcH5 and different Ub mutants, which showed that different types of ubiquitin chains were formed. In contrast to UbcH5 which has no Ub chain linkage specificity with RING E3s, Ubc13/Ube2V1 can exclusively form K63-linked polyubiquitin chains. When tested with TRIM25-RBCC, Ubc13/Ube2V1 retained its ability to form only K63-linked chains.

The physiological substrate of TRIM25 is RIG-I and an interaction occurs between the TRIM25-PRYSPRY and RIG-I-2CARD domains. The crucial role of K63 chains in RIG-I activation is well-established. Polyubiquitin chains linked through K63 are “wrapping” around a homo-tetrameric RIG-I complex which is recognized by other proteins including MAVS and acts as a signalling platform leading to IFN production. However, at the moment there are two models suggested for the K63-linked chain recognition by RIG-I-2CARD. The first model is supported by *in vitro* RIG-I signalling cascade reconstitution assays which showed that unanchored K63 chains were isolated from cells and acted as potent activators of RIG-I signalling [216]. This model is also supported by the crystal structure of the RIG-I-2CARDs bound to K63-linked polyubiquitin chains [219].The second model suggests that K63-linked chains need to be covalently attached to lysine residues of RIG-I-2CARD to induce a stable formation of the tetrameric RIG-I. At present, the precise details that lead to RIG-I activation are less understood. A cooperative mechanism between unanchored and covalently attached K63 chains is possible though, given that a previous study has illustrated using gene silencing techniques that both UbcH5 and Ubc13/Ube2V1 are required for optimal TRIM25-mediated RIG-I activation whereas depletion of either one partially inhibits IFN production [216]. In a simplified version of this

multi-component system, it is possible that in the presence of TRIM25, UbcH5 attaches ubiquitin molecules to RIG-I (initiation), which are then extended to K63-linked polyubiquitin chains through Ubc13/Ube2V1 (elongation). Removal of UbcH5 from this system would still allow formation of unanchored K63 chain which can non-covalently bind and activate RIG-I. Removal of Ubc13/Ube2V1 compromises the efficient formation of long K63 chains. Loss of Ubc13/Ube2V1 could be partially rescued by UbcH5 function but this process is likely to be less efficient. Nevertheless, complexity of this system has increased thanks to a very recent report suggesting that Riplet, another RING E3 ligase, is also involved in RIG-I ubiquitination. Similarly to TRIM25, Riplet recognizes RIG-I-2CARD through its SPRY domain and mediates RIG-I ubiquitination through UbcH5 and Ubc13/Ube2V1 [294]. The authors further suggested that in the context of Riplet, Ubc13/Ube2V1 facilitates the synthesis of polyubiquitin chains while UbcH5 promotes the covalent attachment of those chains to RIG-I. Details of the functional interplay between TRIM25, Riplet and RIG-I along with the interacting E2 enzymes are awaited with great interest.

The E2 enzymes which showed activity with the TRIM25-RBCC construct (UbcH5 and Ubc13/Ube2V1), were further tested with shorter TRIM25 constructs including R, RB1 and RB1B2. These experiments were aimed at providing information about the contribution of each domain of the tripartite motif on the catalytic activity of TRIM25. Results obtained showed that the TRIM25-RING domain sufficiently discharges the thioester-bound UbcH5~Ub and can mediate the formation of K63-linked Ub chains through Ubc13/Ube2V1. The presence of the B-Box domains and the CC region further enhanced the catalytic ability of TRIM25 to discharge UbcH5~Ub but did not affect the formation of K63 chains by Ubc13/Ube2V1.

In order to gain further insights into the catalytic mechanism of TRIM25-RING, the crystal structure of TRIM25-R/UbcH5-Ub was solved. A key observation was that the RING domain crystallized as a dimer, with dimerization mediated by 4 helices on either side of the Zn^{2+}-binding RING core packing closely to each other. This dimerization interface is similar to ones observed for other dimeric RING E3 including Rad18, the heterodimeric E3 BRCA1/BARD1 and TRIM32 [79, 80, 94]. The role of dimerization was biochemically tested using UbcH5~Ub discharge assays and Ubc13/Ube2V1 chain formation assays. These experiments showed that dimerization of the TRIM25-RING is necessary for its

E3 ligase activity and disruption of the RING-RING interface abolishes enzymatic activity. The crystal structure of the TRIM25-R/UbcH5-Ub complex reveals details of the precise molecular determinants that TRIM25 employs for E2~Ub binding and activation. The binding interface of TRIM25 to UbcH5 is similar to all previously described RING/E2 structures. Moreover, the TRIM25-R/UbcH5-Ub structure shows that the E2~Ub conjugate adopts a “closed” conformation in which the Ub molecule binds back towards the E2 enzyme. In this orientation, Ub is primed for transfer onto a substrate. In this complex, both RING domains contact each ubiquitin molecule through residues from the core RING domain but also from the 4-helical bundle. These contacts presumably stabilize the closed conformation as mutational analysis showed that they are important for activity. In all previous structures of dimeric RING/E2-Ub complexes (RNF4 and BIRC7 bound to UbcH5-Ub) the same E2-Ub closed state was observed, indicating that dimeric RING E3s employ this mechanism for activating an E2~Ub conjugate. In addition, the structure described in this thesis shows that TRIM25 uses an additional feature to enforce the closed conformation that is reminiscent of the monomeric E3 Cbl-b that uses a phospho-tyrosine outside the RING domain to stabilise the E2~ubiquitin conjugate [92]. There are no reports of phosphorylation adjacent to the RING domain regulating TRIM catalytic activity and instead TRIM25 uses a glutamate in the N-terminal helix to contact the opposing ubiquitin. This spatial arrangement is highly similar to the pY of Cbl. Interestingly, this glutamate is conserved in many TRIM ligases, including TRIM32 (the structure of which was solved in the Rittinger group), and mutation to arginine severely disrupts catalytic activity in either protein suggesting that its functional role is conserved. At present it is not clear why TRIM ligases would require two different structural features to stabilise the closed E2~Ub conformation but we speculate that it could either provide an additional level of regulation or may be used to further stabilise the closed conformation in cases where RING dimerization is weak or the orientation of the RINGs in the dimer may prevent efficient contact of both RINGs with ubiquitin.

Shortly after publication of our structure, another study reported the TRIM25-RING domain bound to Ubc13-Ub [95]. Interestingly, the authors made the same observations as we described for TRIM25-R/UbcH5-Ub and reached similar conclusions, indicating that TRIM25 activates Ubc13~Ub conjugate in the same manner. Nevertheless, previous studies have shown UbcH5 and Ubc13 have

slightly different operation modes. In the absence of a RING E3, the conjugate of UbcH5~Ub exists in many different conformations, with the majority of them populating an open state. In contrast, Ubc13~Ub adduct occupies mostly closed conformations, explaining why Ubc13~Ub is active with Ube2V1 even in the absence of a RING E3 [88]. The E2~Ub closed state as imposed by RING E3 ligases shifts the reactivity of the E2 thioester towards aminolyis (transfer onto a K residue). In contrast, HECT and RBR E3 ligases rely on an open state of the E2~Ub intermediate, in which transthiolation is favoured (transfer onto a C residue) and aminolysis is suppressed.

Given that structural and biochemical analysis showed that the TRIM25-RING needs to be a dimer for activity, a systematic SEC-MALLS analysis of the different domains of TRIM25 (R, RB1, RB1B2, CC, B1B2CC, PRYSPRY and RBCC) was performed. These data revealed all constructs lacking the CC region were monomeric, whereas the CC and B1B2CC constructs were dimeric. The fact that the RING domain was monomeric under the SEC-MALLS experimental conditions was contradictory to the dimeric state of the TRIM25-RING seen in the crystal structure. NMR relaxation rate experiments were employed in order to observe the oligomeric state of TRIM25-R at the highest concentration of 1 mM. These experiments showed that the TRIM25-R domain has a weak tendency to dimerize, explaining why it was not observed during SEC-MALLS in which the examined concentration of TRIM25-R was much lower.

These results overall suggest that the TRIM25-RING domain is mainly monomeric but has a weak tendency for dimerization which is also required for activation. The complex between the RING and UbcH5a~Ub conjugate crystallized as a dimer suggesting that binding of the ubiquitin–loaded E2 stabilises the otherwise weak RING-RING interaction. Such an increase in apparent affinity most likely explains why catalytic activity could be detected under assay conditions in which the RING is largely monomeric.

Intriguingly, the B-boxes of TRIM25 have no apparent effect on oligomerization, clearly setting them apart from the best studied member of the TRIM family, the retroviral restriction factor TRIM5α. In human TRIM5α, the B-Box2 domain is a trimer in solution, with E118/R119 (in rhesus TRIM5α sequence is E120/R121) at the centre of the interface. Interestingly, in TRIM25 the equivalent positions are occupied by hydrophobic residues (L180/V181) possibly explaining why TRIM25-B-Box2 is not involved in oligomerization. In TRIM5α, higher order

oligomerization is a vital feature for its function as it allows it to bind to the retroviral capsid [178, 184, 292]. Nevertheless, this raises questions about the role of B-boxes in those TRIMs that do not require additional oligomerization domains.

Further SEC-MALLS analysis showed that the RBCC construct was dimeric with a tendency to form higher-order oligomeric species. Given that the B-Box domains have no effect on oligomerization of TRIM25, these observations imply that the dimeric CC may act as platform which favours RING dimerization.

In order to gain structural insights into the TRIM25-RBCC constructs, a series of SAXS experiments was performed. The results showed that the RBCC construct is an elongated, dimeric S-shaped molecule and further SAXS analysis suggests that the RB1B2 domains are flexibly linked to the CC. Given that the RING domain is monomeric and dimerization is a prerequisite for E3 activity, two possible models of activity can apply: a) the RING domains of a CC-mediated dimer fold back over the antiparallel coiled-coil allowing for dimerization of the RING domains in an intra-molecular fashion or b) higher order oligomerization takes place.

The first mode of action proposed is supported by the observation that full-length TRIM25 is dimeric and hence the only mechanism to form a dimeric RING is in an intra-molecular manner [94, 167]. Interestingly, it has recently been shown that the C-terminal PRYSPRY domain of TRIM20 folds back across the coiled-coil [166]. If the PRYSPRY of TRIM25 behaves in a similar fashion, this could result in an overall architecture in which the RING and substrate-binding PRYSPRY domains are located in close proximity along the coiled-coil to facilitate ubiquitin transfer from the E2 onto the substrate (RIG-I). In such an arrangement RING dimerization could potentially be enhanced by substrate binding thereby ensuring that TRIM25 activity is only unleashed in the correct setting. This is particularly interesting in light of the observation that viral proteins such as NS1 bind to the coiled-coil region of TRIM25 [234], which could prevent intramolecular RING dimerization in this model and hence activity (further discussed on chapter 4).

If the second mode of activation applies and TRIM25 requires further oligomerization for catalytic activity, it can be speculated that extra stabilization may be provided by the interaction with the ubiquitin loaded E2 or the substrate. In a recent study, it was reported that binding of RIG-I-2CARD to TRIM25

enhances the E3 ligase activity of the RING domain [95]. These data indicate that substrate binding causes an increase in the local concentration of TRIM25 and thus allow for RING dimerization through avidity effects. Further studies are now required to test these models and examine how RIG-I binding affects TRIM25.

Interestingly, in a parallel study performed within our group, it was shown that TRIM32 has a different self-association mechanism to that I have described here for TRIM25 [94]. The structure of the TRIM32-RING shows that it is also a dimer through the four α-helices as reported for TRIM25. The main difference however, is that the TRIM32-RING is a stable dimer and the TRIM32-RBCC (composed of RING, B-Box2 and CC domains) is an elongated C-shaped tetramer in which the two dimeric RING-B-Box2 domains protrude on either side of the CC [94]. These structural features of TRIM32 are different to TRIM25 and TRIM5α highlighting a remarkable diversity among the TRIM proteins. Further studies on different TRIM members are required to gain further insights which may lead to further categorization according to their oligomeric properties.

Overall, results presented in this chapter reveal novel structural and mechanistic insights into the catalytic activation of TRIM25.

4. Results

Structure and mechanism of NS1-mediated TRIM25 inhibition

4.1 Overview

Influenza viruses have evolved numerous mechanisms to suppress host innate immune responses. Given the crucial role of TRIM25 in the activation of an anti-viral signalling pathway it is not surprising that TRIM25 is itself targeted by influenza A. Previous work has established that the influenza A non-structural protein 1 (NS1) binds directly to the TRIM25-CC region. This event has inhibitory effects on the downstream ubiquitination and activation of the cytosolic pattern recognition receptor RIG-I which is required to activate a signalling pathway that leads to type 1 interferon production. The main aim of the work presented in this chapter was to structurally characterize the interaction between NS1 and TRIM25 and to study the mechanism of NS1-mediated TRIM25 inhibition.

4.2 Initial purification strategies for NS1/TRIM25 complex

NS1 is composed of two domains, the RNA-binding domain (RBD) and the effector domain (ED) which are linked through a short flexible linker region. In some strains, NS1 has a 30 residue-long flexible C-terminal tail (Figure 4.1). Based on mutational analysis reported in literature, it has been suggested that both RBD and ED of NS1 isolated from strain A/Puerto Rico/8/1934 H1N1 (hereafter referred to as NS1) are required for complex formation with TRIM25-CC [234]. Initial efforts were thus focused on identifying soluble NS1 constructs containing both RBD and ED domains. Unfortunately, wild-type NS1-FL readily aggregates and precipitates even at low concentrations. In an effort to examine if binding to TRIM25 stabilizes NS1-FL, the two genes were cloned in different vectors including pET49b (for a GST-tagged), pET5247 (for a His-SUMO tagged, see also section 2.2.2), pET47b (for His_6-tagged) and pET52b (for Strep-II-tagged). Plasmids containing different tagged versions of NS1 and TRIM25-CC were co-transformed in *E.coli* cells and positive colonies were selected on the basis of dual antibiotic resistance (i.e. colonies which grew in the presence of both Kanamycin and Amplicillin were selected for His_6-NS1 and Strep-II-TRIM25). Many different combinations of tags were performed and attempts to purify the complex were unsuccessful as the two proteins were detected in the insoluble fractions. Additionally, vectors expressing either NS1 or TRIM25-CC were transformed separately in *E.coli* cells which were then co-lysed. This strategy did not improve solubility of NS1 and hence of the NS1/TRIM25-CC complex. The same protocols were followed for co-expression and co-purification of the NS1-FL and TRIM25-$RBCC_L$ constructs without any further success. These observations are in agreement though with previous reports mentioning the high aggregation propensity of wt NS1-FL. To circumvent this problem, mutations that suppress this property of NS1-FL have been explored.

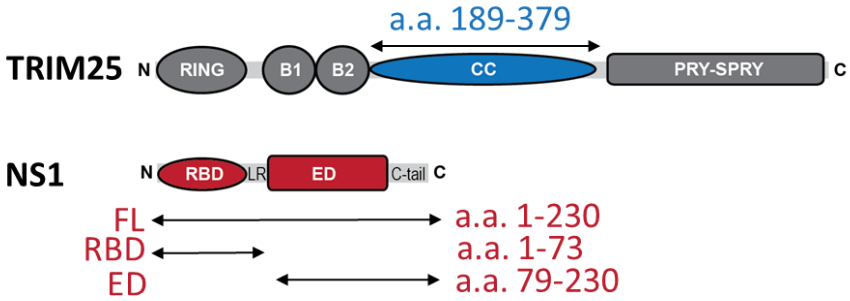

Figure 4.1: NS1 and TRIM25 domains.

Schematic representation of the TRIM25 and NS1 domain structures. The TRIM25-CC region, which is required for interaction with NS1, is shown in blue, along with amino acid boundaries. The different constructs of NS1 used throughout this chapter are shown: full-length (FL), RNA-binding domain (RBD) and effector domain (ED). LR indicates the linker region between RBD and ED. An unstructured C-terminal tail follows the ED.

4.3 Assessment of the oligomeric state of NS1

Previous structural studies on NS1 were carried out using a construct containing two mutations in the RBD (R38A/K41A), which abrogate aggregation and allowed structure determination of full-length NS1 from two different viral strains (H5N1 and H6N6). However, these mutations (R38A/K41A) have been suggested to abolish the interaction with TRIM25-CC [234] so it was evident that other NS1-FL constructs with improved solubility needed to be identified. Nevertheless, this construct was expressed and purified with the intention of using it as a negative control (non-binding to TRIM25-CC). Tryptophan 187 in the effector domain has been shown to mediate dimerization of the isolated ED in a number of studies and therefore the effect of the W187A mutation was tested in the context of the full-length protein. NS1-FL (W187A) has greatly improved solubility compared to the wt NS1.

The oligomeric state of all NS1 constructs and mutants was examined by SEC-MALLS at two concentrations (4.5 and 9 mg/ml) using an S200 10/300 column as described in section 2.11.3 (Figure 4.2). In summary, it was observed that NS1-FL (R38A/K41A) is mostly tetrameric, with some tendency to form higher order oligomers; NS1-FL (W187A) is mostly dimeric with some minor tendency to form higher-order oligomers and NS1-FL (R38A/K41A/W187A) is a stable dimer. Additional SEC-MALLS experiments with the isolated wild-type NS1-RBD and NS1-ED domains showed that while RBD is dimeric, the ED domain is in an

equilibrium between a monomeric/dimeric state (Figure 4.2). These results confirm that NS1 primarily dimerizes through the RBD domain and further self-associates through W187.

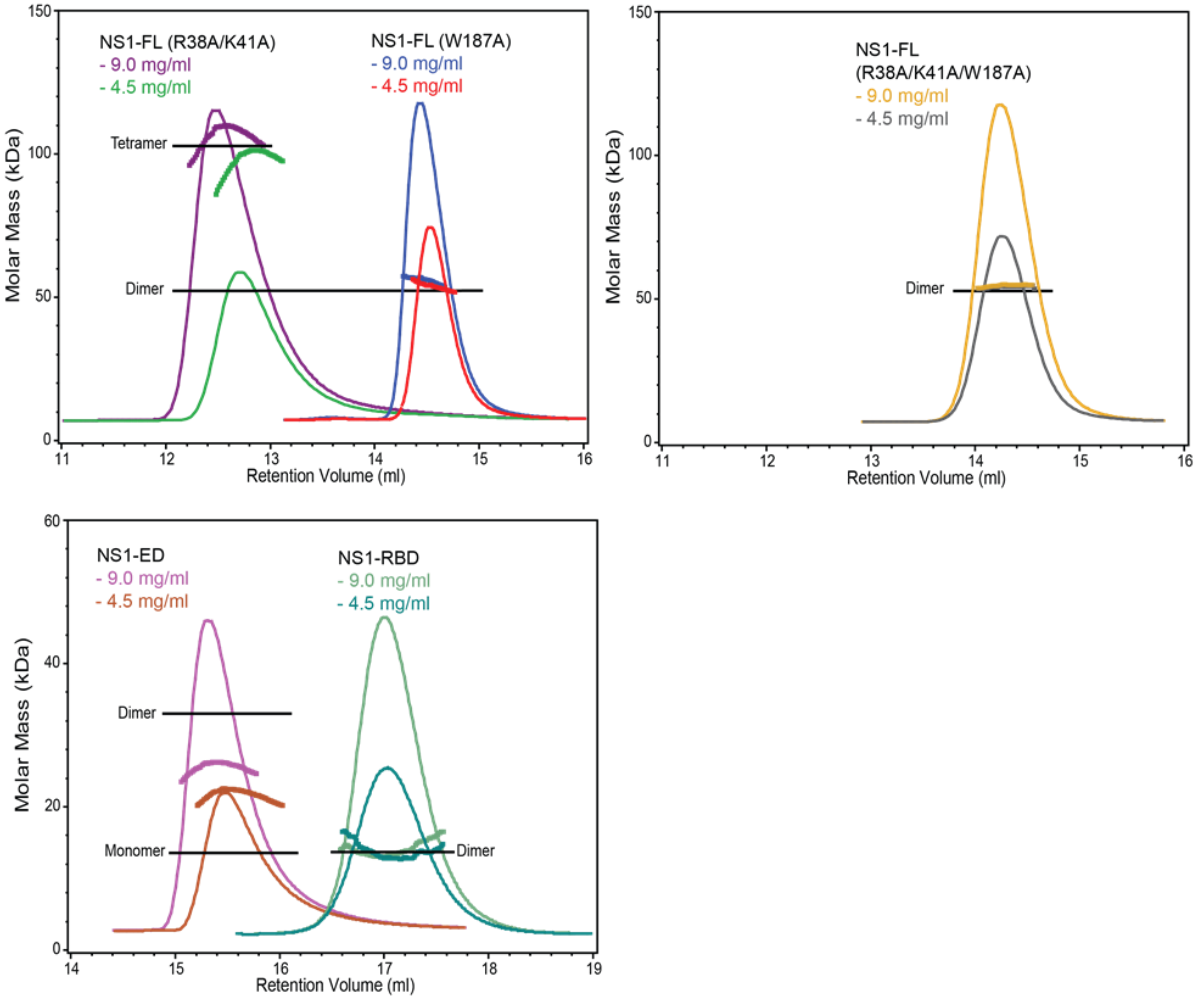

Figure 4.2: SEC-MALLS analysis of NS1 oligomeric state.

The chromatograms show the UV absorbance at 280 nm (curve) and the weight-averaged molecular masses of the samples (dotted-line). The theoretical/expected molecular mass for each construct is shown as a straight line and is parallel-to-the-X-axis. Constructs containing the RBD domain were expected to be dimeric. Only the elution peaks of each sample are shown for clarity. All NS1 samples were run on an S200 10/300 column at two concentrations (9 and 4.5 mg/ml).

4.4 Characterization of the NS1/TRIM25 interaction

To examine the ability of each NS1 construct and mutant to bind TRIM25-CC, pull-down experiments were performed. Strep-II-TRIM25-CC was immobilized on StrepTactin beads which were then incubated with different purified NS1 constructs/mutants and subsequently immune-blotted using an antibody which recognises NS1. Experimental details are described in detail in section 2.10.2.

These experiments show that NS1-FL (W187A) binds Strep-II-TRIM25-CC (Figure 4.3A). Surprisingly, NS1-FL (R38A/K41A) was still able to bind Strep-II-TRIM25-CC, contradicting previous reports that mutation of R38A/K41A abolishes interaction (Figure 4.3A). To confirm this observation, another NS1-FL (R38A/K41A/W187A) construct was tested for binding to TRIM25-CC (Figure 4.3A). This construct can still bind to Strep-II-TRIM25-CC indicating that R38 and K41 are not involved in complex formation. For this NS1-FL mutant, there was less protein observed in the input fraction of NS1-FL (R38A/K41A)/TRIM25-CC compared to the other NS1-FL mutants (Figure 4.3A). An earlier observation was that NS1-FL (R38A/K41A) visibly aggregates when mixed with TRIM25-CC, which might account for the less amount of total protein observed in the pull-down experiment. Despite the less amount seen on the SDS-PAGE, the immunoblotted band that corresponds to NS1-FL (R38A/K41A) and TRIM25-CC complex produces a stronger signal compared to the complexes of NS1 (W187A)/TRIM25-CC and NS1 (R38A/K41A/W187A) (Figure 4.3A). This can be further explained by the fact that NS1 (R38A/K41A) is a tetramer in solution whereas the other two NS1 mutants are dimers and one can speculate that under the experimental conditions a non-stoichiometric NS1 (R38A/K41A)/TRIM25-CC complex is formed (Figure 4.2).

Next, the ability of the individual NS1-RBD and NS1-ED to bind TRIM25-CC was examined in a similar experimental set-up as described above but with wild-type NS1-RBD and ED tested with Strep-II-TRIM25-CC (Figure 4.3B). These experiments establish that ED is sufficient for NS1 binding to TRIM25-CC, whereas NS1-RBD cannot bind.

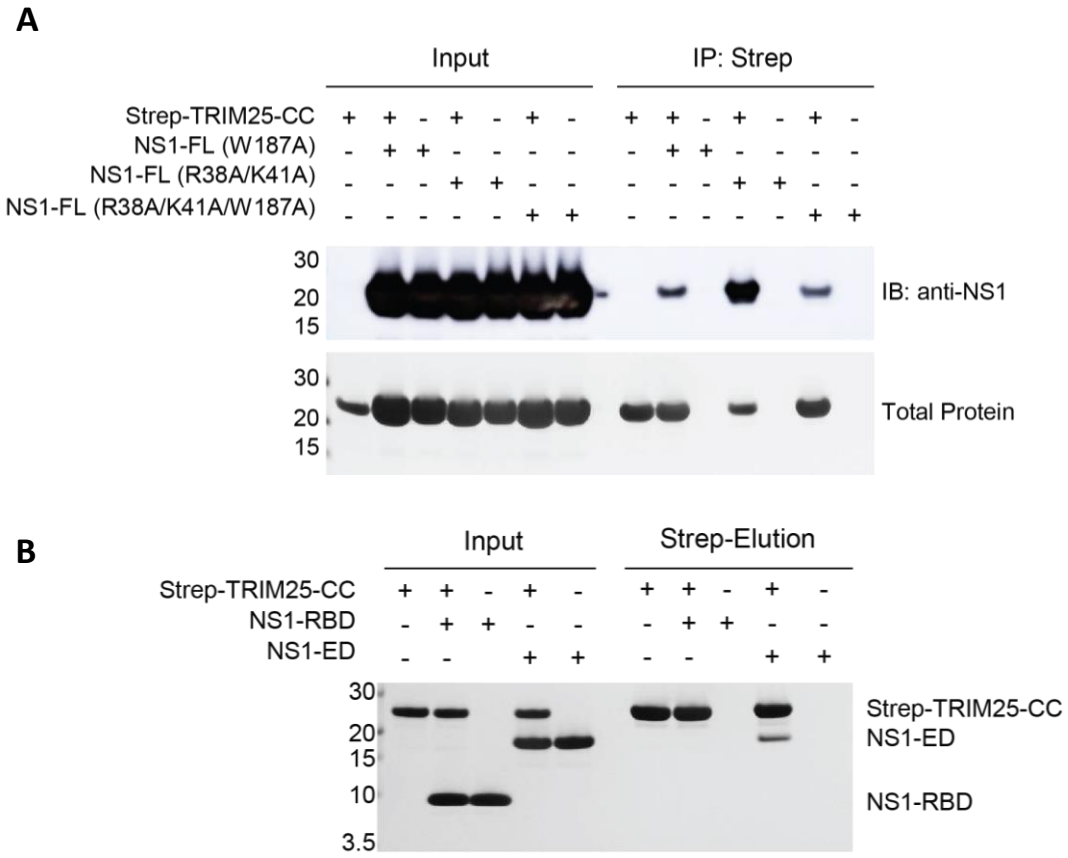

Figure 4.3: Pull-down analysis of TRIM25-CC/NS1 interaction.

A) Strep-II-TRIM25-CC was immobilized on StrepTactin beads and incubated with different NS1 mutants. Input fractions serve as controls and refer to samples removed prior to bead washing and followed by SDS-PAGE analysis and Western blotting or InstantBlue staining. The bands for Strep-tag II-TRIM25-CC (24.5 kDa) and NS1-FL (26.1 kDa) are not well-resolved by SDS-PAGE and were therefore immunoblotted using an anti-NS1 antibody that recognizes residues in the RBD domain. B) Pull-down experiments with Strep-II-TRIM25-CC and NS1-RBD or NS1-ED. Proteins were visualized by InstantBlue stain as anti-NS1 used in A was raised against NS1-RBD did not recognize the ED.

4.5 Crystallization of the NS1-ED/TRIM25-CC complex

To obtain structural insights into the interaction of the NS1-ED with the TRIM25-CC, crystallization experiments were performed. NS1-ED (9 mg/mL) was mixed with TRIM25-CC (10 mg/ml) at a 1:1 molar ratio and protein concentration of 100 µM of each component. Initial hits were optimized by hanging-drop vapour diffusion at 18 °C with a reservoir solution containing 100 mM Tris pH 8.5, 25 % PEG 600 and 200 mM sodium citrate and reaching full size (0.7 mm) after 5 days (Figure 4.4). Crystals were flash-frozen in the reservoir solution containing 30% PEG 600.

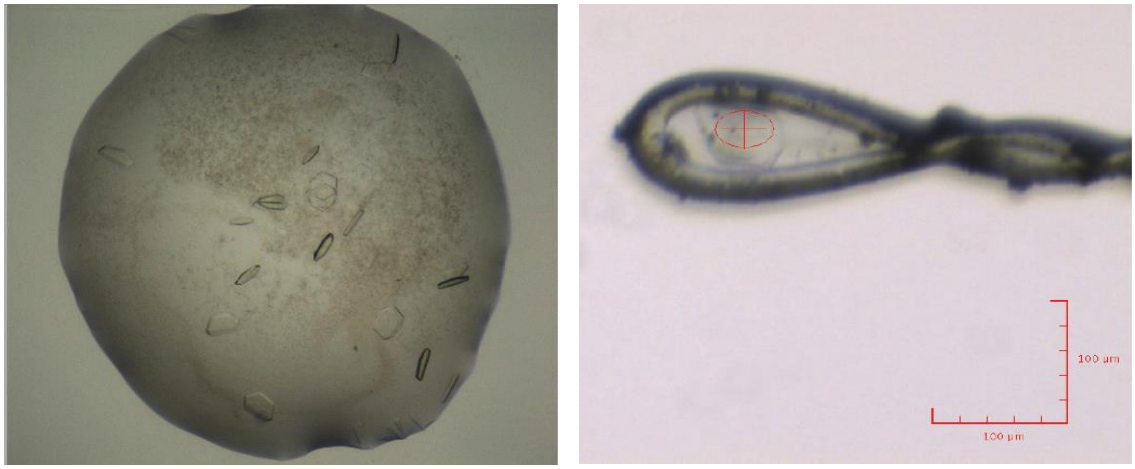

Figure 4.4: Crystals of NS1-ED/TRIM25-CC complex.

Optimized hexagonal crystals of the complex (left image) and mounting of a cryo-protected crystal on a cryo-loop (right image). The red cross indicates the position that the X-ray beamline was aimed to for data collection.

4.6 Structure determination of the NS1-ED/TRIM25-CC complex

Crystals of TRIM25-CC/NS1-ED were collected on beamline IO4 (λ = 0.9795 Å) at the Diamond Light Source (Oxford, UK) and processed using XDS. The structure was solved by molecular replacement (MR) using Phenix software at 2.8 Å resolution using the structure 3O9T.pdb as a search molecule for NS1-ED and 4LTB.pdb for TRIM25-CC in Phaser. Initially, 3 copies of TRIM25-CC in the asymmetric unit were identified by MR and this partial solution was fixed in order to further locate the smaller NS1-ED. Three copies of NS1-ED were also unambiguously identified with an overall translational function Z-score (TFZ) of 19.8. Generally, among other parameters which need to be considered, a TFZ score with a value above 8 might indicate a probable phase solution. The

resulting electron density maps were examined in COOT and the model was further improved by an iterative process of manual building and refinement using REFMAC5 and Phenix-Refine. Electron density is present for TRIM25-CC a.a. 195-362 and NS1-ED a.a. 86-205 in all copies. Residues for which electron density is not present were not modelled. The model of TRIM25-CC/NS1-ED has 97.1% of its residues in favoured regions and 2.9% in allowed regions. The data collection and refinement statistics are summarized on Table 4.1. Coordinates and structure factors were deposited in the Protein Data Bank under the accession code 5NT1.

Crystal	**TRIM25-CC/NS1-ED**
Resolution	48.68 – 2.82 (2.92 – 2.82)
Space group	C 2 2 2
Cell dimensions	
a,b,c (Å)	131.38, 225.23, 146.43
α, β, γ (°)	90.0, 90.0, 90.0
R_{merge}	0.092 (1.287)
Total reflections	355,400
Unique reflections	52,603
Redundancy	6.8
Completeness (%)	99.9
$\langle I/\sigma(I)\rangle$	14.9 (1.4)
$CC_{1/2}$	1.0 (0.6)
Refinement	
R_{work}	0.212
R_{free}	0.236
Number of atoms	6,932
Protein	6,924
Water	8
Average B-factor (Å^2)	79.27
RMS bonds (Å)	0.008
RMS angles (°)	0.90
Ramachandran statistics	
Favoured region (%)	97.1
Allowed region (%)	2.9
Disallowed region (%)	0.0

Table 4.1: X-ray crystallography data collection and refinement statistics.
Data for the highest resolution shells are given in parenthesis.

4.7 Structure of the core NS1-ED/TRIM25-CC complex

The complex crystallized in space group C222 with three copies of each NS1-ED and TRIM25-CC monomer in the asymmetric unit (Figure 4.5A). Given that the TRIM25-CC monomers did not form the previously described dimeric structure [165], crystallographic symmetry operators were applied to examine if the physiological oligomeric unit of TRIM25-CC (i.e. antiparallel dimer) can be seen within the crystallographic unit cell. As anticipated, two TRIM25-CC monomers related by two-fold symmetry form an antiparallel dimer which is the physiological complex (Figure 4.5B) [165]. Further symmetry analysis of the components of the asymmetric unit shows that three TRIM25-CC dimers are bound to six NS1-ED molecules via two interfaces (interface A and interface B) (Figure 4.5B). Given that overall six TRIM25-CC and six NS1-EDs are observed, it is reasonable to assume that two NS1-ED must bind to each TRIM25-CC dimer through the same interface (as we applied a two-fold symmetry to generate this complex). Therefore, further experiments were required to establish whether NS1-ED binds to a dimeric TRIM25-CC through interface A or B under physiological conditions (this is discussed further below).

Structural alignment of NS1-ED seen in this structure with previously reported unbound structures shows r.m.s.d. value ~0.3 Å for both, indicating that complex formation between TRIM25-CC and NS1-ED does not induce major conformational changes in NS1-ED (Figure 4.6A). In contrast, comparison of the unbound TRIM25-CC structure with the NS1-ED-bound structure presented here reveals that binding of NS1-ED causes a slight displacement of the L2 region (Linker 2) of TRIM25-CC (r.m.s.d. 0.9 Å) (Figure 4.6B). Additionally, the first and the last four turns of the long α1 helix of TRIM25-CC are disordered when NS1 is bound, further resulting in disordering of the α2 helix, which in the unbound TRIM25-CC structure is forming a short 3-turn helix (Figure 4.6B). At present, it is not known if this observation has any physiological relevance or it is simply attributed to crystallographic packing.

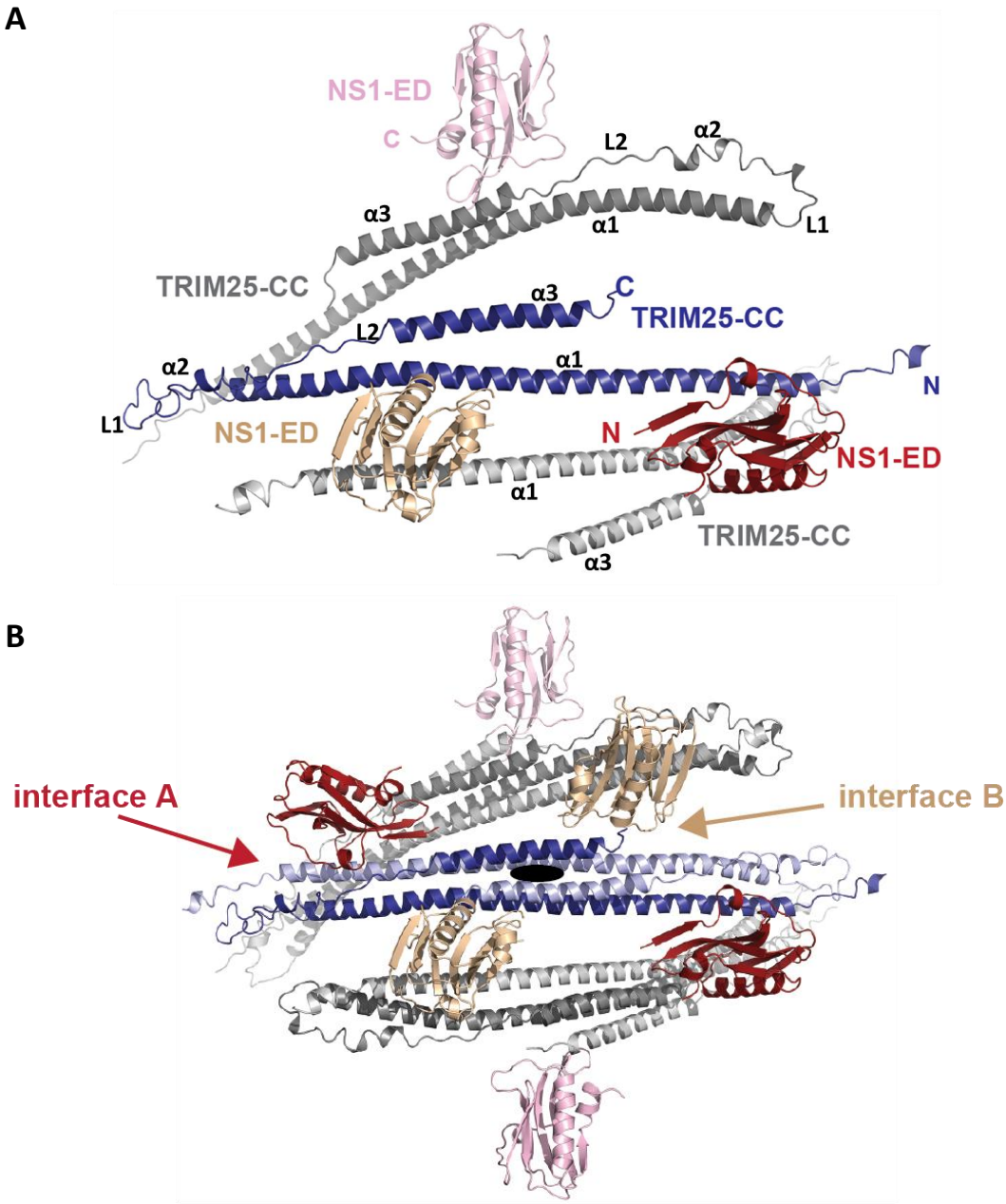

Figure 4.5: Structure of NS1-ED/TRIM25-CC complex.

A) Ribbon representation of the TRIM25-CC/NS1-ED structure. The asymmetric unit of the crystal shows three TRIM25-CC monomers (dark grey, blue, light grey) and three NS1-ED molecules (pink, gold, red). The α-helices (α1-3) and linker regions (L1,2) of the TRIM25-CC are indicated. B) Symmetry analysis through a two-fold symmetry axis (indicated as a dark ellipsoid) shows that NS1-ED binds to a dimeric TRIM25-CC via two distinct interfaces (A and B as indicated). Figure was prepared in Pymol.

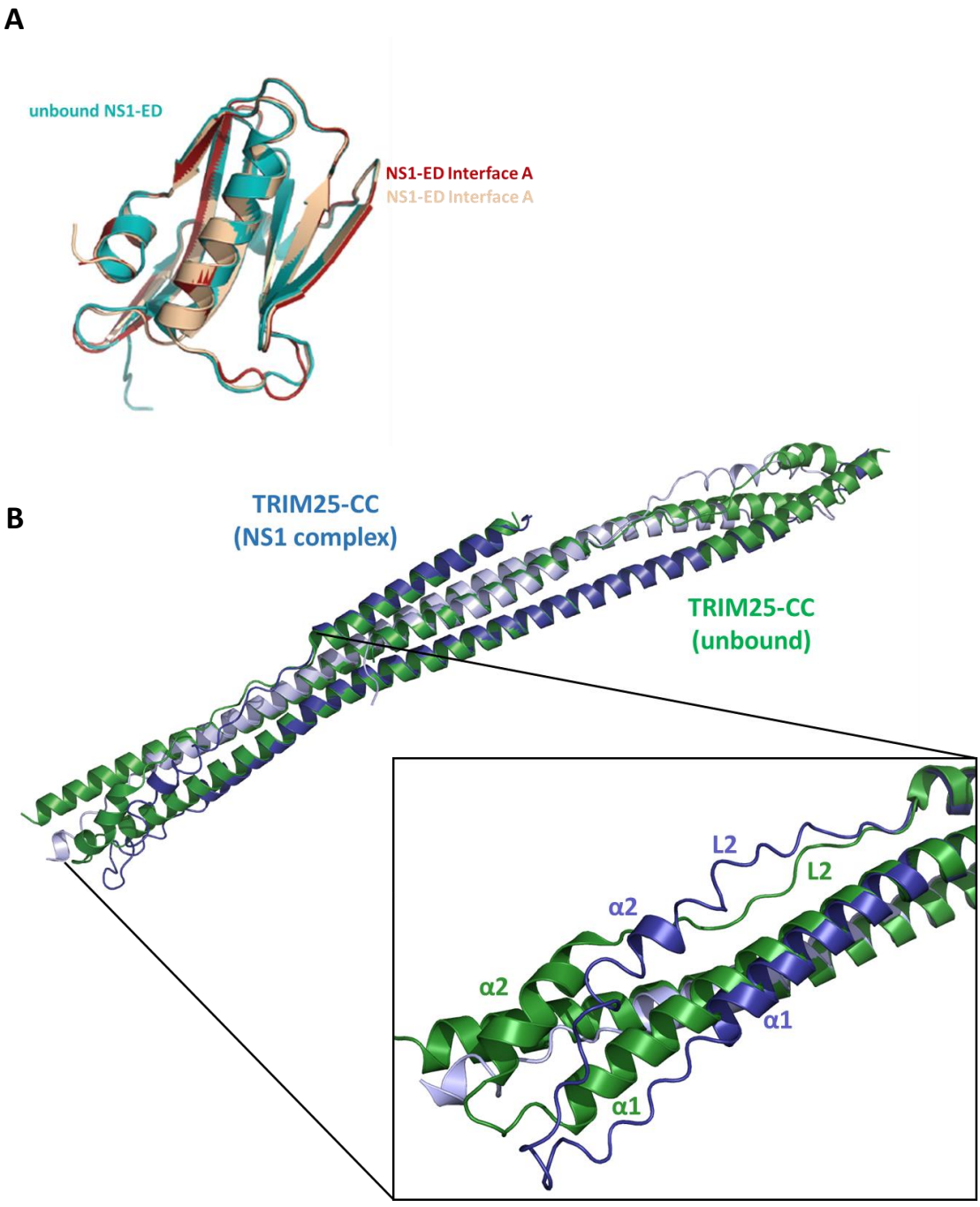

Figure 4.6: Comparison of NS1-ED and TRIM25-CC.

A) Structural alignment of NS1-ED seen in the TRIM25-CC/NS1-ED complex structure (shown in red and gold) with the unbound (apo) structure (cyan) (3O9T.pdb) [251]. No structural changes can be seen. B) Structural overlap of the TRIM25-CC domains (shown in light and dark blue) with their apo structure (in green) (4LTB.pdb) [165]. NS1-ED binding on TRIM25-CC causes slight changes occurring on the α1 and α2 helices and L2 linker region of the CC, as seen in the insert. Figure was prepared in Pymol.

In the structure of TRIM25-CC/NS1-ED presented above, two interacting surfaces are seen (interface A and interface B) (Figure 4.5B). Two plausible scenarios may apply: A) one of them is physiologically relevant and the other is due to crystal lattice formation or B) both interfaces are required for NS1-ED binding to TRIM25, which would suggest a cooperative mechanism that drives higher-order oligomerization of TRIM25-CC.

Interface A utilises a previously identified and highly conserved motif of NS1 that includes a short α-helix composed of a.a. 95-99 that contact the CC (Figure 4.7A). Importantly, previous mutational analysis had identified E96 and E97 of this motif as crucial for TRIM25 binding and inhibition of interferon production [234]. However, the present structure shows that the side chains of E96 and E97 point away from the binding interface with TRIM25 and form a network of contacts within NS1-ED, which may be important to maintain the structural integrity of the α-helix (Figure 4.7A). Instead, the interface between TRIM25 and NS1 involves hydrophobic contacts between $L95_{ED}$ and a hydrophobic pocket formed by $F274_{CC}$, $I277_{CC}$ and polar contacts between the backbone and side-chain of $L95_{ED}$ and $S99_{ED}$ with $E326_{CC}$ and $K320_{CC}$, respectively (Figure 4.7A).

Interface B involves NS1-ED residues spanning 137-143 (Figure 4.7B). These loop-forming residues and especially F138, D139 and R140 contact the central four-helical bundle of TRIM25-CC (Figure 4.7B). However, this interaction only buries 610 $Å^2$ of solvent accessible surface compared to a total of 870 $Å^2$ buried by interface A (the interfaces were calculated using the PISA server from EMBL). To test the relative importance of either interface in solution, interaction studies were carried out with $L95A_{ED}/S99A_{ED}$ or $R140A_{ED}$ and TRIM25-CC. Pull-down experiments were performed using Strep-II-TRIM25-CC and NS1-ED wt/mutants (Figure 4.7C). As described above (sections 2.10.2 and 4.4), Strep-II-TRIM25-CC was immobilized on StrepTactin beads and different NS1-ED proteins were incubated followed by elution and SDS-PAGE analysis. These assays show that the double mutation of $L95A_{ED}/S99A_{ED}$ abolishes the interaction with TRIM25-CC, whereas $R140A_{ED}$ can still bind (Figure 4.7C). Therefore, NS1-ED binds to TRIM25-CC through interface A. Interface B can be attributed to crystal lattice formation with possibly no biological relevance in this system.

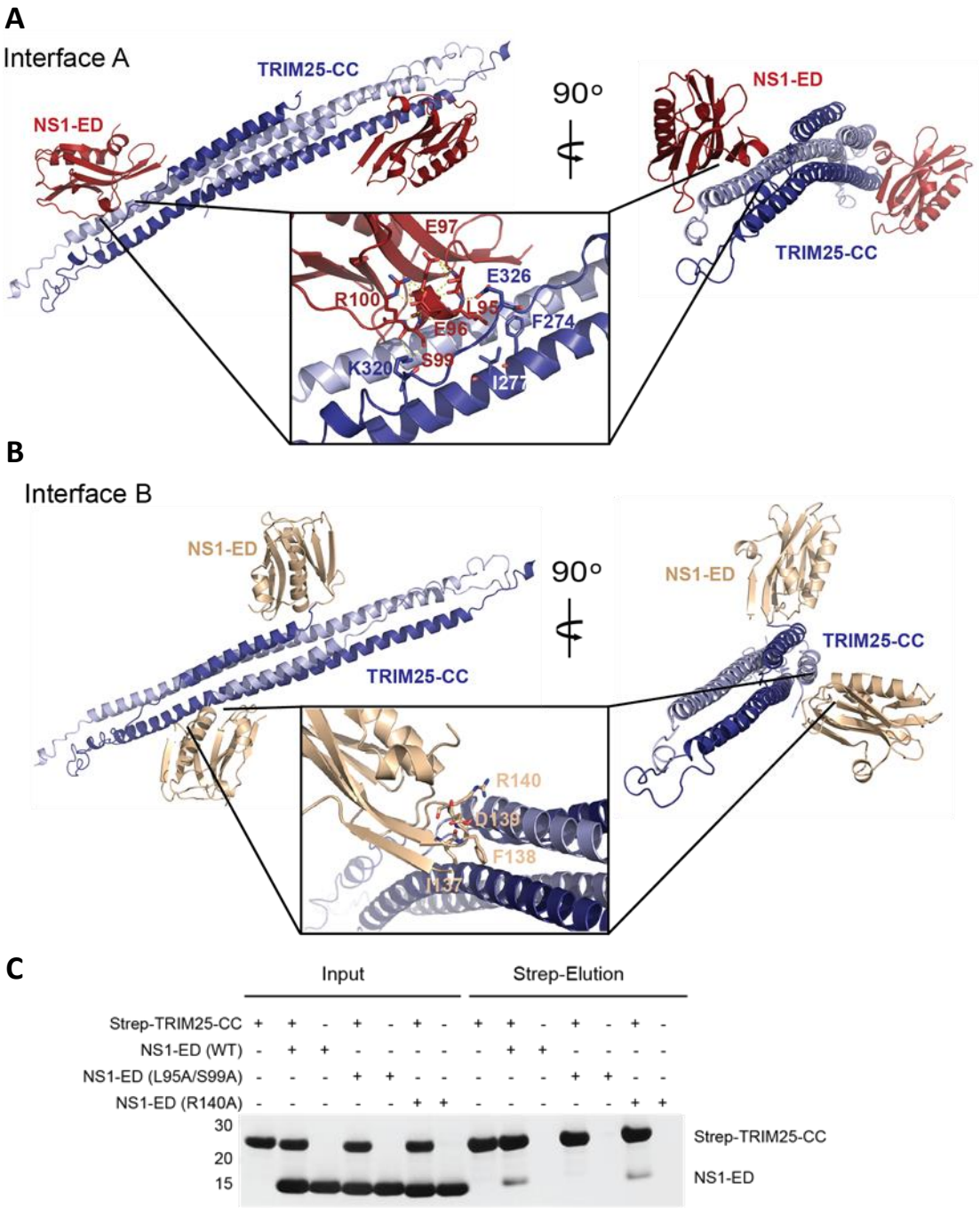

Figure 4.7: Analysis of NS1-ED/TRIM25-CC binding interfaces.

A) NS1-ED/TRIM25-CC interacting through Interface A is shown in two orientations. Interface A is formed by a short NS1-ED α -helix (a.a. residues 95-99) that binds to the TRIM25-CC forming a helical bundle. The insert shows a close-up view of the interface with TRIM25-CC in light and dark blue and NS1-ED in red. The side-chains of the participating residues are indicated. B) Interface B is mediated through a loop-region of NS1-ED spanning residues 137-143 and is shown in two orientations. The insert shows the residues involved in interaction with TRIM25-CC. C) Pull-down experiments with mutant NS1-ED (L95A/S99A for interface A and R140A for interface B) were performed as described previously (Figure 4.3) to validate the physiological interface between NS1-ED and TRIM25-CC. Figures in A and B were prepared in Pymol.

A previous study showed that NS1 proteins derived from different viral strains were able to interact with TRIM25 [234]. A sequence alignment between PR8-NS1 (used in this study) and all the other TRIM25-interacting NS1 proteins shows that the residues involved in the binding are highly conserved across strains (Figure 4.8). Of note, leucine in the position 95 may be substituted with the highly similar isoleucine. Intriguingly, it was reported that PR8-NS1 does not interact with the mouse homologue of TRIM25 but rather targets directly Riplet, another RING E3 ligase which is involved in RIG-I ubiquitination and IFN induction [295]. A sequence analysis of the human and mouse TRIM25 homologues combined with a closer look on the human TRIM25-CC residues involved in NS1-ED binding reveals that $E326_{human}$ is substituted with $K325_{mouse}$. In the TRIM25-CC/NS1-ED structure $E326_{human}$ is involved in polar contacts with the backbone of $L95_{ED}$, indicating that a positive to negative charged side-chain substitution may be sufficient to disrupt TRIM25/NS1 binding (Figure 4.7A).

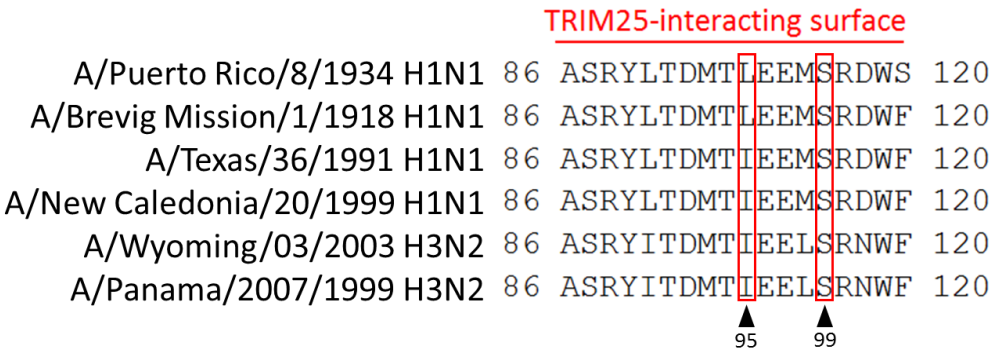

Figure 4.8: Sequence alignment of different NS1 proteins.

The TRIM25-CC-interacting region (interface A, described above) of different NS1 proteins previously shown to bind to TRIM25 were aligned [234]. Indicated residues that are important for binding (L95 and S99 in Puerto Rico (PR8) strain) are highly conserved among different strains.

This NS1-ED/TRIM25-CC complex structure provides the first insight into the oligomeric state of TRIM25 upon binding of NS1. Previous studies have suggested that NS1 may interfere with the oligomeric state of TRIM25 and thereby suppress activity, based on the observation that NS1 binds to the coiled-coil domain of TRIM25 [234]. However, the structure of the TRIM25/NS1 complex now shows that TRIM25 dimerization is unperturbed in the complex and that instead the two NS1-ED molecules bind the dimeric coiled coil at its distal ends in a symmetrical fashion (Figure 4.9A). Previous work on NS1 has also shown that in addition to the strong homo-dimerization mediated by the RBD, there is another, weaker dimerization interface in NS1 contributed by the ED [239, 243, 244, 249-252, 296, 297]. W187, located on α-helix α5 is the key residue responsible for this reciprocal hydrophobic interaction between two NS1-EDs. This interaction has been linked to the ability of NS1 to form higher-order oligomers, which may be important for some of its functions such as dsRNA binding [239, 243, 244, 250, 252]. In the crystal structure of the NS1-ED/TRIM25-CC complex the same W187-mediated interface is observed between two symmetry-related NS1 molecules (Figure 4.9B). However, W187 is not directly involved in the recognition of TRIM25 by NS1, in contrast to the interaction observed between NS1 and the host protein CPSF30 highlighting a structural plasticity that allows NS1 to recognize multiple different binding partners using just a small globular domain [254]. As shown earlier in this chapter, mutation of $W187A_{ED}$ does not affect binding of NS1-FL to TRIM25 (Figure 4.3A).

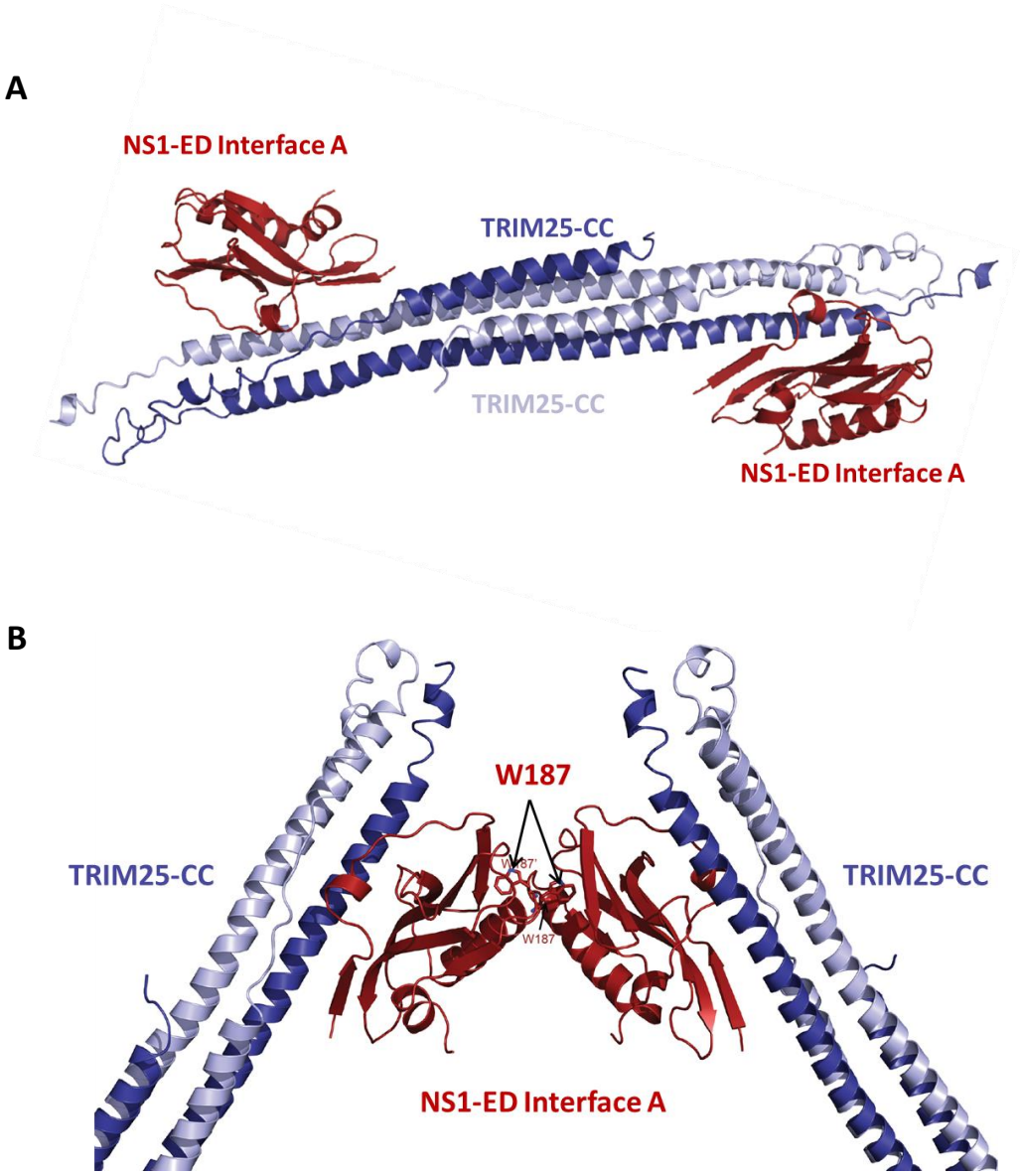

Figure 4.9: NS1-ED binding to TRIM25-CC and crystal packing analysis.
A) NS1-ED (red) binds symmetrically at opposite sides of a dimeric TRIM25-CC (shown in blue/light blue). B) Two symmetry-related NS1-EDs in the crystal are packing against each other through interactions that involve W187 (side-chains shown). NS1-ED W187 is not involved in TRIM25-CC binding. Figures were prepared in Pymol.

4.8 Crystallization of the NS1-FL/TRIM25-CC complex

The binding studies showed that the NS1-ED is sufficient to allow formation of a stable NS1/TRIM25 complex. In order to test if there may be additional stabilisation of the complex through weak interactions with the RBD and to investigate how the restraints imposed by the constantly dimeric RBD domain of full-length NS1 (NS1-FL) may influence the NS1/TRIM25 interaction the structure of the NS1-FL/TRIM25-CC complex was pursued. Unfortunately, complexes with the single (W187A) and double mutants (R38A/K41A) of NS1 did not crystallize and attempts at crystallization were only successful when dimeric NS1-FL (R38A/K41A/W187A), which has no tendency to form higher order oligomers was used. NS1-FL (R38A/K41A/W187A) (8 mg/mL) was mixed with TRIM25-CC (10 mg/ml) at a 1:1 molar ratio and protein concentration of 80 µM of each component. Clustered plates appeared within 3 days and were used for seeding in order to optimize the size and morphology of the crystals. Single cubic crystals of approx. 20-30 µm appeared within 3 days in a seeded drop (0.02 µL seed stock + 0.1 µL protein mixture + 0.1 µL reservoir solution) with a reservoir solution containing 100 mM sodium citrate pH 6.5 and 24% PEG 3350 (Figure 4.10). Crystals were cryoprotected using a step gradient in the reservoir solution containing 5%, 10%, 20% and finally 25% glycerol and flash-frozen (Figure 4.10). Approximately 40 crystals were screened but most diffracted only poorly (~4.5 Å and below). Crystal screening took place in Diamond synchrotron (beamlines I03 and I04).

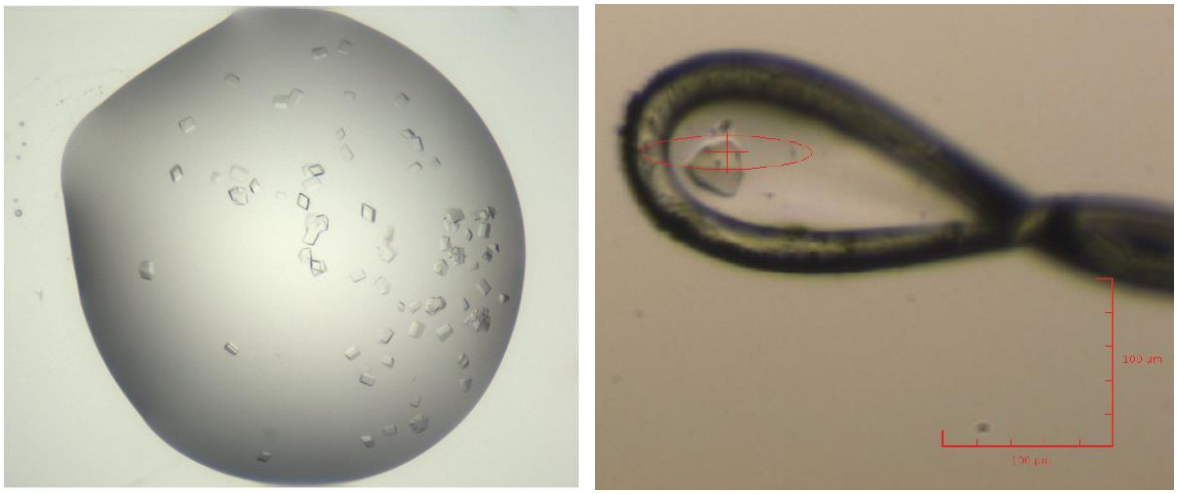

Figure 4.10: Crystals of NS1-FL/TRIM25-CC complex.

Optimized cubic crystals of the complex (left image) and mounting of a cryo-protected crystal on a cryo-loop (right image). The red cross indicates the position that the X-ray beamline was aimed to for data collection.

4.9 Structure determination of the NS1-FL/TRIM25-CC complex

Data for NS1-FL (R83A/K41/W187A) / TRIM25-CC crystals were collected on beamline IO4 (λ = 0.9795 Å) at the Diamond Light Source (Oxford, UK) and processed using autoPROC. The complex crystallised in space group P1 and the structure was solved by MR at 4.26 Å resolution (R/R_{free} = 0.28/0.29) using 5NT1 (TRIM25-CC/NS1-ED) as a search molecule for NS1-ED and TRIM25-CC and 1AIL for NS1-RBD in Phenix-Phaser. Initially, the partial MR solution containing two complexes of NS1-ED/TRIM25-CC in the asymmetric unit (TFZ = 16.5) was identified. Subsequently, this solution was fixed and two out of four molecules of NS1-RBD were located with a TFZ score of 18.6; the other two RBD domains could not be modelled with confidence and are not shown. The model was iteratively improved by manual building in COOT and refined using simulated annealing and rigid body refinement strategies in REFMAC and Phenix-Refine. Additional restraints derived from a higher resolution reference structure (5NT1.pdb) were employed to prevent overfitting at this low resolution. All structural figures were prepared in Pymol. Protein interfaces were calculated using PISA server. The model of TRIM25-CC/NS1-FL has 92.1% of its residues in favoured regions, 6.3% in allowed regions and 1.6% outliers. Structural figures were prepared in Pymol. The data collection and refinement statistics are summarized on Table 4.2. Coordinates and structure factors were deposited in the Protein Data Bank under the accession code 5NT2.

Crystal	**TRIM25-CC/NS1-ED**
Resolution	61.51 - 4.259 (4.411 - 4.259)
Space group	P1
Cell dimensions	
a,b,c (Å)	73.26 Å, 76.30 Å, 92.07 Å
α, *β*, *γ* (°)	100.04, 93.71°, 111.14°
R_{merge}	0.19 (0.597)
Total reflections	32,644
Unique reflections	12,516
Redundancy	2.6
Completeness (%)	98.6
$\langle I/\sigma(I)\rangle$	5.7 (2.5)
$CC_{1/2}$	0.98 (0.91)
Refinement	
R_{work}	0.278
R_{free}	0.295
Number of atoms	20,802
Protein	20,802
Water	0
Average B-factor (Å^2)	77.46
RMS bonds (Å)	0.004
RMS angles (°)	0.91
Ramachandran statistics	
Favoured region (%)	92.1
Allowed region (%)	6.3
Disallowed region (%)	1.6

Table 4.2: X-ray crystallography data collection and refinement statistics.
Data for the highest resolution shells are given in parenthesis.

4.10 Crystal structure of the NS1-FL/TRIM25-CC complex

The asymmetric unit contains 4 molecules of TRIM25 and 4 molecules of NS1 (Figure 4.11A). Electron density is present for all 4 TRIM25-CC and 4 NS1-ED molecules, whereas clear electron density is observed only for 2 NS1-RBD molecules (Figure 4.11B). This could be due to the low resolution of this structure or due to partial occupancy of these domains which can be further attributed to flexibility. Thus, this structure shows 4 TRIM25-CC, 4 NS1-ED and 2 NS1-RBD domains (Figure 4.11A).

This is the first example of a complex between full-length NS1 and a substrate and provides novel insight into the spatial arrangements of the RBD and ED during target binding. An interesting feature of this structure is the observation that the two EDs of a given RBD-mediated NS1 dimer do not contact the same TRIM25-CC molecule but instead connect two CC domains (Figure 4.11A). The two TRIM25-CC dimers are packing against each other with an interface mediated by reciprocal interactions between α1-α1' of the two TRIM25-CC dimers, in an orientation that resembles the letter "X" (Figure 4.11A). This organisation may highlight an important role of the ubiquitous dimeric RBD in imposing further oligomerization of TRIM25-CC, which may be important in a physiological setting.

Interestingly, this structure shows that NS1 makes extensive contacts with TRIM25-CC via NS1-ED whereas there are no contacts seen between NS1-RBD and TRIM25-CC, confirming the pull-down experiments shown in section 4.4 which showed that NS1-ED binds to TRIM25-CC whereas NS1-RBD does not. The two RBD domains form a homodimeric 6 helix arrangement as previously observed in the structure of unbound full-length NS1 (3F5T and 4OPH.pdb) [243, 244], in the structure of NS1-RBD (1AIL.pdb) [242] and in the structure of NS1-RBD in complex with dsRNA (2ZKO.pdb) [246]. In the two NS1 molecules for which density for both RBD and ED is seen, the linker connecting the two domains (NS1-LR) could be traced and modelled (Figure 4.11A). Each NS1-ED is positioned on top of the corresponding NS1-RBD and makes almost no contacts with either the dimeric RBD or the distal ED. The overall architecture of NS1 in the complex resembles the shape of letter "Y", with the NS1-RBD dimer as the base of the stem, the NS1-LR the top part of the stem and each NS1-ED representing one branch (Figure 4.12A). Interestingly, the two NS1 monomers of the homodimer are not symmetrical; while both monomers align well on the NS1-RBD (0.6 Å r.m.s.d.), one NS1-ED is shifted towards the stem in relation to the other (approx. 17 Å) (Figure 4.12B).

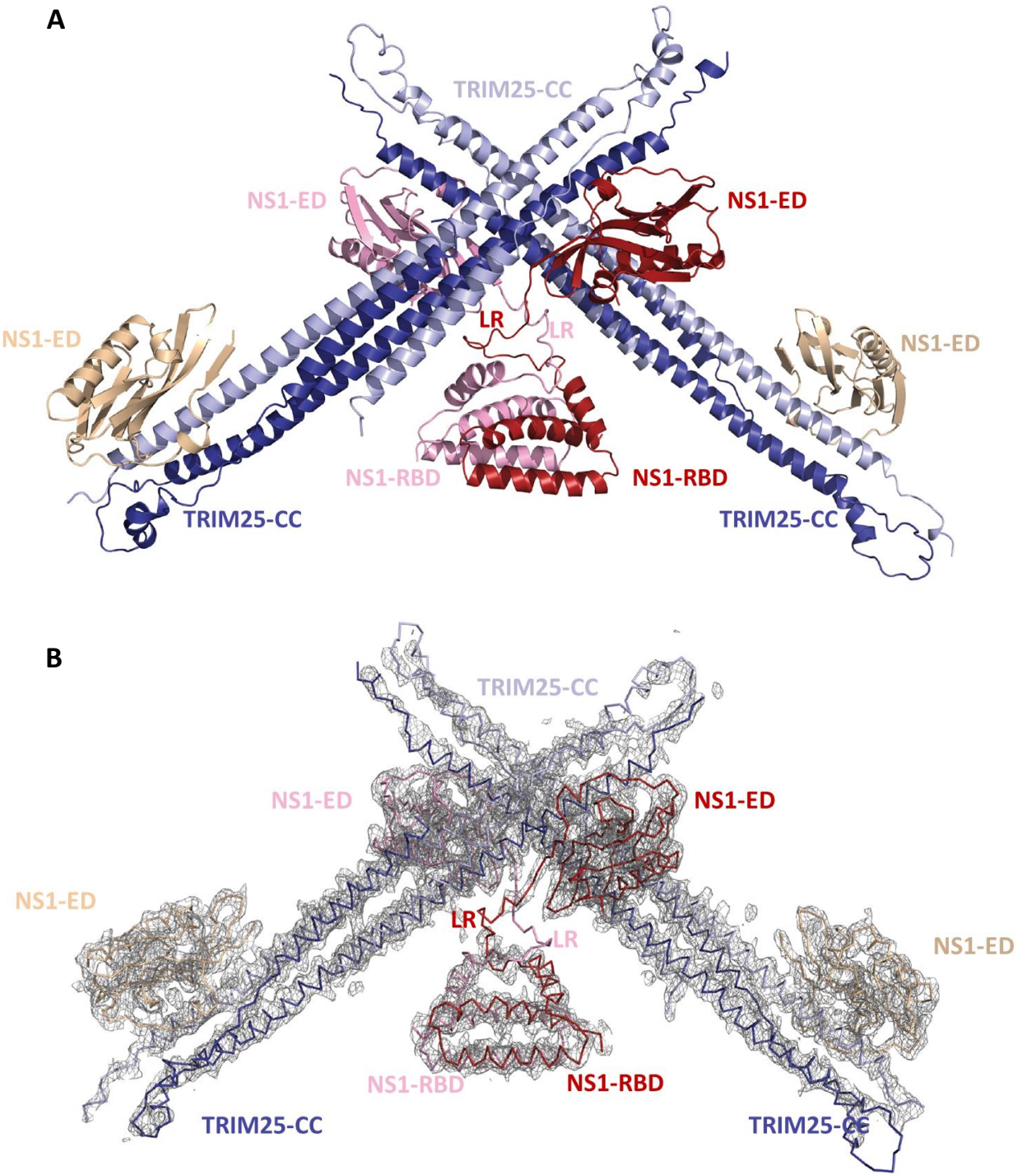

Figure 4.11: Structure of NS1-FL/TRIM25-CC complex.

A) Ribbon representation of the 4.26 Å NS1-FL/TRIM25-CC structure shows four NS1 (two coloured in gold and one in red and pink) bound to two dimeric TRIM25-CC regions (dark/light blue). Only two out of four RBD domains could be modelled as shown. NS1-FL dimerizes through the RBD and binds to both TRIM25-CC dimers which further interact with each other in an orientation that resembles the letter "X". B) The electron density map (contoured at 1 σ) used to build the ribbon model (coloured as in A) is shown as grey mesh. Clear electron density is observed for four TRIM25-CC monomers, four NS1-ED and only two RBD. Figure was prepared in Pymol.

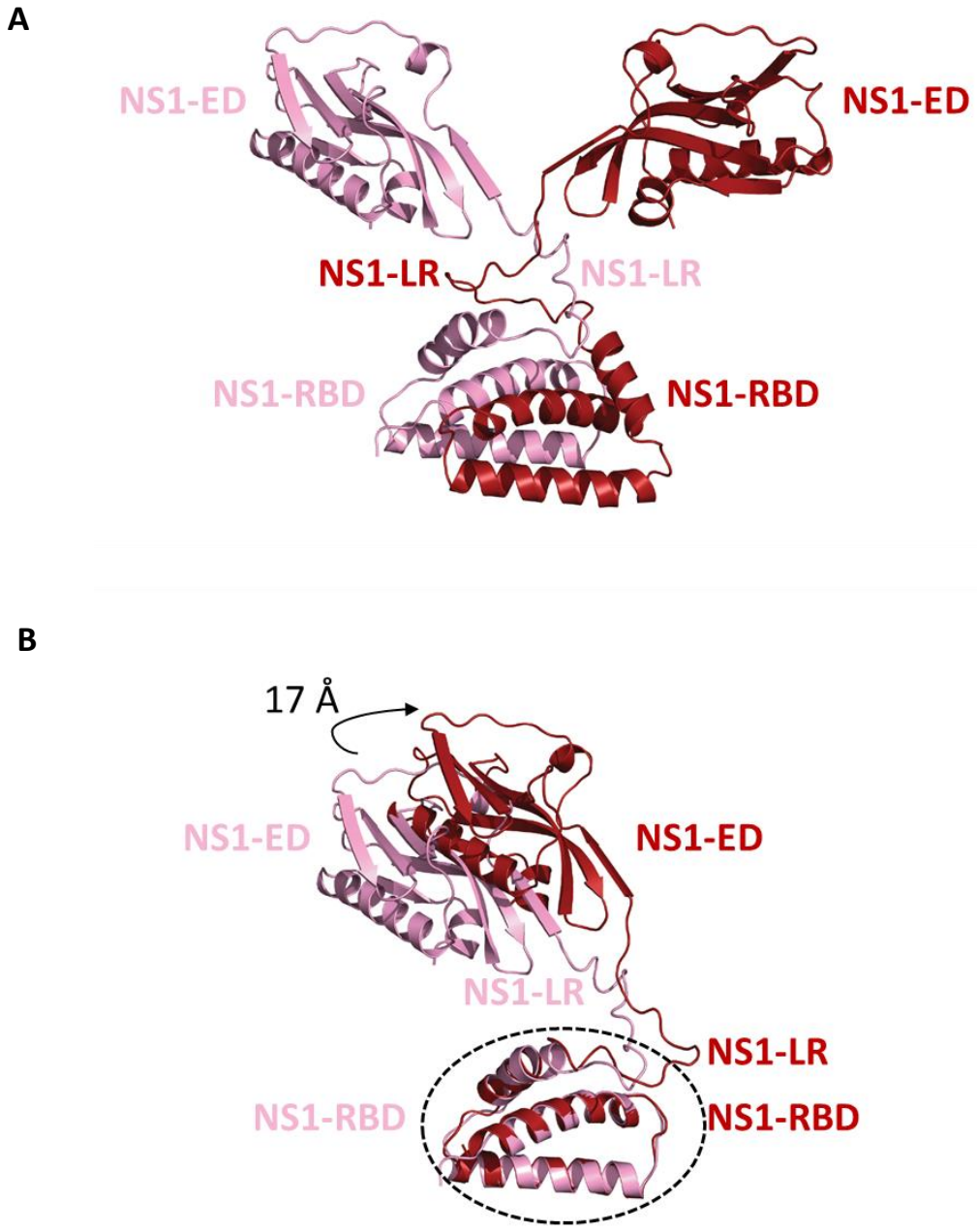

Figure 4.12: The structure of NS1-FL upon TRIM25-CC interaction.

A) Ribbon representation of the NS1-FL dimer (red/pink) seen in the structure of TRIM25-CC/NS1-FL complex (shown in Figure 4.11A). NS1-FL resembles the shape of letter "Y", with the RBD forming a homodimeric 6 helical structure and the effector domains extending outwards without making contact with each other or the RBDs. B) Structural alignment of dimeric NS1-FL from (A) using the RBD (dashed circle) for the overlap shows that the two monomers are not in identical positions, with one ED being shifted by 17 Å in relation to the other owing to the flexible linker region (LR). Figure was prepared in Pymol.

Structural alignment of the NS1-ED/TRIM25-CC complex presented in section 4.7 with that of NS1-FL/TRIM25-CC shows an identical architecture (0.7 Å r.m.s.d.) (Figure 4.13), further supporting the notion that the second CC/ED interface (interface B) seen in the structure of the NS1-ED/TRIM25-CC complex is purely due to crystal packing and not physiologically relevant. It is worth noting that binding of NS1-FL to TRIM25-CC causes the same disordering of the first few turns of the α1 helices as seen in the NS1-ED/TRIM25-CC structure (Figures 4.13 and 4.6B).

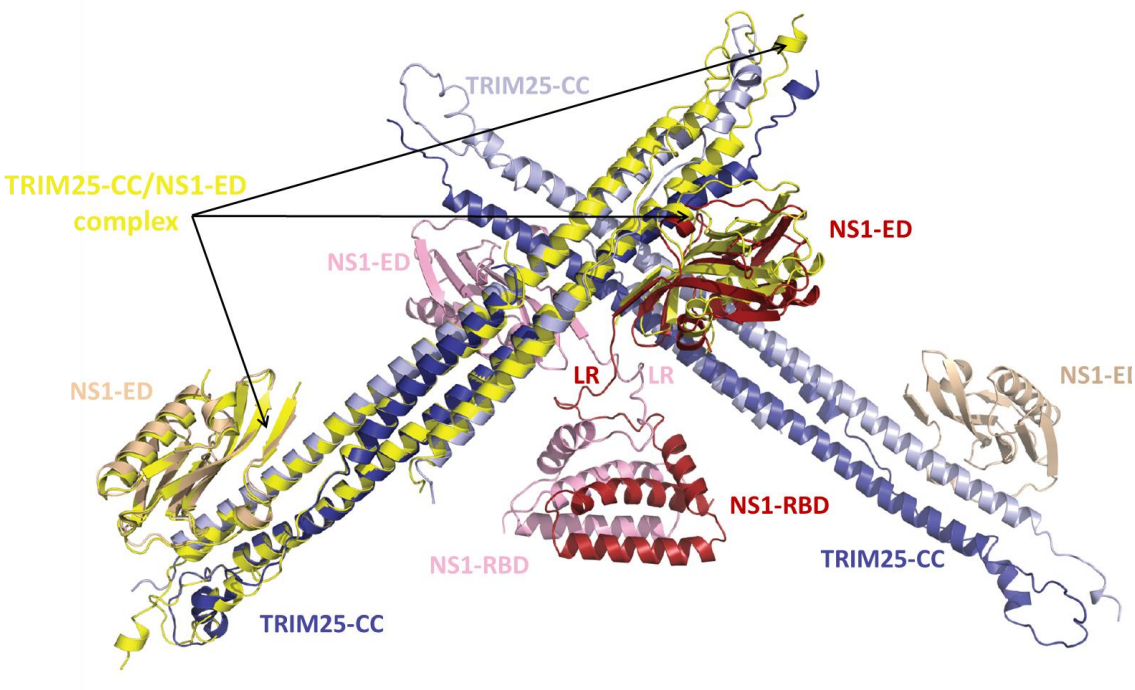

Figure 4.13: The presence of NS1-RBD does not affect TRIM25-CC binding by ED. Structural alignment of the TRIM25-CC/NS1-ED complex (shown in yellow) with the TRIM25-CC/NS1-FL structure (coloured as in Figure 4.11) shows no structural differences in either TRIM25-CC or NS1-ED. Figure was prepared in Pymol.

4.11 TRIM25-FL as a tool to assess the inhibitory role of NS1

The structures of NS1-ED and NS1-FL bound to TRIM25-CC presented above reveal that NS1 does not interfere with the dimerization of TRIM25 coiled-coil domain as was previously hypothesized [234]. Therefore, the key question that arises from these data is what is the mechanism of NS1-mediated TRIM25 inhibition?

To assess if NS1 binding on TRIM25 inhibits directly the RING-mediated catalytic activity, preliminary ubiquitination experiments with TRIM25-RBCC$_L$ and NS1-ED were performed. TRIM25-RBCC$_L$ was used as it contained the NS1-interacting CC region and the RING domains. Ubiquitination assays using UbcH5c, which was shown to be active with TRIM25 (see chapter 3), revealed that auto-ubiquitination of the TRIM25 under these conditions was not affected by NS1-ED (Figure 4.14). However, TRIM25-RBCC$_L$ was multi-autoubiquitinated after 5 min., which might have interfered with NS1-ED recognition and binding; thus additional experiments were required to confirm this preliminary observation (see also the section 4.12 below).

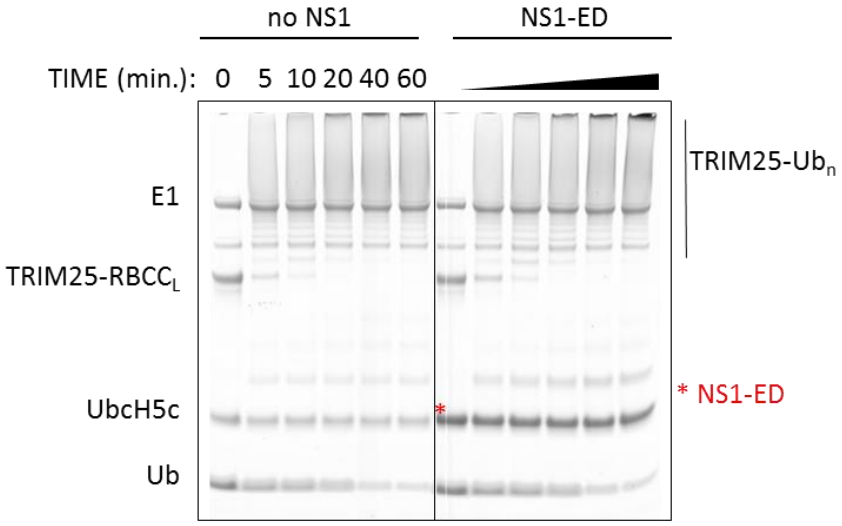

Figure 4.14: Ubiquitination assay with NS1-ED and TRIM25-RBCC$_L$.

An auto-ubiquitination assay with TRIM25-RBCC$_L$ and UbcH5c was performed *in vitro*, in the absence (left panel) and presence (right panel) of NS1-ED. NS1-ED interacts with the TRIM25-CC and the RING domain of TRIM25 is necessary for E3 ligase activity. 1 µM E1, 5 µM E2 (UbcH5c), 5 µM E3 (TRIM25-RBCC$_L$), 0 µM (control) or 10 µM NS1-ED, 100 µM Ub and 10 mM ATP were incubated at 25 °C over time. Samples removed from the reaction at the indicated time points: 0 (before the addition of ATP), 5, 10, 20, 40 and 60 minutes were analysed by SDS-PAGE. Reduction of the TRIM25-RBCC$_L$ band over time is due to auto-ubiquitination and the presence of NS1-ED has no visible effect. The NS1-ED band overlaps with UbcH5c and red asterisk indicates it.

Since NS1-ED did not appear to affect the enzymatic ability of TRIM25-RBCC$_L$ in preliminary auto-ubiquitination assays, I decided to produce the full-length TRIM25 protein (denoted as TRIM25-FL). TRIM25-FL contains the catalytic RING domain and the PRYSPRY domain at its C-terminus which recognizes RIG-I and thus allows me to further test the effect of NS1 *in vitro*.

As described in section 3.2, the quality and yield of TRIM25-FL expressed in *E. coli* was not optimal and hence, a baculovirus-based insect cell expression system was employed with the help of Mr Evangelos Christodoulou (The Francis Crick Institute). Human TRIM25-FL was cloned in an insect cell and baculovirus vector (pIEx/Bac-3) encoding a cleavable N-terminal His$_{10}$-tagged TRIM25-FL. Expression was done in (Sf9) insect cells using standard protocols described in [298]. TRIM25-FL was purified to homogeneity using an optimised strategy and the protein yield and quality were greatly improved compared to previous efforts (Figure 4.15A). SEC-MALLS analysis of TRIM25-FL shows that this construct is mostly dimeric up to 2 mg/ml, which is the highest concentration achieved for this protein, with a tendency to form higher-order oligomers (Figure 4.15B). This is in good accordance to the results obtained for the TRIM25-RBCC$_L$ construct (also a dimer and reported in section 3.4).

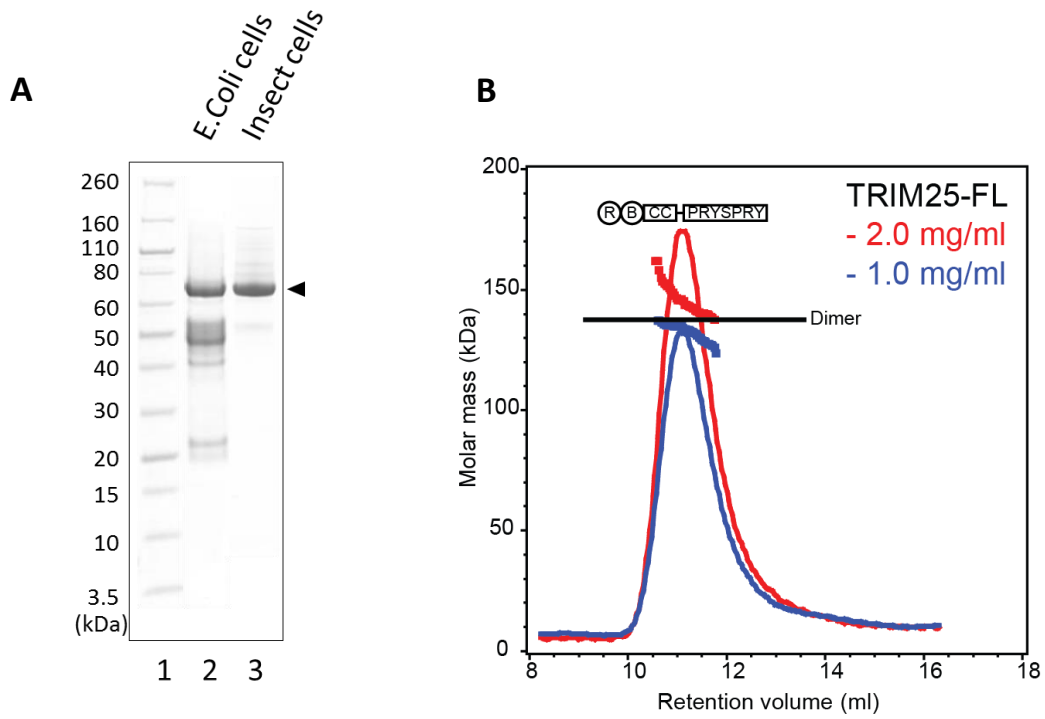

Figure 4.15: Expression and SEC-MALLS analysis of TRIM25-FL.

A) Comparison of final yield and purity of full-length TRIM25 (FL) as analysed by SDS-PAGE. Lane 2 shows TRIM25-FL expressed in *E.coli* cells and lane 3 shows TRIM25-FL expressed and purified from insect (Sf9) cells. Arrow indicates intact full-length TRIM25 whereas bands below are degraded species (in lane 2). B) SEC-MALLS analysis of TRIM25-FL (expressed in insect cells). The chromatograms show the UV absorbance at 280 nm (curve) and the weight-averaged molecular masses of the samples (dotted-line). The theoretical/expected molecular mass for TRIM25-FL (~140 kDa as a dimer) is shown as a straight line and is parallel-to-the-X-axis. Only the elution peaks of each sample are shown for clarity. TRIM25-FL samples were run on an S200 10/300 column at two concentrations (2 and 1 mg/ml).

4.12 NS1 does not affect the intrinsic catalytic activity of TRIM25-FL

Previous studies have suggested that NS1 binding to TRIM25 suppresses RIG-I ubiquitination [234]. In a simplified version of this multicomponent system, I hypothesised that NS1 can either inhibit the intrinsic ability of TRIM25 to discharge an E2~Ub or can have an effect in substrate ubiquitination (for example NS1 may compete with RIG-I for binding to TRIM25).

To assess any potential inhibitory role of NS1 on the catalytic ability of TRIM25-FL, *in vitro* ubiquitination assays were performed with UbcH5 and Ubc13/Ube2V1. The precise molecular details of the TRIM25-mediated activation

of these E2s have been extensively discussed in chapter 3 of this thesis. TRIM25-mediated RIG-I ubiquitination requires the activity of these E2 enzymes [216]. It is likely that UbcH5, which cannot drive the formation of a single type of poly-ubiquitin chain, catalyses the attachment of the first ubiquitin moiety to K172 and other lysine residues of RIG-I-CARD2 (initiation step), which is then extended by Ubc13/Ube2V1 to form a K63-linked poly-ubiquitin chain (elongation step). Previous results presented on chapter 3 of this thesis show that dimerization of the RING domain of TRIM25 is required to discharge UbcH5~Ub onto a nucleophile or to form unattached K63-linked poly-ubiquitin chains with Ubc13/Ube2V1 (Chapter 3 and [94, 95]).

To examine whether binding of NS1 to the CC of TRIM25 interferes with dimerization of the RING domain or its interaction with the E2~Ub conjugate, UbcH5c~Ub discharge assays with TRIM25-FL were performed in the presence of NS1 (Figure 4.16). UbcH5c was pre-charged with Ub which was previously labelled with Atto647N fluorophore (the conjugate is denoted as UbcH5c~AttoUb) as described in section 2.8. UbcH5c~AttoUb discharge assays were initiated by adding TRIM25 only (as control) and TRIM25 plus increasing concentrations (1, 10 and 100 μM) of different NS1 constructs/mutants including NS1-ED, NS1-FL (R38A/K41A/W187A) and NS1-FL (W187A). These data show that the rate of UbcH5c~Ub discharge mediated by TRIM25 is not affected by the presence of any of the NS1 constructs/mutants tested (Figure 4.16).

To further validate this observation, ubiquitination assays with TRIM25-FL and Ubc13/Ube2V1 were performed in order to follow the formation of unanchored-K63 poly-ubiquitin chains in the absence of RIG-I (Figure 4.17). In this case, AttoUb was used to “spike” the K63-linked chain formation in the presence of TRIM25-FL and increasing concentrations (1, 10 and 100 μM) of NS1 constructs/mutants. Addition of AttoUb in these assays provide a “cleaner” readout for activity as only ubiquitin chains are observed on the SDS-PAGE. Similarly to the UbcH5~Ub discharge assays, these experiments clearly show that K63-linked poly-ubiquitin chain formation is also unaffected by the presence of NS1 (Figure 4.17). Taken together, these experiments demonstrate that the intrinsic catalytic activity of TRIM25 is not affected even in the presence of high concentrations of NS1.

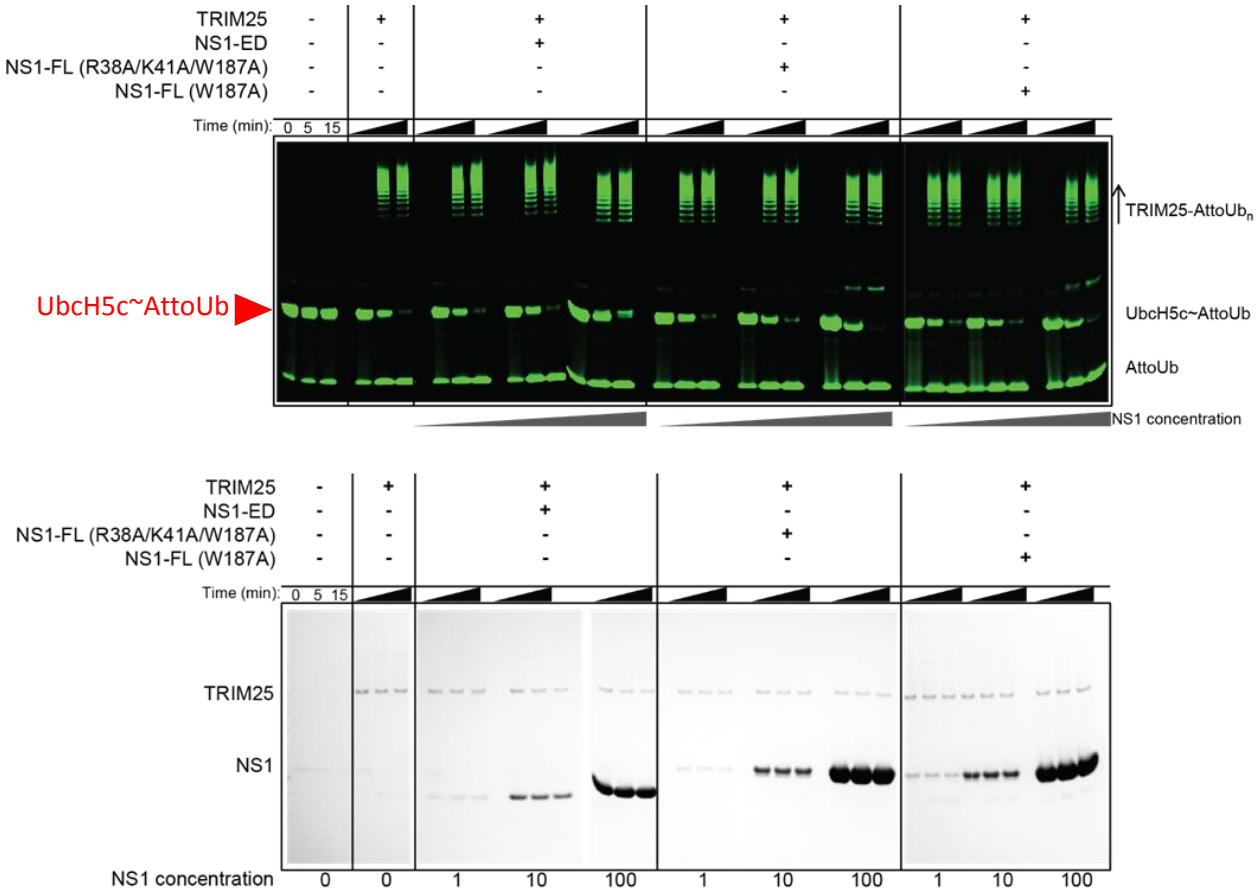

Figure 4.16: NS1 does not affect the TRIM25 ability to discharge UbcH5c~Ub.

The use of fluorescently labeled AttoUb allows monitoring of the UbcH5c~AttoUb discharge rates in the presence of TRIM25-FL and different NS1 constructs. The band corresponding to UbcH5c~AttoUb is indicated by red arrow. NS1 constructs tested here were NS1-ED or NS1-FL (R38A/K41A/W187A or W187A). Assays were carried out with 1 μM UbcH5c~AttoUb and 0 μM (control) or 1 μM of TRIM25-FL incubated with 1 or 10 or 100 μM of different NS1 constructs/mutants in buffer containing 20 mM L-Lysine. Even in the presence of L-Lysine, TRIM25-FL auto-ubiquitinated as indicated by the high molecular weight species. The reaction was monitored over 15 min. Samples taken at the indicated time points (0, 5 and 15 min). Time point 0 indicates the sample taken immediately after the addition of UbcH5c~AttoUb, while the reaction was on ice. Subsequently the reactions were incubated at 25 ˚C. Each sample was treated with loading dye (without DTT) followed by SDS-PAGE analysis. Top panel shows SDS-PAGE scanned at 635 nm wavelength (which is the Atto647N emission wavelength). Bottom panel shows the same SDS-PAGE as in top panel but stained with InstantBlue to visualize total protein content.

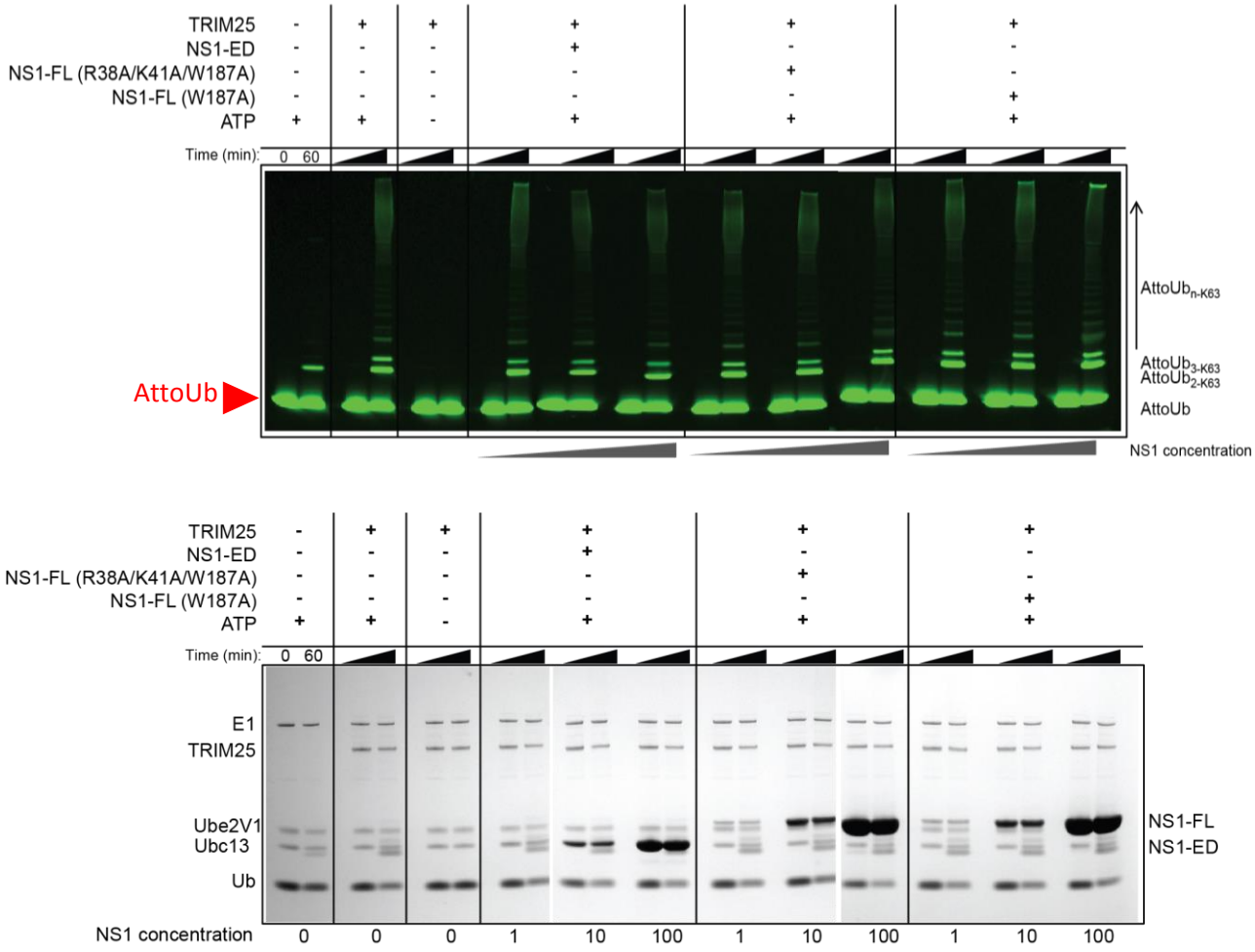

Figure 4.17: NS1 does not affect K63-linked polyubiquitin formation.

The use of fluorescently labeled AttoUb allows monitoring of K63-linked chain formation in the presence of TRIM25-FL and different NS1 constructs. The band corresponding to AttoUb is indicated by red arrow. NS1 constructs tested here were NS1-ED or NS1-FL (R38A/K41A/W187A or W187A). Assays were carried out with 0.5 μM E1, 2.5 μM of each E2 (Ubc13 and Ube2V1), 0 μM (as control) or 1 μM TRIM25-FL, 50 μM unlabeled Ub supplemented with 1 μM AttoUb and three different NS1 concentrations (1 or 10 or 100 μM), as indicated. The reaction was monitored over 60 min. Samples taken at the indicated time points (0 and 60 min). Time point 0 indicates the sample taken before addition of ATP. The reactions were incubated at 25 ˚C and each sample was treated with loading dye (+ DTT) followed by SDS-PAGE analysis. Top panel shows SDS-PAGE scanned at 635 nm wavelength (which is the Atto647N emission wavelength). Bottom panel shows the same SDS-PAGE as in top panel but stained with InstantBlue to visualize total protein content.

4.13 Mechanism of NS1-mediated RIG-I inhibition

Given that the intrinsic activity of TRIM25 remains unaffected by NS1, I hypothesised that RIG-I ubiquitination might be directly perturbed instead. To test this, an *in vitro* RIG-I ubiquitination was set up. As described above, K63-linked poly-ubiquitin formation onto RIG-I requires two different E2s to initiate and subsequently extend the chain (UbcH5 and Ubc13/Ube2V1). In order to be able to quantify any potential changes in RIG-I ubiquitination, a simplified assay that would simulate the initiation reaction *in vitro* was used. Initially, the assay was set up with UbcH5c which was charged with a fluorescently labelled ubiquitin (AttoUb) as described previously and the experiment was performed under E3-rate limiting conditions, large excess of the substrate (RIG-I-2CARD) and NS1 concentration including 0 μM (control), 40 and 100 μM. Experimental details are described in detail in section 2.9.4. Under these conditions, RIG-I-2CARD was ubiquitinated multiple times, both in presence and absence of NS1, and no clear differences could be observed (Figure 4.18). The band corresponding to RIG-I-2CARD-AttoUb$_1$ was then quantified, in an effort to directly compare any changes in RIG-I ubiquitination caused by NS1 (Figure 4.18). Intriguingly, it appears that NS1-FL constructs (either NS1-FL (R38A/K41A/W187A) or NS1-FL (W187A)) moderately inhibit TRIM25-mediated RIG-I-2CARD ubiquitination (~30% reduction) with increasing concentrations of NS1, whereas NS1-RBD which lacks the TRIM25-interacting domain (ED) does not have any effect (Figure 4.18). NS1-ED construct has minimal effect on the RIG-I-2CARD ubiquitination, possibly indicating that RBD-mediated dimerization enhances the inhibitory effect of ED or additional contacts are made through RBD and RIG-I-2CARD (Figure 4.18).

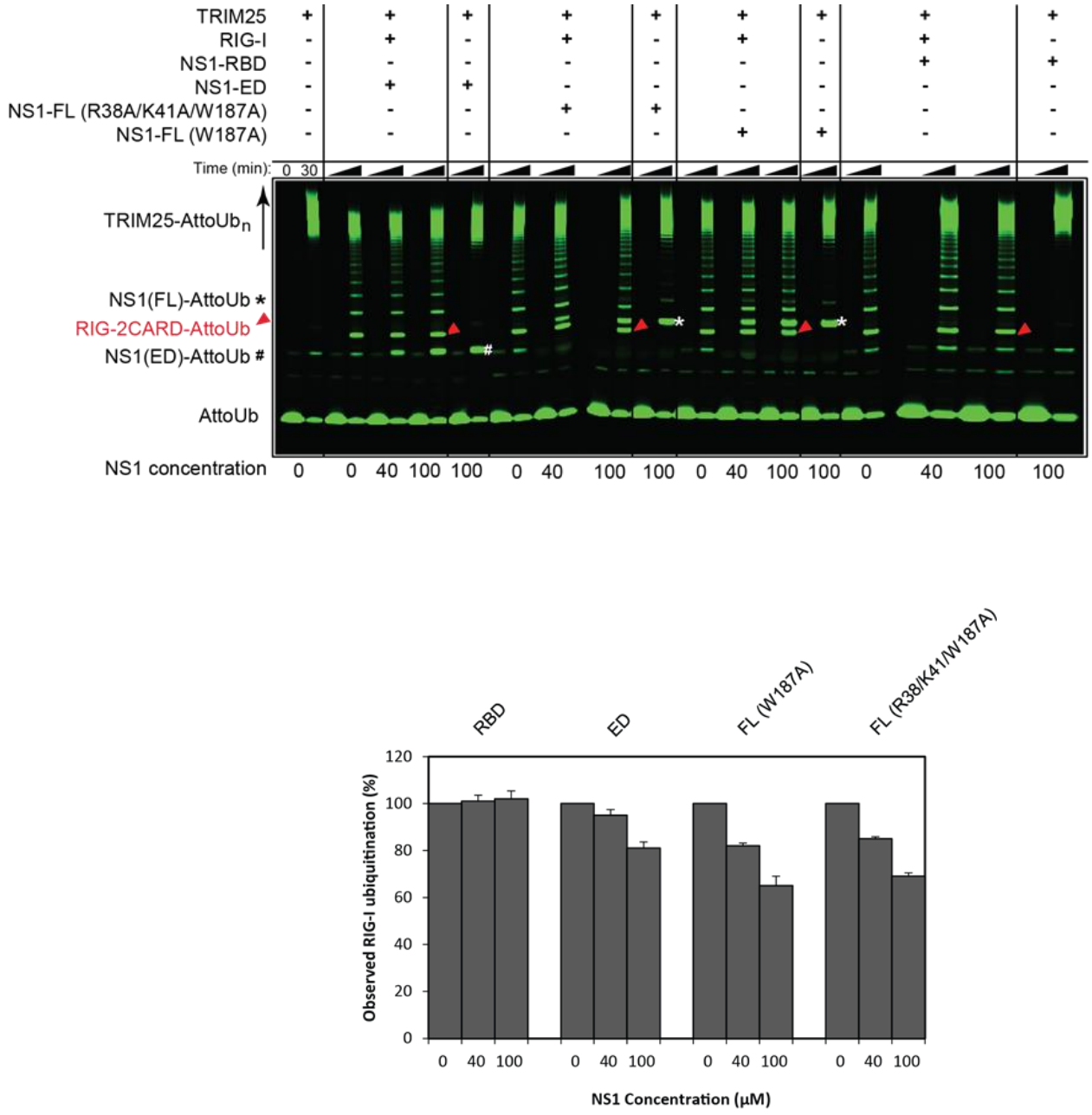

Figure 4.18: Figure description follows in the next page.

Figure 4.18: NS1 inhibits RIG-I ubiquitination by TRIM25/UbcH5c.

The use of fluorescently labeled AttoUb allows monitoring of RIG-I-2CARD ubiquitination in the presence of TRIM25-FL, UbcH5c and different NS1 constructs. As control, a reaction without RIG-I-2CARD and NS1 shows auto-ubiquitination of TRIM25-FL. Further control reactions include TRIM25-FL and RIG-I-2CARD in the absence of NS1. These were used to set a baseline for TRIM25-FL-mediated RIG-I-2CARD ubiquitination. Given that some NS1 constructs (FL and ED) were ubiquitinated in the presence of TRIM25-FL (indicated by # and * symbols), control reactions with TRIM25-FL and NS1 were performed (in the absence of RIG-I-2CARD). NS1 constructs tested here were NS1-RBD, NS1-ED or NS1-FL (R38A/K41A/W187A or W187A). Single-turnover reactions were set up with 4 μM of UbcH5c~AttoUb, 0.5 μM TRIM25-FL, 20 μM RIG-I-2CARD and 0, 40 or 100 μM of different NS1 mutants/constructs, as indicated. The reactions were monitored over 30 min. Samples were taken at the indicated time points (0 and 30 min). Time point 0 indicates the sample taken immediately after the addition of UbcH5c~AttoUb, while the reaction was on ice. Subsequently the reactions were incubated at 30 ˚C. Each sample was treated with loading dye (with DTT) followed by SDS-PAGE analysis. Top panel shows SDS-PAGE scanned at 635 nm wavelength (which is the Atto647N emission wavelength). The band corresponding to RIG-I-2CARD-$AttoUb_1$ is indicated by red arrow. This band was integrated and was plotted as the average of experimental duplicates (± s.d.).

Next, in an effort to develop an assay with a better readout for the potential inhibitory role of NS1 on the TRIM25-mediated RIG-I-2CARD ubiquitination, an earlier observation was further tested. As described in section 3.3.1, in the absence of Ube2V1, Ubc13~Ub will discharge onto TRIM25-RBCC$_L$ (i.e. TRIM25 is auto-ubiquitinated). The same observation was also reported separately in a recent study for TRIM25-FL [95]. This property of Ubc13~Ub was further tested with TRIM25 and RIG-I-2CARD and it was observed that in addition to TRIM25-FL auto-ubiquitination, isolated Ubc13~Ub can also specifically mediate RIG-I mono-ubiquitination (Figure 4.19). The RIG-I lysine residue, which is primarily targeted under these conditions, was identified by mass spectrometry as K190 (using the G-G peptide) (performed by Dr David Frith, The Francis Crick Institute). This ubiquitination site was also previously identified in cell extracts, along with the primary K172 [207]. In this assay, a fluorescently-labelled ubiquitin was used and the band corresponding to the RIG-I-2CARD-AttoUb$_1$ species on the SDS-PAGE was quantified (Figure 4.19). These experiments reveal that NS1-FL (both R38/K41/W187A and W187A) is able to inhibit the mono-ubiquitination of RIG-I by approximately 55%, whereas the isolated effector domain has only a minor effect on RIG-I ubiquitination (Figure 4.19). These results are in good agreement with the data obtained with UbcH5c which showed a moderate decrease of RIG-I ubiquitination only in the presence of NS1-ED and NS1-FL whereas NS1-RBD had no effect (described above). Overall, these results suggest that both RBD and ED of NS1 are required for efficient suppression of RIG-I ubiquitination. Additionally, in these experiments it was observed that NS1 (both NS1-FL and NS1-ED) was mono-ubiquitinated by TRIM25 (Figure 4.19). This follows other reports of post-translational modifications of NS1, although it is currently unknown if this has any physiological relevance during influenza A infection [299-302].

Given the complexity of this multi-component system, the conclusions reached from the RIG-I ubiquitination assays described in the present section are limited. The presence of NS1-FL appears to moderately inhibit ubiquitination of RIG-I. However, these assays were performed with NS1 constructs containing mutations which are required for suppression of aggregation and allow purification. Moreover, TRIM25 is itself auto-ubiquitinated under the assay conditions which might further have an effect on RIG-I ubiquitination. Future experiments are required to further validate the preliminary observations described in this section.

Taken together, the NS1/TRIM25-CC structures and ubiquitination assays presented in this chapter suggest that NS1-binding to TRIM25 inhibits RIG-I ubiquitination either by competing with RIG-I-2CARD for binding on TRIM25 or through steric effects and possibly by masking the RIG-I ubiquitination sites. The implications of these observations are further discussed in the context of other studies in the next section.

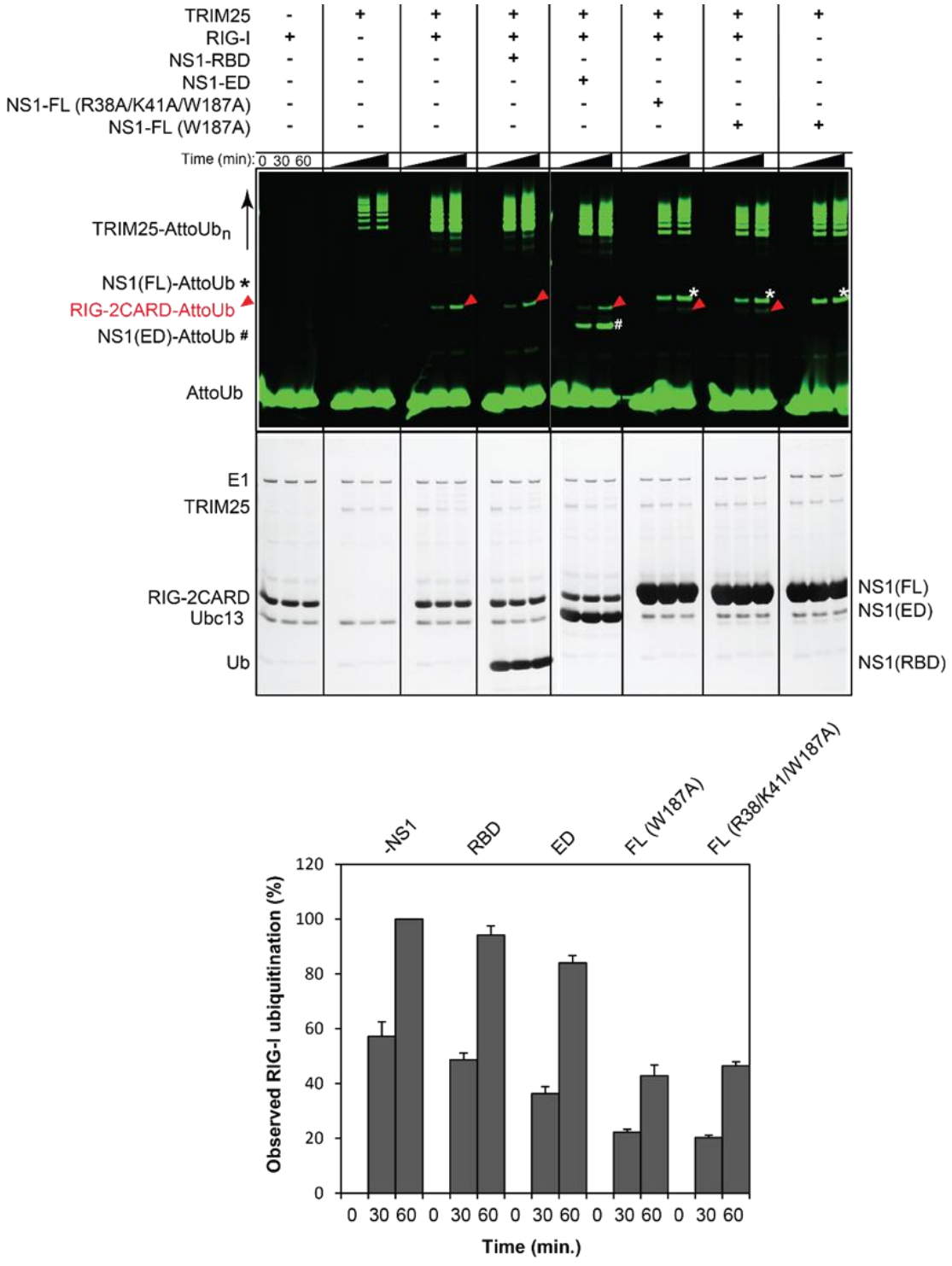

Figure 4.19: Figure description follows in the next page.

Figure 4.19: NS1 inhibits RIG-I ubiquitination by TRIM25/Ubc13.

The use of fluorescently labeled AttoUb allows monitoring of RIG-I-2CARD ubiquitination in the presence of TRIM25-FL, Ubc13 (K92A) and different NS1 constructs. As negative control, a reaction without TRIM25 shows no RIG-I-2CARD ubiquitination. In the presence of TRIM25 and Ubc13, TRIM25 was auto-ubiquitinated (positive control). In the presence of TRIM25-FL and NS1-FL or ED, NS1 is ubiquitinated (indicated by # and * symbols). A reaction with TRIM25 and RIG-I-2CARD was used to set a baseline for TRIM25-FL-mediated RIG-I-2CARD ubiquitination. NS1 constructs tested here were NS1-RBD, NS1-ED or NS1-FL (R38A/K41A/W187A or W187A). Multiple-turnover reactions were set up with 0.5 µM E1, 5 µM Ubc13 (K92A to suppress E2 auto-ubiquitination [93]), 0.5 µM TRIM25-FL, 20 µM RIG-I-2CARD, 1 µM AttoUb and 0 or 100 µM NS1 constructs/mutants, as indicated. The reactions were monitored over 60 min. Samples were taken at the indicated time points (0, 30, 60 min). Time point 0 indicates the sample taken before addition of ATP. The reactions were incubated at 30 ˚C and each sample was treated with loading dye (+ DTT) followed by SDS-PAGE analysis. Top panel shows SDS-PAGE scanned at 635 nm wavelength (which is the Atto647N emission wavelength). Middle panel shows the same SDS-PAGE as in top panel but stained with InstantBlue to visualize total protein content. The band corresponding to RIG-I-2CARD-AttoUb$_1$ is indicated by red arrow on top panel. This band was integrated and was plotted as the average of experimental triplicates (± s.d.).

4.14 Summary and Discussion

RIG-I is an intracellular PRR that plays a key role in the innate immune response against a variety of viruses. Recognition of viral RNA by RIG-I initiates a signalling cascade that culminates in the production of interferons and proinflammatory cytokines. The ubiquitination of RIG-I by TRIM25 is crucial for the activation of the RIG-I signalling pathway establishing TRIM25 as a key player in antiviral immunity. Conversely, viruses have evolved intricate mechanisms to interfere with the host immune response, one of which is the capture of TRIM25 by influenza A virus NS1 to supress its ability to ubiquitinate RIG-I. To understand the mechanism of NS1-mediated inhibition of TRIM25 on a molecular level, this project was aimed at gaining structural insights into the recognition of TRIM25 by NS1. To achieve this, initial efforts were focused on identifying well-behaved NS1 constructs. Due to the increased aggregation observed for the wild-type NS1-FL protein, mutations either in the RBD or ED region had to be introduced in order to produce a better-behaved protein. All constructs were biochemically characterised and their ability to interact with TRIM25-CC was tested.

Using purified proteins, I obtained results which showed that NS1-FL (W187A) is able to bind TRIM25-CC. This observation is in good agreement with a recent study which showed that RIG-I-mediated IFN response was suppressed by infecting cells with Influenza virus A encoding mutant NS1 (W187A) as well as wild-type NS1 [251]. Furthermore, in the present thesis I showed that R38A/K41A mutations do not affect binding of NS1-FL to TRIM25-CC and further established that only NS1-ED interacts with TRIM25-CC whereas NS1-RBD does not. These observations are in contradiction to a previous study suggesting that both domains (RBD and ED) of NS1 are required for binding to TRIM25 and that the mutations R38A/K41A abolish this interaction [234]. However, these assays were performed using cell extracts and therefore it may be possible that in a cellular context there are additional components which stabilize the NS1/TRIM25 interaction. For example, these mutations in the RBD (R38A/K41A) have been shown to abolish binding of dsRNA [242, 246, 303]. Therefore, it is reasonable to speculate that upon viral infection, viral dsRNA is released in the cytoplasm and that both RIG-I and NS1 compete for binding to dsRNA. It is also possible that binding of both proteins to the same dsRNA molecule can lead to co-localization with TRIM25 and also Riplet (which is another RING E3 ligase required for RIG-I activation) [218, 294, 304]. In support of this, recent studies have shown that

NS1 binding to TRIM25 does not interfere with the TRIM25-PRYSPRY/RIG-I-2CARD interaction [234, 304] and that NS1-RBD binds directly to RIG-I-2CARD construct [248]. All these observations point to a model where TRIM25, NS1, RIG-I and dsRNA are all part of the same complex during viral infection. Therefore, mutation in NS1 (R38A/K41A) would destabilize complex formation and reduce the ability of NS1 to inhibit RIG-I-mediated IFN production as described [234].

In order to obtain atomic details of the TRIM25/NS1 interaction, crystallization experiments were pursued for all interacting pairs of NS1 and TRIM25-CC. The crystal structures of the TRIM25-CC domain in complex with NS1-FL and the isolated NS1-ED were solved. These structures show that NS1 binding does not interfere with TRIM25 oligomerization as previously suggested [234] but instead binds both monomers of the dimeric coiled-coil. The pull-down experiments showed that only NS1-ED interacts with TRIM25-CC whereas NS1-RBD does not. These structures validate this observation and further show that the RBD does not make any contacts with the TRIM25-CC even in the context of the NS1-FL. As described above, this contradicts a previous report suggesting that both domains of NS1 are required for interaction with TRIM25-CC [234]. Instead, these structures show that a dimeric NS1-RBD links two TRIM25-CC dimers through interactions with the corresponding NS1-EDs. If we suppose that in solution, a stoichiometric complex is formed of two NS1-FL molecules and two TRIM25-CC domains (forming the antiparallel dimer), two NS1-EDs would bind symmetrically at opposite sites of a dimeric TRIM25-CC as seen in the NS1-ED/TRIM25-CC structure. The distance between these two EDs is measured to be approx. 95 Å. In all reported NS1-FL structures to date, the maximum LR length is measured approx. at 30 Å which raises the question if major conformational rearrangements in NS1 take place or simply the two EDs cannot belong to a single RBD-mediated dimer and that higher-order oligomerization is required, as observed in the TRIM25-CC/NS1-FL structure presented in this thesis. Further studies are required to obtain information about the stoichiometry of the complex in solution. The structures reported in this chapter show the molecular determinants for the NS1/TRIM25 interaction for the first time.

Comparison of the present NS1/TRIM25 structures with the NS1/p85β structure (3L4Q.pdb) reveals remarkable similarities [253]. p85β, a regulatory subunit of the phosphoinositide 3-kinase (PI3K) complex, is a multi-domain protein

containing a rigid elongated coiled-coil domain (β-iSH2) which is targeted by influenza A NS1 leading to stimulated PI3K activity. Intriguingly, the effector domain of NS1 binds to β-iSH2 through exactly the same interface observed in the NS1-ED/TRIM25-CC structure. In both cases, the short NS1 α-helix composed of a.a. 95-99 packs against the substrate CC region, forming a helical bundle (Figure 4.20). This indicates that NS1 can bind multiple helical substrates using the same highly conserved interface.

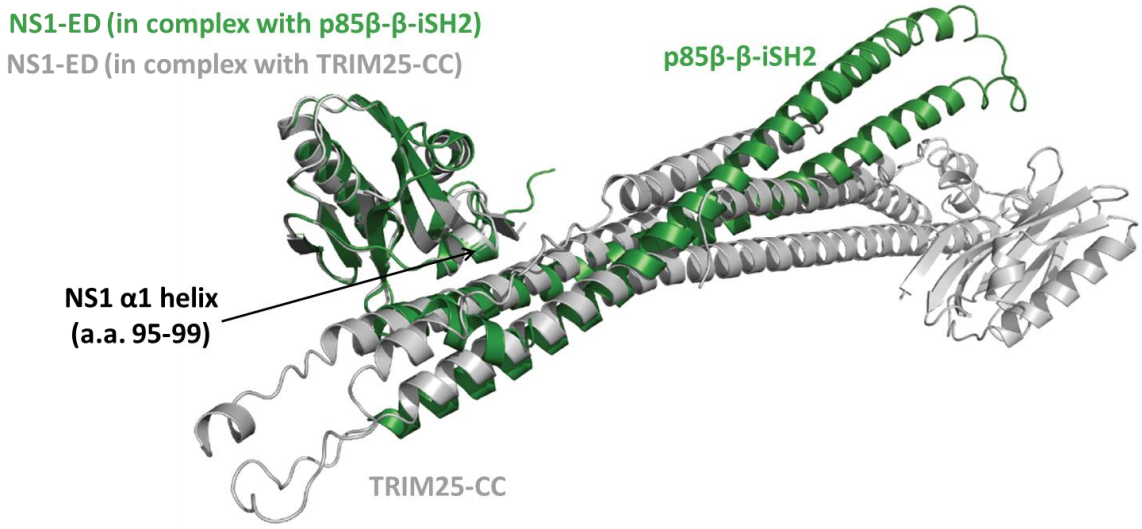

Figure 4.20: Overlap of NS1-ED complexed with TRIM25-CC and p85β.
Structural alignment of the complexes of the effector domain of NS1 bound to TRIM25-CC (grey) and p85β (green) (3L4Q.pdb) reveals similarities [253].

Another interesting feature of NS1 observed in the NS1-FL/TRIM25-CC structure is that the relative arrangement of RBD and ED seen is different from previous structures of full-length NS1. A structural alignment of the NS1-FL (A/Puerto Rico/8/1934) presented in this thesis with the structure of the highly pathogenic H5N1 strain (A/Vietnam/1203/2004(H5N1)) that has an evolutionary conserved 4-residue deletion (LR Δ80-84) and H6N6 NS1 (A/blue-winged teal/MN/993/1980(H6N6)) shows that all three align well on the RBD dimer but the EDs occupy many different positions around it (Figure 4.21). This observation allows me to suggest that the EDs are flexibly linked to the RBD, further supporting the idea that the NS1-LR adds flexibility to NS1 as it acts as a

mechanical hinge to allow movement of ED in relation to RBD to accommodate substrate binding (Figure 4.21) [244].

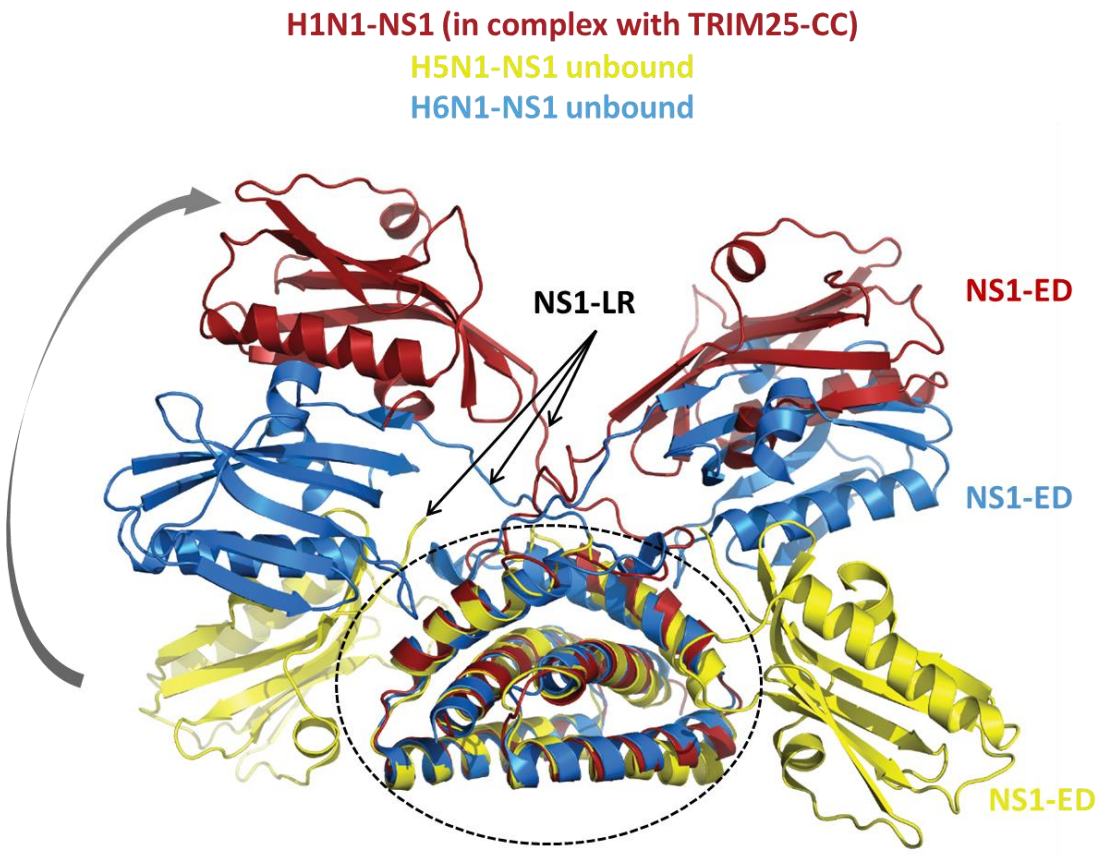

Figure 4.21: Structural comparison of NS1-FL from different viral strains.
Structural alignment of NS1 (as crystallized in complex with TRIM25-CC, shown in red) with the other two available NS1-FL (apo) structures (A/VietNam/1203/2004(H5N1)) shown in yellow (3F5T.pdb) [243] and (A/blue-winged teal/MN/993/1980(H6N6)) shown in blue (4OPH.pdb) [244]. The structures overlap well on the RBD domains (0.8 Å r.m.s.d., circled region) whereas the EDs occupy different positions around the RBD, revealing structural flexibility owing to the linker-region (LR) of NS1.

The two crystal structures of the TRIM25-CC bound to NS1-FL and NS1-ED revealed for the first time that NS1 binding to TRIM25 does not affect CC-mediated dimerization as previously suggested [234]. This indicates that NS1 must execute its inhibitory function by other means. Thus, the next question that my project aimed to answer was what effect does the NS1 binding on TRIM25 have on RIG-I ubiquitination? A recent study reported that a pathogenic *Salmonella* effector (SopA) binds directly to the RING domain of other TRIM

proteins (TRIM56 and TRIM65) [305]. Binding of SopA occludes the E2~Ub binding site on the TRIM-RING and thus renders it inactive. In chapter 3, the structure of TRIM25-RING/UbcH5-Ub complex was reported, showing that TRIM25-RING dimerization is necessary for E3 ligase activity. In an effort to further examine if NS1 directly interferes with TRIM25-RING mediated E2~Ub activation or induces conformational changes that could possibly disrupt RING dimerization, the full-length TRIM25 was produced in insect cells. Enzymatic assays were performed with TRIM25-FL, UbcH5c and Ubc13/Ube2V1 which are required for RIG-I activation [216]. These experiments revealed that the intrinsic E3 ligase ability of TRIM25 remains unaffected by the presence of NS1, indicating that RING-mediated E2~Ub activation and presumably RING dimerization are unperturbed.

Next, the effect of NS1 on TRIM25-mediated RIG-I-2CARD ubiquitination was examined. However, since assays in mammalian cells (such as HEK293T) were not possible at that time, my efforts were focused on reconstituting the enzymatic reactions in an *in vitro* setting. This task had many complications due to the fact that this is a multi-component system and I had to resort to different experimental conditions and combinations. A major disadvantage of this system was that the wild-type NS1-FL protein could not be included in these assays due to its propensity to aggregate. However, simplified versions of the enzymatic cascade showed that TRIM25-FL was able to ubiquitinate RIG-I-2CARD construct using either UbcH5 or even Ubc13 without its physiological partner Ube2V1, *in vitro*. In both cases, the presence of NS1-FL showed a clear reduction in the relative RIG-I ubiquitination levels, under these conditions.

The crystal structures presented in this chapter along with previous published studies indicate that NS1 binding does not interfere with RIG-I recognition by the TRIM25-PRYSPRY domain and hence a ternary complex of TRIM25/RIG-I/NS1 is possibly formed [234, 304]. Therefore, it is reasonable to speculate that NS1 binding to TRIM25 prevents the correct orientation of the RIG-I-binding PRYSPRY domain with respect to the E2~Ub-binding RING domain and thereby prevents efficient ubiquitin transfer (Figure 4.22). In its simplest form, a stoichiometric interaction between TRIM25 and NS1 should suffice to suppress substrate ubiquitination in such a scenario. However, in the experiments reported in section 4.13, an excess of NS1 was required to see inhibition, similar to the observation that the inhibition of RIG-I-induced INF-β promoter activation occurs

in a dose-dependent manner [234]. Given this observation, I speculate that optimal inhibition of RIG-I ubiquitination by NS1 requires the formation of higher order oligomers of NS1, which is absent in the mutants that were used in this study. Intriguingly, the arrangement of NS1-FL and TRIM25-CC observed in the crystal structure, where a given NS1 dimer links two different TRIM25-CC dimers may possibly mimic such a higher order arrangement. In this model NS1-ED interacts with TRIM25-CC and then self-associates, thereby sequestering the available pool of TRIM25 and RIG-I. Additionally, the dsRNA-binding role of NS1 is well-established in the literature and it may be possible that either an dsRNA-mediated interaction is formed between NS1 and RIG-I, further stabilizing a complex composed of TRIM25, RIG-I, NS1 and dsRNA or that binding of NS1-RBD to a dsRNA molecule increases the local concentration of NS1 which can then interact through ED with TRIM25 and RIG-I.

In addition to the well-established role of RIG-I-conjugated poly-ubiquitin chains in MAVS activation, unanchored K63-linked ubiquitin chains have also been shown to be able to oligomerize RIG-I to promote recruitment of MAVS and signal activation [216, 219, 221]. However, the observation that NS1 does not inhibit the ability of TRIM25 to form unanchored K63-linked chains is in apparent contradiction to this report as TRIM25-engagement by NS1 would not suffice to prevent RIG-I activation by unanchored chains. A recent study by Hur and colleagues [219] provides some explanation for this conundrum: whilst binding of unanchored K63 chains to the tandem CARDs of RIG-I does induce a tetrameric CARD arrangement and can initiate signalling, stabilization of this tetrameric arrangement is more efficient with CARDs covalently attached to K63-linked chains than with unattached chains. Furthermore, covalently attached and non-covalent K63-linked ubiquitin chains have been suggested to act in a synergistic manner in an *in vivo* setting and the loss of covalently attached K63 chains might be sufficient to suppress an efficient immune response [306].

Previous studies have reported that TRIM25 is tightly regulated through a negative feedback inhibition mechanism. In cells, TRIM25 undergoes self-mono-ubiquitination [207, 223, 224]. The mono-ubiquitinated TRIM25 species are highly susceptible to further poly-ubiquitination through K48-linked chains, performed by E3 ligases which, to date, remain unidentified [223, 224]. As expected, poly-ubiquitination of TRIM25 with K48-linked chains results in proteasomal degradation and suppression of RIG-I-mediated IFN signaling. In contrast,

TRIM25-specific signaling is sustained through the actions of a de-ubiquitinating (DUB) enzyme (USP15) which binds to the B-Box domains of TRIM25 and removes the K48-linked ubiquitin chains from TRIM25 [224, 225]. The structural and biochemical data presented in chapter 4 show that NS1-binding to TRIM25 allows auto-ubiquitination of the E3. It is thus possible that NS1 may compete with USP15 for binding to poly-ubiquitinated TRIM25 which is then degraded by the proteasome. Degradation of TRIM25 would reduce ubiquitination levels of RIG-I and presumably suppress the IFN-mediated immune response.

Results presented in this chapter reveal for the first time the atomic determinants of the interaction between NS1 protein derived from a highly pathogenic strain (H1N1-PR8) and human TRIM25. Structural characterization and biochemical analysis provided novel insights into the TRIM25 recognition and inhibition of its enzymatic activity mediated by NS1. Further studies are required to examine potential further interactions between NS1 and RIG-I and ultimately determine the structure of a ternary complex composed of TRIM25/RIG-I/NS1 which may provide additional drug targets.

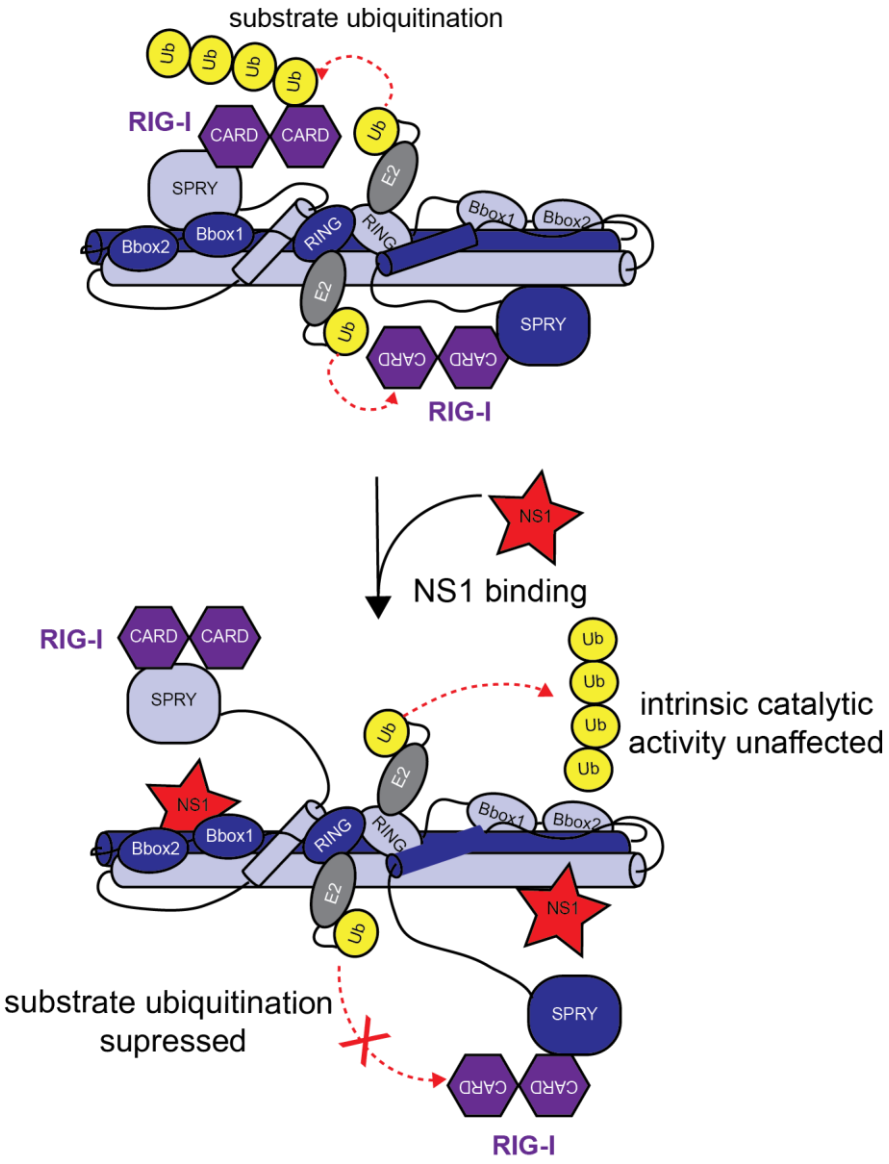

Figure 4.22: Model of NS1-mediated inhibition of TRIM25/RIG-I pathway.

Upon viral infection, RIG-I-2CARD is modified by TRIM25 with K63-linked polyubiquitin chains. NS1 interacts directly with TRIM25 and supresses RIG-I ubiquitination, possibly by interfering with the correct orientation of RIG-I.

5. Overview and Future directions

TRIM proteins compose one of the largest subfamilies of RING E3 ligases and their involvement in the regulation of processes such as innate immune signalling and carcinogenesis suggest that they could constitute interesting targets to combat disease in the future. Work presented in this thesis provides novel insights into the E3 ligase function of TRIM25 and shows how its oligomeric state is linked to the catalytic activity. The crystal structure of a complex between the TRIM25 RING domain and an ubiquitin-loaded E2 identifies the structural and mechanistic features that promote activation of E2~Ub allowing me to propose a model for the regulation of activity in the full-length protein. These conclusions were published in [94]. This was the first thorough and quantitative characterisation of the structure-function relationship of a member of the TRIM E3 ligase family and subsequently other studies show that some of the main principles described here for TRIM25 apply also to other TRIM protein members [94-96, 187]. To date, all studies that focused on TRIM-RING activation of different members including TRIM5α, TRIM23, TRIM25 and TRIM32 have reported that RING dimerization is necessary for activity [94-96, 187]. The structures of all CC domains described so far (TRIM5α, TRIM20, TRIM25, TRIM69) also show long antiparallel dimers which based on bioinformatics analysis appears to be shared among all TRIM proteins [158, 165-167]. However, many of the TRIM proteins described to date show also unique features, as in the case of TRIM5α which oligomerizes through the B-Box2 domain. No other TRIM member appears to share this feature with TRIM5α which acts as a restriction factor by binding to retroviral capsids [177, 179, 181]. Additionally, TRIM32 is a tetramer in solution, mediated by RING and CC dimerization, respectively [94]. Given that the TRIM family is composed of more than 70 proteins, it is necessary to obtain more information about less-studied members, in order to see what are the general features shared and the unique determinants that dictate specificity.

Next, the inhibitory role of Influenza Virus A NS1 protein on TRIM25 was investigated. Biochemical and structural analysis of the TRIM25/NS1 complex identified the interacting regions and helped elucidate how viral infection disrupts the activity of TRIM25. This is the first time these observations are reported and have the potential to form a solid platform for the development of antiviral pharmaceuticals. Work is currently ongoing and the results will be published in the near future.

To my knowledge, this thesis is one of the first studies reporting the atomic details of TRIM/pathogen interactions that lead to suppression of innate immune responses. To date, a *Salmonella* effector protein (SopA) is shown to bind the RING domains of either TRIM65 or TRIM56 [305305, 307]. Here, I reported the structures of Influenza A NS1 bound to TRIM25. Comparison of those revealed that pathogens employ different mechanism for suppression of the catalytic ability of TRIM proteins. Despite the fact that a plethora of studies have identified crucial interactions between pathogen-derived proteins and TRIM members, the structural information about those is scarce. For example, the interaction of IE1 (a human cytomegalovirus protein) with the TRIM19/PML-CC domain is identified but the molecular details of this interaction are not known [205]. Similarly, *Salmonella* effector SseK3 reportedly binds to the C-terminal domain (NHL) of TRIM32 but no structural information is available yet [308]. Obtaining different structural snapshots of these interactions could possibly increase our chances for targeting human pathogens.

Immediate future directions for this project include pursuing structural analysis of the E2~Ub/TRIM25/RIG-I-2CARD complex by X-ray crystallography or cryo-electron microscopy. An optimised purification protocol described in the present thesis results in a homogenous TRIM25 sample with yield and concentration which is sufficient for structural studies. Additionally, charging reactions of E2 enzymes with ubiquitin have also been established before and further described here. Subsequent efforts should be focused in obtaining either a monodisperse RIG-I-2CARD construct or full-length RIG-I which might further require the addition of an RNA molecule for increased stability and release of auto-inhibition. Despite the non-trivial challenges anticipated, a structure of this ternary complex would help elucidating the atomic details of the TRIM25/RIG-I-2CARD interaction and show how RIG-I is modified with K63-linked polyubiquitin chains at specific lysine residues. The NS1/TRIM25-CC structures described in the present thesis provide snapshots of the events that lead to inhibition of TRIM25-mediated RIG-I ubiquitination. Comparison of these structures with a structure of the “active” E2~Ub/TRIM25/RIG-I-2CARD complex could provide further insights into any potential structural changes that NS1 binding might cause to TRIM25 hence testing the NS1/TRIM25 model of inhibition proposed here. For example, NS1

binding might cause displacement of the PRYSPRY domains and hence disrupt efficient ubiquitin transfer.

Collectively, the future work proposed could provide atomic information on RIG-I ubiquitination by TRIM25 and importantly show how NS1 binding to TRIM25 suppressed this.

Long-term future directions of this project include structural and biochemical characterization of the interaction between an RNA molecule from dengue virus and TRIM25. Dengue virus is responsible for dengue fever in humans and currently there is no treatment. In most cases, dengue fever runs naturally its course but some individuals may develop life-threatening dengue haemorrhagic fever. A recent study reported that a subgenomic flaviviral RNA (sfRNA) with a complex secondary structure binds directly to TRIM25 and disrupts the binding of the regulatory DUB enzyme (USP15). Binding of the USP15 to TRIM25 is necessary for sustaining RIG-I-mediated IFN response as described in section 1.9.3. Analysis of the interacting surfaces of TRIM25/sfRNA from dengue virus could provide targets for developing novel pharmaceuticals.

References

1. Komander, D., and Rape, M. (2012). The ubiquitin code. Annual review of biochemistry *81*, 203-229.
2. Hershko, A., and Ciechanover, A. (1998). The ubiquitin system. Annual review of biochemistry *67*, 425-479.
3. Mevissen, T.E.T., and Komander, D. (2017). Mechanisms of Deubiquitinase Specificity and Regulation. Annual review of biochemistry *86*, 159-192.
4. Popovic, D., Vucic, D., and Dikic, I. (2014). Ubiquitination in disease pathogenesis and treatment. Nature medicine *20*, 1242-1253.
5. Baker, R.T., and Board, P.G. (1991). The human ubiquitin-52 amino acid fusion protein gene shares several structural features with mammalian ribosomal protein genes. Nucleic acids research *19*, 1035-1040.
6. Lund, P.K., Moats-Staats, B.M., Simmons, J.G., Hoyt, E., D'Ercole, A.J., Martin, F., and Van Wyk, J.J. (1985). Nucleotide sequence analysis of a cDNA encoding human ubiquitin reveals that ubiquitin is synthesized as a precursor. The Journal of biological chemistry *260*, 7609-7613.
7. Wiborg, O., Pedersen, M.S., Wind, A., Berglund, L.E., Marcker, K.A., and Vuust, J. (1985). The human ubiquitin multigene family: some genes contain multiple directly repeated ubiquitin coding sequences. The EMBO journal *4*, 755-759.
8. Ozkaynak, E., Finley, D., and Varshavsky, A. (1984). The yeast ubiquitin gene: head-to-tail repeats encoding a polyubiquitin precursor protein. Nature *312*, 663-666.
9. Clague, M.J., Heride, C., and Urbe, S. (2015). The demographics of the ubiquitin system. Trends in cell biology *25*, 417-426.
10. Kaiser, S.E., Riley, B.E., Shaler, T.A., Trevino, R.S., Becker, C.H., Schulman, H., and Kopito, R.R. (2011). Protein standard absolute quantification (PSAQ) method for the measurement of cellular ubiquitin pools. Nature methods *8*, 691-696.
11. Yang, X., Brownell, J.E., Xu, Q., Zhu, F., Ma, J., Loke, H.K., Rollins, N., Soucy, T.A., Minissale, J.J., Thomas, M.P., Mallender, W.D., Dick, L.R., Li, P., and Liao, H. (2013). Absolute quantification of E1, ubiquitin-like proteins and Nedd8-MLN4924 adduct by mass spectrometry. Cell biochemistry and biophysics *67*, 139-147.
12. Vijay-Kumar, S., Bugg, C.E., and Cook, W.J. (1987). Structure of ubiquitin refined at 1.8 A resolution. Journal of molecular biology *194*, 531-544.
13. Vijay-Kumar, S., Bugg, C.E., Wilkinson, K.D., and Cook, W.J. (1985). Three-dimensional structure of ubiquitin at 2.8 A resolution. Proceedings of the National Academy of Sciences of the United States of America *82*, 3582-3585.
14. Sloper-Mould, K.E., Jemc, J.C., Pickart, C.M., and Hicke, L. (2001). Distinct functional surface regions on ubiquitin. The Journal of biological chemistry *276*, 30483-30489.
15. Raiborg, C., Slagsvold, T., and Stenmark, H. (2006). A new side to ubiquitin. Trends in biochemical sciences *31*, 541-544.
16. Haririnia, A., Verma, R., Purohit, N., Twarog, M.Z., Deshaies, R.J., Bolon, D., and Fushman, D. (2008). Mutations in the hydrophobic core of ubiquitin differentially affect its recognition by receptor proteins. Journal of molecular biology *375*, 979-996.

17. Wang, Q., Young, P., and Walters, K.J. (2005). Structure of S5a bound to monoubiquitin provides a model for polyubiquitin recognition. Journal of molecular biology *348*, 727-739.
18. Kamadurai, H.B., Souphron, J., Scott, D.C., Duda, D.M., Miller, D.J., Stringer, D., Piper, R.C., and Schulman, B.A. (2009). Insights into ubiquitin transfer cascades from a structure of a UbcH5B approximately ubiquitin-HECT(NEDD4L) complex. Molecular cell *36*, 1095-1102.
19. van der Veen, A.G., and Ploegh, H.L. (2012). Ubiquitin-like proteins. Annual review of biochemistry *81*, 323-357.
20. Streich, F.C., Jr., and Lima, C.D. (2014). Structural and functional insights to ubiquitin-like protein conjugation. Annual review of biophysics *43*, 357-379.
21. Denuc, A., and Marfany, G. (2010). SUMO and ubiquitin paths converge. Biochemical Society transactions *38*, 34-39.
22. Schwertman, P., Bekker-Jensen, S., and Mailand, N. (2016). Regulation of DNA double-strand break repair by ubiquitin and ubiquitin-like modifiers. Nature reviews. Molecular cell biology *17*, 379-394.
23. Yau, R., and Rape, M. (2016). The increasing complexity of the ubiquitin code. Nat Cell Biol *18*, 579-586.
24. Haglund, K., Sigismund, S., Polo, S., Szymkiewicz, I., Di Fiore, P.P., and Dikic, I. (2003). Multiple monoubiquitination of RTKs is sufficient for their endocytosis and degradation. Nat Cell Biol *5*, 461-466.
25. Kirisako, T., Kamei, K., Murata, S., Kato, M., Fukumoto, H., Kanie, M., Sano, S., Tokunaga, F., Tanaka, K., and Iwai, K. (2006). A ubiquitin ligase complex assembles linear polyubiquitin chains. The EMBO journal *25*, 4877-4887.
26. Varshavsky, A. (2017). The Ubiquitin System, Autophagy, and Regulated Protein Degradation. Annual review of biochemistry *86*, 123-128.
27. Peng, J., Schwartz, D., Elias, J.E., Thoreen, C.C., Cheng, D., Marsischky, G., Roelofs, J., Finley, D., and Gygi, S.P. (2003). A proteomics approach to understanding protein ubiquitination. Nature biotechnology *21*, 921-926.
28. Xu, P., Duong, D.M., Seyfried, N.T., Cheng, D., Xie, Y., Robert, J., Rush, J., Hochstrasser, M., Finley, D., and Peng, J. (2009). Quantitative proteomics reveals the function of unconventional ubiquitin chains in proteasomal degradation. Cell *137*, 133-145.
29. Swatek, K.N., and Komander, D. (2016). Ubiquitin modifications. Cell research *26*, 399-422.
30. Komander, D., Reyes-Turcu, F., Licchesi, J.D.F., Odenwaelder, P., Wilkinson, K.D., and Barford, D. (2009). Molecular discrimination of structurally equivalent Lys 63-linked and linear polyubiquitin chains. EMBO reports *10*, 466-473.
31. Weeks, S.D., Grasty, K.C., Hernandez-Cuebas, L., and Loll, P.J. (2009). Crystal structures of Lys-63-linked tri- and di-ubiquitin reveal a highly extended chain architecture. Proteins *77*, 753-759.
32. Bremm, A., Freund, S.M., and Komander, D. (2010). Lys11-linked ubiquitin chains adopt compact conformations and are preferentially hydrolyzed by the deubiquitinase Cezanne. Nature structural & molecular biology *17*, 939-947.
33. Kristariyanto, Y.A., Abdul Rehman, S.A., Campbell, D.G., Morrice, N.A., Johnson, C., Toth, R., and Kulathu, Y. (2015). K29-selective ubiquitin binding domain reveals structural basis of specificity and heterotypic nature of k29 polyubiquitin. Molecular cell *58*, 83-94.

34. Kristariyanto, Y.A., Choi, S.Y., Rehman, S.A., Ritorto, M.S., Campbell, D.G., Morrice, N.A., Toth, R., and Kulathu, Y. (2015). Assembly and structure of Lys33-linked polyubiquitin reveals distinct conformations. The Biochemical journal *467*, 345-352.
35. Virdee, S., Ye, Y., Nguyen, D.P., Komander, D., and Chin, J.W. (2010). Engineered diubiquitin synthesis reveals Lys29-isopeptide specificity of an OTU deubiquitinase. Nature chemical biology *6*, 750-757.
36. Cook, W.J., Jeffrey, L.C., Carson, M., Chen, Z., and Pickart, C.M. (1992). Structure of a diubiquitin conjugate and a model for interaction with ubiquitin conjugating enzyme (E2). The Journal of biological chemistry *267*, 16467-16471.
37. Hershko, A. (2005). The ubiquitin system for protein degradation and some of its roles in the control of the cell-division cycle (Nobel lecture). Angewandte Chemie (International ed. in English) *44*, 5932-5943.
38. Cunningham, C.N., Baughman, J.M., Phu, L., Tea, J.S., Yu, C., Coons, M., Kirkpatrick, D.S., Bingol, B., and Corn, J.E. (2015). USP30 and parkin homeostatically regulate atypical ubiquitin chains on mitochondria. Nat Cell Biol *17*, 160-169.
39. Morris, J.R., and Solomon, E. (2004). BRCA1 : BARD1 induces the formation of conjugated ubiquitin structures, dependent on K6 of ubiquitin, in cells during DNA replication and repair. Human molecular genetics *13*, 807-817.
40. Bremm, A., and Komander, D. (2011). Emerging roles for Lys11-linked polyubiquitin in cellular regulation. Trends in biochemical sciences *36*, 355-363.
41. Hu, H., and Sun, S.C. (2016). Ubiquitin signaling in immune responses. Cell research *26*, 457-483.
42. Michel M , A., Elliott P , R., Swatek K , N., Simicek, M., Pruneda J , N., Wagstaff J , L., Freund S , M.V., and Komander, D. (2015). Assembly and Specific Recognition of K29- and K33-Linked Polyubiquitin. Molecular cell *58*, 95-109.
43. Pan, M., Gao, S., Zheng, Y., Tan, X., Lan, H., Tan, X., Sun, D., Lu, L., Wang, T., Zheng, Q., Huang, Y., Wang, J., and Liu, L. (2016). Quasi-Racemic X-ray Structures of K27-Linked Ubiquitin Chains Prepared by Total Chemical Synthesis. Journal of the American Chemical Society *138*, 7429-7435.
44. Castaneda, C.A., Dixon, E.K., Walker, O., Chaturvedi, A., Nakasone, M.A., Curtis, J.E., Reed, M.R., Krueger, S., Cropp, T.A., and Fushman, D. (2016). Linkage via K27 Bestows Ubiquitin Chains with Unique Properties among Polyubiquitins. Structure (London, England : 1993) *24*, 423-436.
45. Gatti, M., Pinato, S., Maiolica, A., Rocchio, F., Prato, M.G., Aebersold, R., and Penengo, L. (2015). RNF168 promotes noncanonical K27 ubiquitination to signal DNA damage. Cell reports *10*, 226-238.
46. Sparrer, K.M.J., Gableske, S., Zurenski, M.A., Parker, Z.M., Full, F., Baumgart, G.J., Kato, J., Pacheco-Rodriguez, G., Liang, C., Pornillos, O., Moss, J., Vaughan, M., and Gack, M.U. (2017). TRIM23 mediates virus-induced autophagy via activation of TBK1. Nature microbiology.
47. Herhaus, L., and Dikic, I. (2015). Expanding the ubiquitin code through post-translational modification. EMBO reports *16*, 1071-1083.
48. Swaney, D.L., Beltrao, P., Starita, L., Guo, A., Rush, J., Fields, S., Krogan, N.J., and Villen, J. (2013). Global analysis of phosphorylation and

ubiquitylation cross-talk in protein degradation. Nature methods *10*, 676-682.
49. Koyano, F., Okatsu, K., Kosako, H., Tamura, Y., Go, E., Kimura, M., Kimura, Y., Tsuchiya, H., Yoshihara, H., Hirokawa, T., Endo, T., Fon, E.A., Trempe, J.-F., Saeki, Y., Tanaka, K., and Matsuda, N. (2014). Ubiquitin is phosphorylated by PINK1 to activate parkin. Nature *advance online publication*.
50. Richter, B., Sliter, D.A., Herhaus, L., Stolz, A., Wang, C., Beli, P., Zaffagnini, G., Wild, P., Martens, S., Wagner, S.A., Youle, R.J., and Dikic, I. (2016). Phosphorylation of OPTN by TBK1 enhances its binding to Ub chains and promotes selective autophagy of damaged mitochondria. Proceedings of the National Academy of Sciences of the United States of America *113*, 4039-4044.
51. Swaney, D.L., Rodriguez-Mias, R.A., and Villen, J. (2015). Phosphorylation of ubiquitin at Ser65 affects its polymerization, targets, and proteome-wide turnover. EMBO reports *16*, 1131-1144.
52. Grabbe, C., Husnjak, K., and Dikic, I. (2011). The spatial and temporal organization of ubiquitin networks. Nature reviews. Molecular cell biology *12*, 295-307.
53. Kulak, N.A., Pichler, G., Paron, I., Nagaraj, N., and Mann, M. (2014). Minimal, encapsulated proteomic-sample processing applied to copy-number estimation in eukaryotic cells. Nat Meth *11*, 319-324.
54. Schulman, B.A., and Wade Harper, J. (2009). Ubiquitin-like protein activation by E1 enzymes: the apex for downstream signalling pathways. Nature reviews. Molecular cell biology *10*, 319-331.
55. Ye, Y., and Rape, M. (2009). Building ubiquitin chains: E2 enzymes at work. Nature reviews. Molecular cell biology *10*, 755-764.
56. Zheng, N., and Shabek, N. (2017). Ubiquitin Ligases: Structure, Function, and Regulation. Annual review of biochemistry *86*, 129-157.
57. Liu, X., Zhao, B., Sun, L., Bhuripanyo, K., Wang, Y., Bi, Y., Davuluri, R.V., Duong, D.M., Nanavati, D., Yin, J., and Kiyokawa, H. (2017). Orthogonal ubiquitin transfer identifies ubiquitination substrates under differential control by the two ubiquitin activating enzymes. Nature communications *8*, 14286.
58. Lee, I., and Schindelin, H. (2008). Structural insights into E1-catalyzed ubiquitin activation and transfer to conjugating enzymes. Cell *134*, 268-278.
59. Lv, Z., Rickman, K.A., Yuan, L., Williams, K., Selvam, S.P., Woosley, A.N., Howe, P.H., Ogretmen, B., Smogorzewska, A., and Olsen, S.K. (2017). S. pombe Uba1-Ubc15 Structure Reveals a Novel Regulatory Mechanism of Ubiquitin E2 Activity. Molecular cell *65*, 699-714 e696.
60. Olsen, S.K., and Lima, C.D. (2013). Structure of a ubiquitin E1-E2 complex: insights to E1-E2 thioester transfer. Molecular cell *49*, 884-896.
61. Schafer, A., Kuhn, M., and Schindelin, H. (2014). Structure of the ubiquitin-activating enzyme loaded with two ubiquitin molecules. Acta crystallographica. Section D, Biological crystallography *70*, 1311-1320.
62. Lv, Z., Yuan, L., Atkison, J.H., Aldana-Masangkay, G., Chen, Y., and Olsen, S.K. (2017). Domain alternation and active site remodeling are conserved structural features of ubiquitin E1. The Journal of biological chemistry *292*, 12089-12099.

63. Olsen, S.K., Capili, A.D., Lu, X., Tan, D.S., and Lima, C.D. (2010). Active site remodelling accompanies thioester bond formation in the SUMO E1. Nature *463*, 906-912.
64. van Wijk, S.J., and Timmers, H.T. (2010). The family of ubiquitin-conjugating enzymes (E2s): deciding between life and death of proteins. FASEB journal : official publication of the Federation of American Societies for Experimental Biology *24*, 981-993.
65. Tatham, M.H., Plechanovova, A., Jaffray, E.G., Salmen, H., and Hay, R.T. (2013). Ube2W conjugates ubiquitin to alpha-amino groups of protein N-termini. The Biochemical journal *453*, 137-145.
66. Stewart, M.D., Ritterhoff, T., Klevit, R.E., and Brzovic, P.S. (2016). E2 enzymes: more than just middle men. Cell research *26*, 423-440.
67. Cook, W.J., Jeffrey, L.C., Sullivan, M.L., and Vierstra, R.D. (1992). Three-dimensional structure of a ubiquitin-conjugating enzyme (E2). The Journal of biological chemistry *267*, 15116-15121.
68. Eletr, Z.M., Huang, D.T., Duda, D.M., Schulman, B.A., and Kuhlman, B. (2005). E2 conjugating enzymes must disengage from their E1 enzymes before E3-dependent ubiquitin and ubiquitin-like transfer. Nature structural & molecular biology *12*, 933-934.
69. Huang, L., Kinnucan, E., Wang, G., Beaudenon, S., Howley, P.M., Huibregtse, J.M., and Pavletich, N.P. (1999). Structure of an E6AP-UbcH7 complex: insights into ubiquitination by the E2-E3 enzyme cascade. Science (New York, N.Y.) *286*, 1321-1326.
70. Brzovic, P.S., Lissounov, A., Christensen, D.E., Hoyt, D.W., and Klevit, R.E. (2006). A UbcH5/ubiquitin noncovalent complex is required for processive BRCA1-directed ubiquitination. Molecular cell *21*, 873-880.
71. VanDemark, A.P., Hofmann, R.M., Tsui, C., Pickart, C.M., and Wolberger, C. (2001). Molecular insights into polyubiquitin chain assembly: crystal structure of the Mms2/Ubc13 heterodimer. Cell *105*, 711-720.
72. Eddins, M.J., Carlile, C.M., Gomez, K.M., Pickart, C.M., and Wolberger, C. (2006). Mms2-Ubc13 covalently bound to ubiquitin reveals the structural basis of linkage-specific polyubiquitin chain formation. Nature structural & molecular biology *13*, 915-920.
73. Andersen, P.L., Zhou, H., Pastushok, L., Moraes, T., McKenna, S., Ziola, B., Ellison, M.J., Dixit, V.M., and Xiao, W. (2005). Distinct regulation of Ubc13 functions by the two ubiquitin-conjugating enzyme variants Mms2 and Uev1A. The Journal of cell biology *170*, 745-755.
74. Deshaies, R.J., and Joazeiro, C.A. (2009). RING domain E3 ubiquitin ligases. Annual review of biochemistry *78*, 399-434.
75. Barlow, P.N., Luisi, B., Milner, A., Elliott, M., and Everett, R. (1994). Structure of the C3HC4 domain by 1H-nuclear magnetic resonance spectroscopy. A new structural class of zinc-finger. Journal of molecular biology *237*, 201-211.
76. Zheng, N., Schulman, B.A., Song, L., Miller, J.J., Jeffrey, P.D., Wang, P., Chu, C., Koepp, D.M., Elledge, S.J., Pagano, M., Conaway, R.C., Conaway, J.W., Harper, J.W., and Pavletich, N.P. (2002). Structure of the Cul1-Rbx1-Skp1-F boxSkp2 SCF ubiquitin ligase complex. Nature *416*, 703-709.
77. Aravind, L., and Koonin, E.V. (2000). The U box is a modified RING finger - a common domain in ubiquitination. Current biology : CB *10*, R132-134.
78. Budhidarmo, R., Nakatani, Y., and Day, C.L. RINGs hold the key to ubiquitin transfer. Trends in biochemical sciences *37*, 58-65.

79. Huang, A., Hibbert, R.G., de Jong, R.N., Das, D., Sixma, T.K., and Boelens, R. (2011). Symmetry and asymmetry of the RING-RING dimer of Rad18. Journal of molecular biology *410*, 424-435.
80. Brzovic, P.S., Rajagopal, P., Hoyt, D.W., King, M.C., and Klevit, R.E. (2001). Structure of a BRCA1-BARD1 heterodimeric RING-RING complex. Nature structural biology *8*, 833-837.
81. Hashizume, R., Fukuda, M., Maeda, I., Nishikawa, H., Oyake, D., Yabuki, Y., Ogata, H., and Ohta, T. (2001). The RING heterodimer BRCA1-BARD1 is a ubiquitin ligase inactivated by a breast cancer-derived mutation. The Journal of biological chemistry *276*, 14537-14540.
82. Linke, K., Mace, P.D., Smith, C.A., Vaux, D.L., Silke, J., and Day, C.L. (2008). Structure of the MDM2/MDMX RING domain heterodimer reveals dimerization is required for their ubiquitylation in trans. Cell death and differentiation *15*, 841-848.
83. Metzger, M.B., Pruneda, J.N., Klevit, R.E., and Weissman, A.M. (2014). RING-type E3 ligases: master manipulators of E2 ubiquitin-conjugating enzymes and ubiquitination. Biochimica et biophysica acta *1843*, 47-60.
84. Mace, P.D., Linke, K., Feltham, R., Schumacher, F.R., Smith, C.A., Vaux, D.L., Silke, J., and Day, C.L. (2008). Structures of the cIAP2 RING domain reveal conformational changes associated with ubiquitin-conjugating enzyme (E2) recruitment. The Journal of biological chemistry *283*, 31633-31640.
85. Zheng, N., Wang, P., Jeffrey, P.D., and Pavletich, N.P. (2000). Structure of a c-Cbl-UbcH7 complex: RING domain function in ubiquitin-protein ligases. Cell *102*, 533-539.
86. Ozkan, E., Yu, H., and Deisenhofer, J. (2005). Mechanistic insight into the allosteric activation of a ubiquitin-conjugating enzyme by RING-type ubiquitin ligases. Proceedings of the National Academy of Sciences of the United States of America *102*, 18890-18895.
87. Plechanovova, A., Jaffray, E.G., McMahon, S.A., Johnson, K.A., Navratilova, I., Naismith, J.H., and Hay, R.T. (2011). Mechanism of ubiquitylation by dimeric RING ligase RNF4. Nature structural & molecular biology *18*, 1052-1059.
88. Pruneda, J.N., Stoll, K.E., Bolton, L.J., Brzovic, P.S., and Klevit, R.E. (2011). Ubiquitin in motion: structural studies of the ubiquitin-conjugating enzyme approximately ubiquitin conjugate. Biochemistry *50*, 1624-1633.
89. Dou, H., Buetow, L., Sibbet, G.J., Cameron, K., and Huang, D.T. (2012). BIRC7-E2 ubiquitin conjugate structure reveals the mechanism of ubiquitin transfer by a RING dimer. Nature structural & molecular biology *19*, 876-883.
90. Pruneda, J.N., Littlefield, P.J., Soss, S.E., Nordquist, K.A., Chazin, W.J., Brzovic, P.S., and Klevit, R.E. (2012). Structure of an E3:E2~Ub complex reveals an allosteric mechanism shared among RING/U-box ligases. Molecular cell *47*, 933-942.
91. Plechanovova, A., Jaffray, E.G., Tatham, M.H., Naismith, J.H., and Hay, R.T. (2012). Structure of a RING E3 ligase and ubiquitin-loaded E2 primed for catalysis. Nature *489*, 115-120.
92. Dou, H., Buetow, L., Sibbet, G.J., Cameron, K., and Huang, D.T. (2013). Essentiality of a non-RING element in priming donor ubiquitin for catalysis by a monomeric E3. Nature structural & molecular biology *20*, 982-986.

93. Branigan, E., Plechanovova, A., Jaffray, E.G., Naismith, J.H., and Hay, R.T. (2015). Structural basis for the RING-catalyzed synthesis of K63-linked ubiquitin chains. Nature structural & molecular biology *22*, 597-602.
94. Koliopoulos, M.G., Esposito, D., Christodoulou, E., Taylor, I.A., and Rittinger, K. (2016). Functional role of TRIM E3 ligase oligomerization and regulation of catalytic activity. The EMBO journal *35*, 1204-1218.
95. Sanchez, J.G., Chiang, J.J., Sparrer, K.M., Alam, S.L., Chi, M., Roganowicz, M.D., Sankaran, B., Gack, M.U., and Pornillos, O. (2016). Mechanism of TRIM25 Catalytic Activation in the Antiviral RIG-I Pathway. Cell reports *16*, 1315-1325.
96. Dawidziak, D.M., Sanchez, J.G., Wagner, J.M., Ganser-Pornillos, B.K., and Pornillos, O. (2017). Structure and catalytic activation of the TRIM23 RING E3 ubiquitin ligase. Proteins.
97. Galanty, Y., Belotserkovskaya, R., Coates, J., and Jackson, S.P. (2012). RNF4, a SUMO-targeted ubiquitin E3 ligase, promotes DNA double-strand break repair. Genes & development *26*, 1179-1195.
98. Mohapatra, B., Ahmad, G., Nadeau, S., Zutshi, N., An, W., Scheffe, S., Dong, L., Feng, D., Goetz, B., Arya, P., Bailey, T.A., Palermo, N., Borgstahl, G.E., Natarajan, A., Raja, S.M., Naramura, M., Band, V., and Band, H. (2013). Protein tyrosine kinase regulation by ubiquitination: critical roles of Cbl-family ubiquitin ligases. Biochimica et biophysica acta *1833*, 122-139.
99. Ryan, P.E., Sivadasan-Nair, N., Nau, M.M., Nicholas, S., and Lipkowitz, S. (2010). The N terminus of Cbl-c regulates ubiquitin ligase activity by modulating affinity for the ubiquitin-conjugating enzyme. The Journal of biological chemistry *285*, 23687-23698.
100. Kassenbrock, C.K., and Anderson, S.M. (2004). Regulation of ubiquitin protein ligase activity in c-Cbl by phosphorylation-induced conformational change and constitutive activation by tyrosine to glutamate point mutations. The Journal of biological chemistry *279*, 28017-28027.
101. Buetow, L., Gabrielsen, M., Anthony, N.G., Dou, H., Patel, A., Aitkenhead, H., Sibbet, G.J., Smith, B.O., and Huang, D.T. (2015). Activation of a primed RING E3-E2-ubiquitin complex by non-covalent ubiquitin. Molecular cell *58*, 297-310.
102. Das, R., Mariano, J., Tsai, Y.C., Kalathur, R.C., Kostova, Z., Li, J., Tarasov, S.G., McFeeters, R.L., Altieri, A.S., Ji, X., Byrd, R.A., and Weissman, A.M. (2009). Allosteric activation of E2-RING finger-mediated ubiquitylation by a structurally defined specific E2-binding region of gp78. Molecular cell *34*, 674-685.
103. Metzger, M.B., Liang, Y.H., Das, R., Mariano, J., Li, S., Li, J., Kostova, Z., Byrd, R.A., Ji, X., and Weissman, A.M. (2013). A structurally unique E2-binding domain activates ubiquitination by the ERAD E2, Ubc7p, through multiple mechanisms. Molecular cell *50*, 516-527.
104. Hibbert, R.G., Huang, A., Boelens, R., and Sixma, T.K. (2011). E3 ligase Rad18 promotes monoubiquitination rather than ubiquitin chain formation by E2 enzyme Rad6. Proceedings of the National Academy of Sciences of the United States of America *108*, 5590-5595.
105. Wright, J.D., Mace, P.D., and Day, C.L. (2016). Secondary ubiquitin-RING docking enhances Arkadia and Ark2C E3 ligase activity. Nature structural & molecular biology *23*, 45-52.

106. Pierce, N.W., Kleiger, G., Shan, S.O., and Deshaies, R.J. (2009). Detection of sequential polyubiquitylation on a millisecond timescale. Nature *462*, 615-619.
107. Christensen, D.E., Brzovic, P.S., and Klevit, R.E. (2007). E2-BRCA1 RING interactions dictate synthesis of mono- or specific polyubiquitin chain linkages. Nature structural & molecular biology *14*, 941-948.
108. Jin, L., Williamson, A., Banerjee, S., Philipp, I., and Rape, M. (2008). Mechanism of ubiquitin-chain formation by the human anaphase-promoting complex. Cell *133*, 653-665.
109. Garnett, M.J., Mansfeld, J., Godwin, C., Matsusaka, T., Wu, J., Russell, P., Pines, J., and Venkitaraman, A.R. (2009). UBE2S elongates ubiquitin chains on APC/C substrates to promote mitotic exit. Nat Cell Biol *11*, 1363-1369.
110. Brown, N.G., Watson, E.R., Weissmann, F., Jarvis, M.A., VanderLinden, R., Grace, C.R., Frye, J.J., Qiao, R., Dube, P., Petzold, G., Cho, S.E., Alsharif, O., Bao, J., Davidson, I.F., Zheng, J.J., Nourse, A., Kurinov, I., Peters, J.M., Stark, H., and Schulman, B.A. (2014). Mechanism of polyubiquitination by human anaphase-promoting complex: RING repurposing for ubiquitin chain assembly. Molecular cell *56*, 246-260.
111. Brown, N.G., VanderLinden, R., Watson, E.R., Weissmann, F., Ordureau, A., Wu, K.P., Zhang, W., Yu, S., Mercredi, P.Y., Harrison, J.S., Davidson, I.F., Qiao, R., Lu, Y., Dube, P., Brunner, M.R., Grace, C.R.R., Miller, D.J., Haselbach, D., Jarvis, M.A., Yamaguchi, M., Yanishevski, D., Petzold, G., Sidhu, S.S., Kuhlman, B., Kirschner, M.W., Harper, J.W., Peters, J.M., Stark, H., and Schulman, B.A. (2016). Dual RING E3 Architectures Regulate Multiubiquitination and Ubiquitin Chain Elongation by APC/C. Cell *165*, 1440-1453.
112. Lu, Y., Wang, W., and Kirschner, M.W. (2015). Specificity of the anaphase-promoting complex: a single-molecule study. Science (New York, N.Y.) *348*, 1248737.
113. Bosu, D.R., and Kipreos, E.T. (2008). Cullin-RING ubiquitin ligases: global regulation and activation cycles. Cell division *3*, 7.
114. Petroski, M.D., and Deshaies, R.J. (2005). Function and regulation of cullin-RING ubiquitin ligases. Nature reviews. Molecular cell biology *6*, 9-20.
115. Hua, Z., and Vierstra, R.D. (2011). The cullin-RING ubiquitin-protein ligases. Annual review of plant biology *62*, 299-334.
116. Rotin, D., and Kumar, S. (2009). Physiological functions of the HECT family of ubiquitin ligases. Nature reviews. Molecular cell biology *10*, 398-409.
117. Wenzel, D.M., Lissounov, A., Brzovic, P.S., and Klevit, R.E. (2011). UBCH7 reactivity profile reveals parkin and HHARI to be RING/HECT hybrids. Nature *474*, 105-108.
118. Kamadurai, H.B., Qiu, Y., Deng, A., Harrison, J.S., Macdonald, C., Actis, M., Rodrigues, P., Miller, D.J., Souphron, J., Lewis, S.M., Kurinov, I., Fujii, N., Hammel, M., Piper, R., Kuhlman, B., and Schulman, B.A. (2013). Mechanism of ubiquitin ligation and lysine prioritization by a HECT E3. eLife *2*, e00828.
119. Maspero, E., Valentini, E., Mari, S., Cecatiello, V., Soffientini, P., Pasqualato, S., and Polo, S. (2013). Structure of a ubiquitin-loaded HECT ligase reveals the molecular basis for catalytic priming. Nature structural & molecular biology *20*, 696-701.

120. Kim, H.C., and Huibregtse, J.M. (2009). Polyubiquitination by HECT E3s and the determinants of chain type specificity. Molecular and cellular biology *29*, 3307-3318.
121. Lechtenberg, B.C., Rajput, A., Sanishvili, R., Dobaczewska, M.K., Ware, C.F., Mace, P.D., and Riedl, S.J. (2016). Structure of a HOIP/E2~ubiquitin complex reveals RBR E3 ligase mechanism and regulation. Nature *529*, 546-550.
122. Stieglitz, B., Morris-Davies, A.C., Koliopoulos, M.G., Christodoulou, E., and Rittinger, K. (2012). LUBAC synthesizes linear ubiquitin chains via a thioester intermediate. EMBO reports *13*, 840-846.
123. Smit, J.J., Monteferrario, D., Noordermeer, S.M., van Dijk, W.J., van der Reijden, B.A., and Sixma, T.K. (2012). The E3 ligase HOIP specifies linear ubiquitin chain assembly through its RING-IBR-RING domain and the unique LDD extension. The EMBO journal *31*, 3833-3844.
124. Rittinger, K., and Ikeda, F. (2017). Linear ubiquitin chains: enzymes, mechanisms and biology. Open biology *7*.
125. Dove, K.K., and Klevit, R.E. (2017). RING-Between-RING E3 Ligases: Emerging Themes amid the Variations. Journal of molecular biology.
126. Buetow, L., and Huang, D.T. (2016). Structural insights into the catalysis and regulation of E3 ubiquitin ligases. Nature reviews. Molecular cell biology *17*, 626-642.
127. Duda, D.M., Olszewski, J.L., Schuermann, J.P., Kurinov, I., Miller, D.J., Nourse, A., Alpi, A.F., and Schulman, B.A. (2013). Structure of HHARI, a RING-IBR-RING ubiquitin ligase: autoinhibition of an Ariadne-family E3 and insights into ligation mechanism. Structure (London, England : 1993) *21*, 1030-1041.
128. Trempe, J.F., Sauve, V., Grenier, K., Seirafi, M., Tang, M.Y., Menade, M., Al-Abdul-Wahid, S., Krett, J., Wong, K., Kozlov, G., Nagar, B., Fon, E.A., and Gehring, K. (2013). Structure of parkin reveals mechanisms for ubiquitin ligase activation. Science (New York, N.Y.) *340*, 1451-1455.
129. Kane, L.A., Lazarou, M., Fogel, A.I., Li, Y., Yamano, K., Sarraf, S.A., Banerjee, S., and Youle, R.J. (2014). PINK1 phosphorylates ubiquitin to activate Parkin E3 ubiquitin ligase activity. The Journal of cell biology *205*, 143-153.
130. Kazlauskaite, A., Kondapalli, C., Gourlay, R., Campbell, D.G., Ritorto, M.S., Hofmann, K., Alessi, D.R., Knebel, A., Trost, M., and Muqit, M.M. (2014). Parkin is activated by PINK1-dependent phosphorylation of ubiquitin at Ser65. The Biochemical journal *460*, 127-139.
131. Kumar, A., Chaugule, V.K., Condos, T.E.C., Barber, K.R., Johnson, C., Toth, R., Sundaramoorthy, R., Knebel, A., Shaw, G.S., and Walden, H. (2017). Parkin-phosphoubiquitin complex reveals cryptic ubiquitin-binding site required for RBR ligase activity. Nature structural & molecular biology *24*, 475-483.
132. Kelsall, I.R., Duda, D.M., Olszewski, J.L., Hofmann, K., Knebel, A., Langevin, F., Wood, N., Wightman, M., Schulman, B.A., and Alpi, A.F. (2013). TRIAD1 and HHARI bind to and are activated by distinct neddylated Cullin-RING ligase complexes. The EMBO journal *32*, 2848-2860.
133. Scott, D.C., Rhee, D.Y., Duda, D.M., Kelsall, I.R., Olszewski, J.L., Paulo, J.A., de Jong, A., Ovaa, H., Alpi, A.F., Harper, J.W., and Schulman, B.A. (2016). Two Distinct Types of E3 Ligases Work in Unison to Regulate Substrate Ubiquitylation. Cell *166*, 1198-1214 e1124.

134. Stieglitz, B., Rana, R.R., Koliopoulos, M.G., Morris-Davies, A.C., Schaeffer, V., Christodoulou, E., Howell, S., Brown, N.R., Dikic, I., and Rittinger, K. (2013). Structural basis for ligase-specific conjugation of linear ubiquitin chains by HOIP. Nature *503*, 422-426.
135. Ronau, J.A., Beckmann, J.F., and Hochstrasser, M. (2016). Substrate specificity of the ubiquitin and Ubl proteases. Cell research *26*, 441-456.
136. Hatakeyama, S. (2017). TRIM Family Proteins: Roles in Autophagy, Immunity, and Carcinogenesis. Trends in biochemical sciences *42*, 297-311.
137. Napolitano, L.M., and Meroni, G. (2012). TRIM family: Pleiotropy and diversification through homomultimer and heteromultimer formation. IUBMB life *64*, 64-71.
138. Hatakeyama, S. (2011). TRIM proteins and cancer. Nature reviews. Cancer *11*, 792-804.
139. Petrera, F., and Meroni, G. (2012). TRIM proteins in development. Advances in experimental medicine and biology *770*, 131-141.
140. Kawai, T., and Akira, S. (2011). Regulation of innate immune signalling pathways by the tripartite motif (TRIM) family proteins. EMBO molecular medicine *3*, 513-527.
141. Marin, I. (2012). Origin and diversification of TRIM ubiquitin ligases. PloS one *7*, e50030.
142. Micale, L., Chaignat, E., Fusco, C., Reymond, A., and Merla, G. (2012). The tripartite motif: structure and function. Advances in experimental medicine and biology *770*, 11-25.
143. Reymond, A., Meroni, G., Fantozzi, A., Merla, G., Cairo, S., Luzi, L., Riganelli, D., Zanaria, E., Messali, S., Cainarca, S., Guffanti, A., Minucci, S., Pelicci, P.G., and Ballabio, A. (2001). The tripartite motif family identifies cell compartments. The EMBO journal *20*, 2140-2151.
144. Sardiello, M., Cairo, S., Fontanella, B., Ballabio, A., and Meroni, G. (2008). Genomic analysis of the TRIM family reveals two groups of genes with distinct evolutionary properties. BMC evolutionary biology *8*, 225.
145. Ikeda, K., and Inoue, S. (2012). TRIM proteins as RING finger E3 ubiquitin ligases. Advances in experimental medicine and biology *770*, 27-37.
146. Massiah, M.A., Simmons, B.N., Short, K.M., and Cox, T.C. (2006). Solution structure of the RBCC/TRIM B-box1 domain of human MID1: B-box with a RING. Journal of molecular biology *358*, 532-545.
147. Borden, K.L. (1998). RING fingers and B-boxes: zinc-binding protein-protein interaction domains. Biochemistry and cell biology = Biochimie et biologie cellulaire *76*, 351-358.
148. Tao, H., Simmons, B.N., Singireddy, S., Jakkidi, M., Short, K.M., Cox, T.C., and Massiah, M.A. (2008). Structure of the MID1 tandem B-boxes reveals an interaction reminiscent of intermolecular ring heterodimers. Biochemistry *47*, 2450-2457.
149. Esposito, D., Koliopoulos, M.G., and Rittinger, K. (2017). Structural determinants of TRIM protein function. Biochemical Society transactions *45*, 183-191.
150. Wallenhammar, A., Anandapadamanaban, M., Lemak, A., Mirabello, C., Lundstrom, P., Wallner, B., and Sunnerhagen, M. (2017). Solution NMR structure of the TRIM21 B-box2 and identification of residues involved in its interaction with the RING domain. PloS one *12*, e0181551.

151. Huang, S.Y., Naik, M.T., Chang, C.F., Fang, P.J., Wang, Y.H., Shih, H.M., and Huang, T.H. (2014). The B-box 1 dimer of human promyelocytic leukemia protein. Journal of biomolecular NMR *60*, 275-281.
152. Mrosek, M., Meier, S., Ucurum-Fotiadis, Z., von Castelmur, E., Hedbom, E., Lustig, A., Grzesiek, S., Labeit, D., Labeit, S., and Mayans, O. (2008). Structural analysis of B-Box 2 from MuRF1: identification of a novel self-association pattern in a RING-like fold. Biochemistry *47*, 10722-10730.
153. Keown, J.R., and Goldstone, D.C. (2016). Crystal structure of the Trim5alpha Bbox2 domain from rhesus macaques describes a plastic oligomerisation interface. Journal of structural biology *195*, 282-285.
154. Borden, K.L., Martin, S.R., O'Reilly, N.J., Lally, J.M., Reddy, B.A., Etkin, L.D., and Freemont, P.S. (1993). Characterisation of a novel cysteine/histidine-rich metal binding domain from Xenopus nuclear factor XNF7. FEBS letters *335*, 255-260.
155. Komander, D., Lord, C.J., Scheel, H., Swift, S., Hofmann, K., Ashworth, A., and Barford, D. (2008). The structure of the CYLD USP domain explains its specificity for Lys63-linked polyubiquitin and reveals a B box module. Molecular cell *29*, 451-464.
156. Du, H., Huang, Y., Zaghlula, M., Walters, E., Cox, T.C., and Massiah, M.A. (2013). The MID1 E3 ligase catalyzes the polyubiquitination of Alpha4 (alpha4), a regulatory subunit of protein phosphatase 2A (PP2A): novel insights into MID1-mediated regulation of PP2A. The Journal of biological chemistry *288*, 21341-21350.
157. Torok, M., and Etkin, L.D. (2001). Two B or not two B? Overview of the rapidly expanding B-box family of proteins. Differentiation; research in biological diversity *67*, 63-71.
158. Goldstone, D.C., Walker, P.A., Calder, L.J., Coombs, P.J., Kirkpatrick, J., Ball, N.J., Hilditch, L., Yap, M.W., Rosenthal, P.B., Stoye, J.P., and Taylor, I.A. (2014). Structural studies of postentry restriction factors reveal antiparallel dimers that enable avid binding to the HIV-1 capsid lattice. Proceedings of the National Academy of Sciences of the United States of America *111*, 9609-9614.
159. Wagner, J.M., Roganowicz, M.D., Skorupka, K., Alam, S.L., Christensen, D., Doss, G., Wan, Y., Frank, G.A., Ganser-Pornillos, B.K., Sundquist, W.I., and Pornillos, O. (2016). Mechanism of B-box 2 domain-mediated higher-order assembly of the retroviral restriction factor TRIM5alpha. eLife *5*.
160. Crick, F. (1953). The packing of [alpha]-helices: simple coiled-coils. Acta Crystallographica *6*, 689-697.
161. Pauling, L., and Corey, R.B. (1953). Compound Helical Configurations of Polypeptide Chains: Structure of Proteins of the [alpha]-Keratin Type. Nature *171*, 59-61.
162. Lupas, A.N., and Bassler, J. (2017). Coiled Coils - A Model System for the 21st Century. Trends in biochemical sciences *42*, 130-140.
163. Javanbakht, H., Yuan, W., Yeung, D.F., Song, B., Diaz-Griffero, F., Li, Y., Li, X., Stremlau, M., and Sodroski, J. (2006). Characterization of TRIM5alpha trimerization and its contribution to human immunodeficiency virus capsid binding. Virology *353*, 234-246.
164. Cao, T., Borden, K.L., Freemont, P.S., and Etkin, L.D. (1997). Involvement of the rfp tripartite motif in protein-protein interactions and subcellular distribution. Journal of cell science *110 (Pt 14)*, 1563-1571.

165. Sanchez, J.G., Okreglicka, K., Chandrasekaran, V., Welker, J.M., Sundquist, W.I., and Pornillos, O. (2014). The tripartite motif coiled-coil is an elongated antiparallel hairpin dimer. Proceedings of the National Academy of Sciences of the United States of America *111*, 2494-2499.
166. Weinert, C., Morger, D., Djekic, A., Grutter, M.G., and Mittl, P.R. (2015). Crystal structure of TRIM20 C-terminal coiled-coil/B30.2 fragment: implications for the recognition of higher order oligomers. Scientific reports *5*, 10819.
167. Li, Y., Wu, H., Wu, W., Zhuo, W., Liu, W., Zhang, Y., Cheng, M., Chen, Y.G., Gao, N., Yu, H., Wang, L., Li, W., and Yang, M. (2014). Structural insights into the TRIM family of ubiquitin E3 ligases. Cell research *24*, 762-765.
168. Short, K.M., and Cox, T.C. (2006). Subclassification of the RBCC/TRIM superfamily reveals a novel motif necessary for microtubule binding. The Journal of biological chemistry *281*, 8970-8980.
169. Nisole, S., Stoye, J.P., and Saib, A. (2005). TRIM family proteins: retroviral restriction and antiviral defence. Nature reviews. Microbiology *3*, 799-808.
170. Grutter, C., Briand, C., Capitani, G., Mittl, P.R., Papin, S., Tschopp, J., and Grutter, M.G. (2006). Structure of the PRYSPRY-domain: implications for autoinflammatory diseases. FEBS letters *580*, 99-106.
171. Rhodes, D.A., de Bono, B., and Trowsdale, J. (2005). Relationship between SPRY and B30.2 protein domains. Evolution of a component of immune defence? Immunology *116*, 411-417.
172. D'Cruz, A.A., Kershaw, N.J., Chiang, J.J., Wang, M.K., Nicola, N.A., Babon, J.J., Gack, M.U., and Nicholson, S.E. (2013). Crystal structure of the TRIM25 B30.2 (PRYSPRY) domain: a key component of antiviral signalling. The Biochemical journal *456*, 231-240.
173. Rajsbaum, R., Garcia-Sastre, A., and Versteeg, G.A. (2013). TRIMmunity: The roles of the TRIM E3-ubiquitin ligase family in innate antiviral immunity. Journal of molecular biology.
174. Versteeg, G.A., Rajsbaum, R., Sanchez-Aparicio, M.T., Maestre, A.M., Valdiviezo, J., Shi, M., Inn, K.S., Fernandez-Sesma, A., Jung, J., and Garcia-Sastre, A. (2013). The E3-ligase TRIM family of proteins regulates signaling pathways triggered by innate immune pattern-recognition receptors. Immunity *38*, 384-398.
175. Versteeg, G.A., Benke, S., Garcia-Sastre, A., and Rajsbaum, R. (2014). InTRIMsic immunity: Positive and negative regulation of immune signaling by tripartite motif proteins. Cytokine & growth factor reviews *25*, 563-576.
176. Ozato, K., Shin, D.M., Chang, T.H., and Morse, H.C., 3rd (2008). TRIM family proteins and their emerging roles in innate immunity. Nature reviews. Immunology *8*, 849-860.
177. Pertel, T., Hausmann, S., Morger, D., Zuger, S., Guerra, J., Lascano, J., Reinhard, C., Santoni, F.A., Uchil, P.D., Chatel, L., Bisiaux, A., Albert, M.L., Strambio-De-Castillia, C., Mothes, W., Pizzato, M., Grutter, M.G., and Luban, J. (2011). TRIM5 is an innate immune sensor for the retrovirus capsid lattice. Nature *472*, 361-365.
178. Li, Y.L., Chandrasekaran, V., Carter, S.D., Woodward, C.L., Christensen, D.E., Dryden, K.A., Pornillos, O., Yeager, M., Ganser-Pornillos, B.K., Jensen, G.J., and Sundquist, W.I. (2016). Primate TRIM5 proteins form hexagonal nets on HIV-1 capsids. eLife *5*.

179. Stremlau, M., Owens, C.M., Perron, M.J., Kiessling, M., Autissier, P., and Sodroski, J. (2004). The cytoplasmic body component TRIM5alpha restricts HIV-1 infection in Old World monkeys. Nature *427*, 848-853.
180. Grutter, M.G., and Luban, J. (2012). TRIM5 structure, HIV-1 capsid recognition, and innate immune signaling. Current opinion in virology *2*, 142-150.
181. Ribeiro, C.M.S., Sarrami-Forooshani, R., Setiawan, L.C., Zijlstra-Willems, E.M., van Hamme, J.L., Tigchelaar, W., van der Wel, N.N., Kootstra, N.A., Gringhuis, S.I., and Geijtenbeek, T.B.H. (2016). Receptor usage dictates HIV-1 restriction by human TRIM5α in dendritic cell subsets. Nature *540*, 448-452.
182. Biris, N., Yang, Y., Taylor, A.B., Tomashevski, A., Guo, M., Hart, P.J., Diaz-Griffero, F., and Ivanov, D.N. (2012). Structure of the rhesus monkey TRIM5alpha PRYSPRY domain, the HIV capsid recognition module. Proceedings of the National Academy of Sciences of the United States of America *109*, 13278-13283.
183. Stremlau, M., Perron, M., Lee, M., Li, Y., Song, B., Javanbakht, H., Diaz-Griffero, F., Anderson, D.J., Sundquist, W.I., and Sodroski, J. (2006). Specific recognition and accelerated uncoating of retroviral capsids by the TRIM5alpha restriction factor. Proceedings of the National Academy of Sciences of the United States of America *103*, 5514-5519.
184. Diaz-Griffero, F., Qin, X.R., Hayashi, F., Kigawa, T., Finzi, A., Sarnak, Z., Lienlaf, M., Yokoyama, S., and Sodroski, J. (2009). A B-box 2 surface patch important for TRIM5alpha self-association, capsid binding avidity, and retrovirus restriction. Journal of virology *83*, 10737-10751.
185. Keown, J.R., Yang, J.X., Douglas, J., and Goldstone, D.C. (2016). Characterisation of assembly and ubiquitylation by the RBCC motif of Trim5alpha. Scientific reports *6*, 26837.
186. Fletcher, A.J., Christensen, D.E., Nelson, C., Tan, C.P., Schaller, T., Lehner, P.J., Sundquist, W.I., and Towers, G.J. (2015). TRIM5alpha requires Ube2W to anchor Lys63-linked ubiquitin chains and restrict reverse transcription. The EMBO journal *34*, 2078-2095.
187. Yudina, Z., Roa, A., Johnson, R., Biris, N., de Souza Aranha Vieira, D.A., Tsiperson, V., Reszka, N., Taylor, A.B., Hart, P.J., Demeler, B., Diaz-Griffero, F., and Ivanov, D.N. (2015). RING Dimerization Links Higher-Order Assembly of TRIM5alpha to Synthesis of K63-Linked Polyubiquitin. Cell reports *12*, 788-797.
188. McEwan, W.A., Mallery, D.L., Rhodes, D.A., Trowsdale, J., and James, L.C. (2011). Intracellular antibody-mediated immunity and the role of TRIM21. BioEssays : news and reviews in molecular, cellular and developmental biology *33*, 803-809.
189. Foss, S., Watkinson, R., Sandlie, I., James, L.C., and Andersen, J.T. (2015). TRIM21: a cytosolic Fc receptor with broad antibody isotype specificity. Immunological reviews *268*, 328-339.
190. Foss, S., Watkinson, R.E., Grevys, A., McAdam, M.B., Bern, M., Hoydahl, L.S., Dalhus, B., Michaelsen, T.E., Sandlie, I., James, L.C., and Andersen, J.T. (2016). TRIM21 Immune Signaling Is More Sensitive to Antibody Affinity Than Its Neutralization Activity. Journal of immunology *196*, 3452-3459.
191. Mallery, D.L., McEwan, W.A., Bidgood, S.R., Towers, G.J., Johnson, C.M., and James, L.C. (2010). Antibodies mediate intracellular immunity through

tripartite motif-containing 21 (TRIM21). Proceedings of the National Academy of Sciences of the United States of America *107*, 19985-19990.
192. McEwan, W.A., Tam, J.C., Watkinson, R.E., Bidgood, S.R., Mallery, D.L., and James, L.C. (2013). Intracellular antibody-bound pathogens stimulate immune signaling via the Fc receptor TRIM21. Nature immunology *14*, 327-336.
193. Fletcher, A.J., and James, L.C. (2016). Coordinated Neutralization and Immune Activation by the Cytosolic Antibody Receptor TRIM21. Journal of virology *90*, 4856-4859.
194. Keeble, A.H., Khan, Z., Forster, A., and James, L.C. (2008). TRIM21 is an IgG receptor that is structurally, thermodynamically, and kinetically conserved. Proceedings of the National Academy of Sciences of the United States of America *105*, 6045-6050.
195. Dos Santos, G.A., Kats, L., and Pandolfi, P.P. (2013). Synergy against PML-RARa: targeting transcription, proteolysis, differentiation, and self-renewal in acute promyelocytic leukemia. The Journal of experimental medicine *210*, 2793-2802.
196. de Thé, H., and Chen, Z. (2010). Acute promyelocytic leukaemia: novel insights into the mechanisms of cure. Nature reviews. Cancer *10*, 775-783.
197. Chang, H.R., Munkhjargal, A., Kim, M.J., Park, S.Y., Jung, E., Ryu, J.H., Yang, Y., Lim, J.S., and Kim, Y. (2017). The functional roles of PML nuclear bodies in genome maintenance. Mutation research.
198. Ishov, A.M., Sotnikov, A.G., Negorev, D., Vladimirova, O.V., Neff, N., Kamitani, T., Yeh, E.T., Strauss, J.F., 3rd, and Maul, G.G. (1999). PML is critical for ND10 formation and recruits the PML-interacting protein daxx to this nuclear structure when modified by SUMO-1. The Journal of cell biology *147*, 221-234.
199. Scherer, M., and Stamminger, T. (2016). Emerging Role of PML Nuclear Bodies in Innate Immune Signaling. Journal of virology *90*, 5850-5854.
200. Dutrieux, J., Maarifi, G., Portilho, D.M., Arhel, N.J., Chelbi-Alix, M.K., and Nisole, S. (2015). PML/TRIM19-Dependent Inhibition of Retroviral Reverse-Transcription by Daxx. PLoS pathogens *11*, e1005280.
201. Kahle, T., Volkmann, B., Eissmann, K., Herrmann, A., Schmitt, S., Wittmann, S., Merkel, L., Reuter, N., Stamminger, T., and Gramberg, T. (2015). TRIM19/PML Restricts HIV Infection in a Cell Type-Dependent Manner. Viruses *8*.
202. Masroori, N., Cherry, P., Merindol, N., Li, J.X., Dufour, C., Poulain, L., Plourde, M.B., and Berthoux, L. (2017). Gene Knockout Shows That PML (TRIM19) Does Not Restrict the Early Stages of HIV-1 Infection in Human Cell Lines. mSphere *2*.
203. Shen, T.H., Lin, H.K., Scaglioni, P.P., Yung, T.M., and Pandolfi, P.P. (2006). The mechanisms of PML-nuclear body formation. Molecular cell *24*, 331-339.
204. Lee, H.R., Kim, D.J., Lee, J.M., Choi, C.Y., Ahn, B.Y., Hayward, G.S., and Ahn, J.H. (2004). Ability of the human cytomegalovirus IE1 protein to modulate sumoylation of PML correlates with its functional activities in transcriptional regulation and infectivity in cultured fibroblast cells. Journal of virology *78*, 6527-6542.
205. Scherer, M., Klingl, S., Sevvana, M., Otto, V., Schilling, E.M., Stump, J.D., Muller, R., Reuter, N., Sticht, H., Muller, Y.A., and Stamminger, T. (2014). Crystal structure of cytomegalovirus IE1 protein reveals targeting of TRIM

family member PML via coiled-coil interactions. PLoS pathogens *10*, e1004512.
206. Schilling, E.M., Scherer, M., Reuter, N., Schweininger, J., Muller, Y.A., and Stamminger, T. (2017). The Human Cytomegalovirus IE1 Protein Antagonizes PML Nuclear Body-Mediated Intrinsic Immunity via the Inhibition of PML De Novo SUMOylation. Journal of virology *91*.
207. Gack, M.U., Shin, Y.C., Joo, C.H., Urano, T., Liang, C., Sun, L., Takeuchi, O., Akira, S., Chen, Z., Inoue, S., and Jung, J.U. (2007). TRIM25 RING-finger E3 ubiquitin ligase is essential for RIG-I-mediated antiviral activity. Nature *446*, 916-920.
208. Brubaker, S.W., Bonham, K.S., Zanoni, I., and Kagan, J.C. (2015). Innate immune pattern recognition: a cell biological perspective. Annual review of immunology *33*, 257-290.
209. Reikine, S., Nguyen, J.B., and Modis, Y. (2014). Pattern Recognition and Signaling Mechanisms of RIG-I and MDA5. Frontiers in immunology *5*, 342.
210. Yoneyama, M., Kikuchi, M., Natsukawa, T., Shinobu, N., Imaizumi, T., Miyagishi, M., Taira, K., Akira, S., and Fujita, T. (2004). The RNA helicase RIG-I has an essential function in double-stranded RNA-induced innate antiviral responses. Nature immunology *5*, 730-737.
211. Kowalinski, E., Lunardi, T., McCarthy, A.A., Louber, J., Brunel, J., Grigorov, B., Gerlier, D., and Cusack, S. (2011). Structural basis for the activation of innate immune pattern-recognition receptor RIG-I by viral RNA. Cell *147*, 423-435.
212. Maharaj, N.P., Wies, E., Stoll, A., and Gack, M.U. (2012). Conventional protein kinase C-alpha (PKC-alpha) and PKC-beta negatively regulate RIG-I antiviral signal transduction. Journal of virology *86*, 1358-1371.
213. Gack, M.U. (2014). Mechanisms of RIG-I-like receptor activation and manipulation by viral pathogens. Journal of virology *88*, 5213-5216.
214. Pichlmair, A., Schulz, O., Tan, C.P., Naslund, T.I., Liljestrom, P., Weber, F., and Reis e Sousa, C. (2006). RIG-I-mediated antiviral responses to single-stranded RNA bearing 5'-phosphates. Science (New York, N.Y.) *314*, 997-1001.
215. Rawling, D.C., Fitzgerald, M.E., and Pyle, A.M. (2015). Establishing the role of ATP for the function of the RIG-I innate immune sensor. eLife *4*.
216. Zeng, W., Sun, L., Jiang, X., Chen, X., Hou, F., Adhikari, A., Xu, M., and Chen, Z.J. (2010). Reconstitution of the RIG-I pathway reveals a signaling role of unanchored polyubiquitin chains in innate immunity. Cell *141*, 315-330.
217. Wies, E., Wang, M.K., Maharaj, N.P., Chen, K., Zhou, S., Finberg, R.W., and Gack, M.U. (2013). Dephosphorylation of the RNA sensors RIG-I and MDA5 by the phosphatase PP1 is essential for innate immune signaling. Immunity *38*, 437-449.
218. Oshiumi, H., Miyashita, M., Matsumoto, M., and Seya, T. (2013). A distinct role of Riplet-mediated K63-Linked polyubiquitination of the RIG-I repressor domain in human antiviral innate immune responses. PLoS pathogens *9*, e1003533.
219. Peisley, A., Wu, B., Xu, H., Chen, Z.J., and Hur, S. (2014). Structural basis for ubiquitin-mediated antiviral signal activation by RIG-I. Nature *509*, 110-114.
220. Liu, H.M., Loo, Y.M., Horner, S.M., Zornetzer, G.A., Katze, M.G., and Gale, M., Jr. (2012). The mitochondrial targeting chaperone 14-3-3epsilon

regulates a RIG-I translocon that mediates membrane association and innate antiviral immunity. Cell host & microbe *11*, 528-537.
221. Wu, B., Peisley, A., Tetrault, D., Li, Z., Egelman, E.H., Magor, K.E., Walz, T., Penczek, P.A., and Hur, S. (2014). Molecular imprinting as a signal-activation mechanism of the viral RNA sensor RIG-I. Molecular cell *55*, 511-523.
222. Peisley, A., Wu, B., Yao, H., Walz, T., and Hur, S. (2013). RIG-I forms signaling-competent filaments in an ATP-dependent, ubiquitin-independent manner. Molecular cell *51*, 573-583.
223. Inn, K.S., Gack, M.U., Tokunaga, F., Shi, M., Wong, L.Y., Iwai, K., and Jung, J.U. (2011). Linear ubiquitin assembly complex negatively regulates RIG-I- and TRIM25-mediated type I interferon induction. Molecular cell *41*, 354-365.
224. Pauli, E.K., Chan, Y.K., Davis, M.E., Gableske, S., Wang, M.K., Feister, K.F., and Gack, M.U. (2014). The Ubiquitin-Specific Protease USP15 Promotes RIG-I-Mediated Antiviral Signaling by Deubiquitylating TRIM25. Science signaling *7*, ra3.
225. Torre, S., Polyak, M.J., Langlais, D., Fodil, N., Kennedy, J.M., Radovanovic, I., Berghout, J., Leiva-Torres, G.A., Krawczyk, C.M., Ilangumaran, S., Mossman, K., Liang, C., Knobeloch, K.P., Healy, L.M., Antel, J., Arbour, N., Prat, A., Majewski, J., Lathrop, M., Vidal, S.M., and Gros, P. (2017). USP15 regulates type I interferon response and is required for pathogenesis of neuroinflammation. Nature immunology *18*, 54-63.
226. Kwon, S.C., Yi, H., Eichelbaum, K., Föhr, S., Fischer, B., You, K.T., Castello, A., Krijgsveld, J., Hentze, M.W., and Kim, V.N. (2013). The RNA-binding protein repertoire of embryonic stem cells. Nature structural & molecular biology *20*, 1122-1130.
227. Choudhury, N.R., Nowak, J.S., Zuo, J., Rappsilber, J., Spoel, S.H., and Michlewski, G. (2014). Trim25 Is an RNA-Specific Activator of Lin28a/TuT4-Mediated Uridylation. Cell reports *9*, 1265-1272.
228. Zou, W., Wang, J., and Zhang, D.E. (2007). Negative regulation of ISG15 E3 ligase EFP through its autoISGylation. Biochemical and biophysical research communications *354*, 321-327.
229. Zou, W., and Zhang, D.E. (2006). The interferon-inducible ubiquitin-protein isopeptide ligase (E3) EFP also functions as an ISG15 E3 ligase. The Journal of biological chemistry *281*, 3989-3994.
230. Ketscher, L., Basters, A., Prinz, M., and Knobeloch, K.P. (2012). mHERC6 is the essential ISG15 E3 ligase in the murine system. Biochemical and biophysical research communications *417*, 135-140.
231. Oudshoorn, D., van Boheemen, S., Sánchez-Aparicio, M.T., Rajsbaum, R., García-Sastre, A., and Versteeg, G.A. (2012). HERC6 Is the Main E3 Ligase for Global ISG15 Conjugation in Mouse Cells. PloS one *7*, e29870.
232. Manokaran, G., Finol, E., Wang, C., Gunaratne, J., Bahl, J., Ong, E.Z., Tan, H.C., Sessions, O.M., Ward, A.M., Gubler, D.J., Harris, E., Garcia-Blanco, M.A., and Ooi, E.E. (2015). Dengue subgenomic RNA binds TRIM25 to inhibit interferon expression for epidemiological fitness. Science (New York, N.Y.) *350*, 217-221.
233. Hale, B.G., Albrecht, R.A., and Garcia-Sastre, A. (2010). Innate immune evasion strategies of influenza viruses. Future microbiology *5*, 23-41.
234. Gack, M.U., Albrecht, R.A., Urano, T., Inn, K.S., Huang, I.C., Carnero, E., Farzan, M., Inoue, S., Jung, J.U., and Garcia-Sastre, A. (2009). Influenza

A virus NS1 targets the ubiquitin ligase TRIM25 to evade recognition by the host viral RNA sensor RIG-I. Cell host & microbe *5*, 439-449.
235. Wright, P.F., and Webster, R.G. (2001). Orthomyxoviruses. In: Knipe DM, Howley PM, eds. Fields virology. 4th ed. Philadelphia: Lippincott Williams & Wilkins, 1533-1579.
236. Taubenberger, J.K., and Morens, D.M. (2010). Influenza: the once and future pandemic. Public health reports (Washington, D.C. : 1974) *125 Suppl 3*, 16-26.
237. Krug, R.M., and García-Sastre, A. (2013). The NS1 protein: A master regulator of host and viral functions. In Textbook of Influenza. (John Wiley & Sons, Ltd), pp. 114-132.
238. Dundon, W.G., and Capua, I. (2009). A Closer Look at the NS1 of Influenza Virus. Viruses *1*, 1057-1072.
239. Hale, B.G. (2014). Conformational plasticity of the influenza A virus NS1 protein. The Journal of general virology *95*, 2099-2105.
240. Long, J.X., Peng, D.X., Liu, Y.L., Wu, Y.T., and Liu, X.F. (2008). Virulence of H5N1 avian influenza virus enhanced by a 15-nucleotide deletion in the viral nonstructural gene. Virus genes *36*, 471-478.
241. Bornholdt, Z.A., and Prasad, B.V. (2006). X-ray structure of influenza virus NS1 effector domain. Nature structural & molecular biology *13*, 559-560.
242. Liu, J., Lynch, P.A., Chien, C.Y., Montelione, G.T., Krug, R.M., and Berman, H.M. (1997). Crystal structure of the unique RNA-binding domain of the influenza virus NS1 protein. Nature structural biology *4*, 896-899.
243. Bornholdt, Z.A., and Prasad, B.V. (2008). X-ray structure of NS1 from a highly pathogenic H5N1 influenza virus. Nature *456*, 985-988.
244. Carrillo, B., Choi, J.M., Bornholdt, Z.A., Sankaran, B., Rice, A.P., and Prasad, B.V. (2014). The influenza A virus protein NS1 displays structural polymorphism. Journal of virology *88*, 4113-4122.
245. Chien, C.Y., Tejero, R., Huang, Y., Zimmerman, D.E., Rios, C.B., Krug, R.M., and Montelione, G.T. (1997). A novel RNA-binding motif in influenza A virus non-structural protein 1. Nature structural biology *4*, 891-895.
246. Cheng, A., Wong, S.M., and Yuan, Y.A. (2009). Structural basis for dsRNA recognition by NS1 protein of influenza A virus. Cell research *19*, 187-195.
247. Wang, W., Riedel, K., Lynch, P., Chien, C.Y., Montelione, G.T., and Krug, R.M. (1999). RNA binding by the novel helical domain of the influenza virus NS1 protein requires its dimer structure and a small number of specific basic amino acids. RNA (New York, N.Y.) *5*, 195-205.
248. Jureka, A.S., Kleinpeter, A.B., Cornilescu, G., Cornilescu, C.C., and Petit, C.M. (2015). Structural Basis for a Novel Interaction between the NS1 Protein Derived from the 1918 Influenza Virus and RIG-I. Structure (London, England : 1993) *23*, 2001-2010.
249. Hale, B.G., Barclay, W.S., Randall, R.E., and Russell, R.J. (2008). Structure of an avian influenza A virus NS1 protein effector domain. Virology *378*, 1-5.
250. Aramini, J.M., Hamilton, K., Ma, L.C., Swapna, G.V., Leonard, P.G., Ladbury, J.E., Krug, R.M., and Montelione, G.T. (2014). (19)F NMR reveals multiple conformations at the dimer interface of the nonstructural protein 1 effector domain from influenza A virus. Structure (London, England : 1993) *22*, 515-525.
251. Kerry, P.S., Ayllon, J., Taylor, M.A., Hass, C., Lewis, A., Garcia-Sastre, A., Randall, R.E., Hale, B.G., and Russell, R.J. (2011). A transient homotypic

interaction model for the influenza A virus NS1 protein effector domain. PloS one *6*, e17946.
252. Aramini, J.M., Ma, L.C., Zhou, L., Schauder, C.M., Hamilton, K., Amer, B.R., Mack, T.R., Lee, H.W., Ciccosanti, C.T., Zhao, L., Xiao, R., Krug, R.M., and Montelione, G.T. (2011). Dimer interface of the effector domain of non-structural protein 1 from influenza A virus: an interface with multiple functions. The Journal of biological chemistry *286*, 26050-26060.
253. Hale, B.G., Kerry, P.S., Jackson, D., Precious, B.L., Gray, A., Killip, M.J., Randall, R.E., and Russell, R.J. (2010). Structural insights into phosphoinositide 3-kinase activation by the influenza A virus NS1 protein. Proceedings of the National Academy of Sciences of the United States of America *107*, 1954-1959.
254. Das, K., Ma, L.C., Xiao, R., Radvansky, B., Aramini, J., Zhao, L., Marklund, J., Kuo, R.L., Twu, K.Y., Arnold, E., Krug, R.M., and Montelione, G.T. (2008). Structural basis for suppression of a host antiviral response by influenza A virus. Proceedings of the National Academy of Sciences of the United States of America *105*, 13093-13098.
255. Reinhard, L., Mayerhofer, H., Geerlof, A., Mueller-Dieckmann, J., and Weiss, M.S. (2013). Optimization of protein buffer cocktails using Thermofluor. Acta crystallographica. Section F, Structural biology and crystallization communications *69*, 209-214.
256. Huynh, K., and Partch, C.L. (2015). Current Protocols in Protein Science: Analysis of protein stability and ligand interactions by thermal shift assay. Current protocols in protein science / editorial board, John E. Coligan ... [et al.] *79*, 28.29.21-28.29.14.
257. Phillips, K., and de la Pena, A.H. (2011). The combined use of the Thermofluor assay and ThermoQ analytical software for the determination of protein stability and buffer optimization as an aid in protein crystallization. Current protocols in molecular biology *Chapter 10*, Unit10 28.
258. Tarazona, M.P., and Saiz, E. (2003). Combination of SEC/MALS experimental procedures and theoretical analysis for studying the solution properties of macromolecules. Journal of biochemical and biophysical methods *56*, 95-116.
259. Arakawa, T., and Wen, J. (2001). Size-exclusion chromatography with on-line light scattering. Current protocols in protein science *Chapter 20*, Unit 20 26.
260. Harding, S.E., and Jumel, K. (2001). Light Scattering. In Current protocols in protein science. (John Wiley & Sons, Inc.).
261. Delaglio, F., Grzesiek, S., Vuister, G.W., Zhu, G., Pfeifer, J., and Bax, A. (1995). NMRPipe: A multidimensional spectral processing system based on UNIX pipes. Journal of biomolecular NMR *6*, 277-293.
262. Vranken, W.F., Boucher, W., Stevens, T.J., Fogh, R.H., Pajon, A., Llinas, M., Ulrich, E.L., Markley, J.L., Ionides, J., and Laue, E.D. (2005). The CCPN data model for NMR spectroscopy: Development of a software pipeline. Proteins: Structure, Function, and Bioinformatics *59*, 687-696.
263. Kay, L.E., Torchia, D.A., and Bax, A. (1989). Backbone dynamics of proteins as studied by nitrogen-15 inverse detected heteronuclear NMR spectroscopy: application to staphylococcal nuclease. Biochemistry *28*, 8972-8979.

264. Dosset, P., Hus, J.-C., Blackledge, M., and Marion, D. (2000). Efficient analysis of macromolecular rotational diffusion from heteronuclear relaxation data. Journal of biomolecular NMR *16*, 23-28.
265. García de la Torre, J., Huertas, M.L., and Carrasco, B. (2000). HYDRONMR: Prediction of NMR Relaxation of Globular Proteins from Atomic-Level Structures and Hydrodynamic Calculations. Journal of Magnetic Resonance *147*, 138-146.
266. Dmitri, I.S., and Michel, H.J.K. (2003). Small-angle scattering studies of biological macromolecules in solution. Reports on Progress in Physics *66*, 1735.
267. Putnam, C.D., Hammel, M., Hura, G.L., and Tainer, J.A. (2007). X-ray solution scattering (SAXS) combined with crystallography and computation: defining accurate macromolecular structures, conformations and assemblies in solution. Quarterly reviews of biophysics *40*, 191-285.
268. Jacques, D.A., and Trewhella, J. (2010). Small-angle scattering for structural biology--expanding the frontier while avoiding the pitfalls. Protein science : a publication of the Protein Society *19*, 642-657.
269. Petoukhov, M.V., Franke, D., Shkumatov, A.V., Tria, G., Kikhney, A.G., Gajda, M., Gorba, C., Mertens, H.D., Konarev, P.V., and Svergun, D.I. (2012). New developments in the ATSAS program package for small-angle scattering data analysis. Journal of applied crystallography *45*, 342-350.
270. Rambo, R.P., and Tainer, J.A. (2013). Accurate assessment of mass, models and resolution by small-angle scattering. Nature *496*, 477-481.
271. Franke, D., and Svergun, D.I. (2009). DAMMIF, a program for rapid ab-initio shape determination in small-angle scattering. Journal of applied crystallography *42*, 342-346.
272. Shi, Y. A Glimpse of Structural Biology through X-Ray Crystallography. Cell *159*, 995-1014.
273. Rupp, B. (2010). Biomolecular crystallography: Principles, practice, and application to structural biology., (New York: Garland Science).
274. Battye, T.G., Kontogiannis, L., Johnson, O., Powell, H.R., and Leslie, A.G. (2011). iMOSFLM: a new graphical interface for diffraction-image processing with MOSFLM. Acta crystallographica. Section D, Biological crystallography *67*, 271-281.
275. Kabsch, W. (2010). XDS. Acta crystallographica. Section D, Biological crystallography *66*, 125-132.
276. Evans, P.R., and Murshudov, G.N. (2013). How good are my data and what is the resolution? Acta crystallographica. Section D, Biological crystallography *69*, 1204-1214.
277. Winn, M.D., Ballard, C.C., Cowtan, K.D., Dodson, E.J., Emsley, P., Evans, P.R., Keegan, R.M., Krissinel, E.B., Leslie, A.G., McCoy, A., McNicholas, S.J., Murshudov, G.N., Pannu, N.S., Potterton, E.A., Powell, H.R., Read, R.J., Vagin, A., and Wilson, K.S. (2011). Overview of the CCP4 suite and current developments. Acta crystallographica. Section D, Biological crystallography *67*, 235-242.
278. McCoy, A.J., and Read, R.J. (2010). Experimental phasing: best practice and pitfalls. Acta crystallographica. Section D, Biological crystallography *66*, 458-469.
279. Terwilliger, T.C., Adams, P.D., Read, R.J., McCoy, A.J., Moriarty, N.W., Grosse-Kunstleve, R.W., Afonine, P.V., Zwart, P.H., and Hung, L.W. (2009). Decision-making in structure solution using Bayesian estimates of

map quality: the PHENIX AutoSol wizard. Acta crystallographica. Section D, Biological crystallography *65*, 582-601.
280. Emsley, P., Lohkamp, B., Scott, W.G., and Cowtan, K. (2010). Features and development of Coot. Acta crystallographica. Section D, Biological crystallography *66*, 486-501.
281. Emsley, P., and Cowtan, K. (2004). Coot: model-building tools for molecular graphics. Acta crystallographica. Section D, Biological crystallography *60*, 2126-2132.
282. Evans, P., and McCoy, A. (2008). An introduction to molecular replacement. Acta crystallographica. Section D, Biological crystallography *64*, 1-10.
283. Stein, N. (2008). CHAINSAW: a program for mutating pdb files used as templates in molecular replacement. Journal of applied crystallography *41*, 641-643.
284. L Patterson, A. (1934). A Fourier Series Method for the Determination of the Components of Interatomic Distances in Crystals, Volume 46.
285. McCoy, A.J. (2007). Solving structures of protein complexes by molecular replacement with Phaser. Acta crystallographica. Section D, Biological crystallography *63*, 32-41.
286. Terwilliger, T.C., Grosse-Kunstleve, R.W., Afonine, P.V., Moriarty, N.W., Zwart, P.H., Hung, L.W., Read, R.J., and Adams, P.D. (2008). Iterative model building, structure refinement and density modification with the PHENIX AutoBuild wizard. Acta crystallographica. Section D, Biological crystallography *64*, 61-69.
287. Ramachandran, G.N., Ramakrishnan, C., and Sasisekharan, V. (1963). Stereochemistry of polypeptide chain configurations. Journal of molecular biology *7*, 95-99.
288. Afonine, P.V., Grosse-Kunstleve, R.W., Echols, N., Headd, J.J., Moriarty, N.W., Mustyakimov, M., Terwilliger, T.C., Urzhumtsev, A., Zwart, P.H., and Adams, P.D. (2012). Towards automated crystallographic structure refinement with phenix.refine. Acta crystallographica. Section D, Biological crystallography *68*, 352-367.
289. Vagin, A.A., Steiner, R.A., Lebedev, A.A., Potterton, L., McNicholas, S., Long, F., and Murshudov, G.N. (2004). REFMAC5 dictionary: organization of prior chemical knowledge and guidelines for its use. Acta crystallographica. Section D, Biological crystallography *60*, 2184-2195.
290. Terwilliger, T.C. (2013). Finding non-crystallographic symmetry in density maps of macromolecular structures. Journal of structural and functional genomics *14*, 91-95.
291. Urzhumtsev, A., Afonine, P.V., and Adams, P.D. (2013). TLS from fundamentals to practice. Crystallography reviews *19*, 230-270.
292. Li, X., and Sodroski, J. (2008). The TRIM5alpha B-box 2 domain promotes cooperative binding to the retroviral capsid by mediating higher-order self-association. Journal of virology *82*, 11495-11502.
293. Zhang, M., Windheim, M., Roe, S.M., Peggie, M., Cohen, P., Prodromou, C., and Pearl, L.H. (2005). Chaperoned Ubiquitylation—Crystal Structures of the CHIP U Box E3 Ubiquitin Ligase and a CHIP-Ubc13-Uev1a Complex. Molecular cell *20*, 525-538.
294. Shi, Y., Yuan, B., Zhu, W., Zhang, R., Li, L., Hao, X., Chen, S., and Hou, F. (2017). Ube2D3 and Ube2N are essential for RIG-I-mediated MAVS aggregation in antiviral innate immunity. Nature communications *8*, 15138.

295. Rajsbaum, R., Albrecht, R.A., Wang, M.K., Maharaj, N.P., Versteeg, G.A., Nistal-Villan, E., Garcia-Sastre, A., and Gack, M.U. (2012). Species-specific inhibition of RIG-I ubiquitination and IFN induction by the influenza A virus NS1 protein. PLoS pathogens *8*, e1003059.
296. Ayllon, J., Russell, R.J., Garcia-Sastre, A., and Hale, B.G. (2012). Contribution of NS1 effector domain dimerization to influenza A virus replication and virulence. Journal of virology *86*, 13095-13098.
297. Kerry, P.S., Long, E., Taylor, M.A., and Russell, R.J. (2011). Conservation of a crystallographic interface suggests a role for beta-sheet augmentation in influenza virus NS1 multifunctionality. Acta crystallographica. Section F, Structural biology and crystallization communications *67*, 858-861.
298. Martino, L., Holland, L., Christodoulou, E., Kunzelmann, S., Esposito, D., and Rittinger, K. (2016). The Biophysical Characterisation and SAXS Analysis of Human NLRP1 Uncover a New Level of Complexity of NLR Proteins. PloS one *11*, e0164662.
299. Zheng, W., Cao, S., Chen, C., Li, J., Zhang, S., Jiang, J., Niu, Y., Fan, W., Li, Y., Bi, Y., Gao, G.F., Sun, L., and Liu, W. (2017). Threonine 80 phosphorylation of non-structural protein 1 regulates the replication of influenza A virus by reducing the binding affinity with RIG-I. Cellular microbiology *19*.
300. Kathum, O.A., Schrader, T., Anhlan, D., Nordhoff, C., Liedmann, S., Pande, A., Mellmann, A., Ehrhardt, C., Wixler, V., and Ludwig, S. (2016). Phosphorylation of influenza A virus NS1 protein at threonine 49 suppresses its interferon antagonistic activity. Cellular microbiology *18*, 784-791.
301. Hsiang, T.Y., Zhou, L., and Krug, R.M. (2012). Roles of the phosphorylation of specific serines and threonines in the NS1 protein of human influenza A viruses. Journal of virology *86*, 10370-10376.
302. Zhao, C., Hsiang, T.Y., Kuo, R.L., and Krug, R.M. (2010). ISG15 conjugation system targets the viral NS1 protein in influenza A virus-infected cells. Proceedings of the National Academy of Sciences of the United States of America *107*, 2253-2258.
303. Qian, X.Y., Chien, C.Y., Lu, Y., Montelione, G.T., and Krug, R.M. (1995). An amino-terminal polypeptide fragment of the influenza virus NS1 protein possesses specific RNA-binding activity and largely helical backbone structure. RNA (New York, N.Y.) *1*, 948-956.
304. Sanchez-Aparicio, M.T., Ayllon, J., Leo-Macias, A., Wolff, T., and Garcia-Sastre, A. (2017). Subcellular Localizations of RIG-I, TRIM25, and MAVS Complexes. Journal of virology *91*.
305. Fiskin, E., Bhogaraju, S., Herhaus, L., Kalayil, S., Hahn, M., and Dikic, I. (2017). Structural basis for the recognition and degradation of host TRIM proteins by Salmonella effector SopA. Nature communications *8*, 14004.
306. Davis, M.E., and Gack, M.U. (2015). Ubiquitination in the antiviral immune response. Virology *479-480*, 52-65.
307. Kamanova, J., Sun, H., Lara-Tejero, M., and Galán, J.E. (2016). The Salmonella Effector Protein SopA Modulates Innate Immune Responses by Targeting TRIM E3 Ligase Family Members. PLoS pathogens *12*, e1005552.
308. Yang, Z., Soderholm, A., Lung, T.W.F., Giogha, C., Hill, M.M., Brown, N.F., Hartland, E., and Teasdale, R.D. (2015). SseK3 Is a Salmonella Effector That Binds TRIM32 and Modulates the Host's NF-κB Signalling Activity. PloS one *10*, e0138529.